KADIR HAS UNIVERSITY

SCHOOL OF GRADUATE STUDIES

DEPARTMENT OF BIOINFORMATICS AND GENETICS

SCREENING OF NOVEL AND SELECTIVE INHIBITORS FOR NEURONAL NITRIC OXIDE SYNTHASE (nNOS) VIA STRUCTURE-BASED DRUG DESIGN TECHNIQUES

SARAH BOUMEZBER

DOCTOR OF PHILOSOPHY THESIS

ISTANBUL, JANUARY, 2022

Sarah Boumezber

Ph.D. Thesis

2022

SCREENING OF NOVEL AND SELECTIVE INHIBITORS FOR NEURONAL NITRIC OXIDE SYNTHASE (nNOS) VIA STRUCTURE-BASED DRUG DESIGN TECHNIQUES

SARAH BOUMEZBER

A thesis submitted to
the School of Graduate Studies of Kadir Has University
in partial fulfilment of the requirements for the degree of
Doctor of Philosophy in
Bioinformatics and Genetics

Istanbul, January, 2022

APPROVAL

This thesis titled SCREENING OF NOVEL AND SELECTIVE INHIBITORS FOR NEURONAL NITRIC OXIDE SYNTHASE (nNOS) VIA STRUCTURE-BASED DRUG DESIGN TECHNIQUES, submitted by SARAH BOUMEZBER, in partial fulfillment of the requirements for the degree of Doctor of Philosophy in Bioinformatics and Genetics is approved by

Prof. Dr. Kemal Yelekçi (Advisor)
Kadir Has University

Asst. Prof. Ebru Bilget Güven
Kadir Has University

Asst. Prof. Muhammet Mustafa Çetin
Kadir Has University

Prof. Dr. Özkan Daniş
Marmara University

Prof. Dr. Atilla Akdemir
Bezmialem Vakif University

I confirm that the signatures above belong to the aforementioned faculty members.

_____

Prof. Dr. Mehmet Timur Aydemir
Director of the School of Graduate Studies
Date of Approval: 12.01.22

DECLARATION ON RESEARCH ETHICS AND
PUBLISHING METHODS

I, SARAH BOUMEZBER; hereby declare

- that this Ph.D. Thesis that I have submitted is entirely my own work and I have cited and referenced all material and results that are not my own in accordance with the rules;

- that this Ph.D. Thesis does not contain any material from any research submitted or accepted to obtain a degree or diploma at another educational institution;

- and that I commit and undertake to follow the "Kadir Has University Academic Codes of Conduct" prepared in accordance with the "Higher Education Council Codes of Conduct".

In addition, I acknowledge that any claim of irregularity that may arise in relation to this work will result in a disciplinary action in accordance with the university legislation.

Sarah Boumezber

_____

Date (12.01.22)

To My parent, thanks for everything ...

ACKNOWLEDGEMENT

SCREENING OF NOVEL AND SELECTIVE INHIBITORS FOR NEURONAL NITRIC OXIDE SYNTHASE (nNOS) VIA STRUCTURE-BASED DRUG DESIGN TECHNIQUES

ABSTRACT

The overproduction of nitric oxide (NO) by neuronal nitric oxide synthase (nNOS) is the main cause of several neurodegenerative diseases such as Alzheimer's Disease (AD), Parkinson's Disease (PD), and Multiple Sclerosis (MS). NO is produced in many cell types by three isoforms of NOS (nNOS, iNOS, and eNOS) and has various biological functions, generally, for its significant reactivity with proteins. NOS isoforms share a high sequence and structure similarity, specifically in the active site, which makes the development and design of nNOS inhibitors extremely challenging; mainly, no-selective inhibitors can affect iNOS and eNOS physiological roles. To date, there is no selective inhibitor against nNOS in the market with desirable ADMET (absorption, distribution, metabolism, elimination, and toxicity) properties, and pass the blood-brain barrier (BBB). With improvement of computational drug design techniques and accessibility of the X-ray crystal structures, development of novel drugs became less expensive and faster. Our research benefited from the structure-based drug design approaches to investigate proficient and selective inhibitors against nNOS. After structure-based virtual screening, the selective top-ranked compounds were filtered according to the ADMET prediction; then, the candidates with a high affinity with a suitable ADMET profile were subject to 100 ns molecular dynamics (MD) simulations. The stability through the 100 ns run has been evident for some nominated inhibitors, which are valuable lead compounds that can be optimized to reach the greatest physicochemical properties in addition to the selectivity.

Keywords: Nitric oxide, structure-based drug design, neuronal nitric oxide synthase, neurodegenerative diseases, ADMET properties, selective nNOS inhibitors, molecular dynamics simulation.

NÖRONAL NITRIK OKSIT SENTAZ (nNOS) IÇIN YENI VE SEÇICI
INHIBITÖRLERIN YAPI BAZLI ILAÇ TASARIM TEKNIKLERI ILE
TARANMASI

ÖZET

Nöronal nitrik oksit sentaz (nNOS) tarafından aşırı nitrik oksit (NO) üretimi, Alzheimer
Hastalığı (AD), Parkinson Hastalığı (PD) ve Multipl Skleroz (MS) gibi çeşitli
nörodejeneratif hastalıkların ana nedenidir. NO, birçok hücre tipinde üç NOS izoformu
(nNOS, iNOS ve eNOS) tarafından üretilir ve genellikle proteinlerle olan önemli
reaktivitesi nedeniyle çeşitli biyolojik fonksiyonlara sahiptir. NOS izoformları, özellikle
aktif bölgede, nNOS inhibitörlerinin geliştirilmesini ve tasarımını son derece zorlaştıran
yüksek bir dizi ve yapı benzerliği paylaşır; esas olarak, seçici olmayan inhibitörler,
iNOS ve eNOS'un fizyolojik rollerini etkileyebilir. Bugüne kadar piyasada nNOS'a karşı
iyi ADMET (absorpsiyon, dağılım, metabolizma, eliminasyon ve toksisite) özellikleri
ve yüksek biyoaktiviteye sahip seçici bir inhibitörü yoktur. Hesaplamalı ilaç tasarım
tekniklerinin gelişmesi ve X-ışını kristal yapılarının erişilebilirliği ile yeni ilaçların
geliştirilmesi daha ucuz ve daha hızlı hale geldi. Araştırmamız, nNOS'a karşı etkili ve
seçici inhibitörleri araştırmak için yapı temelli ilaç tasarımı yaklaşımlarından yararlandı.
Yapıya dayalı sanal taramadan sonra, seçici üst sıradaki bileşikler, ADMET tahminine
göre filtrelendi; daha sonra, iyi bir ADMET profiline sahip yüksek afiniteye sahip
adaylar, 100 ns moleküler dinamik (MD) simülasyonlarına tabi tutuldu. Bazı aday
bileşikler için 100 ns simülasyon sonucunda kararlılık sağlandı. Seçiciliğe ek olarak
fizikokimyasal özellikleri çok uygun olan önemli öncü bileşiklerin optimimize
edilebileceği görüldü.

Anahtar kelimier: Nitrik oksit, yapı temelli ilaç tasarımı, nöronal nitrik oksit sentaz,
nörodejeneratif hastalıklar, ADMET özellikleri, seçici nNOS inhibitörleri, moleküler
dinamik simülasyonu.

TABLE OF CONTENTS

LIST OF FIGURES

LIST OF TABLES

LIST OF ACRONYMS AND ABBREVIATIONS

3D QSAR	3D quantitative structure activity relationships
AC	Adenylate cyclase
AD	Alzheimer's disease
ADMA	Asymmetric dimethylarginine
AGEs	Advanced glycation end products
ALS	Amyotrophic lateral sclerosis
AMPK	AMP-activated protein kinase
ANS	Autonomic nervous system
AP-1	Activating protein-1
bp	Base pairs
CADD	Computer aided drug design
CADD	Computer-aided drug design
CAMD	Computer-aided molecular design
CaMKII	Ca^{2+}/calmodulin-dependent protein kinase II
CAMM	Computer-aided molecular modeling
Cav1	Caveolin-1
Cav3	Caveolin-3
cGMP	$3'$-$5'$-cyclic guanosine monophosphate
CM	Cutaneous melanoma
CM	Cytokine mixture
cNOSs	Mammalian constitutive NOS
CNS	Central nervous system
CPR	Cytochrome P450 reductase protein
CRH	Corticotropin-releasing hormone
DALYs	Disability-adjusted life-years
DHAP	Dihydroxyacetone phosphate
DSM-5	The 5th edition of the Diagnostic and Statistical Manual of Mental Disorders
EDRF	Endothelium derived relaxing factor
eNOS	Neuronal nitric oxide synthase

ENS	Enteric nervous system
ERK	Extracellular signal-regulated kinase
FAD	Flavin adenine dinucleotide
FMN	Flavin mononucleotide
GAP	Glyceraldehyde 3-phosphate
GBD	Global Burden of Disease
GC	Guanyl cyclase
GHRH	Growth hormone-releasing hormone
GnRH	Gonadotropin-releasing hormone
GTP	Guanosine 5′-triphosphate
GW	Gestational week
H4B	(6R)-5,6,7,8-tetrahydrobiopterin
Hbα	Haemoglobin α
HD	Huntington's disease
HPO	Human Phenotype Ontology
HSCR	Hirschsprung disease
hsp90	Heat shock protein 90
HTS	High-throughput screening
IDDM	Insulin dependent diabetes mellitus
iNOS	Inducible nitric oxide synthase
JNK	c-Jun amino-terminal kinase
^{L}-NMMA	N^G-monomethyl-^{L}-arginine
LBDD	Ligand-based drug design
LPS	Lipopolysaccharide
MAPKs	Mitogen-activated protein kinases
mtNOS	Mitochondrial nitric oxide synthase
NADPH	Nicotinamide adenine dinucleotide phosphate
NANC	Nonadrenergic noncholinergic
NCC	Neural crest cells
NCDs	Neurodegenerative diseases
NIA–AA	National Institute on Aging–Alzheimer's Association
NIDDM	Non-insulin dependent diabetes mellitus

NINDS	National Institute of Neurological Disorders and Stroke
NMDAR	N-methyl-D-aspartate receptor
nNOS	Neuronal nitric oxide synthase
NO	Nitric oxide
NO^+	Nitrosyl cation
NO^-	Nitrosyl anion
NO_2^-	Nitrite
NO_3^-	Nitrate
NOHA	N^ω-hydroxy-L-arginine
$ONOO^-$	Peroxynitrite
PD	Parkinson's disease
PDE-3	Phosphodiesterase 3
PDE-5.	Phosphodiesterase 5
PH	Pulmonary hypertension
PI3	Phosphatidylinositol-3
PKA	Protein kinase A
PKG	Protein kinase G
PNS	Peripheral nervous system
PSD	Post-synaptic density
PTB	Phosphotyrosine binding
RBPs	RNA-binding proteins
RNS	Reactive nitrogen species
ROS	Reactive oxygen species
SBDD	Structure based drug design
SCZ	Schizophrenia
SDMA	N^G,N^G-symmetric dimethylarginine
SNPs	Single nucleotide polymorphisms
SNS	Sympathetic nervous system
SoNS	Somatic nervous system
SPECT	Single-photon emission computed tomography
TNF-α	Tumor necrosis factor-α
TPI	Triose-phosphate isomerase

TRH	Thyrotropin-releasing hormone
TTP	Tristetraprolin
uORF	Upstream open reading frame
VEGF	Vascular endothelial growth factor
VNTRS	Variable number of tandem repeats
VSO	Vascular superoxide
WHO	World health organization
ZnS$_4$	Zinc tetrathiolate

1. INTRODUCTION

Neurodegenerative diseases (NDs) pose a severe threat to human health. These age-related disorders have become more frequent due to an increase in the aged population in recent years (Gitler, Dhillon and Shorter, 2017, pp. 499–502). Brain aging, peripheral infections, and other factors make the central nervous system (CNS) more vulnerable to damage (Stephenson et al, 2018, pp. 204–219; Pihlstrøm, Wiethoff and Houlden, 2017, pp. 309–323). NDs are severe, multifactorial disorders of the nervous system. Conferring to the World Health Organization (WHO) data, NDs millions of people worldwide. The organization has predicted that NDs affecting motor function will become the second-most prevalent cause of death in the next 20 years (Durães, Pinto, and Sousa, 2018, p. 44).

Neuronal damage is a pathological characteristic of Alzheimer's disease (AD) and Parkinson's disease (PD), amyotrophic lateral sclerosis (ALS), Huntington's disease (HD), spinocerebellar ataxia, and multiple sclerosis (MS), but ND is also noticed after neurotropic viral infections, stroke, genetic white matter diseases, and paraneoplastic disorders (Xie et al, 2014, p. 648740; Stephenson et al, 2018, pp. 204–219; Ghasemi, Razavi and Nikzad 2017, pp. 1–10). These diseases have distinct epidemiology, clinical symptomatology, laboratory and neuroimaging characteristics, neuropathology, and therapy (Erkkinen, Kim and Geschwind, 2018, p. a033118). In many cases, they are expressed via impairing memory, cognition, and locomotion (Durães, Pinto and Sousa, 2018, p. 44).

In ND, oxidative and nitrergic stress are thought to initiate several pathogenic processes that further accelerate the existing neurodegeneration (Bourgognon et al, 2021, p. e2009579118). 3 N-terminal tail (3-NT) of -amyloid (A) oligomers, for instance, provides a direct mechanism for boosting oligomer steadiness and toxicity. Notably, A42 oligomerization plays a vital function in enhancing nitrergic stress, in other words, triggering 3-NT in a variety of neuronal proteins (Bourgognon et al, 2021, p. e2009579118; Heinrich, Gorath and Richter-Landsberg, 1999, pp. 244–255). The

enzyme triose-phosphate isomerase (TPI), one of the targeted proteins, controls glycolytic circulation by interconverting dihydroxyacetone phosphate (DHAP) and glyceraldehyde 3-phosphate (GAP). TPI's enzymatic activity is reduced by the nitrergic post-translational alteration generated by the A42 peptide, which changes the metabolite balance toward DHAP production. Following that, DHAP is immediately converted into the toxic metabolic 'by-product methylglyoxal.' In patients with Alzheimer's disease, a nitro-oxidative condition promotes elevated amounts of 3-nitrotyrosinated TPI, and the inactivation of this enzyme results in nonenzymatic methylglyoxal-mediated protein glycation and the development of final advanced glycation products (AGEs) (Orosz, Oláh and Ovádi 2006, pp. 703–715; Bourgognon et al, 2021, p. e2009579118). Aggregation and accumulation of AGEs are seen in TAU positive intracellular aggregates and Aβ plaques in AD with AGE-mediated protein cross-linking, considerably accelerating amyloid polymerization. Glycation at specific residues affects the ability to produce amyloid fibrils, revealing that this change plays a role in the accumulation of AGEs (Rajmohan and Reddy, 2017, pp. 975–999).

Unfortunately, no ND is treatable, and present treatments only manage symptoms or delay disease development. As a result, new therapies for this disease category are desperately needed (Golde, 2009, p. 8; Durães, Pinto and Sousa, 2018, p. 44). The fundamental restriction of the anti-neurodegenerative disease drug efficacy is their failure to penetrate the blood-brain barrier (BBB); in fact, more than 98% of small molecules and nearly 100% of large molecules cannot reach the brain. Initially, invasive techniques, such as neurosurgery-based cerebral infusions or implants and physical or chemical disruption of the BBB to allow drug access via osmotic shift, were used to pass the BBB (Cascione et al, 2020, p. 566767). These approaches are dangerous, causing brain tissue destruction, and are likely to cause chronic neuropathological sequelae in patients treated (Cascione et al, 2020, p. 566767) (**Table 1.1).**

Table 1.1 Current drugs used for neurodegenerative (ND) disorders and their restrictions (Cascione et al, 2020, p. 566767).

Drug	Bioactivities	Limits
Rivastigmine	Acetylcholinesterase inhibitor	(-) BBB (-) Bioavailability.
Donepezil	Acetylcholinesterase inhibitor	(-) Bioavailability (-) BBB
Curcumin	Amyloid protein aggregation inhibitor	(-) Solubility (-) Bioavailability
Quercetin	Antioxidant capacity Enhance cognitive and memory function	(-) ADME (-) BBB
Resveratrol	Facilitates non-amyloidogenic degradation of amyloid precursor proteins, increases amyloid-peptide elimination, and reduces neuronal damage	(-) solubility (-) Bioavailability
Levodopa (SHM)	Dopamine precursor	Cytotoxicity Dyskinesia (-) BBB

Neuronal nitric oxide synthase (nNOS) is an enzymatic target for the therapy of ND (and other neuronal-damaged) (Cinelli et al, 2017, pp. 3958–3978). nNOS can become hyperactive or overexpressed during neuroinflammatory or neurodegenerative phenotypes, which causes the formation of a high amount of nitric oxide (NO). This produced NO by itself can be dangerous or can interact with other molecules to generate other species such as peroxynitrite. (Cinelli et al, 2017, pp. 3958–3978).

3

nNOS is active in homodimeric form and transforms L-arginine to L-citrulline and NO via electron conduction involving five cofactors (Förstermann and Sessa, 2012, pp. 829–837). Each monomer includes oxygenase and reductase domains connected by a linker domain where calmodulin attaches and stimulates the enzyme due to the increased calcium levels (Rao, Chaudhury and Goyal, 2008, pp. G627–G634). When the enzyme is active, electron transfer begins from the reductase domain bound reduced nicotinamide adenine dinucleotide phosphate (NADPH) to flavin adenine dinucleotide (FAD), then to flavin mononucleotide (FMN), and finally to the FMN subdomain of one monomer towards the oxygenase domain of the other monomer through (6R)-5,6,7,8-tetrahydrobiopterin (H4B). Lastly, the attached L-arginine is oxidized in the presence of molecular oxygen at the active heme center (Cinelli et al, 2017, pp. 3958–3978; Förstermann and Sessa, 2012, pp. 829–837; McCabe et al, 2000, pp. 6123–6128).

The majority of nNOS inhibitors compete with the substrate L-arginine and have physicochemical features similar to it (**Figure 1.1**) (Boer et al, 2000, pp.1026–1034). However, these compounds are polar, ionizable with high-pKa, which lead to low bioavailability and BBB permeability. These characteristics limit their therapeutic utility (Pajouhesh and Lenz, 2005, pp. 541–553). the design of a selective inhibitor against nNOS over eNOS and iNOS is highly challenging because the inhibition of eNOS may induce cardiovascular risks , and the inhibition of iNOS may impair immune system function. This is a complex undertaking because all three NOS isoforms have similar sequences and structures (Ji et al, 2009, pp. 209–217; Melikian et al, 2009, pp. 256–262; Pensa et al, 2017, pp. 7146–7165).
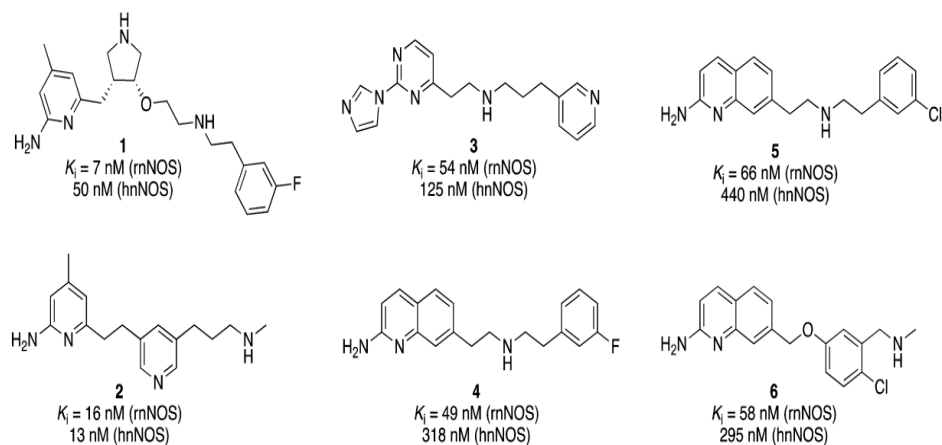
Figure 1.1 Earlier designed human nNOS inhibitors (Pensa et al, 2017, pp. 7146–7165).

The process of discovering and developing new medicines is time-consuming, risky, and costly. Many techniques to speeding the research cycle and decreasing the cost and probability of failure in drug development were explored. Computer-aided drug design (CADD) is one of the most successful ways to attain these goals (Ou-Yang et al, 2012, pp. 1131–1140). Structure-based drug design (SBDD), ligand-based drug design (LBDD), and sequence-based techniques are the most frequently employed computational drug discovery methodologies. SBDD approaches, including molecular docking and de novo drug design, depend on the target macromolecule's structure, mainly collected via crystal structures, NMR data, and homology modeling (Aparoy, Kumar Reddy and Reddanna, 2012, pp.3763–3778). In the most of these techniques, the LBDD approach is used in the absence of receptor three-dimensional (3D) data. This method requires a well-understanding of drugs that interact to the biological target of interest. The essential techniques in LBDD are 3D quantitative structure-activity relationships and pharmacophore modeling because they give predictive models employed to identify and optimize drugs (Acharya et al, 2011, pp. 10–22).

1.1. Research Objectives

- This Dissertation aims to design selective and potent human neuronal nitric oxide synthase (nNOS) inhibitors using CADD approaches.
- Structure-based drug design techniques were employed, including molecular docking, virtual screening, and MD simulations.
- Human NOS structures were used to have a close evaluation of isoform selectivity.

2. NITRIC OXIDE

2.1. Structure of Nitric Oxide (NO)

NO is, also named nitrogen oxide or nitrogen monoxide, is an essential gaseous signaling radical (molecular weight =30 Da) (Bignon et al,2019, pp. 415–429; Yang et al, 2015, pp. 49–68). It was discovered by Robert Furchgott, Louis Ignarro, and Ferid Murad in 1987, and they were awarded the Nobel prize in physiology or medicine in 1998 (Lancaster, 2015, p. FSO59; Bignon et al, 2019, pp. 415–429; Levine, Punihaole and Levine T, 2012, pp. 55–68). NO is composed of a double covalent bond between oxygen and nitrogen (Lancaster, 2015, p. FSO59). Since NO is electrically neutral, it can cross biological membranes at a rate of $848*10^{-6}$ m/s in the aortic wall. This property considerably boots its role as a second messenger. NO's action is limited by its reactivity due to the nitrogen atom's lack of 1 electron in its sp2 orbital, which reduces the NO half-life to 1–10 s. As a result, its production and half-life are determined by the type and the pathophysiological condition of the tissues (Picón-Pagès et al, 2019, pp. 1949–1967). NO is a major signaling molecule that regulates many physiological processes in many tissues, including vasodilation, neuronal function, inflammation, and immune function (Shahani and Sawa, 2012, pp. 736–742).

2.2. Nitric Oxide (NO) Production Pathways

The human body produces NO via different pathways in the different locations of the body. Its production involves a variety of enzyme isoforms (Endogenous NO) or 'the enzymatic pathway,' which is catalyzed by NOS via a series of redox reactions with L-arginine degradation to L-citrulline and NO (Luiking, Engelen, and Deutz, 2010, pp. 97–104).

NO is also produced in many tissues by four distinct isoforms of NOS: neuronal NOS (nNOS), inducible NOS (iNOS), endothelial NOS (eNOS), and mitochondrial NOS (mtNOS) (Levine, Punihaole and Levine T, 2012, pp. 55–68). NOSs have very similar structures but vary in expression and activities (Mittal and Kakkar,2020, p. 228). Each one is encoded by a specific gene (Król and Kepinska, 2021, p. 56).

2.2.1. Nitrate- Nitrite- Nitric oxide (NO) pathway

The non-enzymatic pathways produce NO from nitrite through various routes, primarily in acidic conditions, and occur mostly in tissues. Nitrite reduction below is the primary pathway (Luiking, Engelen, and Deutz, 2010, pp. 97–104):

$$2H^+ + NO_2^- + e^- \rightarrow NO + H_2O. \tag{2.1}$$
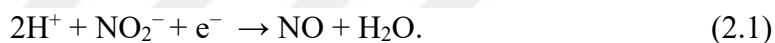
Given that the half-life of NO in the blood is only 2 ms and less than 2 s in tissues, stabilization of NO to nitrite (NO_2^-) and nitrate (NO_3^-) is a suitable method of storing bioavailable NO because these anions can be reduced back to NO under hypoxia (Bryan and Grisham, 2007, pp. 645–657; Park et al, 2020, p. 13166). After being concentrated from the blood by salivary glands, nitrate absorbed from nutritional sources can be converted to nitrite, primarily by commensal bacterial nitrate reductases in the oral cavity. The nitrite in tissues is reduced to NO by several enzymatic systems, such as deoxyhemoglobin, deoxymyoglobin, and molybdenum containing enzymes (Park et al, 2020, p. 13166). The nitrate- nitrite- NO pathway can be considered as a complement to the classical L-arg-NOS pathway, they also work in tandem to some extent., but nitrite reduction to NO becomes more significant under hypoxic conditions and when NOS activity is restricted (Lundberg, Weitzberg and Gladwin, 2008, pp. 156–167; Luiking, Engelen, and Deutz, 2010, pp. 97–104). The rate of formation and degradation of NO define its steady-state concentration (Kelm, 1999, pp. 273–289).

2.3. Nitric Oxide (NO) Derivatives

NO can quickly pass through hydrophobic areas (like plasma membrane) due to its low solubility in water (1.9 mM at 20°C) and liposome/water partition coefficient around 4.4 (Zacharia and Deen, 2005, pp. 214–222). It can also interact with multiple desired targets to produce a wide range of end products (Thomas et al, 2008, pp. 18–31).

NO has its other derivatives, including nitrosyl cation (NO^+), nitrosyl anion (NO^-), and peroxynitrite ($ONOO^-$), which belong to reactive nitrogen species (RNS)that are distinguished by their high chemical reactivity owing to their unpaired electrons. RNS with reactive oxygen species (ROS) together have the potential to destroy cellular structures, and their uncontrolled production results in a phenomenon similar to oxidative stress (Król and Kepinska, 2021, p. 56; Tuteja et al, 2004, pp. 227–237).

2.4. Nitric Oxide (NO) Signaling Mechanisms

2.4.1. Guanylate cyclase activation

NO activates soluble guanylate cyclase (GC) (*i.e.*, guanyl cyclase or guanylyl cyclase) by binding to its heme group producing 3′-5′-cyclic guanosine monophosphate (cGMP or cyclic GMP) from guanosine 5′-triphosphate (GTP) (Levine, Punihaole and Levine T, 2012, pp. 55–68). cGMP is a crucial intracellular signaling molecule that controls a wide range of physiological and pathophysiological mechanisms in various tissues (Ivanova and Hemmersbach, 2020, p. 1139). Once cGMP is produced, it can have a wide range of effects in cells, which of most are governed by the activation of protein kinase G (PKG). In the NO/cGMP/PKG signaling pathway, NO as the "first messenger" triggers a cascade of phosphorylation reactions, in which the level of each step is enzymatically amplified. This process is critical for the biological mechanisms like blood vessel relaxation (vasodilation), activating several transcription factors which can lead to changes in gene expression, inhibition of platelet aggregation, and improvement in cognitive functions (Francis,Busch, and Corbin, 2010, pp. 525 LP – 563; Russwurm and Koesling, 2004, pp. 4443–4450).

- **Smooth muscle relaxation:** The relaxation of smooth muscle through the NO sGC-cGMP pathway is a historical and vital function of NO. Following the discovery of Endothelium derived relaxing factor (EDRF) by Robert Furchgott in 1980, NO has been studied as a signaling molecule (Moncada and Higgs, 2006, pp. S193–S201; Martin, 2009, pp.633–637). Furchgott demonstrated endothelial cells' capacity to produce substance that caused the vascular segment's relaxation of the underlying smooth muscle (Moncada and Higgs, 2006, pp. S193–S201; Martin, 2009, pp.633–637). Later, Ignarro, and Murad performed some experiments to see if EDRF produced from the artery might activate sGC and thus accounts for increased cGMP in response to ACh or bradykinin (Nava and Llorens, 2016, pp. 125–145; Ignarro et al, 1986, pp. 893 – 900). EDRF activation of sGC, such as NO activation, was heme dependent. EDRF was NO discovered in 1988 (Garthwaite, Charles and Chess-Williams, 1988, pp. 385–388; Priviero and Webb, 2010, pp. 229–233). The binding of the 1st messengers initiates vasodilation signaling (Félétou, 2011). This binding activates the inositol triphosphate (IP3) mechanism, in which IP3 binds to Ca_2^+ channels in the endoplasmic reticulum, causing Ca_2^+ ions to be released into the cytosol (Foskett et al, 2007, pp. 593–658). This event causes the Ca_2^+/calmodulin complex to bind to the NOS, initiating NO synthesis from L-arginine to L-citrulline.

The NO then passes via the cell membrane to its sGC receptor in the smooth muscle cells surrounding the artery. The sGC involves cGMP formation from GTP, resulting in the activation of cGMP-dependent protein kinases (PKG) in smooth muscle cells. Phosphodiesterase 5 (PDE-5) is an enzyme that controls intracellular cGMP levels by catalyzing the hydrolytic cleavage 3′ phosphodiester bond of the cyclic nucleotide. PKG promotes Ca_2^+ reuptake and opening of the KCa channels in the smooth muscle membrane (Friebe, Sandner and Schmidtko, 2020, pp. 287–302). The decrease in Ca_2^+ concentration in the cytoplasm indicates that the myosin light-chain kinase will no longer phosphorylate the myosin molecule, blocking the cross-bridge cycle and causing smooth muscle cell relaxation (Webb, 2003, pp. 201–206).

Abnormality of the NO-cGMP signaling pathway in arteries has been linked to cardiovascular disorders, such as systemic arterial and pulmonary hypertension (PAH), coronary artery disease, peripheral vascular disease, and atherosclerosis (Bork and Nikolaev, 2018, p. 801). Pulmonary hypertension (PH) is a type of high blood pressure in the lung vasculature caused by thinning of blood vessels related to and within the lungs (Bazan and Fares, 2015, pp. 11–1221). Fibrosis, another disorder, is a mechanism in which affected blood vessels stiffen and thicken (Harvey et al., 2016, pp. 659–668).

The rise in the heart's activity induces right ventricular hypertrophy, reducing the heart's ability to pump blood toward the lungs (Ryan and Archer, 2014, pp. 176–188). One more case PAH pathology, which is caused by pulmonary endothelial cell dysfunction. It is characterized by dysfunction of multiple signaling pathways like reduced NO synthesis, prostacyclin production, and higher concentrations of endothelin-1, thromboxane A2, and serotonin (Lai et al, 2014, pp. 115–130; Rose-Jones and Mclaughlin, 2015, pp. 73–79; Morrell et al, 2009, pp. S20–S31). O_2^- may also react with NO to produce $ONOO^-$, which oxidizes and uncouples eNOS, affecting NO synthesis and inducing uncoupled eNOS to produce reactive oxygen species (Förstermann and Li, 2011, pp. 213–223). Consequently, oxidative stress causes sGC heme group oxidation, making it low receptive to NO and cause heme separation from sGC (Shah et al, 2018, pp. 97–104). ROS also plays a role in acute inflammation, where vascular abnormalities occur as the result of a multistep phenomenon (Yang et al, 2017, p. 600).

- **Platelet aggregation:** Platelets are circulating sentinels of vascular integrity which are stimulated, inhibited, or controlled by a wide range of hormones, vasoactive substances, and drugs (Jurk and Walter, 2019, pp. 140–151). The NO/sGC/cGMP pathway functions in platelet activation have been studied for more than three decades (Gambaryan, Friebe, and Walter, 2012, pp. 5335–5336).

There are two principal controversies about the NO-cGMP pathway's involvement in platelets: (1) if the NO-cGMP pathway plays a stimulatory, inhibitory, or both role during platelet activation; and (2) if the inhibitory impact of NO donors on platelet function is cGMP-dependent or not (Makhoul et al, 2018, pp.71–80). The amounts of free cytosolic cAMP and cGMP are regulated by their synthesis via adenylate cyclase (AC) and sGC (Bassil and Anand-Srivastava, 2007, pp. 99–108).

The normal endothelial cells produce NO, endothelial-ADPase, and PGI_2, which inhibit platelet activation, where endothelial-ADPase lowers the platelet activator ADP. Active Ca_2^+ efflux is maintained in resting platelets by a cyclic AMP-activated Ca_2^+ pump. Platelet activation status is determined by intracellular calcium concentration, which causes platelet degranulation and structural alteration. cAMP and cGMP signaling systems, cooperate to regulate the suppression or stimulation of granule liberation (Jin and Loscalzo, 2010, pp. 147–162; Smolenski, 2012, pp. 167–176; Marcus et al, 1997, pp. 1351–1360).

G-protein-coupled receptor signaling activates adenylate cyclase located in platelets. The linkage of PGI_2 from endothelial cells to its IP receptor on the platelet surface stimulates the GPCRs (Midgett et al, 2011, pp. 517–528). Platelets contain a large amount of sGC, which is stimulated by NO produced in platelets or passed via the platelet membrane from endothelium. The second messenger, cGMP, which sGC synthesizes from GTP, stimulates PKG and blocks phosphodiesterase 3 (PDE-3), the enzyme which degrades cAMP (Patra et al, 2020, pp. 738–745).

Protein kinase A (PKA), a recognized blocker of platelet aggregation, is activated by cAMP. Consequent substrate phosphorylation induces the inhibition of small G-proteins from the Ras and Rho families, the inhibition of Ca_2^+ produced from intracellular reserves, and the modification of actin cytoskeleton dynamics (Robichaux and Cheng, 2018, pp. 919–1053; Robinson-White and Stratakis, 2002, pp. 256–270). In addition, phosphodiesterases degrade both cAMP and cGMP, which can reduce signaling to particular subcellular compartments (Stangherlin and Zaccolo, 2012, pp. H379–H390).

The extreme level of junction between stimulating and cAMP/cGMP-dependent inhibitory signaling pathways at all stages, like cAMP/cGMP biosynthesis and decomposing, and PKA/PKG-mediated substrate phosphorylation, is a developing principle of cyclic nucleotide signaling in platelets. As a result, abnormalities in the cAMP/cGMP pathways may lead to platelet hyperactivity in cardiovascular diseases (Nagy and Smolenski, 2018, pp. 558–571).

- **Cell cycle:** NO has been proposed as a physiological cell proliferation regulator, capable of causing the downregulation in the majority of cases (Villalobo, 2006, pp. 307–316; Napoli et al, 2013, pp. 89–95). The direct association of NO-sensitive GC with chromosomes during mitosis is a process involved in cell cycle regulation.

Furthermore, via class II histone deacetylases, NO has been shown to modulate chromatin folding in human endothelial cells (Napoli et al, 2013, pp. 89–95).

NO appears to be anti-apoptotic at low concentrations, in part by inhibiting caspase activity through nitrosation. In contrast, at greater level, it cannot directly stimulate caspases, where caspase-9 can be modified by nitrosylation (Parrish, Freel, and Kornbluth, 2013, p. a008672). In the presence of an excess of NO or peroxynitrite, the NO-cGMP apoptotic signaling is activated, resulting in the initiation of cytotoxicity toward cancerous cells and adjacent tissues through Cyt c production from mitochondria, p53 accretion, and JNK/SAPK stimulation (Ha et al, 2003, pp. 1036–1047).

Apoptosis can be prevented by inhibiting sGC with 1H- [1, 2, 4] oxadiazolo [4,3, -a] quinoxalin-1-one (ODQ) or the cGMP-PKG inhibitor KT5822 (Sirotkin et al, 2000, pp. 1–9; Feelisch et al, 1999, pp. 243-53). Moreover, in undisturbed neurons (NG108-15 and N1E-115 cells), inhibition of sGC and reduction of basal cGMP levels induce apoptosis. The cGMP/PKG pathway plays a vital role in preventing the stimulation of a proapoptotic mechanism, consequently promoting neural cell survival (Fiscus, 2002, pp. 175–190).

2.4.2. S-Nitrosylation as a post-translational modification

The covalent modification of protein cysteine thiols by NO to form S-Nitrosothiols at a physiological pH range is defined as S-Nitrosylation, suggested as a signaling pathway for NO that modulates cGMP-independent effects (Fulton, 2016, pp. 29–64). A variety of mechanisms are regulated by S-Nitrosylation, comprising transcription, DNA impairment repair, cellular growth/differentiation, and apoptosis.

There are 4 different types of S-Nitrosylation reactions:

- When NO reacts with oxygen (O_2), it produces a series of nitrogen oxides. Nitrite and nitrosothiol are formed when N_2O_3 interacts with a protein thiol (Fernando et al, 2019, p. 404).
- NO reacts with O_2 producing NO_2, which then combines with a thiol to form a thiol radical and nitrite. NO is then reacted with a thiol radical to form nitrosothiol (Fernando et al, 2019, p. 404).
- When NO encounters a thiol radical, it immediately reacts with the radical to form nitrosothiol (Fernando et al, 2019, p. 404).
- Nitrosonium (NO^+) is formed when a transition metal oxidizes NO. Nitrosonium after that reacted with a thiol nearby the catalytic center producing nitrosothiol (Fernando et al, 2019, p. 404).

2.4.3. Mitogen-activated protein kinases (MAPKs)

Mitogen-activated protein kinases (MAPKs) are a type of serine/threonine kinases that are activated quickly in response to growth factor stimulation (Barman, 2005, pp. 325–335). MAPKs control critical cellular processes like proliferation, stress tolerance, apoptosis, and immune response defense (Soares-Silva et al, 2016, p. 183), and can be detected in the cytoplasm and nucleolus of different cell types (Yong et al, 2005, pp. 1–9). Different MAPKs, such as extracellular signal-regulated kinase (ERK), c-Jun amino-terminal kinase (JNK)/stress-activated protein kinase, and p38 MAPK, have been detected in mammalian cells. In addition, the intracellular production of peroxynitrite ($ONOO^-$) from the reaction of NO with superoxide (O_2^-) causes the activation of

MAPKs (Nabeyrat et al, 2003, pp. L1112-L1120; Pacher, Beckman and Liaudet, 2007, pp. 315–424). MAPK plays a pivotal role in cardiac myocyte hypertrophy that is mediated by a variety of factors, and NO clearly inhibits that pathway (Yong et al, 2005, pp. 1–9). Both NO and MAPK signal pathways are tightly correlated to immune system functions, and it is well recognized that heavy metals, such as mercury, can seriously damage mammalian immunity. Mercury prevents NO synthesis by inhibiting the NF-kappa B pathway and controls cytokine expression by activating the p38 MAPK pathway in macrophage cells (Kim, Johnson and Sharma, 2002, pp. 67–74).

3. NITRIC OXIDE SYNTHASE

3.1. Historical Introduction

NOS was first discovered and described by Knowles in 1989; they reported that the NADPH-dependent formation of NO and citrulline from L-arginine was catalyzed by a soluble enzyme derived from the rat forebrain (Knowles et al, 1989, pp. 5159 LP – 5162). Between 1991 and 1994, the three main types of NOSs were cloned and isolated. In 1998 and 1999, the first X-ray crystal structures of NOS subdomains were exhibited and documented. (Alderton, Cooper and Knowles, 2001, pp. 593–615). NOSs are responsible for the enzymatic formation of NO (Luiking, Engelen, and Deutz, 2010, pp. 97–104). The NOS is the primary source of NO in humans and mammals (Li et al, 2014, p. 5272).

3.2. NOS Isoforms

To comprehend the importance and function of NO, it must first become acquainted with the enzyme responsible for its production and the structural differences between enzyme isoforms. NOS is a homodimer multidomain enzyme and has two constitutively expressed and Ca_2^+-dependent isoforms, nNOS [neuronal NOS, NOS1, NOS I] and eNOS [endothelial NOS, NOS3, NOS III], as well as an inducible and Ca_2^+-independent isoform (iNOS, NOS2, NOS II) (Oliveira et al, 2013, pp. 1537–1551; Tejero et al, 2019, pp. 7904–7916). As a result of its expression in neurons and the brain, NOS1 is recognized as nNOS. Since its expression can be triggered by cellular activation, NOS2 is known as iNOS, and for its association with the endothelium, NOS3 is also identified as eNOS. NOSs are expressed in wide cell types despite their names, frequently with an overlapping distribution. (Mattila and Thomas, 2014, p. 478). The 3 NOS isoforms have been classified in mammals, sharing 50–60% sequence identity with the tremendous variability in the amino-terminal despite ~ 400 million years of evolution. Besides that, NOS isoforms are very conserved between species, and homology for a given isoform

may range from 85 to 92% (Fedorov et al, 2004, pp. 5892 LP – 5897; Pradhan, Bertels and Akerman, 2018, pp. 391–401; Gantner, LaFond and Bonini, 2020, p. 101550).

The principal sequence difference between mammalian constitutive isoforms (cNOSs) and iNOSs is a sequence insertion found only in cNOSs and serving as an autoinhibitory control feature (Ghosh and Salerno, 2003, p. 193). The structure of the 3 enzymes is identical, each one containing a reductase and an oxygenase domain (Alderton, Cooper and Knowles, 2001, pp. 593–615). Calmodulin (CaM) binding was discovered to be necessary for all isoforms of NOS activity and is regulated by intracellular calcium (Ca^{2+}) levels. The Ca^{2+} requirement varies between the three isoforms. nNOS and eNOS need higher intracellular Ca^{2+} concentrations for function, while CaM is thought to be very closely bound to the iNOS enzyme, requiring only low levels of Ca^{2+} for activation (Schmidt et al, 1992, pp. 427–434) (**Table 3.1**).

Table 3.1 The main binding site residues in hNOSs (Curtin et al, 2015, pp. 2558–2579).

iNOS	eNOS	nNOS
Methionine 120	Valine 104	Methionine 341
Threonine 121	Phenylalanine 105	Histidine 342
Alanine 262	Serine 246	Serine 482
Glutamine 263	Glutamine 247	Glutamine 483
Arginine 266	Arginine 250	Arginine 486
Valine 352	Valine 336	Valine 572
Phenylalanine 369	Phenylalanine 353	Phenylalanine 589
Asparagine 370	Serine 354	Serine 590
Glycine G371	Glycine 355	Glycine 591
Tryptophan 372	Tryptophan 356	Tryptophan 592
Tyrosine 373	Tyrosine 357	Tyrosine 593
Glutamic acid 377	Glutamic acid 361	Glutamic acid 597
Aspartic acid 382	Asparagine 366	Aspartic acid 602
Tyrosine 491	Tyrosine 475	Tyrosine 711

The heNOS structure shows residues Lys67–Trp480, matching to residues Lys69–Trp482 in beNOS. In addition, the frequently disarranged loop area (Arg109–Pro120) in bovine eNOS also is absent in heNOS (Arg107–Pro118) (Li et al, 2014, p. 5272) (**Table 3.2**). Both iNOS and nNOS are cytosolic enzymes, but eNOS is membranaire (Raman et al, 1998, pp. 939–950).

Table 3.2 Sequence variation beyond the heme active site in a binding pocket (Li et al, 2014, p. 5272).

Rat nNOS	hnNOS	beNOS	heNOS	miNOS	hiNOS
Met336	Met341	Val106	Val104	Met114	Met120
Leu337	His342	Leu107	Phe105	Asn115	Thr121
Tyr706	Tyr711	Tyr477	Tyr475	Tyr485	Tyr491
Trp306(B)	Trp311(B)	Trp76(B)	Trp74(B)	Trp84(B)	Trp90(B)

3.3. Molecular Genetics of NOS

Marsden and his collaborators separated genomic clones encoding heNOS and defined the gene's structural arrangement. Identification of the eNOS gene's 5-prime-flanking region showed that it lacks TATA and has proximal promoter elements linked with a constitutively expressed gene, specifically, SP1 and GATA motifs. (Marsden et al, 1993, pp.17478–17488). Later, Janssens and collaborators separated a cDNA encoding a human vascular NO. The human protein was 1294 AA long and had 52% of its AA sequence with brain NOS in common. According to the researchers, the cDNA encodes a Ca_2^+-regulated, constitutively expressed eNOS able to generat EDRF in the vessels (Janssens et al, 1992, pp. 14519–14522). Marsden et al. also cloned and sequenced heNOS. Their cDNA clones estimated a 1203 AA with approximately 60% identity to the rat brain NOS isoform and 94% identity with the bovine endothelial protein. NOS has been divided into two groups: (i) a constitutively expressed, Ca_2^+-regulated category found in the brain, neutrophils, and endothelial cells, and (ii) Ca_2^+-independent class found in endotoxin or cytokine-istimulated macrophages and endothelial cells. (Marsden et al, 1992, pp. 287–293).

hnNOS gene is found on chromosome 12q24.26 and contains 29 exons and extends over 100 kb. Moreover, heNOS gene is located on chromosome 7q35-7q36 and comprises 26 exons over a span of 21 kb. The 37 kb gene coding for hiNOS is situated on chromosome 17cen-q11.2 and contains 26 exons as well (Wang and Marsden, 1995, pp. 71–90).

3.4. Structure of NOS

NOS is a homodimeric enzyme composed of many domains (modules) comprising of an N-terminal oxygenase domain (NOSox), where NO is produced, contains iron protoporphyrin IX (heme) and tetrahydrobiopterin (BH4), and binds L-arg and a C-terminal reductase domain that has binding sites for two-electron carriers flavin adenine dinucleotide (FAD) and flavin mononucleotide (FMN), also nicotinamide adenine dinucleotide phosphate(NADPH) which serves as the electron source (Venema et al, 1997, pp. 1276–1282; Fedorov et al, 2004, pp. 5892 LP – 5897; Sharma and Patel, 2017, pp.11–22; Gantner, LaFond and Bonini, 2020, p. 101550). Linked by a flexible hinge (R-Hinge) localized between the two flavin sites that regulate enzymatic activity is a site of diversity between NOS family members. (Astashkin et al, 2019, pp. 7075–7086; Gantner, LaFond and Bonini, 2020, p. 101550).

Another regulatory domain is the oxygenase-reductase hinge (OR-Hinge), governing the transfer of electrons from the NOSred domain to the NOSox domain. Such transfer is facilitated by structural modifications caused by the Ca_2^{+-}dependent adaptor calmodulin (CaM) binding. Cam binding has been found to be essential for the activity of all NOS isoforms and is controlled by intracellular calcium rates (Piazza, Guillemette and Dieckmann, 2015, pp. 1989–2000; Gantner, LaFond and Bonini, 2020, p. 101550). The last monitoring domain is the PSD/Disc-Large/ZO-1 (PDZ), which alters the enzyme's subcellular position through protein-protein interactions; as a result, the obtainability of substrates and accessibility to NO's targets (Gantner, LaFond and Bonini, 2020, p. 101550).

3.4.1. The oxygenase domain

NOSox has a single heme domain with a heme-porphyrin catalytic center, a structural zinc tetrathiolate (ZnS_4) motif, and the BH4 cofactor. The geometry of the binding pocket is strongly conserved between NOS isoforms and mammalian species (Li et al, 2014, p. 5272; Bignon et al, 2019, pp. 415–429). Heme is axially coordinated to a cysteine thiolate (Cys420 in nNOS); the porphyrin is the binding site for the dioxygen molecule necessary for L-arginine oxidation (Li and Poulos, 2005, pp. 293–305; Bignon et al, 2019, pp. 415–429). The binding of NOS with heat shock protein 90 (hsp90), the structural modifications that allows heme availability to its binding cleft in the protein while endorsing NOS dimerization as well, can favor heme enclosure within the NOSox domain (Sarkar et al, 2015, pp. 21615–21628; Ghosh, Chawla-Sarkar and Stuehr, 2011, pp. 2049–2060; Bignon et al, 2019, pp. 415–429).

Studies have revealed that a conserved glutamate residue (Glu597 in nNOS) is crucial in substrate binding (Bignon et al, 2019, pp. 415–429). The pterin redox cofactor links nearby the binding site via attachment with the heme propionate groups, yet this mechanism is supposed to facilitate L-Arg adhesion. This network effectively promotes the preservation of the NOSox dimer interface and L-Arg binding to NOS (Chartier and Couture, 2004; Bignon et al, 2019, pp. 415–429).

Nearby the active site, conserved aromatic residues form assembling binding with the porphyrin moiety (Trp414 and Phe589 in nNOS) and the pterin cofactor (Trp683 in nNOS), which is implicated in a vast hydrogen-bond network. It has been suggested that an essential tryptophan residue located at the back of the heme pocket (Trp592 in nNOS) transports the electron from the FMN cofactor to heme (Monni et al, 2015, pp. 5602–5606; Bignon et al, 2019, pp. 415–429). The ZnS_4 motif is another component that causes dimerization. The zinc ion is tetra-coordinated with two thiolates (Cys331 and Cys336 in nNOS) from each monomer, which helps to preserve NOS architecture by connecting the two NOSox domains. The lack of this cation, or the adjustment of one of the coordinated cysteines, severely disrupts the dimer, decreasing NOS catalytic activity (Chreifi et al,2014; Bignon et al, 2019, pp. 415–429).

3.4.2. The reductase domain

The NOS reductase (NOSred) domain is divided into 3 subdomains: NADPH, FAD, and FMN, which individually bind to a different cofactor for electron transfer (Feng et al, 2014, pp. 130–140). CPR has 60% sequence homology with NOSred and catalyzes the similar electron transfer from NADPH to the P450 reactive region. The NADPH and FAD domains involve in creating the 'FNR-like' unit, while the single FMN component is thought to be behaving as an electron shuttle toward the heme center, similar to CPR. A helix hinge segment binds the FMN and FAD subdomains, ensuring that the two flavins are appropriately aligned to facilitate electron transfer. The electron is transferred from NADPH to FAD and then to the FMN. Once activated, the FMN domain produces large-scale motions for docking on the NOSox domain and inhibits electron transfer to the heme center. This mechanism is caused by calmodulin binding and happens in trans (from one monomer's reductase domain to the other monomer's NOSox) (Bignon et al, 2019, pp. 415–429; Wang et al, 1997, pp. 8411–8416; Gachhui et al, 1996, pp. 20594–20602). Examining the FMN/FAD domain interface showed significant hydrophobic interactions and salt bridges, particularly between the Glu816 and Arg1229 residues, preserved in cNOSs. It has been proposed that Arg1400, which is found in both nNOS and eNOS (Arg1165), plays a significant role in the selective binding of NADPH and the lodging of FMN in its electron-acceptor state in the lack of calmodulin. Phe1395, a FAD-shielding residue, is suggested to be important in inhibiting electron transfer in the calmodulin-free form by serving as an aromatic barrier between NADPH and FAD (**Figure 3.1**) (Bignon et al, 2019, pp. 415–429; Wang et al, 1997, pp. 8411–8416; Gachhui et al, 1996, pp. 20594–20602).
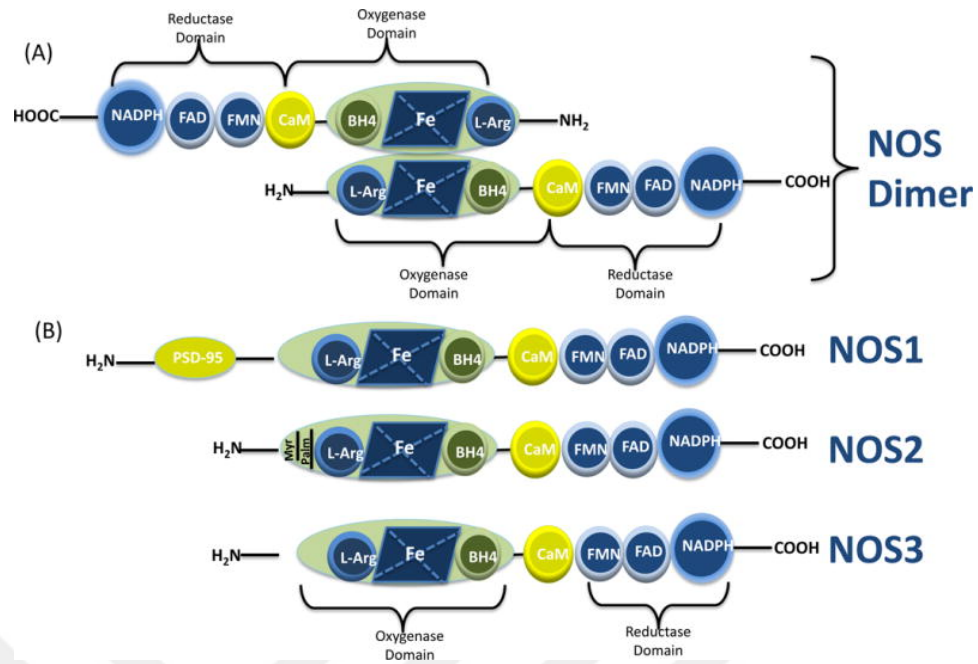
Figure 3.1 (A) Molecular structure of NOS dimer. (B) Protein structure of NOS isoforms, where PSD95 is postsynaptic density protein (Sharma and Patel, 2017, pp.11–22).

3.5. Tissue Specificity and Cellular Distribution of NOS Isoforms

The effects of NO in biological systems are determined by its steady-state level and the location where it is generated. Therefore, the organ in which NO is made is essential, and the types of cells that contribute to NO formation appear to be a primary factor in its impact. NOS2 has recently been shown to be fundamentally expressed in neurons, kidney, liver, lung, colon, and keratinocytes, while NOS3 may be expressed at a higher concentration than the constitutive one in different situations, like physical activities, estrogen activation, hyperthermia (Villanueva and Giulivi, 2010, pp. 307–316) (**Table 3.3**).

Table 3.3 Recapitulate mammalian NOS isoform's properties (Ignarro, 2000; Bivalacqua, Champion and Hellstrom, 2002, pp. 345–352; Taylor, Alarcon and Billiar, 1998, pp. 766–781; Alderton, Cooper and Knowles, 2001, pp. 593–615; Geller and Billiar, 1998).

Structural and enzymatic parameters	nNOS (NOS 1, NOS I)	eNOS (NOS 3, NOS III)	iNOS (NOS 2, NOS II)
Subunit molecular mass	160 kDa 1433 aa	135 kDa 1153 aa	125–130 kDa 1203 aa
Gene structure and size	29 exons, 28 introns, complex structural organization, locus over a region of >200 kbp	26 exons, 25 introns, 21–22 kbp	26 exons, 25 introns, 37 kbp
cDNA size	10.0 kb	4.4 kb	4.1 kb
Inducibility	Constitutive	Constitutive	Inducible
Calmodulin binding	$\sim$30 * 10^{-9} M	$\sim$30 * 10^{-9} M	Subunit-like (>> 30* 10^{-9} M)
Cofactors	H4B, FAD, FMN, heme, Zn	H4B, FAD, FMN, heme, Zn	H4B, FAD, FMN, heme, Zn
Substrates	NADPH, L-Arg, O_2	NADPH, L-Arg, O_2	NADPH, L-Arg, O_2
Protein variants	µ,a,ß,d tissue-specific isoforms	-	-
Posttranslational modifications	Specific phosphorylation sites present	Myristoylation, palmitoylation, phosphorylation sites present	Specific phosphorylation site present
Sources of superoxide formation	Heme domain, reductase domain	Mainly heme domain	Mainly reductase domain
Protein-protein	PSD-95, caveolin3, phosphofructokinas	Caveolin1, HSP 90, CAT-2,	-

interactions	e M	bradykinin receptor	
Major physiological function	Neurotransmission	Vasodilatation	Cytotoxicity
Role in disease	Stroke Muscular dystrophy Ischemia reperfusion injury	Endothelial dysfunction hypercholesterolemia hypertension	Toxic shock inflammation autoimmune disease
Chromosome	12q24.2–12q24.3 of chromosome 12	7q35–7q36 of chromosome 7	17cen–q11.2 of chromosome 17
NO production	Low (pM)	Low (pM)	High (mM)
Regulation	Ca^{2+}/calmodulin	Ca^{2+}/calmodulin	Gene transcription
Stimuli	acetylcholine; bradykinin; ATP; ADM; proliferation; shear stress	neuro-excitatory amino acids; estrogens	IL-1; TNF-a; NF-kB; IFN; endotoxin; injury

3.6. NOS Reactivity

The NOS enzyme is active to produce NO only as a dimer (Feng et al, 2014, pp. 130–140). The urea dissociation studies show that the absolute dimer potencies are respectively: NOSIIIoxy ≫ NOSIoxy > NOSIIoxy (endothelial NOSoxy (eNOSoxy) ≫ neuronal NOSOXY (nNOSoxy) > inducible NOSoxy (iNOSoxy)) (Panda et al, 2002, pp. 31020–31030). The L-Arg, is converted to NO and citrulline by 2 consecutive monooxygenation interactions. The intermediate, N^{ω}-hydroxy-L-arginine (NOHA), Throughout the enzymatic turnover, it remains associated at the active site, albeit dissociation and following NOHA build-up have been reported in some scenarios. (Daff, 2010, pp.1–11). L-Arg is transported inside the cells by a cationic amino acid transporter (CAT) (Prado, Martins and Tibério, 2011, p. 832560) (**Figure 3.2**).

L-Arg + 1.5 NADPH + 1.5 H$^+$ + 2 O$_2$ → 1.5 NADP$^+$ + Citrulline + NO + 1.5 H$_2$O (3.1)

(Feng et al, 2014, pp. 130–140).

Figure 3.2 NO synthesis from L-arginine (Daff, 2010, pp.1–11).

The biochemical reaction is started in the NOSred domain. A functional NOS transfers electron from NADPH to heme in the amino-terminal oxygenase domain through the flavin FAD and FMN in the carboxy-terminal reductase domain (Förstermann and Sessa, 2012, pp. 829–837).

NADPH is transformed NADP$^+$. This liberates electrons to reduce FAD, which later passes electrons to FMN. Even though NOS monomers have NOSox and redu domains, they do not transfer electrons within the same protein chain. However, as a dimer, this transition happens successfully when the FMN group of one monomer passes electrons to the heme group in the NOSox domain of the other monomer, known as the trans phenomenon. This transition is a rate-limiting step in the reaction and targets extreme regulation of enzymatic activities of NOS family members. CaM binding to the linker domain induces significant modifications in the accessibility of the FMN domain, allowing electron transfer to the heme group (Bignon et al, 2019, pp. 415–429; Gantner, LaFond and Bonini, 2020, p. 101550).

NOS's NOSred domain is analogous to the NADPH-dependent diflavin NOSred enzyme, which supplies electrons to cyt P450 enzyme domains. The oxygenase domain is where NO is formed since the heme-BH4 groups accept electrons and transfer them to molecular oxygen, which then oxidizes L-Arg to NOHA. NOHA is then oxygenated again by transforming it to L-citrulline, releasing NO, and completing the reaction (Gantner, LaFond and Bonini, 2020, p. 101550; Tejero and Stuehr, 2013, pp. 358–365).

4. NEURONAL NITRIC OXIDE SYNTHASE

4.1. nNOS Molecular Structure

Neuronal nitric oxide synthase (also known as Constitutive NOS; IHPS1; N-NOS; NC-NOS; Neuronal NOS; nitric oxide synthase 1; nitric oxide synthase 1 (neuronal); Nitric oxide synthase, brain; nNOS; NOS; NOS type I; NOS1; Peptidyl-cysteine S-nitrosylase NOS1) (Mattila and Thomas, 2014, p. 478; Costa et al, 2016, p. 206) is a constitutive enzyme (Sánchez-Ruiloba et al, 2014, p. e95191) that composed of 1434 amino acids, and has an estimated molecular weight of 160.8 kDa. nNOS is the principal NO source in the central nervous system (Freudenberg, Alttoa and Reif, 2015, pp. 46–63). nNOS monomer has a bidomain structure with an oxygenase domain (N-terminal) extended PSD/Discs-large/ZO-1 homologous (PDZ) domain (Mungrue and Bredt, 2004), by which it can interact with other proteins containing PDZ domains (Freudenberg, Alttoa and Reif, 2015, pp. 46–63; Zhou and Zhu, 2009, pp. 223–230), and a reductase domain (C-terminal) which are separated by a calmodulin-binding motif (Zhou and Zhu, 2009, pp. 223–230). nNOS is calmodulin-regulated (Gerber and de Montellano, 1995, pp. 17791–17796). CaM activates nNOS reversibly in a Ca^{2+}dependent manner. The N-terminal NOSox domain comprises heme and tetrahydrobiopterin cofactors, L-Arg binding site, and C-terminal diflavin reductase domain with the NADPH binding sites and the cofactors FAD and FMN (Sobolewska-Stawiarz et al, 2014, pp. 11725–117). Furthermore, the binding site of Zn facilitates nNOS dimerization (Delker et al, 2010, pp. 10803–10810) (**Figure 4.1**).

In 2002, the crystal structure of nNOS became accessible (Mukherjee et al, 2014, pp. 6814–6838). Brain nNOS is present in cells in particulate and soluble forms, and its distinct subcellular distribution can lead to its different functions (Förstermann and Sessa, 2012, pp. 829–837).
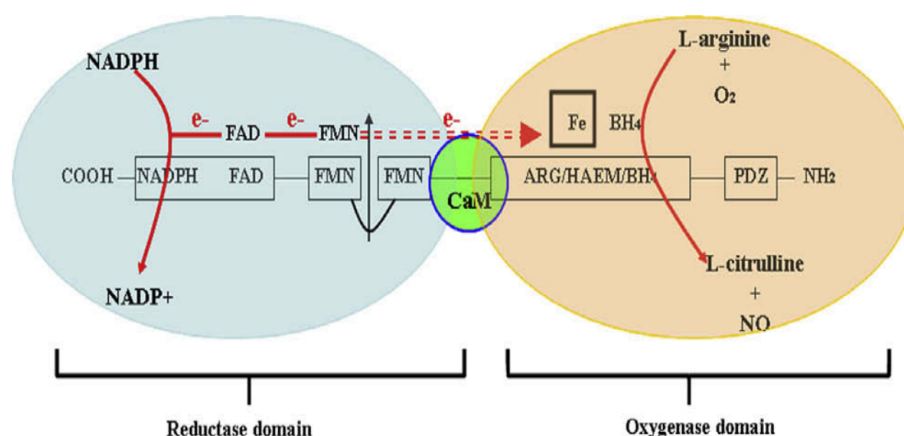
Figure 4.1 nNOS structure and NO formation (Zhou and Zhu, 2009, pp. 223–230).

4.2. The Active Site of Human nNOS

The two isoform-specific residues, Met341 and Asp602 in human nNOS are conserved; His342 is located in the hydrophobic pocket, which might be critical for inhibitor binding (Li et al, 2014, pp.2667–2674) in addition to Met336 and Tyr706 (Li et al, 2014, pp.2667–2674). According to Li and his colleagues, Asp597 residue, as an important active site, mainly maintains selectivity (Li et al, 2018; Li et al, 2014, pp.2667–2674). Olsbu and his group suggest that Val567 has a crucial function in maintaining the dependability of the active site for substrate binding, stability of heme-bound gaseous ligands, and possible NO generation (Olsbu et al, 2018, pp. 1553–1566).

4.3. Gene Expression of nNOS

nNOS gene (NOS1) was the first cloned and characterized human NOS gene (Jeffrey Man, Tsui and Marsden, 2014, pp. 161–192). It is located on chromosome 12q24.2 (Kishimoto et al, 1992, pp. 802–804; Reif et al, 2006, pp. 286–300; Wang, Newton and Marsden, 1999, pp. 21–43; Freudenberg, Alttoa and Reif, 2015, pp. 46–63; González-Castro et al, 2019, pp. 967–977) and spreads over an area up to 200 kb in human genomic DNA and comprises 4299 nucleotides which encode for 1434 amino acids (Costa et al, 2016, p. 206); it consists of 28 coding exons (Freudenberg, Alttoa and Reif, 2015, pp. 46–63).

The nNOS gene produces various mRNA transcripts via mechanisms, such as alternative promoter use, alternative splicing, cassette insertions/deletions, changing sites for 3-untranslated region cleavage, polyadenylation, and allelic diversity in mRNA structure (Panda et al, 2003, pp. 37122–37131; Wang, Newton and Marsden, 1999, pp. 21–43); 130 kb 'variable region' with 12 alternative first exons besides the unique promoters (labeled exons 1a - 1l) (Freudenberg, Alttoa and Reif, 2015, pp. 46–63) (**Figure 4.2**).

The tissue and cell-specific expressions of nNOS employ a larger variety of particular promoters and linked exon 1 variants than every human gene. The majority of basically expressed nNOS variants have low translational performance (Jeffrey Man, Tsui and Marsden, 2014, pp. 161–192).

nNOS transcripts are susceptible to various stimuli and generate diverse isoforms due to differences in transcriptional initiation, processing and translational performance, stability, and localization. Up to this point, there are five splice variants of nNOS that have been identified, nNOS α, nNOS β, nNOS γ, nNOS μ, and nNOS2 (Zhang et al, 2014, pp. 3189–3200; Balke, Zhang and Percival, 2019, pp. 35–47; Panda et al, 2003, pp. 37122–37131). That is why nNOS is one of the most complicated genes of the human genome (Freudenberg, Alttoa and Reif, 2015, pp. 46–63).
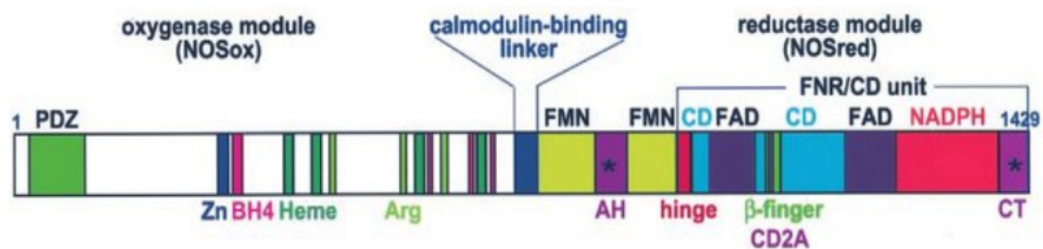
Figure 4.2 Domain organization of NOS1 (Garcin et al, 2004, pp. 37918–37927).

4.4. Localization of nNOS

Although the name of nNOS comes from the tissue (neuronal tissue) where it was first purified (Dai et al, 2013, p. 891581), it is also present in skeletal, cardiac, smooth muscle (Tengan et al, 2012), the kidney, heart, and endothelial cells (Dai et al, 2013, p. 891581). In cardiac myocytes, nNOS differs from eNOS in terms of location because nNOS is located in the sarcoplasmic reticulum (SR) and the plasma membrane (Zhang et al, 2014, pp. 3189–3200). Generally, nNOS is found in the brain expressed in immature and mature neurons (Zhou and Zhu, 2009, pp. 223–230), mainly in the cerebellum, basal ganglia, hippocampus, frontal cortex (Freudenberg, Alttoa and Reif, 2015, pp. 46–63).

The wide range of proteins with PDZ domains may connect with the PDZ domain of nNOS, which affects the subcellular distribution and (or) behavior of the enzyme in the brain and muscle (Zhou and Zhu, 2009, pp. 223–230). There are two kinds of nNOS–expressing neurons in the cortex: Type I and Type II (Perrenoud et al, 2012, p. 36). Type I, where nNOS neurons are limited, is mainly located in deeper levels and expresses nNOS at elevated amounts. In this type, various neuromodulatory inputs are obtained by nNOS neurons. Type I nNOS neurons have very wide, long-range projecting axonal arbors that place them in an advantageous position to influence the vasculature. Type II nNOS neurons, on the other hand, are a diverse group of interneurons located predominantly in deep and superficial layers of the cortex, including mechanisms that can cover many layers. (Echagarruga et al, 2020, p. e60533). Rothe and coworkers reported that neuronal nNOS immunoreactivity was primarily found in the cytosol, far from the membranes, in a patch-like mode (Zhou and Zhu, 2009, pp. 223–230).

4.5. Formation of nNOS Products

nNOS enzymatic activity involves the dimerization of two nNOS monomers based on Ca^{2+} and calmodulin-binding (Freudenberg, Alttoa and Reif, 2015, pp. 46–63). nNOS catalyzes NO's production from L-arginine in two phases: the hydroxylation of L-Arg to the intermediate NOHA, which will then be oxidized to L-citrulline and NO (Costa et al, 2016, p. 206; Zhou and Zhu, 2009, pp. 223–230). NADPH transfers electrons to FAD and FMN during the first stage, reducing molecular oxygen to superoxide (O_2^-). Simultaneously, an electron from a flavin-mononucleotide (FMNH) reduces Fe^{3+} to Fe^{2+} in the heme group. The Fe^{3+} reduction allows O_2 binding, which leads to an $O_2^- - Fe^{2+}$ complex. The electron of the complex switches between Fe^{2+} and O_2, leading to the $O_2 - Fe^{3+}$ intermediate. Likewise, this intermediate may receive an electron by forming $O_2^- - Fe^{3+}$, which produces H_2O_2 and Fe^{3+} once combined with H^+. BH4 binding to the $O_2^- - Fe^{3+}$ present in the heme group is critical for the catalysis of L-Arg (Costa et al, 2016, p. 206). nNOS proceeds the transfer of electrons to the heme and thus oxidize NADPH at a rapid frequency, while eNOS and iNOS will accomplish the same process at a much slower rate (Saravi, 2017). The nNOS enzyme is dimeric in its active form, demanding heme binding and dimer stabilization through L-arginine and BH4 binding (Dunbar et al, 2004, pp. 964 LP – 969).

In the absence of CaM, NADPH interaction is expected to lock the nNOS reductase domain into a conformation that limits the mobility of the FMN-binding domain. Electron transfer from FMN to the NOSox domain is prevented in this locked conformation, and NO production is interrupted. This "conformational lock" is believed to be mediated by Arg-1400 in the C-tail, the impacts of which are alleviated by CaM joining (Freudenberg, Alttoa and Reif, 2015, pp. 46–63).

nNOS can also generate ROS at saturating levels of L-Arg or NOHA before the formation of NO (Costa et al, 2016, p. 206). Moreover, BH4 significantly boosts H_2O_2 output at the expense of O_2 (Shimizu et al, 2003, pp. 1343–1352). In addition, there is an autoinhibitory loop that controls nNOS activity within the FMN binding domain (Zhou and Zhu, 2009, pp. 223–230).

4.6. Factors Regulating nNOS Function

nNOS is a strictly modulated enzyme controlled at the transcriptional and posttranslational levels through protein-protein interactions and modifications, such as phosphorylation, ubiquitination, and sumoylation. The enzymatic activity of nNOS is affected by the optimum substrate concentration, cofactors, and interaction with controlling proteins (Sharma and Patel,2017, pp.11–22).

4.6.1. Extrinsic factors

- **nNOS dimerization:** The active form of nNOS is the dimeric form with two strong affinity binding sites for BH4 and L-Arg (Rao, Chaudhury and Goyal, 2008, pp. G627–G634; Zhou and Zhu, 2009, pp. 223–230). The two monomers are connected by a disulfide bridge and bind a zinc ion. In addition, the dimer is maintained by the 'N-terminal hook' domain. BH4, heme, and L-Arg stabilize the dimer of nNOS (Hemmens and Mayer, 1998. pp. 1-32), where the dimerization protects nNOS from proteolysis. Low-temperature SDS-PAGE experiments indicate the dimer strength of NOSs in the order of eNOS> nNOS >iNOS (Panda et al, 2002, pp. 31020–31030). According to Okada, BH4-dependent dimer stabilization protects nNOS from PKC phosphorylation and hydrolyzed by trypsin (Okada, 1998, pp. 261–264; Zhou and Zhu, 2009, pp. 223–230).

- **Phosphorylation:** nNOS phosphorylation is crucial for enzymatic activity. PKA, CaM-kinases (CaM-KI and CaMKII), PKC, and phosphatase 1 regulate nNOS activity; nNOS is then regulated by extracellular and intracellular signals (Costa et al, 2016, p. 206; Zhou and Zhu, 2009, pp. 223–230). The dephosphorylation of nNOS boosts nNOS enzymatic activity (Rameau, Chiu and Ziff, 2003, pp.1123–1133). Ca^{2+}/calmodulin (CaM)-dependent protein kinase II (CaMKII) can phosphorylate nNOS at Ser847 that reduces NOS activity in neurons (Osuka et al, 2002, pp. 1098–1106). CaMKII binds to the C-terminal domain of the NR2B subunit near nNOS attached by PSD-95 and phosphorylates S847 of nNOS (Cao et al, 2005, pp. 117–126; Rameau et al, 2007, pp. 3445–3455). Rameau and his collaborators demonstrated that the phosphorylation of

Ser1412 by Akt is necessary for activating nNOS by the N-methyl-D-aspartate receptor (NMDAR). The C-terminal tail of nNOS possesses a potential phosphorylation site at Ser1412 (Rameau et al, 2007, pp. 3445–3455; Costa et al, 2016, p. 206).

Phosphatidylinositol-3 (PI3) kinase binds to tyrosine-phosphorylated NR2B, causing phosphoinositide phosphorylation and the recruitment and stimulation of Akt at the plasma membrane that could phosphorylate nNOS (Rameau et al, 2007, pp. 3445–3455). CaM-KI phosphorylation at Ser741 in transfected cells also induces nNOS enzymatic activity (Song et al, 2004, pp. 133–137; Zhou and Zhu, 2009, pp. 223–230) **(Figure 4.3).**
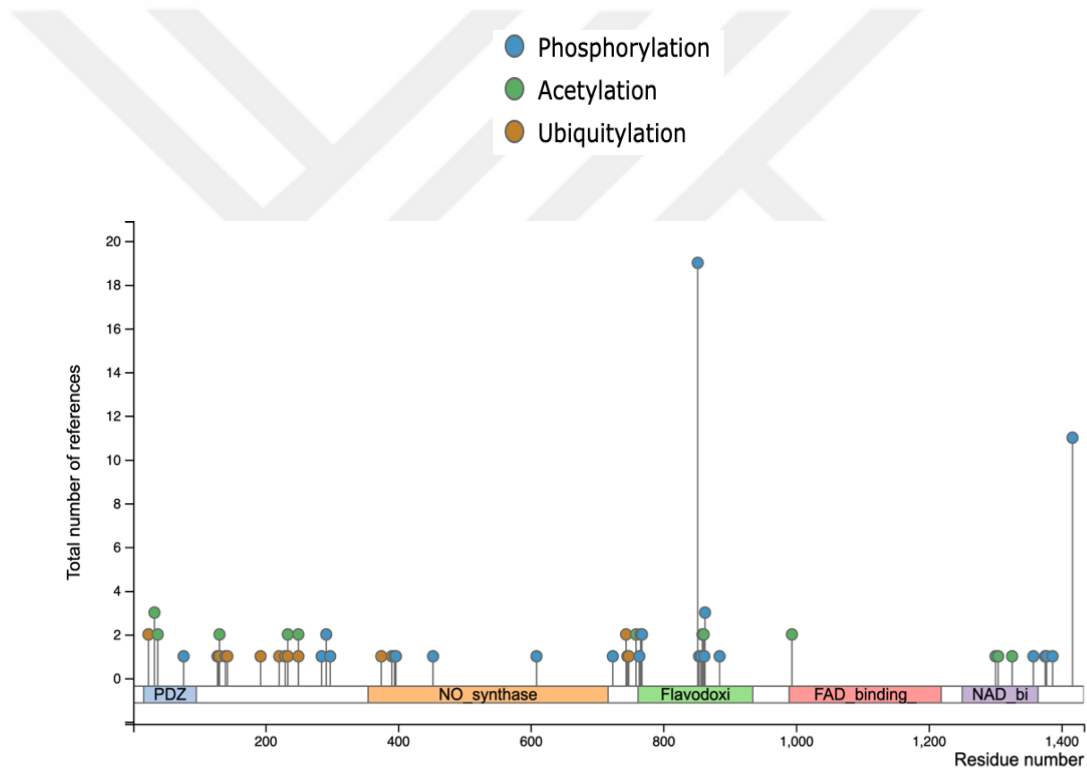
Figure 4.3 Phosphorylation, Acetylation and Ubiquitylation sites (post-translational modifications (PTM) sites) in nNOS (Hornbeck et al, 2015, pp. D512–D520).

- **Protein-Protein interactions (PPIs):** Unlike endothelial and inducible NOS, nNOS has a PDZ (PSD-95/Dlg/ZO-1) domain at its N-terminal implicated in subcellular targeting. The PDZ domain of nNOS appears to have class I, II, and III joining specificity. The PDZ domain of nNOS will bind to C-terminal sequences with acidic residues at the P-2 location with reduced micromolar binding constants, just like a real class III PDZ domain. Conjugation to C-terminal sequences with a hydrophobic residue at the P-2 position and an acidic residue at the P-3 position (class II) is also possible (Merino-Gracia et al, 2016, pp. 11581–11595; Manjunath, Ramanujam and Galande, 2018, pp.155–171).

nNOS can be attached to precise subcellular structures via mediating PPIs due to the post-synaptic density (PSD) domain. There are abundant PDZ domains in Scaffold proteins which are crucial for the organization of supramolecular signaling complexes (Gu and Zhu, 2021, pp. 1–10).

The protein carboxy-terminal PDZ ligand of nNOS (CAPON) is believed to be selectively linked with nNOS and have comparable regional distribution (Esplugues, 2002, pp. 1079–1095) that has a C-terminal PDZ domain binding to the N-terminal PDZ domain of nNOS and N-terminal phosphotyrosine binding (PTB) domain (Zhou and Zhu, 2009, pp. 223–230). CAPON controls NO formation in CNS neurons by determining the amount of nNOS connected to the plasma membrane. CAPON also binds nNOS to other macromolecules, such as the small G-protein Dexras-1 (Zhang et al, 2018, p. e12754; Fang et al, 2000, pp. 183–193). CAPON is also involved in regulating dendritic morphology, dendrite patterning, and dendritic spine growth (Zhang et al, 2018, p. e12754).

- **nNOS uncoupling:** BH4 and L-Arg are critical cofactors for nNOS. In the case of deficiency of such cofactors, nNOS enzymes remain "uncoupled," generating reactive oxygen species (ROSs) instead of NO (Landmesser et al, 2003, pp. 1201–1209; Wu et al, 2014, pp. 815–824; Costa et al, 2016, p. 206). Pressure overload-induced heart failure, hypertension, ischemia/reperfusion damage, and atrial fibrillation are exacerbated by BH4 deficiency and nNOS uncoupling. Accumulation of methylarginine and S-Glutathionylation of nNOS enhance uncoupling (Alkaitis and Crabtree, 2012, pp. 200–210; Hemmens et al, 2000, pp. 35786–35791).

- **Protein inhibitor of nNOS (PIN):** The PIN is a small molecular weight endogenous protein, dynein light chain, which inhibits nNOS by destabilizing the dimer isoform. There is a binding site at the NH_2-terminus of nNOS for PIN (Costa et al, 2016, p. 206; Lajoix et al, 2004, pp. 1467–1474). PIN has been shown to bind to a 17-residue peptide fragment of nNOS (Met-228 to His-244), thus destabilizing the dimeric structure of nNOS resulting in a catalytically inactive monomeric state. Since PIN shares similarities with the light chains of myosin and dynein, it is possible that PIN is involved in the interaction of nNOS with the neuronal cytoskeleton during axonal transport (Sharma and Patel, 2017, pp.11–22; Zhou and Zhu, 2009, pp. 223–230).

The overexpression of PIN reduces the erectile response to electrical field activation, whereas shRNA-mediated knockdown of PIN aids in the reversal of age-related ED. PIN colocalizes with nNOS in neurons and physically cooperates with nNOS, destabilizing nNOS dimers to catalytically inhibited monomers vulnerable to fragmentation (Sharma and Patel, 2017, pp.11–22; Zhou and Zhu, 2009, pp. 223–230).

4.6.2. Intrinsic factors

• **Auto-Inhibitory domain and c-terminal tail:** The sequence of 40–50 AA found in the FMN domain destabilizes CaM binding to the enzyme and inhibiting intra- and inter-module electron transferring, which cause the nNOS auto-inhibition (Costa et al, 2016, p. 206). Calmodulin appears to serve as an allosteric activator of nNOS; when CaM and Ca^{2+} are not present, electron flow from FAD to FMN decreases. At basal intracellular Ca^{2+} concentrations, nNOS is inactive. Though stimulating factors raise intracellular Ca^{2+} levels, calmodulin binds to nNOS and activates it. (Zhou and Zhu, 2009, pp. 223–230). At the C-terminus of nNOS, there is a tail sequence of 21–42 amino acids linked to enzyme inhibition (Roman et al, 2000, pp. 29225–29232). The elimination of this extension enhances electron flow transfer rates in the NOSred domain. Even though CaM is still necessary to promote electron transfer from the FMN domain to the heme for NO processing, removing the auto-inhibitory domain and C-terminal tail results in CaM-independent electron transfer via the NOSred domain (Tejero et al, 2010, pp. 27232–27240; Costa et al, 2016, p. 206).

• **Dimer stability:** The ability of the N-terminal domain to sustain dimerization is critical for the enzymatic activity of nNOS. If this domain does not properly process, the electron transport and formation of nNOS products do not occur (Panda et al, 2003, pp. 37122–37131). The cysteines are found in all recognized nNOS sequences, with the N-terminal of the dimer located about 30–35 residues from the oxygenase domain boundary. Zinc binding has an important role in dimer stabilization (Costa et al, 2016, p. 206; Hemmens et al, 2000, pp. 35786–35791).

4.7. nNOS Gene Polymorphism

At least 124 commons (Minor allele frequency (MAF) > 0.05) single nucleotide polymorphisms (SNPs) in the nNOS gene, but none in the coding regions. As a result, the existence of SNPs in the promoter region may be significant. For instance, the guanine to adenine (GàA) transition positioned in the promoter of nNOS exon 1c

(-84GàA) and a cytosinetothymine (CàT) transition identified at 276 base pairs (bp) downstream from the translation termination site (276CT; rs2682826) is associated with impaired expression of the nNOS gene. Li and his group suggested that selected functional SNPs in the nNOS genes relate to the risk of cutaneous melanoma (CM) (Li et al, 2007, pp. 1570–1578).

Few investigations have been done to date to explore the relationship between nNOS gene polymorphism and Ischemic Stroke (IS) pathogenesis (Dai et al, 2013, p. 891581). Some findings indicated that the NOS1 gene polymorphism (rs1483757, rs7308402, rs2293050, and rs2139733) was linked to IS disease (Dai et al, 2013, p. 891581).

Two polymorphisms in the promoter region of the NOS1 gene (a VNTR and rs41279104) have been linked to schizophrenia (SCZ) in addition to another SNP in intron 3 (rs3782206), and SNP (rs6490121) in intron 2 is among the most critical SNPs that showed associations with SCZ (Zhang et al, 2015, pp. 1383–1394). As a neurotransmitter for bronchodilator nonadrenergic noncholinergic (NANC) nerves, neurally derived NO that is provided by NOS1 is physiologically linked to asthma. Previous findings in Caucasian populations have linked asthma diagnosis and IgE levels to chromosome 12q14–24.2 (Grasemann et al, 2000, pp. 391–394; Martínez et al, 2007, pp. 105–113).

Several gene polymorphisms of NOS1 were identified as potential risk factors for Parkinson's disease (Huang et al, 2016, p. e4982). There is a connection between 2 single nucleotide polymorphisms (SNPs) of NOS1 and the pathology. NOS1 exon18 has been linked to Parkinson's disease in four studies (Huang et al, 2016, p. e4982).

5. nNOS IMPLICATIONS IN THE CENTRAL NERVOUS SYSTEM

5.1. Implications of the Neuronal Nitric Oxide Synthase in the Physiological Central Nervous System

NO is involved in various neurobiological processes. Such a controlling molecule has been linked to many roles in the nervous system, including the mechanism of endothelial-dependent vasodilation in neurotransmission and host-defense functions (Džoljić, Grabatinić and Kostić, 2015, pp. 159–163; Araki et al, 2020, p. 7997). In physiological conditions, NO levels vary within a narrow range of 100 pM (or below) up to 5 nM orders of magnitude (Džoljić, Grabatinić and Kostić, 2015, pp. 159–163; Hall and Garthwaite, 2009).

nNOS is found in the cytoplasm of a small subpopulation of GABA-ergic cells in the cortex and hippocampus. It is also located in a much larger excitatory neuron population, but only in the spine head. nNOS is the source of 95% of the NO in the cortex and plays a crucial role in synaptic plasticity (Hardingham, Dachtler and Fox 2013, p.190). As a free radical and a small gas molecule, NO can diffuse through membranes and serve as a second messenger in signaling pathways (Reierson et al, 2011, pp. 715–727; Džoljić, Grabatinić and Kostić, 2015, pp. 159–163). The activation of NMDA (N-methyl-d-aspartate) receptors, in particular, has been shown to raise postsynaptic NO synthesis by Ca^{2+}-calmodulin-dependent nNOS (Araki et al, 2020, p. 7997). The diffusible NO will then induce sGC, culminating in presynaptic cGMP output and neurotransmitter production (Hardingham, Dachtler and Fox 2013, p.190; Reierson et al, 2011, pp. 715–727). NO has a suppressive activity on synaptic GABA-ergic transmission. NO functions on ion channels and ion exchangers via cGMP-dependent mechanisms with an immediate impact on membrane excitability. Besides that, NO signaling influences synaptic repression in the superior paraolivary nucleus through cGMP-dependent inhibition of a potassium ion/chloride co-transporter. Since

NO serves as a stopper of inhibition intensity at the post-synaptic point, this allows for altering the information processing (Džoljić, Grabatinić and Kostić, 2015, pp. 159–163).

5.1.1. Neuroprotection process of nitric oxide

NO provides neuroprotection across a variety of processes such as (Calabrese et al, 2007, pp. 766–775):

- **Akt and CREB:** NO and Akt have survival-promoting effects and play critical roles in CNS development and plasticity. The kinase Akt and the transcription factor CREB are implicated in the NO-induced survival mechanism in cerebellar granule cells (Mejía-García et al, 2013, pp. 2424–2439; Calabrese et al, 2007, pp. 766–775). The Impact of NO on Akt and CREB is thought to be mediated by cGMP and the sequential activation of PKG, an essential intermediate in the NO-mediated stimulation of Akt and CREB (Mejía-García et al, 2013, pp. 2424–2439; Calabrese et al, 2007, pp. 766–775).

- **Neuroprotection through S-Nitrosylation*:*** In the NMDA-mediated neurotoxicity model, where persistent activation of NMDA receptors induces excitotoxic cell damage, NO provides neuroprotection by the S-nitrosylating NMDA receptors NR1 and NR2 subunits that decrease the intracellular Ca^{2+} influx causing neurodegeneration (Calabrese et al, 2007, pp. 766–775). Neurons expressing elevated amounts of NMDA receptors, for instance, for people with neurodegenerative disorders, injection of NMDA receptor agonists further into the striatum of rodents or non-human primates mimics the process of neurodegeneration have been seen in Huntington's disease (Dong, Wang and Qin, 2009, pp. 379–387).

- **Neuroprotection by the overexpression of heme oxygenase*:*** Heme oxygenase-1 (HO-1) is an enzyme with 32 kDa weight (Si and Wang, 2020, pp. 1259–1272) that degrades heme to carbon monoxide (CO), free iron II (Fe^{2+}), and biliverdin. Protecting cells against oxidative stress is essential, which may be a potential therapeutic goal for neuroprotection. Biliverdin is transformed to bilirubin by the action of biliverdin reductase (BVR), which can scavenge hydroxyl radicals, singlet oxygen, and superoxide anions and inhibit protein and lipid peroxidation, exerting a potent antioxidant, anti-apoptotic, and anti-inflammatory action. CO has anti-apoptotic and anti-inflammatory properties by influencing the sGC and MAPK mechanisms. Free iron II production

promotes the formation of a heavy chain of ferritin, which quenches free iron II and stimulates the membrane transporter Fe-ATPase. This process allows cytosolic iron efflux to lower intracellular free Fe^{2+} ion concentration and stops cellular oxidative damage caused by the Fenton reaction. (Jazwa and Cuadrado, 2010, pp.1517–1531; Nitti et al, 2018, p. 2260).

5.2. Implications of Neuronal Nitric Oxide Synthase in the Pathological Central Nervous System Condition

In latest years, studies have associated with NO as a central mediator of neurodegeneration in a variety of nervous system impairment, particularly PD, AD, ALS, HD, and ischemic brain injury (Knott and Bossy-Wetzel, 2009, pp. 541–554). Probable NO-based neurotoxicity pathways include protein nitrosylation and nitrotyrosination, excitotoxicity, mitochondrial respiratory complex repression, organelle fragmentation, and zinc (Zn^{2+}) release from intracellular stores. In pathological conditions, including brain ischaemia or neurological diseases, NO is generated in abundance by overactivated NMDA receptors in neurons (Moncada and Bolaños, 2006, pp. 1676–1689; Knott and Bossy-Wetzel, 2009, pp. 541–554).

Initially, animal models of 1-methyl-4-phenyl-1,2,3,6-tetrahydropyridine (MPTP)-induced neurotoxicity studies have found NOS inhibition delays in disease progression (Jakowec and Petzinger, 2004, pp.497–513; Knott and Bossy-Wetzel, 2009, pp. 541–554; Zhu and Gong, 2020, p. e9209). MPTP is a neurotoxin that destroys substantia nigra neurons while preventing complex I of the mitochondrial respiratory chain. Due to its lipophilicity, MPTP effectively passes the blood-brain barrier (BBB) and is oxidized to a toxic compound, MPP^+ (1-methyl-4-phenylpyridinium), via monoamine oxidase in glial cells. The dopamine carrier transports MPP^+ through dopaminergic neurons, where it gathers in the mitochondria. MPP^+ prevents the mitochondrial complex I in the electron transport chain by blocking electron flow, decreasing ATP output, and enhancing ROS production (Subramaniam and Chesselet, 2013, pp. 17–32). In addition to many studies on NO in PD models, a proteomic analysis suggested an association between β-amyloid aggregation and nitration in a variety of proteins in AD patients

(Butterfield, Swomley and Sultana, 2013, pp. 823–835). The mutant huntingtin (mtHTT), a pathologically mutated protein in HD, can bind with glyceraldehyde-3-phosphate dehydrogenase (GAPDH) and Seven in absentia homolog 1 (SIAH-1), a protein complex that interacts with NO in cell cultures (Schulte and Littleton, 2011, pp. 65–78; Bossy-Wetzel, E., Petrilli and Knott, 2008, pp. 609–616).

5.3. Potential Mechanisms of NO-Mediated Neurodegeneration

5.3.1. S-Nitrosylation

Protein nitrosylation is a well-known mechanism of protein adjustment and regulation. Several S-nitrosylated proteins have been identified in the literature (Knott and Bossy-Wetzel, 2009, pp. 541–554). S-Nitrosylation is a redox-mediated post-translational modification that controls protein function by covalently binding nitric oxide (NO)-based species with the cysteine thiol group of the target protein within the biologycal circumstances (Nakamura et al, 2013, pp. 596–614; Nakamura and Lipton, 2008, pp. 87–101; Okamoto and Lipton, 2015, pp. 1588–1593). Nevertheless, in the case of aging or environmental contaminants that produce intense NO, abnormal S-Nitrosylation reactions can occur, which change protein misfolding, mitochondrial fragmentation, synaptic role, apoptosis, or autophagy (Nakamura and Lipton, 2011, pp. 1479–1492).

- **Parkin:** The ubiquitin E3 ligase controls ubiquitin insertion on specific substrates (Chung et al, 2004, pp. 1328–1331). In the case of Parkin nitrosylation, experiments discovered an increased level in E3 ubiquitin ligase activity before a substantial loss of activity (Knott and Bossy-Wetzel, 2009, pp. 541–554).

- **Prx2:** By interacting with NO (forming SNO-Prx2), peroxiredoxin 2 (PRX2), a component of a class of abundant antioxidants that uses cysteine residues to decompose peroxides, remains S-Nitrosylated. In human PD brains, S-Nitrosylation of Prx2 blocked both its enzymatic activity and defensive action against oxidative stress. Dopaminergic neurons, which are damaged in PD, are especially susceptible (Fang et al, 2007, pp. 18742 LP – 18747; Low, Hampton and Winterbourn, 2008, pp. 1621–1630; Knott and Bossy-Wetzel, 2009, pp. 541–554).

- **Protein-disulfide isomerase (PDI):** Protein-disulfide isomerase (PDI) is a third nitrosylated protein relevant to both PD and AD, and it is an endoplasmic reticulum

(ER)-associated chaperone protein that protects neurons from ER stress and protein misfolding. Relying on the cellular environment, PDI may also act as an NO receptor or donor (Perri et al, 2016, p. 80; Knott and Bossy-Wetzel, 2009, pp. 541–554; Grek and Townsend, 2014, pp. 4–17). In addition, NO-induced S-Nitrosylation of PDI inhibits the enzymatic activity of PDI and leads to the accumulation of polyubiquitinated proteins. PDI protects against neurotoxicity coupled with ER stress and protein misfolding; however, NO inhibits this neuroprotective consequence in neurodegenerative diseases by S-Nitrosylating PDI. In the AD brain, the expression of the ER stress marker, growth arrest, and DNA damage protein (GADD34) was dramatically amplified in neurons and oligodendrocytes (Honjo et al, 2017, pp. 495–50).

- **Heat-shock protein 90 (Hsp90):** Hsp90 is a molecular chaperone that plays a critical role in pathogenic transformation. Furthermore, in addition to its well-known roles in cancer, Hsp90 plays a role in preserving the functional stability of neuronal proteins with abnormal potential, if mutated or over-activated, and enabling and maintaining the concentrations of toxic aggregates. Moreover, Hsp90 controls the function of the transcription factor heat shock factor-1 (HSF-1), which is the key molecule of the heat shock response, a process that cells are using to protect themselves when stressed (Luo et al, 2010, p. 24). In the AD case, inactivation of Hsp90 can cause tau and amyloid-β aggregates to concentrate in the brain. As a result, S-Nitrosylation of Hsp90 inhibits ATPase activity, which is essential for its chaperone role (Knott and Bossy-Wetzel, 2009, pp. 541–554).

- **GAPDH:** Glyceraldehyde-3-phosphate dehydrogenase (Lazarev et al, 2018, pp. 1003–1008) has different roles beyond conventional aerobic glucose metabolism. GAPDH can interact with a wide range of small molecules, proteins, membranes, and other molecules that contribute to normal and pathologic cell activities due to its various isoforms and cellular positions. GAPDH is shown to connect with proteins associated with neurodegenerative disorders, such as the β-amyloid precursor protein (AβPP) (Butera et al, 2019, p. 2062). According to Sen and collaborators, the S-Nitrosylation (SNO) of GAPDH was enhanced by the high amount of NO; S-Nitrosylated GAPDH (GAPDH-SNO) stimulated the acetylation and the activation of acetyltransferase p300, also promoted nitrosylation and inhibiting the deacetylase sirtuin1 (SIRT1) (Sen, Saha and Sen N, 2018, p. eaao6765; Kornberg et al, 2010, pp.

1094–1100). Within the pathological conditions, NO S-nitrosylates GAPDH at the catalytic cysteine residue (Cys152 in humans) and S-nitrosylated GAPDH is suggested to contribute to nuclear signaling events leading to apoptotic cell death (Hara et al, 2005, pp. 665–674). Enzymatic activity of GAPDH is interrupted by S-Nitrosylation, allowing GAPDH to bind to SIAH1, an E3 ubiquitin ligase. SIAH1 brings GAPDH to the nucleus and also has a nuclear localization signal. GAPDH regulates SIAH1 in the nucleus and enables nuclear proteins to be degraded by ubiquitination (Lee et al, 2012, pp. 65–76). As a result, the GAPDH/SIAH1 ubiquitination and cell death pathway could be a key mechanism in the pathology of a variety of neurological disorders (Ko et al, 2019, pp. 15435–15445).

- **MMP-9:** Matrix metalloproteinase-9 (MMP-9) (Knott and Bossy-Wetzel, 2009, pp. 541–554) is a Zn^{2+} dependent endopeptidase that is present in several kinds of cells, namely neurons and glia, endothelial cells, glandular epithelia, protective connective tissue, and muscle cells (Reinhard, Razak and Ethell, 2015, p. 280). MMP-9 is among the most frequently studied MMPs, which controls pathological remodeling mechanisms in cardiovascular disease that include inflammation and fibrosis (Yabluchanskiy et al, 2013, pp. 391–403; McCarthy et al, 2008, pp. 5832–5840). The controlled function of MMP-9 is essential for the development of the CNS. MMP-9, in particular, plays a significant role in the development of sensory circuits during the crucial periods of early Postpartum development. It also governs sensory-mediated, local circuit reorganization by controlling synaptogenesis, axonal pathfinding, and myelination. While the activity-dependent stimulation of MMP-9 at particular synapses is critical in multiple plasticity pathways in the CNS, uncontrolled stimulation of the enzyme has been linked to a variety of neurodegenerative diseases, such as traumatic brain injury, MS, Fragile X Syndrome, and AD (Reinhard, Razak and Ethell, 2015, p. 280). Numerous findings suggest that by S-Nitrosylation of the pro-domain Cys residue, NO participates in activating MMPs or associated metalloproteinases (McCarthy et al, 2008, pp. 5832–5840). MMPs are a subject for S-Nitrosylation during pathological processes characterized by highly dynamic rises in NO bioavailability due to NOS activation. S-Nitrosylation of MMP-9 has been linked to neurodegeneration (Underly and Shih, 2021, p. 619230).

5.3.2. 3-Nitrotyrosination

While ONOO$^-$, produced by the reaction of NO and O$_2$, targets proteins, it frequently induces 3-nitrotyrosination of tyrosine residues to form 3-nitrotyrosine (3-NT). 3-NT is a considerably specific marker of peroxynitrite-mediated oxidative damage (Bandookwala and Sengupta, 2020, pp. 1047–1062; Ahsan, 2013, pp. 1392–1399). Protein nitration at the subcellular level generates conformational changes that harm the cytoskeleton and cause neurodegeneration (Bandookwala and Sengupta, 2020, pp. 1047–1062; Mihm et al, 2001, p. RC149).

Tohgi and his group suggested that tyrosine nitration stimulation could be implicated in brain aging and cause AD. They found that the 3-nitrotyrosine level and the 3-nitrotyrosine/tyrosine proportion raised significantly with age, while the tyrosine level remained unchanged. The 3-nitrotyrosine level and the 3-nitrotyrosine/tyrosine ratio augmented dramatically (>6-fold) in patients with AD compared to control group patients of similar age and dropped considerably with declining cognitive functions, while the tyrosine level did not alter (Tohgi et al, 1999, pp. 52–54).

5.3.3. Glutamate excitotoxicity

Glutamate and aspartate are the most important excitant neurotransmitter in the brain. Glutamate links and activates ligand-gated ion channels (ionotropic glutamate receptors) and a group of GPCRs. Whereas intracellular glutamate rates in the brain are millimolar, excitatory AA transporters which import glutamate and aspartate through astrocytes and neural synapses keep extracellular glutamate levels in the reduced micromolar range (Lewerenz and Maher, 2015, p. 469; Sheldon and Robinson, 2007, pp. 333–355).

Excitotoxicity is frequent in several NDs, such as ischemic stroke, AD, ALS, and HD (Prentice, Modi, and Wu, 2015, p. 964518; Sheldon and Robinson, 2007, pp. 333–355). Glutamate excitotoxicity is a cell death process caused by high glutamate release from neurons and glial cells. Overstimulation of synaptic glutamate receptors leads to

increased Ca^{2+} influx and neuronal damage (Knott and Bossy-Wetzel, 2009, pp. 541–554; Belov Kirdajova et al, 2020, pp. 14 -51; Sheldon and Robinson, 2007, pp. 333–355). NO can effectively protect from excitotoxicity by preventing NMDA-receptor activation. Increased intracellular Ca^{2+} levels, caused by glutamate receptor activation, such as NMDA receptors, induce nNOS to generate additional NO. NO is extremely important in excitotoxicity, and under circumstances of excessive glutamate receptor activation, NO binds with O_2^- to form the toxic molecule $ONOO^-$ (Prentice, Modi, and Wu, 2015, p. 964518; Knott and Bossy-Wetzel, 2009, pp. 541–554).

6. NOS INHIBITORS

NOS became a drug target after discovering that this enzyme is responsible for NO biosynthesis. Following identifying the different NOS isoforms, such inhibitor studies have rapidly expanded. NOS quickly has become apparent that the isoform selectivity poses a significant problem due to the similarity of the active site structures of the three human NOS isoforms, nNOS, eNOS, and iNOS. NOSs have the same structural architecture, with 16 of 18 residues within 6 Å of the substrate-binding site being the same and causing selective inhibitor development challenging (Raman et al. 2001, pp. 26486–26491; Annedi S, 2015, pp. 1064–1066; Poulos and Li, 2017, pp. 68–77).

The upregulation or increased production of NO by any specific NOS isoform plays an essential role in many diseases, involving septic shock, stroke, NDs (PD, ALS, MS, and AD), pain (migraine, chronic tension-type headache, visceral and neuropathic pain), arthritis, diabetes, and ischemia-reperfusion injury (Mukherjee et al, 2014, pp. 6814–6838; Annedi S, 2015, pp. 1064–1066).

Due to the absence of NOS crystal structure, early selective NOS inhibitor design (between the 1980s and 1990s) was established on the substrate L-Arginine (**Figure 6.1**). This process resulted in the first-generation NOS inhibitors, L-arginine mono- and disubstituted derivatives. Whereas most of these preliminary inhibitors were found to be effective, many of them demonstrated bad selectivity among the 3 NOS isoforms (Silverman, 2009, pp. 439–451; Annedi S, 2015, pp. 1064–1066). Since the 3D structures of all NOS isoforms became known in the late 1990s and early 2000s, developed inhibitor synthesis became increasingly valuable (Víteček et al, 2012, p. 318087; Annedi S, 2015, pp. 1064–1066).
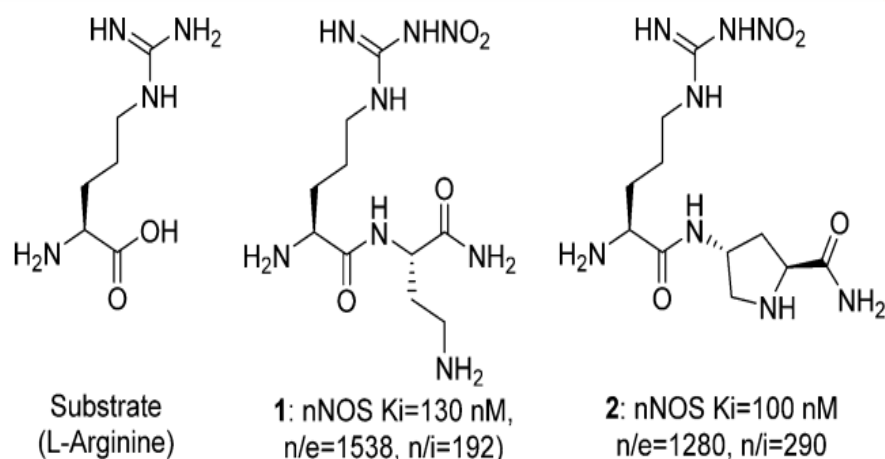
Figure 6.1 L-Arginine-based first-generation NOS inhibitors. (Annedi S, 2015, pp. 1064–1066)

6.1. Classification of Nitric Oxide Synthase Inhibitors

NOS inhibitors can be categorized according to their different characteristics (Víteček et al, 2012, p. 318087), such as chemical properties, isoform selectivity, and binding site (Sundaresan, Giri and Chatterjee, 2016, pp. 81–107) **(Table 6.1)**.

Table 6.1 NOS inhibitors with pharmacological examples depending on binding sites (Sundaresan, Giri and Chatterjee, 2016, pp. 81–107).

Binding site	Pharmacological inhibitors
Substrate binding site	L-N$^{\omega}$-Methylarginine
Pterin binding site	4-amino pteridine derivatives 2,4-diamino-5-(3',4'dichlorophenyl) pyrimidine 7-Nitroindazole
Inhibitor which binds with the heme group	S-Methyl-L thiocitrulline
flavin/ NADPH site	Diphenyleneiodonium chloride

According to their mechanism of action, NOS inhibitors can be categorized to:

- Reversible inhibitors (subgroups: competitive, uncompetitive, non-competitive, and mixed type).

- Irreversible inhibitors.

- Reaction-based inhibitors, whose activity is contingent on the enzymatic reaction, can be distinguished using the classical enzymological reaction.

- This classification matches the classical enzymological approach (Víteček et al, 2012, p. 318087).

In addition, NOS inhibitors are classified into four classes based on their mechanism of action:

- Arginine analogs: which can be attached to the substrate-binding site. Many arginine-based analogs are included in this category, including L-NMA, L-NAME, and others.

- Agents with a structure similar to tetrahydrobiopterin, for example, derivatives of 4-amino pteridine.

- Inhibitors link to the heme, interacting with monomer dimerization and enzymatic activities. S-Methyl-L thiocitrulline (SMTC), for instance.

- Molecules that interfere with flavin cofactors (DPI) such as Diphenyleneiodonium chloride (DPI) (Sundaresan, Giri and Chatterjee, 2016, pp. 81–107).

Depending on the chemical properties, NOS inhibitors can be classified into two groups: the first group is an amino acide -based. Most of them are arginine products and analogs, while the other class contains a variety of ligands with structures that differ from arginine (Sundaresan, Giri and Chatterjee, 2016, pp. 81–107).

6.1.1. Arginine-based inhibitors of NOS

Since Arginine-based inhibitors were supposed to compete with Arginine for the active site of NOS, they were initially proposed as inhibitors for experimental purposes, in which some objectives have been met. Furthermore, certain members of this class of inhibitors can function as reaction-based inhibitors (Víteček et al, 2012, p. 318087).

The widely investigated compounds are L-N$^{\omega}$-Nitroarginine, LN -Nitroarginine methyl ester, and N^G-propyl-L-arginine (Sundaresan, Giri and Chatterjee, 2016, pp. 81–107).

6.1.2. Non-amino acid-based inhibitors

Non-amino acid-based NOS inhibitors have been studied for the particular selectivity and therapeutic efficacy in order to enhance the selectivity and therapeutic potential of L-Arg products (Saleron et al, 2002, pp. 177–200; Garvey et al, 1994, pp. 26669–26676), such as Guanidines, Isothioureas, Amidines, Thiazines, Imidazoles, Indazoles, Benzoxazoles, Pyridines, and Pteridines. These compounds can be sub-classified into two major classes by their chemical properties: amidinic compounds and heterocyclic compounds (Saleron et al, 2002, pp. 177–200).

6.1.3. Amidinic compounds

All compounds with a carbamidine carbon bound to N (guanidines), S (isothioureas), or another carbon (simple amidines) are presented in **Figure 6.2** (Mukherjee et al, 2014, pp. 6814–6838; Saleron et al, 2002, pp. 177–200).
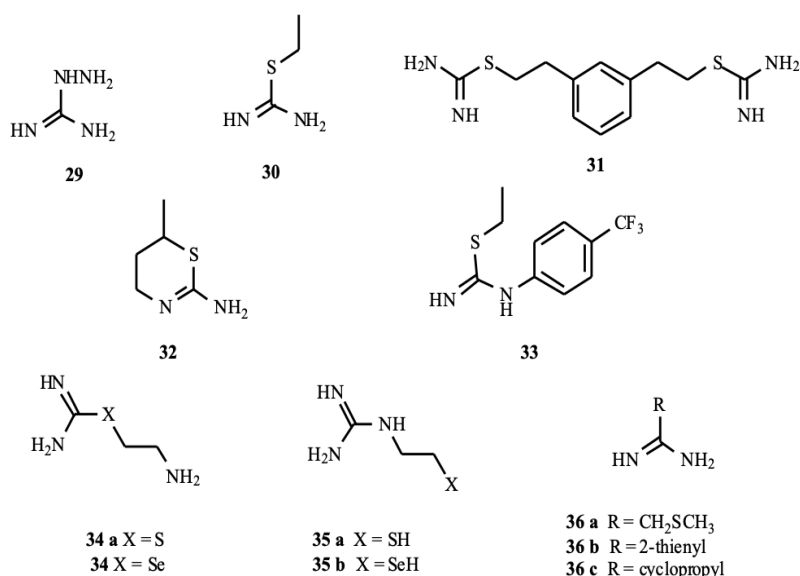
Figure 6.2 Non-amino acid-based NOS inhibitors: Amidinic compounds (Saleron et al, 2002, pp. 177–200).

6.1.4. Heterocyclic compounds

The other non-amino acid-based NOS inhibitors consist of heterocyclic compounds, such as indazoles, imidazoles, and tetrahydrobiopterine analogs (**Figure 6.3**) as the most common ones.

47 a -j

48 a - r

49 a R = H, R' = CF$_3$, R" = H
49 b R = SH, R' = CF$_3$, R" = H
49 c R = H, R' = Cl, R" = H
49 d R = H, R' = R" = F

50 a R = NO$_2$
50 b R = NH$_2$
50 c R = H

51 a n = 0, R = H; **51 b** n = 1, R = H; **51 c** n = 2, R = H; **51 d** n = 3, R = H;
51 e n = 4, R = H; **51 f** n = 1, R = C$_6$H$_5$; **51 g** n = 2, R = C$_6$H$_5$; **51 h** n = 3, R = C$_6$H$_5$

52 a n = 1, X = N, Y = CH
52 b n = 2, X = N, Y = CH
52 c n = 1, X = CH, Y = N
52 d n = 2, X = CH, Y = N

53 a n = 1, X = N, Y = CH
53 b n = 2, X = N, Y = CH
53 c n = 1, X = CH, Y = N
53 d n = 2, X = CH, Y = N
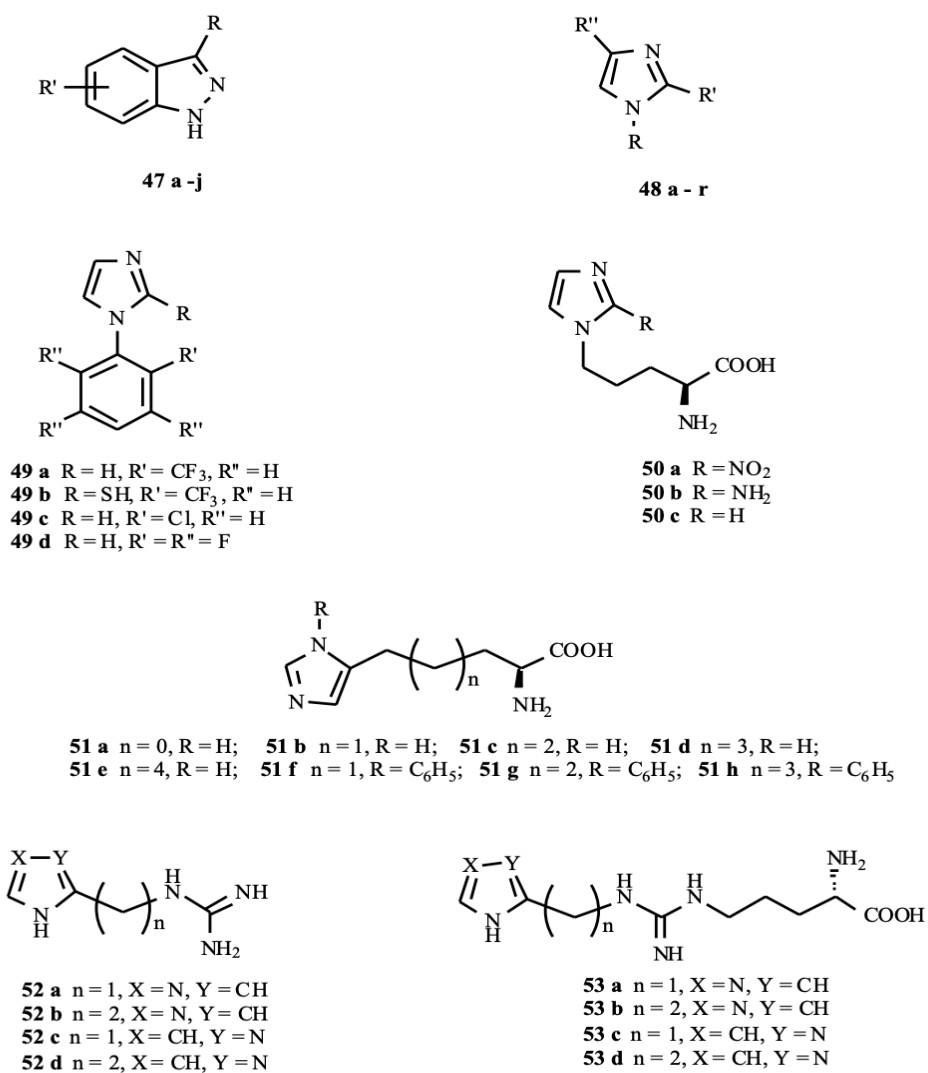
Figure 6.3 Structures of non-amino acid-based inhibitors: heterocyclic compounds (Saleron et al, 2002, pp. 177–200).
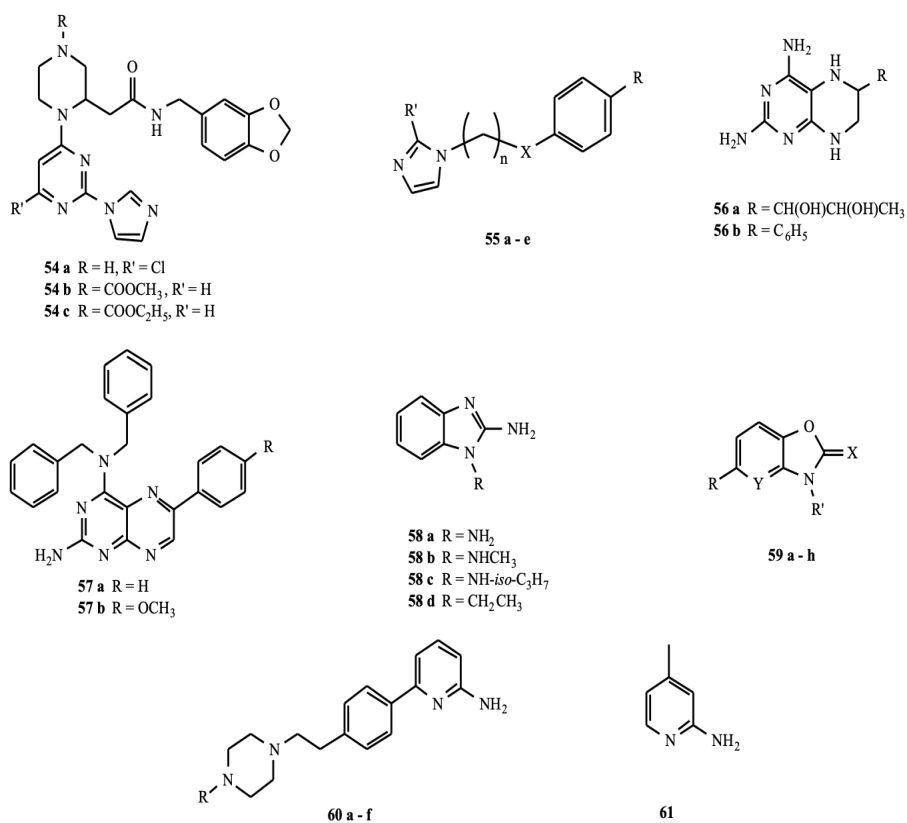
Figure 6.4 Structures of non-amino acid-based inhibitors: heterocyclic compounds (Saleron et al, 2002, pp. 177–200).

6.2. nNOS Inhibitors

After discovering the function of nNOS in neurodegenerative disorders and pain, several efforts were made to block or deactivate nNOS selectively over its otherisoformsfor the treatment of diseases, as inhibition of the incorrect isoform may result in damaging consequences (Mukherjee et al, 2014, pp. 6814–6838). The first challenge in designing nNOS inhibitors is to achieve selective ligands that do not affect iNOS and eNOS (Maccallini and Amoroso, 2016, pp. 1731–1734). Earlier nNOS inhibitors, which were substrate analogs or arginine-based dipeptides, have been rejected by the researchers because they caused undesirable cardiovascular complications (hypertension, heart failure, etc.) due to their weak isoform selectivity (Baylis, 2006, pp. 209–220; Maccallini and Amoroso, 2016, pp. 1731–1734;

Papageorgiou et al, 2015, pp. 1741–1750). Sterically hindered amidines, non-aminoacidic compounds are selectively capable of inhibiting nNOS (Compounds **1** and **2** presented in **Figure 6.5**). Since they are liable with the desirable interactions inside the nNOS catalytic region, these compounds' phenyl and isopropyl groups are the main segments granting the desired selectivity. Thienyl-carbamidines generated affirmative outcomes, as they were victorious against hnNOS and demonstrated neuroprotective effects in ischemia models and neuropathic pain (Compounds **3** and **4** presented in **Figure 6.5**). In addition, compounds **5** and **6** in **Figure 6.5** demonstrated high potency against nNOS as the most successful candidates (Maccallini and Amoroso, 2016, pp. 1731–1734).
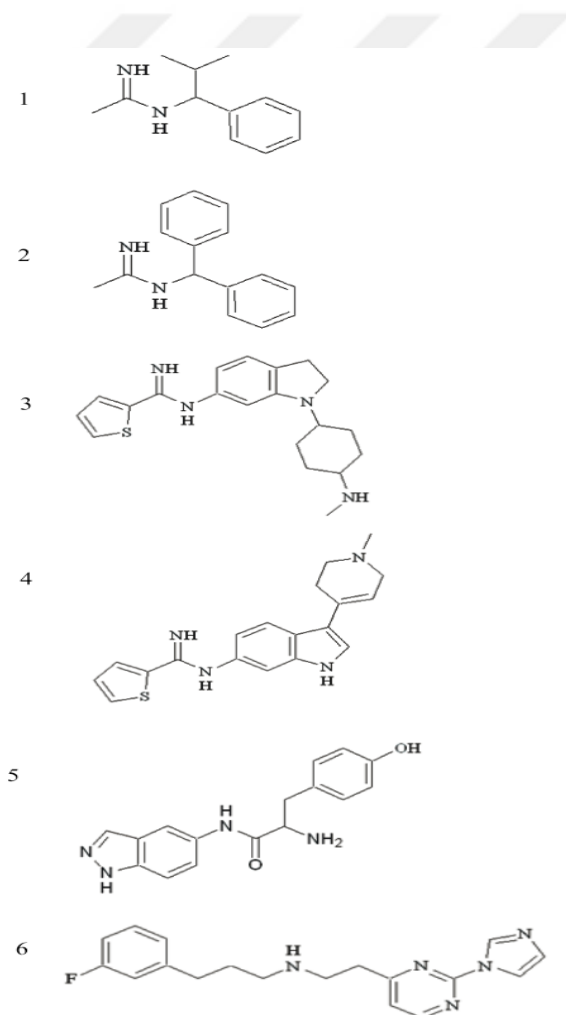
Figure 6.5 Inhibitors of neuronal nitric oxide synthase (Maccallini and Amoroso, 2016, pp. 1731–1734).

6.2.1. Different approaches to neuronal nitric oxide synthase inhibition

there are many methods of inhibition, which vary from minor inhibition through substrate or cofactor imitation (Competitive inhibition) (Furfine et al, 1993, pp. 8512–8517) and mechanism-based inactivation to inhibition of protein-protein interactions inside nNOS (Dimer inhibition) (Palumbo, Astarita and d'Ischia, 2001, pp. 105–110) or between enzyme and associated proteins (CaM antagonism) (Fukunaga et al, 2000, pp. 693–699). Initiatives to suppress nNOS in combination with other targets involved in neurodegenerative disorders and pain are made (Dual inhibition) (Mukherjee et al, 2014, pp. 6814–6838) (**Figure 6.6**).
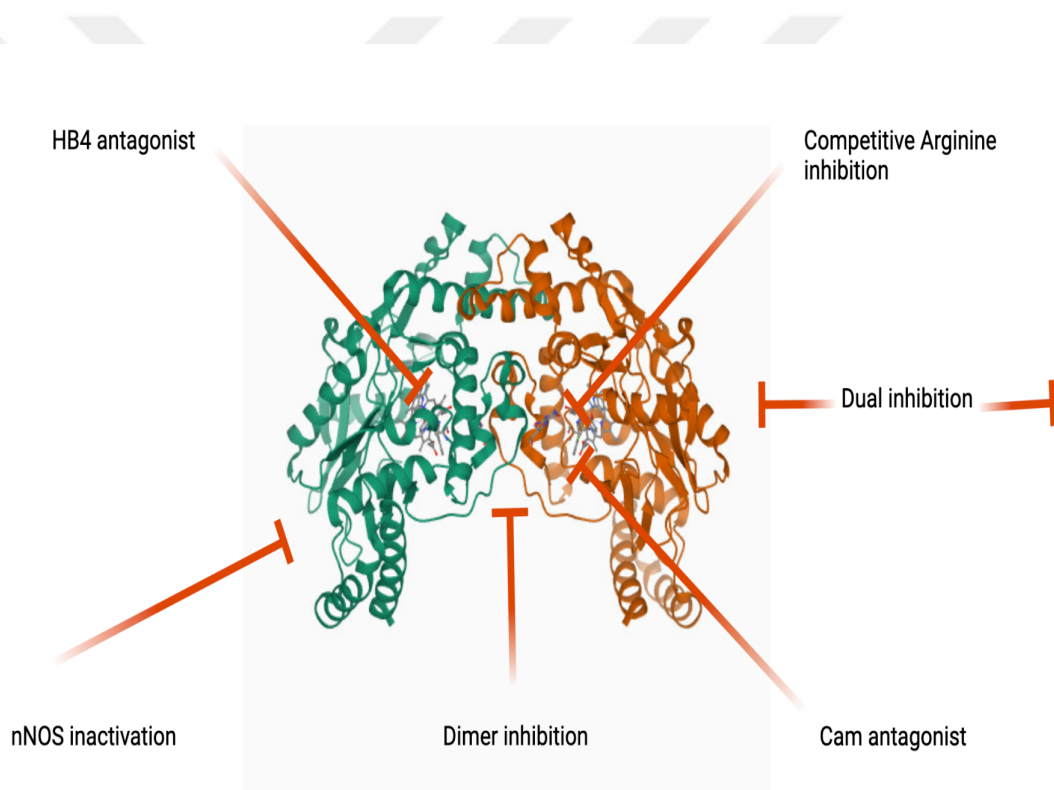
Figure 6.6 Neuronal nitric oxide synthase inhibition modes (PDB ID: 5VV5).

For instance, L-N$^{\omega}$-Nitroarginine is a competitive inhibitor of nNOS which adheres to the active site of the enzyme and prevents substrate binding. Still, this competitive inhibitor has low selectivity over eNOS. Unfortunately, extreme hypertension is triggered by the methyl ester of L-N$^{\omega}$-nitroarginine, a prodrug for L-nitroarginine, and is

stimulated by esterase-catalyzed hydrolysis to L-N$^\omega$-nitroarginine (Ji et al, 2009, pp. 209–217; Lajoix et al, 2004, pp. 1467–1474). According to Zhou and his group, ischemia causes nNOS to interfere with postsynaptic density protein-95 (PSD-95). Increased N-terminal AA residues 1-133 of nNOS (nNOS-N (1-133)) prevent glutamate-induced excitotoxicity and cerebral ischemic endangerment. ZL006 was created to inhibit the ischemia-induced nNOS-PSD-95 association selectively. ZL006 easily penetrated the blood-brain barrier without implying violent behavior and disrupting NMDAR action, nNOS catalytic activity, or spatial memory (Zhou et al, 2010, pp. 1439–1443).

The compound 6-(((3R,4R)-4-(2-((3-fluorophenethyl) amino) ethoxy) pyrrolidin-3-yl) methyl)-4-methylpyridin-2-amine showed a high potency and selectivity, but poor membrane permeability due to the 2 secondary amino groups (Drerup, Ermert, and Coenen, 2016, pp.1160). The compound IC87201 has also been shown to be a potent inhibitor of the nNOS/ PSD-95 protein-protein interaction *in vitro* and *in vivo* studies (Bach et al, 2015, p. 12157).

7. COMPUTER-AIDED DRUG DESIGN (CADD)

The term ′drug design‵ refers to the systematic, rational search for new drugs with biological activity. It is essentially based on experimental data from the expected target molecule or a related biomolecule (direct drug design) and/or recognized binders of this target (indirect drug design) (Talevi, 2018, pp. 1–19).

The drug production and discovery process are complex, costly, and time-consuming (Mohs and Greig, 2017, pp. 651–657). In the last years, drug design noticeably increased due to the advancement of computational techniques and methods (Bibi and Sakata, 2016, pp. 167–177). CADD, also recognized as *in silico* screening, computational drug design, computer-aided molecular design (CAMD), computer-aided molecular modeling (CAMM), rational drug design, *in silico* drug design, computer-aided drug discovery and development, and computer-aided rational drug design, is becoming a potent tool in recent years due to its importance in different phases of drug discovery and development using multiple innovative tools (Kapetanovic, 2008, pp. 165–176; Macalino et al, 2015, pp. 1686–1701).

Fortune magazine released a news article titled "The Next Industrial Revolution: Designing Drugs by Computer at Merck" on October 5, 1981(Merck makes ethical drugs and fine chemicals (Brown et al, 2017, pp. 255–266)). Many considered this the beginning of remarkable progress in the future of computer-aided drug design (Sliwoski, 2013, pp. 334–395).

Novel therapeutic agents are discovered through the combination of rational drug design and structural biology. CADD partners with structure biologists, biophysicists, and computational researchers to find acceptable chemical compounds (Chegkazi et al, 2018, pp. 89–111).

Drug development and discovery require a minimum of 10-15 years of process and 0.8-1.8 billion USD expense (Macalino et al, 2015, pp. 1686–1701) (**Figure 7.1**). Besides this, the number of new molecular entities (NMEs) effectively commercialized has declined in recent years (Myers and Baker, 2001, pp. 727–730). For that, the use of CADD techniques and strategies by many major pharmaceutical firms and research institutions has become critical for the primitive stage of drug discovery to speed up the drug delivery in a much more cost-effective manner and to reduce failures in the final stage (Leelananda and Lindert, 2016, pp.2694–2718; Macalino et al, 2015, pp. 1686–1701).
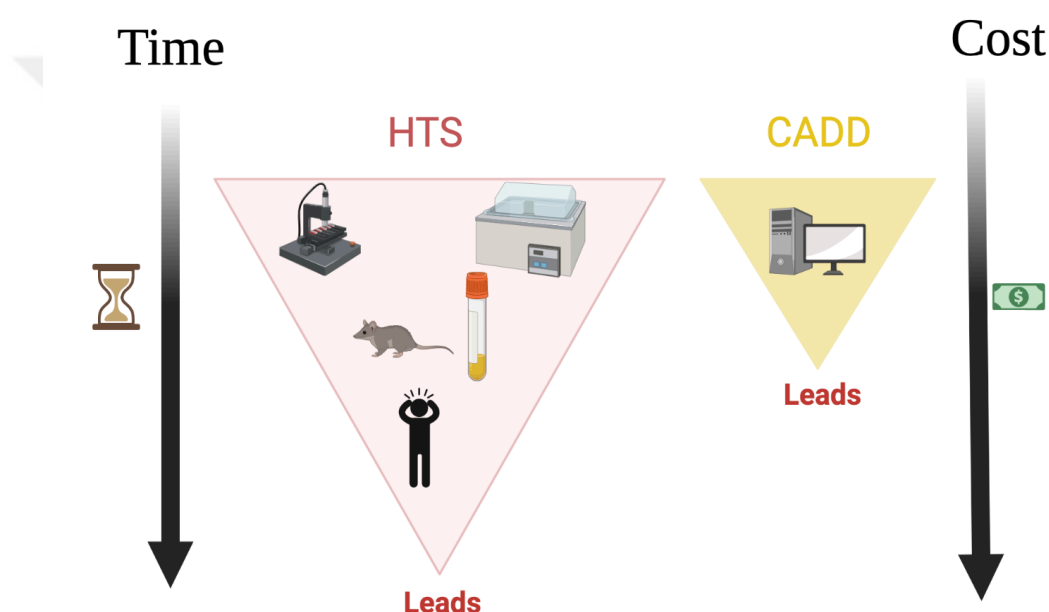
Figure 7.1   The traditional HTS and CADD.

 Using computational tools may minimize drug production costs by 50% (Katsila et al, 2016, pp. 177–184). CADD tools distinguish lead drug molecules for development, estimate the efficacy and potential side effects, and help improving the bioavailability of potential drug molecules (Talevi, 2018, pp. 1–19; Sliwoski, 2013, pp. 334–395). For instance, in a recent CADD research, it was revealed that by adding a triphenylphosphine group into the base molecule pyridazinone (Yang et al, 2016, pp. 2801–2805), it would be possible to acquire proteasome inhibitors (Fricker, 2020).

Moreover, analogs with high potency have been developed using this starting pattern. Several findings demonstrate that CADD can impact the production of novel treatments (Leelananda and Lindert, 2016, pp.2694–2718).

In addition, the Pfizer company has also employed CADD tools to screen for inhibitors of tyrosine phosphatase-1B, an enzyme involved in diabetes (Taylor, 2003, pp. 759–782). The virtual screening generated 365 compounds, of which 127 inhibited effectively, yielding a hit rate of approximately 35%. This group also ran a standard high-throughput screening (HTS) (Entzeroth, Flotow and Condron, 2009, pp. 9.4.1-9.4.27) against the same target at the same time as the standard HTS. Only 81 of the evaluated 400,000 compounds demonstrated inhibition, generating a hit rate of 0.021 %. This comparative study clearly illustrates the working capacity of CADD tools (**Table 7.1**) (Johnson, Ermolieff and Jirousek, 2002, pp. 696–709; Sliwoski, 2013, pp. 334–395; Vijayakrishnan, 2009).

Table 7.1   A brief history of CADD

Year	Research	References
1900	The 'Lock and Key' concept of protein-ligand binding of P. Ehrich (1909) and E. Fisher (1894)	(Tripathi and Bankaitis, 2017, p. 10.16966/2575-0305.106)
1970s	Quantitative structure-activity relationships (QSAR)	(Cherkasov et al, 2014, pp. 4977–5010)
1980s	CADD Molecular Biology X-ray crystallography multi-dimensional NMR Molecular modeling Computer graphics	(Baig et al, 2018, pp. 740–748)
1990s	Human genome bioinformatics Combinatorial chemistry High-throughput screening	(Chaguturu, 2013, p.1; Kore et al, 2012, pp. 139–148)

Many approved drugs that attribute their development in large portion to CADD techniques, such as Dorzolamide, a carbonic anhydrase inhibitor approved in 1995 (Sugrue, 1996, pp. 363–376), captopril that is an angiotensin-converting enzyme (ACE) inhibitor approved in 1981 as being an anti-hypertensive drug (Bicket, 2002, pp. 461–468). In addition to HIV drug discoveries: saquinavir was approved in 1995 (James, 1995, pp. 1–2), ritonavir (Lea and Faulds, 1996, pp. 541–548) as well as indinavir (Plosker and Noble, 1999, pp. 1165–1203), both approved in 1996, and tirofiban that is a fibrinogen antagonist approved in 1998 (McClellan and Goa, 1998, pp. 1067–1080).

7.1. CADD Position in the Drug Discovery Pipelines

Since CADD utilizes a more focused search than standard HTS and combinatorial chemistry, it can improve the hit rate of innovative drugs. This serves not only to understand the molecular basis of therapeutic action but to potentially identify compounds that might enhance efficacy (Liao et al, 2011, pp. 21–54). CADD is generally used for three main reasons in drug development (Sliwoski, 2013, pp. 334–395): **(i)** Utilization of computational resources to speed up the drug discovery and production mechanism, **(ii)** Applying chemical and biological knowledge about ligands and (or) targets to define and improve new drugs, and **(iii)** *in silico* filter design to remove compounds with undesirable properties like limited activity and/or bad ADMET, but instead, to find the most suitable candidate (Kapetanovic, 2008, pp. 165–176).

7.2. General Computer Aided Techniques for Drug Discovery

Computational techniques have developed vital tools for target recognition, drug discovery, and drug candidate target optimization (Ou-Yang et al, 2012, pp. 1131–1140). In conjunction with statistics and chemoinformatic methods, technological advances differ depending on disorder pathways and phenotypes, identifying new drug targets that can be validated using HTS Technologies (Katsila et al, 2016, pp. 177–184).

7.2.1. Target identification and validation

With the release of the maps of the human genome and an initial conclusion that the human genome contains approximately 21000 genes, there is a significant expectation that several new disease-specific molecular targets must quickly be defined, and this will therefore serve as the foundation for many novel drug development projects (Williams, 2003, pp. 571–577). Identifying drug targets from vast numbers of candidate drugs is critical and complicated as the 1st stage in the drug discovery process (Ou-Yang et al, 2012, pp. 1131–1140; Tang et al, 2006, pp. 307–313). Many tools are used frequently effectively employed for this purpose, for instance: **(i)** Chemical structure similarity searching, **(ii)** data mining/machine learning, **(iii)** panel docking, and **(iv)** bioactivity spectra-based algorithms (Katsila et al, 2016, pp. 177–184).

Target identification may be established as target-based or reverse chemical genetics at the beginning of the biological screening or as phenotype-based or forward chemical genetics at the end (Macalino et al, 2015, pp. 1686–1701). The online target identification databases play essential roles, and there is no doubt that an immensely detailed collection is easily accessible nowadays.

High-resolution 3D structures are the most important resource of structural data for drug discovery, notably for proteins varying in size from a few AA to 998 kD (Singh, Malik, and Sharma, 2006, pp. 314–320). The crystal structure data must be checked for diffracted amplitude resolution, such as reliability or R factors, coordinate error, T^0 factors, and chemical correctness (Smyth and Martin, 2000, pp. 8–14; Maveyraud and Mourey, 2020, p. 1030). The 3D structures defined with R ranging under 2.5 Å are usually appropriate for drug design because they provide a good data to parameter ratio and a prominent position of residues in the electron density map (Wlodawer et al, 2008; Singh, Malik, and Sharma, 2006, pp. 314–320). A homology model may also be used for drug discovery if no experimentally defined structure is available. For instance, SWISS MODEL generates a confidence factor per residue to analyze a homology model, representing the amount of structural knowledge used to construct that model section (Singh, Malik, and Sharma, 2006, pp. 314–320; Vyas et al, 2012). Many *in*

silico methods are available to start the drug design process if the target has been determined. Each of these methods is determined by the target's nature and information on the framework (Bajorath, 2015; Katsila et al, 2016, pp. 177–184; Liao et al, 2011, pp. 21–54). In general, there are 2 approaches to computational drug design, structure-based (SB) and ligand-based (LB) (Macalino et al, 2015, pp. 1686–1701; Leelananda and Lindert, 2016, pp.2694–2718; Sliwoski et al, 2013, pp. 334–395; Katsila et al, 2016, pp. 177–184; Liao et al, 2011, pp. 21–54).

7.3. Structure-Based Drug Design (SBDD)

Structure-Based Drug Design (SBDD) is a cyclic process that involves the acquisition of information in steps as inputs for the further next steps. This pathway is carried out to recognize probable compounds starting from a known target structure (Ferreira et al, 2015, pp. 13384–13421). Structure determination techniques, such as X-ray crystallography (Zheng et al, 2014, pp. 125–137) and nuclear magnetic resonance (NMR) (Pellecchia et al, 2008, pp. 738–745), have quickly progressed in the last few years. As a result, several three-dimensional (3D) structures of biomolecules have been identified, creating a new phase of SBDD in drug discovery and development (Wang et al, 2018, pp. D1074–D1082). The 3D-structures of biomolecules, especially those established by X-ray crystallography, are frequently regarded as the "gold standard" of data identifying the molecular architecture of crucial proteins and nucleic acids (Davis, Teague and Kleywegt, 2003, pp. 2718–2736; Zheng et al, 2014, pp. 125–137).

Furthermore, the accessible number of macromolecular structures has dramatically increasedsince its beginning in 1971, with the increase in the range of deposition of such structures to the PDB (Burley et al, 2017, pp. 627–641). Moreover, several NMR applications for SBDD have been generated since the 1970s (Pellecchia et al, 2008, pp. 738–745). The standard NMR task is identifying a particular inhibitor and studying its binding mode (Shi and Zhang, 2021, p. 576). The SBDD can represent the binding process of the compounds to the target (enzymes, proteins, or receptors), and estimate the main binding pocket sites and affinity of compounds to their target, which seem to be essential for their related biological activities, once the 3D-structural details

of targets are defined, that is usually obtained experimentally or via computational homology modeling (Batool, Ahmad and Choi, 2019, p. 2783; Wang et al, 2018, pp. D1074–D1082). This knowledge is then used to obtain high affinity compounds with the essential properties for expected pharmacological and therapeutic results (Wang et al, 2018, pp. D1074–D1082). The SBDD is a common computational technique used by drug companies and researchers, with which various drugs that are still on the market have been defined (**Table 7.2**) (Batool, Ahmad and Choi, 2019, p. 2783).

Table 7.2   The successful example of drug discovery by the SBDD technique.

Drug	Target	Disease	Approved in Year	References
Raltitrexed	Thymidylate synthase	HIV	2007	(Batool, Ahmad and Choi, 2019, p. 2783; Baig et al, 2016, pp. 572–581)
Amprenavir	Antiretroviral protease	HIV	1999	(Noble and Goa, 2000, pp. 1383–1410; Batool, Ahmad and Choi, 2019, p. 2783)
Isoniazid	InhA	Tuberculosis	-	(Batool, Ahmad and Choi, 2019, p. 2783; Jagadeb, Rath and Sonawane, 2019, pp. 3388–3398)
Pim-1 Kinase Inhibitors	Pim-1 Kinase	Cancer	2009	(Arrouchi, Lakhlili and Ibrahimi, 2019, pp. 116–120; Batool, Ahmad and Choi, 2019, p. 2783)
Epalrestat	Aldose Reductase	Diabetic neuropathy	-	(Batool, Ahmad and Choi, 2019, p. 2783; Steele, Faulds and Goa, 1993, pp. 532–555; National Center for Biotechnology Information, 2021b)

Flurbiprofen	Cyclooxygenase-2	Rheumatoid arthritis, Osteoarthritis	1987	(Batool, Ahmad and Choi, 2019, p. 2783; National Center for Biotechnology Information, 2021a)
STX-0119	STAT3	Lymphoma	-	(Batool, Ahmad and Choi, 2019, p. 2783; Choi et al, 2019)
Norfloxacin	Topoisomerase II, IV	Urinary tract infection	1983	(Batool, Ahmad and Choi, 2019, p. 2783; Rowen, Michel and Thompson, 1987, pp. 92–110)
Dorzolamide	Carbonic anhydrase	Glaucoma, cystoid macular edema	1994	(Batool, Ahmad and Choi, 2019, p. 2783; Balfour and Wilde, 1997, pp. 384–403)

7.3.1. Structure-based drug design workflow

The SBDD comprises many steps, including protein structure preparation, active site recognition, ligand library preparation, docking, MD simulation, and scoring functions (Anderson, 2011, pp.359–366; Wang et al, 2018, pp. D1074–D1082). Virtual screening (VS) and de novo drug discovery (DNDD) are two cutting-edge structure-based drug design methods that are effective and alternative methods to HTS (Lionta et al, 2014, pp. 1923–1938).

The VS is an *in-silico* process used in drug discovery (Ekins, Mestres and Testa, 2007, pp. 9–20). A wide range of databases of known 3D structures is mechanically analyzed during VS by the employment of computational methods (Green, 2003, pp. 61–97). The VS is a filter that picks the successful compounds for *in vitro* experiments (Maia et al, 2020, p. 343). There are three types of VS: **(i)** Structure-based virtual screening

(SBVS), **(ii)** ligand-based virtual screening, and **(iii)** fragment-based virtual screening (Lavecchia and Di Giovanni, 2013, pp. 2839–2860; Maia et al, 2020, p. 343).

The SBVS is a computational method used during the primary phase of drug development to scan a chemical compound library for novel bioactive molecules vs. a aimed drug target. The 3D structure of the biomolecule determined by X-ray, NMR, or computational modeling is used to dock a series of chemical compounds into the binding pocket and pick a portion among these compounds for the next steps based on the predicted binding results (Li and Shah, 2017, pp. 111–124). The SBVS aims to estimate the strongest interaction mode between two molecules to create a stable system and employs scoring functions to determine the force of non-covalent interactions between the compound and the protein (Maia et al, 2020, p. 343).

7.3.2. Target structure preparation

The critical step in the SBDD is to prepare the structure of the target (Wang et al, 2018, pp. D1074–D1082). Some target structure preparation steps are reviewed:

- Hydrogens are added to macromolecular structures because the crystal structures with resolutions lower than 1 Å generally miss hydrogens (Anderson, 2011, pp.359–366).

- Estimation and identification of individual residue charges (Anderson, 2011, pp.359–366).

- Identifying the active site of the target macromolecule (Wang et al, 2018, pp. D1074–D1082; Anderson, Chen and Linusson, 2010, pp. 1408–1422). Binding sites in the target can experimentally be obtained via site-directed mutagenesis or X-ray crystallography. In addition, many studies on proteins co-crystallized with their substrates or known inhibitors give data about the active site (Wang et al, 2018, pp. D1074–D1082). When no data about the binding site is present, there are numerous web servers and software that can assist in acquiring information about the binding site in the target protein, including the DoGSite Scorer server, CASTp, NSiteMatch, metal pocket, DEPTH, LISE, and MSpocket (Yang, Roy and Zhang, 2013, pp. 2588–2595; Wang et al, 2018, pp. D1074–D1082; Xie et al, 2013, pp. W292–W296). If the binding site is known, the volume of the binding pocket can be determined using computational tools

or web servers, like EpockTRAnsient Pockets in Proteins (TRAPP) (Stank et al, 2017, pp. W325–W330) as well as POVME (Durrant, de Oliveira and McCammon, 2011, pp. 773–776).

- At this stage, the choice to retain any metals or cofactors attached to the docking site is taken. Metals and cofactors may also be involved in the complex formation with the compound and, if so, they are counted as part of the binding sites. Nevertheless, if the removal of the metal or cofactor is needed, it must be extracted to make the functional groups to which they link accessible to the compound (Chai, Lu and Ye, 2009; Anderson, 2011, pp.359–366).

- At this level, a determination is taken to preserve or remove the water molecules that remain in the binding sites. If the water molecules are essential to compound binding, they can stay in the binding domain; otherwise, they can be extracted (Schiebel et al, 2018, p. 3559).

- The sum and nature of flexible residues and the degree of flexibility are established if the docking software requires target elasticity to fit conformational changes caused by the compound (Lexa and Carlson, 2012, pp. 301–343).

7.3.3. Structure based virtual screening

7.3.3.1. Ligand library preparation for the structure based virtual screening

The library preparation diverges according to the target and the type of research (for example, drug production, toxin detection, pesticide improvement); we can build the ligands library, which can be chosen from NPs, public repositories, or commercial resources (**Table 7.3)**. The library may include existing known drug substances for repositioning, synthetic substances analogous to lead or drug compounds for subsequent structural optimization, or other natural or xenobiotic ligands (Glaab, 2016, pp. 352–366; Wang et al, 2018, pp. D1074–D1082).

The ligand library can be screened at the start to identify compounds that are more expected to be bioavailable in the final phase. Many parameters, such as molecular weight, number of rotatable bonds, and number of HD and HA, can be used for the

screening (Anderson, 2011, pp.359–366; Glaab, 2016, pp. 352–366). Besides that, the compounds should be evaluated for the restrictions of "Lipinski's rule of five" (logP values, molecular weight, number of HD and HA) to increase efficiency (Giménez et al, 2010, pp. 148–152). Before docking, ligands' ADMET risk score (absorption, distribution, metabolism, excretion, and toxicity) (Guan et al, 2018, pp. 148–157) and risk parameters (size, charge, water solubility, volume of distribution, severe rat toxicity, carcinogenicity, serum glutamic oxaloacetic transaminase acceleration, hepatotoxicity, and inhibition of 3A4 oxidation of midazolam) should be evaluated earlier than the docking and are effective in finding bioactive compounds with pharmacokinetic properties and drug safety (Mansoor and Mahabadi, 2020; Wang et al, 2018, pp. D1074–D1082; Campos et al, 2011, pp. 1387–1393). Then, the compounds must be analyzed for proper geometry, such as bond distances and angles (Long et al, 2017, pp. 103–111). If needed, the conformation of the compounds can be minimized to ensure optimum structure (Mirzaei et al, 2015, pp. 1063–1076; Anderson, 2011, pp.359–366). Furthermore, compounds can be protonated following the pH of the target solution (Onufriev and Alexov, 2013, pp. 181–209).

Table 7.3 List of some accessible databases

Database	Website	Availability	References
PubChem	www.pubchem.ncbi.nlm.nih.gov/	Public	(Kim et al,2016, pp. D1202–D1213)
ChEMBL	www.ebi.ac.uk/chembl/	Public	(Gaulton et al, 2012, pp. D1100–D1107)
BindingDB	www.bindingdb.org/bind/index.jsp	Public	(Liu et al, 2007, pp. D198–D201)
ZINC	www.zinc.docking.org/	Public	(Irwin et al, 2012, pp. 1757–1768)
ChemSpider	www.chemspider.com/	Public	(Williams et al, 2010, p. O16)

DrugBank	www.drugbank.com/	Public	(Wishart et al, 2018, pp. D1074–D1082)
ChemBridge	www.chembridge.com/	Commercial	(Desai et al, 2004, pp. 6609–6615)
Maybridge	www.fishersci.com/us/en/brands/I 9C8LZ4U/maybridge.html	Commercial	(Major and Smith l, 2011, p. 389364)
ChemDiv	www.chemdiv.com/	Commercial	(Patnaik, 2020, p. 254)
Life Chemicals	www.lifechemicals.com/	Commercial	(Wang Et al, 2018, pp. D1074–D1082)
Specs	www.specs.net/	Commercial	(Zhang, Zhu and Li, 2013, pp. 301–310)
Enamine	https://enamine.net/	Commercial	(Pérez-Regidor et al, 2016, p. 1508)

7.3.3.2. Docking and scoring functions

Molecular docking has gained much importance as a drug discovery tool since the mid-1970s. The molecular docking strategy is used to study the interaction between a ligand and a protein at the atomic scale, permitting us to characterize small molecule activity in target protein active sites and explain essential biological processes (Meng et al, 2011, pp. 146–157; Pinzi and Rastelli, 2019, p. 4331).

The docking technique consists of two basic procedures: estimating the ligand conformation and its location and orientation inside this pocket (typically called pose) and determining the binding affinity of the ligand-receptor complexes (Ferreira et al, 2015, pp. 13384–13421; Meng et al, 2011, pp. 146–157). In other words, sampling, and scoring (Huang and Zou, 2010b, pp. 262–273). Fisher proposed the Lock–Key Model hypothesis in 1894, and it was 1st used to describe the theoretical model of receptor–

ligand interaction, which claimed that ligands and receptors might distinguish each other via geometric and energy coordinates (Chen, Seukep, A and Guo, 2020, p. 545; Pagadala, Syed and Tuszynski, 2017, pp. 91–102), and either the ligand or the receptor were considered as rigid bodies (Meng et al, 2011, pp. 146–157; Pagadala, Syed and Tuszynski, 2017, pp. 91–102).

In 1958, Koshland suggest the Induced Fit Theory regarding the disadvantages of the Lock–Key Model and the modifications in enzyme conformation caused by substrate induction during the enzyme-substrate interaction (Chen, Seukep, A and Guo, 2020, p. 545; Pagadala, Syed and Tuszynski, 2017, pp. 91–102). According to this principle, the ligand and receptor should be flexible during docking. As a result, it may identify the binding events more effectively than the rigid procedure (Meng et al, 2011, pp. 146–157).

Given the limitations of computer resources, docking has just been conducted for an extended period with a flexible compoundand a rigid receptor. It continues to be a powerful method used nowadays. Several attempts have been principally made to deal with receptor flexibility; furthermore, flexible target docking, notably backbone flexibility in receptors, makes it very difficult for current docking approaches (Meng et al, 2011, pp. 146–157; Pagadala, Syed and Tuszynski, 2017, pp. 91–102).

- **Molecular docking methodologies**

a.   *Rigid docking:* The conformations of the ligands and target do not modify in the Rigid Docking computation; just the spatial location and posture of the 2 molecules vary (Meng et al, 2011, pp. 146–157). The dimensional conformation of the ligand and receptor is assumed to be unchanged in this molecular docking. Specifically, because of the easiest measurement challenge and calculation amount, this docking method is the most useful (Chen, Seukep, A and Guo, 2020, p. 545). As a result, it is appropriate for studying docking systems with pretty large structures, like protein-protein and protein-nucleic acid complexes (Vakser, 2014, pp. 1785–1793). DOCK, FLOG, and some protein-protein docking software, including FTDOCK, used an approach that held the

ligand and receptor rigid throughout the docking process (Meng et al, 2011, pp. 146–157; Chen and Zhi, 2001, pp. 217–226).

b. *Flexible docking:* The conformations of the ligand and target are enabled to modify spontaneously during the flexible docking measurement. Since this sort of molecular docking is remarkably accurate and strongly matches the real docking circumstance, it is frequently employed to study the identification between two molecules (Pagadala, Syed and Tuszynski, 2017, pp. 91–102). Due to the geometric development of variables with the atomic number in the model, the flexible docking approach is computationally expensive and time-consuming, necessitating high demands on PC software and hardware devices. FlexX is a very well-known molecular docking software for this docking (Meng et al, 2011, pp. 146–157; Chen and Zhi, 2001, pp. 217–226; Pagadala, Syed and Tuszynski, 2017, pp. 91–102).

c. *Semi-flexible docking:* The receptor's conformation is rigid and constant throughout the semi-flexible docking calculation process. Only the ligand's conformation can adjust within a certain limit, like adjusting the bond angle and bond length of certain non-critical elements. To measure and estimate the model, such a docking approach is usually used in docking simulations between ligands and target (proteins, enzymes, and nucleic acids). FlexX, Dock, AutoDock, and other semi-flexible docking programs are currently used in this docking (Meng et al, 2011, pp. 146–157; Chen and Zhi, 2001, pp. 217–226; Pagadala, Syed and Tuszynski, 2017, pp. 91–102).

- **Molecular docking software**

In the last decades, over than 50 different docking tools and software for both academic and commercial use have been developed like such as DOCK, AutoDock, FlexX, Surflex, GOLD, ICM, Glide, Cdocker, LigandFit, MCDock, FRED, MOE-Dock, LeDock, AutoDock Vina, rDock, UCSF Dock, and many others (Pagadala, Syed and Tuszynski, 2017, pp. 91–102Glaab, 2016, pp. 352–366). Most of them are docking software for small molecules (ligands) and proteins (receptors) and docking software for protein-protein, protein–DNA, and protein–RNA molecules. This docking system had

been launched by laboratories and was initially freely available. When software is updated with only a few bugs, it can be obtained by a professional commercial software firm and used as an element in a complex software kit (Chen, Seukep, A and Guo, 2020, p. 545).

• **Molecular docking scoring functions**

Docking software tools cover a wide scale of structure representation and search strategies, supplemented by a similarly diverse variety of scoring functions used to analyze docking poses (Glaab, 2016, pp. 352–366). The scoring function's goal is to separate valid poses from inaccurate poses or binders from inactive compounds in a decent time. On the other hand, scoring functions imply predicting instead of measuring the Ki between the target and the ligand, and these functions use a variety of predictions and simplifications (Meng et al, 2011, pp. 146–157).

There are three types of approaches for docking software according to the scoring function (Teramoto and Fukunishi, 2007, pp. 526–534, pp. 526–534; Meng et al, 2011, pp. 146–157), force-field, empirical, and knowledge-based (Huang, Grinter and Zou, 2010, pp. 12899–12908; Huang and Zou, 2010a, pp. 3016–3034):

a. **Classical molecular mechanics or force field-based methods**: Classical force-field-based scoring functions determine the free energy by adding the non-bonded (electrostatics and van der Waals) interactions. In addition, Hydrogen bonds, solvations, and entropy contributions are all considered in extensions of force-field-based scoring functions (Meng et al, 2011, pp. 146–157).

Extended force fields like AMBER and CHARMM and variants applied in Dock, GoldScore, and AutoDock (Huang, Grinter and Zou, 2010, pp. 12899–12908; Ferreira et al, 2015, pp. 13384–13421; Meng et al, 2011, pp. 146–157).

$$V = W_{vdw} \sum_{ij} \left(\frac{A_{ij}}{r_{ij}^{12}} - \frac{B_{ij}}{r_{ij}^6} \right) + W_{hbond} ij(t) \left(\frac{C_{ij}}{r_{ij}^{12}} - \frac{D_{ij}}{r_{ij}^{10}} \right) + W_{elec} ij \frac{q_i q_j}{e(r_{ij}) r_{ij}} +$$

$$W_{sol} \sum_{ij} (SiVj + SiVj) e(-r_{ij}^2 / 2\sigma^2) \qquad (7.1)$$

The total of van der Waals, hydrogen bond, coulomb energy, and desolvation is used to calculate the pair-wise atomic energy of two atoms I j. The weighted factors W are used to adjust the empirical free energy (Meng et al, 2011, pp. 146–157).

b. **Empirical scoring functions:** Estimated by regression analysis of experimental structural and binding score details (Guedes, Pereira and Dardenne, 2018, p. 1089; Eldridge et al, 1997, pp. 425–445). ChemScore, FlexX/F-Score, X-Score, GlideScore, LUDI, PLP, Cyscore, ID-Score, and Surflex are examples of software programs that provide such functions to users (Ferreira et al, 2015, pp. 13384–13421; Huang, Grinter and Zou, 2010, pp. 12899–12908; Meng et al, 2011, pp. 146–157). Founded on the concept that the free energy of binding can be connected to several unrelated parameters (Böhm, 1994; Guedes, Pereira and Dardenne, 2018, p. 1089).

For example, the empirical scoring function from FlexX:

$$\Delta G = \Delta G_0 + \Delta G_{rot} \times N_{rot} + \Delta G_{hb} \sum_{neutral\ H-bond} f(\Delta R, \Delta \alpha) +$$

$$\Delta G_{io} \sum_{ion\ init} f(\Delta R, \Delta \alpha) + \Delta G_{aro} \sum_{aro\ init} f(\Delta R, \Delta \alpha) + \Delta G_{lipo} \sum_{lipo\ cont} f^*(\Delta R) \quad (7.2)$$

Where:

ΔG: The calculatedfree free energy

ΔG_0: The regression constant

$\Delta G_{rot}, \Delta G_{hb}, \Delta G_{io}, \Delta G_{aro}, \Delta G_{lipo}$: Regression coefficients

$f(\Delta R, \Delta \alpha)$: Scaling function penalizing deviations

N_{rot}: The free rotate bonds that are immobilized in the system

(Meng et al, 2011, pp. 146–157).

c. **Knowledge-based scoring functions**: Generated from knowledge obtained from solved crystal structures. Software like DrugScore, DSX, PMF, ITScore, SMoG, STScore, and ASP profide that (Ferreira et al, 2015, pp. 13384–13421; Meng et al, 2011, pp. 146–157; Huang, Grinter and Zou, 2010, pp. 12899–12908).

$$PM\_score = \sum_{kIr < rij_{cut-off}} A_{ij}(r) \qquad (7.3a)$$

$$A_{ij}(r) = -\kappa_B T \ln \left[f^i_{vol_corr}(r) \frac{\rho^{ij}_{seg}(r)}{\rho^{ij}_{bulk}} \right] \qquad (7.3b)$$

Where:

k_B: The Boltzmann constant

T: The Temperature

r: The atom pair distance

$f_{Vol\_corr}(r)$: The compound volume correction factor

$\rho^{ij}_{seg}(r)$ / ρ^{ij}_{bulk}: The radial distribution function of a protein atom of type i and a compound atom of type j (Meng et al, 2011, pp. 146–157).

- **Consensus scoring**

Consensus scoring is a technique of protein-ligand docking and not a specific scoring function. It increases the chances of discovering an accurate result by integrating scoring information from different scoring functions to compensate the failures of the individual scoring functions (Teramoto and Fukunishi, 2007, pp. 526–534; Teramoto and Fukunishi, 2008, pp. 747–754). As a result, the major challenge in consensus scoring is finding how to establish the combination rule for individual scores so that proper binder can be distinguished from others using the consensus calculation, for example of consensus scoring methods MultiScore and X-Cscore (Huang and Zou, 2010b, pp. 262–273; Obiol-Pardo and Rubio-Martinez, pp. 134–142, 2007; Teramoto and Fukunishi, 2007, pp. 526–534). In addition, "rank-by-number" is a consensus scoring method in which each binding pose's consensus score is the mean of the values calculated by correspondingly independent scoring function in a defined consensus scoring scheme (Liu et al, 2012, p. e38086).

7.3.3.3. MD simulations

MD simulations are defined as the science that imitates a system of particles (Karplus and Petsko, 1990, pp. 631–639). MD simulations calculate how each atom in a target or other molecular system may migrate over time based on a general physics model governing interatomic interactions. Although, the first simple gasses MD simulations were performed in the 1950s, and the first protein MD simulation in the 1970s, the foundation that enabled these simulations was among the accomplishments

acknowledged by the 2013 Nobel Prize in Chemistry (Hollingsworth and Dror, 2018, pp. 1129–1143). In addition, the history of molecular dynamics can be traced from Galileo's time (1564-1642) to the present day (Hoover et al, 1983, pp.29–46).

i.   MD applications: For decades, X-ray crystallography has been the most important experimental technique to explain the three-dimensional structure of biological macromolecules; conversely, it can only give a static snapshot of a functional state of a protein **(**Srivastava et al, 2018, p. 3401). Therefore, Nuclear magnetic resonance (NMR) spectroscopy has been rapidly used because it offers many features: Over a large range of timescales, the dynamics of protein folding, structural fluctuations, internal mobility, and chemical exchange of target molecules can be studied. Furthermore, physiological conditions may be employed to study protein-protein or protein–ligand interactions (Sugiki, Kobayashi and Fujiwara, 2017, pp. 328–339).

 NMR spectroscopy has some limitations. Consequently, MD simulations are often used to help understand NMR dynamic experiments and to discover new leads that can be followed up experimentally. MD may also be used to conduct experiments that aren't possible with NMR, such as focusing on a single molecule instead of an ensemble average (Fisette et al, 2012, p. 254208).

MD offers energetic information about protein and ligand interactions and solve some hard problems which cannot be solved by experimental methods alone, as the pathogenic pathway of diseases due to the protein misfolding, VS, and drug resistance mechanisms caused by target mutations (Liu et al, 2018, pp. 23–37).

ii.   Molecular dynamics simulations principles: Newton's second law, also known as the equation of motion, supports the MD simulation process to study the time independent performance of the systems (De Vivo et al, 2016, pp. 4035-4061):

$$f_i\left(t\right) = m_i a_i(t) = -\frac{\sigma V\left(x(t)\right)}{\sigma x_i(t)} \qquad (7.4)$$

f_i (t): The net potency applicated on the $_i$th atom of the system at a fixed point in time t

a_i (t): The acceleration

m_i: The mass

In (7.4), the location of the N interacting atoms in the Cartesian space, expressed by the sudden configuration of the system i denoted by the vector x(t).

The empirical potential power function is introduced V(x) in (7.4), the FF or MM is the model that results from this simplified representation:

$$V = \sum_i^{bonds} \frac{k_{l;i}}{2} \left(l_i - l_{0,i}\right)1^2 + \sum_i^{angles} \frac{k_{\alpha,i}}{2} \left(\alpha_i - \alpha_{0,i}\right)^2 +$$

$$\sum_i^{torsion} \left\{ \sum_k^M \frac{V_{ik}}{2} \left[1 + cos\left(n_{ik}.\theta - \theta_{0,ik}\right)\right] \right\} + \sum_{i,j}^{pairs} \varepsilon_{ij} \left[\left(\frac{r_{0,ij}}{r_{ij}}\right)^{12} - \right.$$

$$\left. 2\left(\frac{r_{0,ij}}{r_{ij}}\right)^6 \right] + \sum_{i,j}^{pairs} \frac{q_i q_j}{4\pi\epsilon_0\epsilon_r r_{ij}} \tag{7.5}$$

In (7.5):

1.   The 1st three terms are the intramolecular interactions of the atoms
2.   The 4th and 5th terms are van der Waals and electrostatic interactions between atoms or "non-bonded" at the time (t + δt) are estimated by current positions, velocities (v(t)), and accelerations given by:

$$x_i(t + \delta t) = x_i(t) + v_i(t)\delta t + \frac{1}{2}a_i(t)\delta t^2 \tag{7.6}$$

After that, the velocities are generated in the following manner:

$$v_i(t + \delta t) = v_i(t) + \frac{1}{2}[a_i(t) + a_i(t + \delta t)]\delta t \tag{7.7}$$

iii.   **Advantages and limitations:** The main advantage of MD simulations is in specifically treating structural elasticity and entropic effects (De Vivo et al, 2016, pp. 4035-4061).

Besides the calculations in the simulations involving high computational and memory costs (Nicolas-Barreales, Sujar and Sanchez, 2021, pp. 1–18), MD simulations are still constrained by major issues:

- The force fields used need refinement in certain cases to an ineffective sampling of conformational states (Durrant and McCammon, 2011, p. 71).
- The time scales are too short of addressing several interesting and important molecular events (Elber, 2016, p. 60901).

iv. **Popular molecular dynamics simulations software:** There are many software tools available for MD of biomolecules (Salo-Ahen et al, 2020, pp. 71):

- **ACEMD:** A production-class biomolecular dynamics (MD) engine which supports CHARMM and AMBER force fields. Free Serial Version (for Academia). It is capable of supercomputing scale efficiency of 40 ns per day for all-atom protein systems with over 23 000 atoms due to its GPU-specific design (Harvey, Giupponi and Fabritiis, 2009, pp. 1632–1639).
- **Amber:** A paid MD Engines supports AMBER force fields, GAFF (the general AMBER force field) (Case et al, 2005, pp. 1668–1688).
- **CHARMM:** CHARMM (Chemistry at Harvard Molecular Mechanics). It is a free serial high-performance version supporting large-scale parallelism and GPUs, supporting CHARMM and Amber force fields (Brooks et al, 2009, pp. 1545–1614).
- **Desmond:** A free MD Engines, available in a graphics processing unit (GPU) accelerated version (Gioia et al,2017). Supported force fields by Desmond are: CHARMM (22,27,32,36), AMBER (94,96,99,03), and OPLS (2001,2005), in addition to several in-house-developed variants (such as CHARMM22 and AMBER99SB-ILDN) (Bowers et al, 2006, p. 43).
- **GROMACS:** It is an open-source and free tool that supports GPU. All commonly used molecular mechanics force fields can be included, and 15 AMBER's varieties, CHARMM, GROMOS, and OPLS, have been validated and included (Abraham et al, 2015, pp. 19–25).

- **DL_POLY:** A highly parallel molecular dynamics simulation program provides a highly efficient range of methods and algorithms. It is accessible at no charge to academic scientists performing non-commercial research, supporting GPU (Todorov et al, 2006, p. 1911).

- **NAMD:** Or Nanoscale Molecular Dynamics, a parallel molecular dynamics application crafted for high-performance simulations of very large biological objects using CPU and GPU architectures, was the first fully featured MD kit to take advantage of GPU acceleration. It was also an early adopter of GPU-accelerated clusters. It utilizes CHARMM, AMBER, OPLS, and GROMOS biomolecular force fields (Phillips et al, 2020, p. 044130). NAMD is Based on Charm++ parallel objects and can scale to hundreds of cores for standard simulations and further than 500,000 cores for the most complex simulations. (Acun et al,2018, pp. 4:1-4:9).

v.   **Force fields used in molecular dynamics simulations:** MD simulations are created according by elucidating Newton's equations of motion using molecular mechanics or empirical force field (FF) to obtain the necessary forces (Lin and MacKerell, 2019, pp. 21–54). The FF is a mathematical term that describes the relationship between a system's energy and its particle coordinates. It consists of a series of parameters that enter into an analytical form of the interatomic potential energy, U. Gavezzotti provides a historical account of the progress of FFs in relation to molecular mechanics (González, 2011, pp. 169–200). For different types of molecules, several forces fields have been developed (**Table 7.4)** (Salo-Ahen et al, 2020, pp. 71).

Table 7.4 Generally used FF in MD simulations (Salo-Ahen et al, 2020, pp. 71).

Molecule	FF
Proteins	AMBER CHARMM GROMOS OPLS-AA GAFF CGenFF
Small organic molecules	CGenFF) MMFF OPLS3 GROMOS96
Lipids	GROMOS (45A3, 53A6, 54A7/8) Berger lipid FF CHARMM (C36 lipid FF C36-UA) Slipids FF AMBER (LIPID14 FF)

8. MATERIALS AND METHODS

8.1. Target Identification and Validation

The first critical phases in the drug discovery pipeline are target classification and validation. Drug target validation could be highly beneficial for potential drug discovery and development and increase the knowledge of the pathophysiology of target-related disorders. The protein database (http://www.rcsb.org/) is frequently used to obtain the macromolecular structure. The most widely employed structures for drug design are those found by X-ray diffraction data, though solution structures produced by NMR methods and homology models can also be beneficial (Anderson, 2011, pp. 359–366). A good target must be efficient, nontoxic, satisfy clinical and commercial requirements, and, above all else, be 'druggable.' A druggable target is available to the potential drug molecule, whether it is a small molecule or a larger biological structure, and when bound induces a biological response which can be quantified *In vitro* and *In vivo* (Hughes et al, 2011, pp. 1239–1249).

Because NO is a free radical that is usually assumed to lead to oxidative stress and the damage of molecules and tissues, it is interesting that it has so many critical physiological benefits. Apart from some pathological states where extra NO is released, the cell is defended from NO's negative impacts. Tissue damage and oxidative stress can occur in this circumstance, resulting in many maladies such as rheumatoid arthritis, AD, PD, and others. It has been demonstrated in many cases that targeting NOS has a beneficial effect and regulates NO rate. One hundred forty-three crystal structures of NOS were collected from the Research Collaborators for Structural Bioinformatics Protein Data Bank (RCBS PDB). The website (https://www.rcsb.org/) can be simply checked for 3-D protein structures using different search possibilities such as authors, macromolecules, sequence, and ligand (Parasuraman, 2012, pp. 351–352).
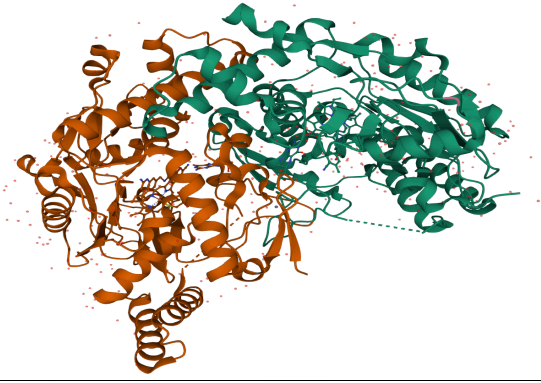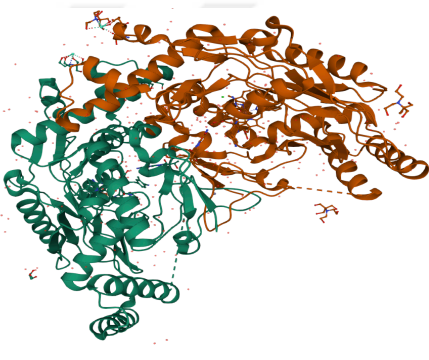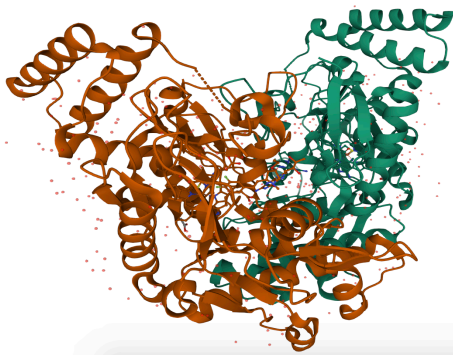
8.1.1. Sequence alignment and structural superimposition

Superposition is a popular procedure for measuring the spatial resemblance of 3D objects in fields such as computer vision, image science, and molecular biology. Superposition is used in molecular biology and structural bioinformatics to facilitate a wide variety of objectives (Lu et al, 2016, p. 18). Sequence alignment viewers are a handy technique for visualizing similarities and differences in the amino acid sequences of related proteins. In certain situations, the simple one-letter amino acid codes are supplemented with colors to represent a unique identity of each residue, like hydrophobicity, or recognized properties, such as the presence of post-translational changes. This concept has been expanded to analyze the folded protein's residue structure or microenvironment (Pitt, Montalvão and Blundell, 2014, p. 324).

For the sequence alignment and structural superimposition of NOS, we randomly selected three human NOS isoforms hnNOS: 5VV5, heNOS: 5VVB, and hiNOS: 3E7G, to measure the sequence and structure similarity between the three NOS isoforms within the same species. To evaluate the sequence and structure similarity of the neuronal NOS isoform of different species, we selected the following enzymes human neuronal NOS: 5VV5, and rat neuronal NOS: 6NHE **(Table 8.1).**

For that purpose, we used BIOVIA Discovery Studio (DS) "Align Sequences" tool kit (https://www.3ds.com/); BIOVIA DS is a sophisticated tools package for studying and modeling molecular structures sequences and other information of interest to life scientists. The program contains data viewing and editing capabilities, as well as tools for performing fundamental data analysis.

Table 8.1 NOS isoforms used for Sequence alignment and structural superimposition.

PDB ID	Type	Structure
5VV5	Human nNOS	
5VVB	Human eNOS	
3E7G	Human iNOS	
6NHE	Rat nNOS	

8.1.2. Structure-based phylogenetic analysis

Johnson and colleagues were the first to use 3-D structures to construct phylogenetic trees for a range of protein families. It compares evolutionary relationships between homologous protein families determined simply from amino acid sequences to those derived purely from 3-D structures (Balaji and Srinivasan, 2007, pp. 83–96).

The phylogenetic tree was produced and visualized via the webserver: www.phylogeny.fr/simple_phylogeny.cgi (Dereeper et al, 2010, p. 8), to see if the three NOS isoforms form one related group or that different groups could be notable. The following NOS isoforms were picked randomly and used in this step:

- Human neuronal NOS: PDB ID 5VV5
- Human endothelial NOS: PDB ID 5VVB
- Human inducible NOS: PDB ID 3E7G
- Rat neuronal NOS : PDB ID 6NHE

8.1.3. Molecular docking with known inhibitors

To reproduce experimental crystallographic poses 'docking' method was employed, where the native ligands were docked to the binding site in a target (NOS isoforms). The docking programs' accuracy differs significantly between software and structures in the validation data when predicting the complex's crystallographic pose. We used the crystal structures of NOS isoforms containing co-crystallized small molecules obtained from the Protein Data Bank and mentioned above. The known inhibitors available were scored using AutoDock Tools (ADT) (Morris, Huey and Olson, 2008).

i.   **Requirements:** In order to perform molecular docking, we used the software shown in **Table 8.2**.

Table 8.2   The software used for molecular docking.

MGL tools	www.mgltools.scripps.edu/downloads
Cygwin	http://www.cygwin.com/install.html
DS Visualizer	www.accelrys.com/products/discovery-studio/visualization-download.php
Binary files	www.autodock.scripps.edu

ii.   **AutoDock and AutoDock tools:** AutoDock and AutoDock Tools have been free tools since 1990, which were widely cited in the previous works as an indispensable tool in structure-based drug discovery. (El-Hachem et al, 2017, pp. 391–403). The graphical user interface for AutoDock is found on http://autodock.scripps.edu/. AutoDock is a C program suite that estimates the binding conformations of a small, flexible compound to the specific target. The method integrates simulated annealing for conformation searches with a fast grid-based energy performance measure (Goodsell, Morris and Olson, 1996, pp. 1–5).

The scoring function in AutoDock is the calculated docking energy of the ligand to the target. The ideal docking is the one that uses the minimum energy. AutoDock adopts a grid-based technique to accelerate the measurement of the energy function. Initially, the protein is pre-processed by a tool called AutoGrid, which adds probe atoms and charges at grid points mostly around protein and determines and records the energy function for further usage. Following that, AutoDock employs trilinear interpolation between grid points to calculate energy terms individually for each atom of the ligand. After that, it combines them to determine the amount of energy of the conformation (Rizvi, Shakil and Haneef, 2013, pp. 831–857). To evaluate a specific docking task, AutoDock provides several search algorithms. Monte Carlo Simulated Annealing (SA), a Genetic

Algorithm (GA), and a hybrid local search GA, also referred to as the Lamarckian Genetic Algorithm (LGA), are among them. The LGA outperforms the SA, GA, and LGA in determining the system's lowest energy (Dupanloup, Schneider and Excoffier, 2002, pp. 2571–2581). Generally, the initial step is to obtain the desired Ligand.pdb and Target.pdb files from relevant databases. Step two is to use AutoDock to prepare PDBQT format files for Target and Ligand (Target.pdbqt, Ligand.pdbqt) as well as Grid and Docking parameter files (System.gpf and system.dpf). The third step is to use Cygwin to execute MD, and then the outputs are evaluated (Forli et al, 2016, pp. 905–919).

iii.   **Targets and ligands preparation and optimization process:** First, we separated the native ligands or the inhibitors from the complexes selected above, and we deleted water and Zinc molecules and kept just Chain A (Because NOS is a homo-dimer enzyme, for that reason, one chain is enough to work with) with Heme and H4B as cofactors in each enzyme using BIOVIA DS. After that, we Refined the target structure (or Chain A), including adjusting the side chain orientations, adding missing residues, adding hydrogens because hydrogens are usually absent from the 3D structures determined with data at resolutions lower than 1 Å or for other reasons. Then we picked the appropriate protonation states. This step can be done using the AutoDock tool 1.5.6 (ADT) or BIOVIA DS. In the end, the targets were saved in pdb format for later. To prepare the ligand, we used BIOVIA DS 'Sketch and edit molecule' tool to draw the structure of the ligands like the native ligands deleted from the complexes earlier. In addition, we added hydrogen and fixed the chirality and the valence if needed. Finally, we used the 'Clean geometry' tool and saved the ligands in pdb format.

iv.   **Re-docking:** The coordinates x, y, and z of each native ligand were identified using BIOVIA DS to perform the molecular docking using AutoDock. The gpf outputs were prepared with 60^3 Å grid points selected for three-dimension of the grid box to make sure that it covered the whole ligand as well as the binding site, 'Center on macromolecule' option was selected to move the ligands to the target binding site during the docking, docking space was kept by default at 0.375 Å, Population size 150, the maximum number of "evals" depending on the number rotatable bonds, and the

number of Genetic Algorithms GA Runs were 20. We added polar HB and Gasteiger charges, as well as the necessary number of torsional trees. Last, we used the Lamarckian Genetic Algorithm (LGA) to simulate the docking.

The following Windows and Unix commands were utilized for molecular docking:

Step 1:

> **Windows:**
>
> .\autogrid4.exe -p system.gpf -l system.glg
>
> **Unix:**
>
> autogrid4 -p system.gpf -l system.glg

Step 2:

> **Windows:**
>
> .\autodock4.exe -p system.dpf -l system.dlg
>
> **Unix:**
>
> autodock4 -p system.dpf -l system.dlg

8.1.4. Pearson correlation coefficient calculation

Correlation, in its widest sense, is a calculation of the strength of a connection between variables. Thus, a modification in the scale of one variable relates to a modification in the scale of another variable, in the same ((+) correlation) or reverse manner ((-) correlation) in linked data (Schober, Boer and Schwarte, 2018, pp. 1763–1768).

To measure the relationship between the experimental results from literature and the calculated docking results of the known inhibitors, we employed a primary method which is Pearson correlation coefficient calculation, to compare the correlation between the results and also to validate the docking tool 'AutoDock' and to select the candidates from the list of targets re-docked to use them for the next stage of the research.

For bilaterally normal distributions, the Pearson correlation coefficient is often adopted (data that follow a bivariate normal distribution) (Schober, Boer and Schwarte, 2018, pp. 1763–1768).

The Pearson correlation coefficient formula used is:

$$r = \left.\sum(xi - \bar{x})(yi - \bar{y})\middle/\sqrt{\sum(xi - \bar{x})2 \sum(yi - \bar{y})2}\right. \tag{8.1}$$

r: Correlation coefficient

xi: Values of the x-variable in a sample

$\bar{x}$: Mean of the values of the x-variable

yi: Values of the y-variable in a sample

$\bar{y}$: Mean of the values of the y-variable

The scale r $\pm$ 1 means an excellent positive correlation, and a perfect negative correlation.

8.2. Structure-Based VS

The use of f speedy and economical computational algorithms to discover potentially active compounds using virtual databases is known as virtual screening (Dos Santos, Ferreira and Andricopulo, 2018, pp. 31–50). VS is becoming more popular in research. It is seen as a complementary technique to experimental screening (HTS); however, when combined with structural biology, it guarantees to improve the number of projects in the lead identification stage of the discovery phase while also improving their effectiveness (Lyne, 2002, pp.1047–1055). VS can be divided into 2 types: LBVS and RBVS. The ligand-based technique approach exploits data supplied by a ligand or group of ligands known to bind to the required target to detect additional compounds in the databases with similarities (Gimeno et al, 2019, p. 1375).

In our research, the target protein's structure is known. Therefore, receptor-based computational approaches were used. Protein-ligand docking was deployed for SBVS.

The protein's crystal structures (NOS) were used to estimate how the ligands in the VS library could interact with the binding pocket of different isoforms.

The SBVS method used involves the following steps:

- Molecular target identification and minimization.
- Compound database collection
- MD
- Finding's analysis

8.2.1. Characterization of the macromolecular target

The targets were selected from the last step of redocking and validation, the X-ray structures of NOS isoforms were nominated to be used in the following stages.

5VV0, 4CX7, and 6AV7 were retrieved from the PDB (http://www.rcsb.org). The targets were optimized by BIOVIA DS tools; only chain A with co-factors (Heme and BH4) were kept, and the native ligands, the water, and zinc molecules were deleted. We added charges, checked the ionizations, and assigned the tautomers, and minimized the energies (**Table 8.3)**.

Table 8.3 The enzymes used for the docking process.

PDB ID	Isoform	Resolution (Å)	Organism	Chains	Sequence Length	Details
5VV0	nNOS	1.8	Homo sapiens	A, B	421	*EC:* 1.14.13.39
6AV7	eNOS	1.92	Homo sapiens	A, B, C, D	440	*EC:* 1.14.13.39
4CX7	iNOS	3.16	Homo sapiens	A, B, C, D	431	*EC:* 1.14.13.39

8.2.2. Ramachandran plots and other structure's evaluation

Sasisekharan established the use of torsion angles to characterize polypeptide and protein conformation while studying the structure of collagen chains as a doctoral student in G.N. Ramachandran's research team. The effectiveness of this strategy was immediately apparent, and its application spread swiftly. Given the new definitions, this so-called Ramachandran plot aka, ϕ, ψ-plot has been essentially unaltered over the last 50 years, a vital technique for protein structure research (Hollingsworth and Karplus, 2010, pp. 271–283).

The Ramachandran plot is a two-dimensional visualization of the protein backbone's φ-ψ torsion angles. It offers a fundamental perspective of a protein's structure. In the Ramachandran plot, the φ-ψ angles cluster into several zones, each corresponding to a unique secondary structure. Ramachandran plots are organized into four categories based on the stereochemistry of the AA: generic (it refers to the 18 non-glycine non-proline amino acids), glycine, proline, and pre-proline (which relates to residues preceding a proline) (Ho and Brasseur, 2005, p. 14). The Ramachandran plots and other evaluations of NOSs's structures were accomplished via the online server: https://saves.mbi.ucla.edu/.

8.2.3. Binding site prediction

In a structure-based drug discovery method, identifying druggable cavities or pockets on a target molecule is critical for developing novel techniques. Binding sites (BSs), whether with or without ligand, are typically referred to as cavities on the protein surface and come in a wide range of different shapes and sizes (Harigua-Souiai et al, 2015, p. 93). Potential H-bond donors and acceptors, unique hydrophobic surfaces, and molecular surface size are binding site properties that are critical for the ligand binding (Andersson, Chen and Linusson, 2010, pp. 1408–1422).

The binding sites and the binding residues involved were generated using the webserver GalaxyWEB (http://galaxy.seoklab.org/). The GalaxyWEB server uses template-based modeling to predict protein structure from sequence and structure-based modeling to

optimize loop or terminal regions. This web server is based on the technology known as 'Seok-server,' which was evaluated as one of the best ranked template-based modeling platforms in CASP9 (9th Critical Assessment of Techniques for Protein Structure Prediction) (Ko et al, 2012, pp. W294–W297).

8.2.4.   Grid generation

The size of a search space used to find minimum energy binding poses of drug candidates is among the essential factor for ligand docking. Many of the currently accessible docking programs include a default approach for estimating box size; but several of these approaches have not been well validated.

Molecular docking is usually done with the default grid box size, which is determined based on the coordinates of the native ligand binding to the target protein in the experimental structure. Furthermore, unlike their chemical structures, the coordinates of bound ligands are not usually available. Moreover, the radius of gyration, Rg, a commonly used scale of a molecule's dimensions and mass distribution, can efficiently represent its size (Feinstein and Brylinski, 2015,p. 18).

In this study, the targets grid were generated around the binding site residues identified using AutoDock according to the literature review and confirmed by BIOVIA discovery studio and HotSpot Wizard 3.0 webserver (https://loschmidt.chemi.muni.cz/hotspotwizard/), which is used generally in semi-rational protein design for the automated discovery of hotspots to optimize protein stability, catalytic activity, substrate specificity, and enantioselectivity (Sumbalova et al, 2018, pp. W356–W362).

8.2.5. Database's collection

It is well known that a compound library's content and structure quality have significant implications for the success of a DBVS project. The databases frequently contain lots of small-molecule compounds, ranging from tens of thousands to millions. Therefore, designing a specialized library for specific purposes may be a more object-oriented and efficient method. (Cheng et al, 2012, pp. 133–141). It is imperative to have an easy-access database of purchasable compounds. Databases are classified into four types: a) generic virtual high throughput (vHTS) databases, which comprise massive amounts of ligands; b) diversity-oriented databases that contain highly chemically diverse compounds; c) target-oriented databases that are constructed with a precise, clear aim; d) molecular property diversity databases, that are constructed with particular molecular property statuses (namely solubility, lipophilicity, etc.), and e) natural product databases (Lionta et al, 2014, pp. 1923–1938) (**Table 8.4**).

- **ZINC15 Database:** ZINC gives access to high-value molecules such as metabolites, drugs, natural products, and annotated compounds from the research. Compounds can be obtained through the genes for which they are annotated and through the major and minor target classes to which those genes relate. Thus, it provides new analytic tools that are simple for non-specialists. ZINC preserves its original three-dimensional basis; all molecules are accessible in biologically relevant, prepared formats. ZINC is accessible for free at http://zinc15.docking.org (Sterling and Irwin, 2015, pp. 2324–2337).

- **Otava Chemicals Database:** It is a universal science-based chemical firm that operates in researching and manufacturing specialized chemicals, bio-chemicals, and bioanalytical reagents. They provide over 200,000 compounds for high-throughput screening (HTS), comprising more than 200 target-focused libraries (PK, Proteases, GPCRs, Ion Channels, Epigenetic receptors, and others), as well as libraries of Fragments, Lead-like, Drug-like, and CNS compounds. Additionally, special library design is available if needed (https://www.otavachemicals.com/).

- **PubChem Bioassay Database:** Provides unique, validated chemical structures (small molecules) that may be found by searching for names, synonyms, or keywords. If multiple depositors provided the same structure, the compound data might be associated

with more than one PubChem Substance data. All Compound entries provide approved chemical representation information that has been supplied to characterize compounds in PubChem Substance. PubChem Compounds structures are pre-clustered and cross-referenced by identity and similarity categories. Furthermore, calculated characteristics and descriptors can be used to find and filter chemical structures (https://pubchem.ncbi.nlm.nih.gov/).

- **ChEMBL Database:** ChEMBL is a freely accessible, manually maintained library of bioactive molecules having drug-like characteristics. The database is exceptional in its concentration on all elements of drug discovery as well as its size, with data on over 1.5 million compounds and over 10 million data on their impacts on biological systems (https://www.ebi.ac.uk/training/online/courses/chembl-quick-tour/what-is-chembl/).

- **Drug Bank:** Drug Bank (www.drugbank.ca) is a web-based database that contains detailed molecular data about drugs, their functions, interactions, and receptors. Includes data on the effects of hundreds of drugs on metabolite levels (Pharmaco-metabolomics), gene expression levels (pharmaco-transcriptomics), and protein expression levels (pharmaco-transcriptomics) (Pharmaco-proteomics) (Wishart et al, 2018, pp. D1074–D1082). Drug Bank has been extensively implemented to facilitate the discovery of *In silico* drug targets, drug design, drug docking or screening, drug metabolism prediction, drug interaction prediction (Wishart et al, 2008, pp. D901–D906).

Table 8.4 The databases used for the SBVS.

Database	Compounds retrieved	Website
ZINC15	230 000000	www.zinc15.docking.org/
Otava chemicals	270000	www.otavachemicals.com/
Protein-protein interactions (PPI-lib)	500000	www.asinex.com/ppi/
PubChem Database	3574650	www.pubchem.ncbi.nlm.nih.gov/
Food library	26941	www.foodb.ca/
ChEMBL	1961462	www.ebi.ac.uk/chembl/
Natural product compound collection (NP-lib)	380,000	www.lifechemicals.com/screening-libraries/natural-product-like-compound-library
Drug Bank	9591	www.drugbank.ca/
SuperDrug2	3992	www.cheminfo.charite.de/superdrug2/index.html
SMMDB	6509	www.bsbe.iiti.ac.in/bsbe/smmdb/

8.2.6. Databases preparation for SBVS

Because there is no "perfect" chemical database, we must expend considerable effort in cleaning up the Collection, regardless of whether it contains Virtuals, Reals, or Tangibles (Bologa and Oprea, 2012, pp. 125–143).

Many chemical suppliers offer their specific approach to this issue. FILTER is our preferred option. Despite the technique, we made specific fundamental changes to the collection's "make-up." One apparent solution is to eliminate "unwanted" compounds.

Furthermore, compounds are typically derived from databases in some form of one-dimensional (1D) format (SMILES, InChI, fingerprints, etc.), and many in-silico procedures are mandated to transform each of them to a proper 3D structure in order to conduct molecular docking, especially if all relevant enantiomers and tautomers at physiological pH are to be regarded (Radusky et al, 2017, pp. 1741–1746). In this study, BIOVIA DS was used to adjust the geometry by minimizing the energy with correct chiralities of ligands, and the missed hydrogens were added, and the duplicated compounds were deleted.

8.2.7. Screening using AutoDock Vina

AutoDock Vina, an original MD and VS software, was developed in the same research facility as the well-known AutoDock 4 (Jaghoori, Bleijlevens and Olabarriaga, 2016, pp. 237–249). Compared to earlier molecular docking tools (AutoDock 4), AutoDock Vina achieves a two-order-of-magnitude performance improvement. Autodock vina is free for academics, available from http://vina.scripps.edu/download.html. Vina's own optimization process employs a great gradient optimization algorithm. The gradient computation effectively gives the optimization algorithm with a "sense of direction" from one evaluation. Vina can accelerate calculating by employing multithreading multiple CPUs or CPU cores (Trott and Olson, 2010, pp. 455–461).

When starting the docking experiments, the maximum number of concurrent threads can be specified (by the command-line option CPU). Vina attempts to produce as many threads as the number of possible cores by default (Jaghoori, Bleijlevens and Olabarriaga, 2016, pp. 237–249). Because of the randomized seeding of the computations, performing the same execution on the same ligand-protein can result in different binding modes. However, Vina enables us to manually select an initial randomization seed to recreate the docking outcomes (Jaghoori, Bleijlevens and

Olabarriaga, 2016, pp. 237–249). Running Vina on a multi-core processor is the simplest approach to screen a ligand database, although this is only appropriate for smaller databases. Several studies utilized freely available scripts to consecutively evaluate all the compounds in the database (Abreu et al, 2010, p. 10). AutoDock Vina employs an evolutionary search and a powerful hybrid scoring function (empirical and knowledge-based) to find the lowest-energy docking conformations (Hassan et al, 2017, p. 15451). In our study, the exhaustiveness, or time invested in the analysis, was already intuitively adjusted based on the number of atoms and flexibility. The parameters used in the docking process via Vina are mentioned in the following table (**Table 8.5**).

Table 8.5 Grid mapping parameters used for virtual screening docking against respective enzymes.

Center (Å)	x	y	z
5VV0 (h nNOS)	121.76	248.52	357.46
4CX7 (h iNOS)	120.02	245.95	360.55
6AV7 (h eNOS)	63.11	29.13	-184.71
Size	x	y	z
	22	22	22
Exhaustiveness		8	

The following process and command lines were used to do SBVS using vina on Ubuntu:

- Autodock vina (www.vina.scripps.edu/download.html)
- Python (https://www.python.org/downloads/)
- Pymol (https://pymol.org/2/)
- Openbabel (openbabel.org/wiki/Main_Page)

a. Receptor's preparation

We used these command lines to convert pdb files to pdbqt :

```
for i in `ls receptor*pdb`;do echo $i;grep ATOM $i | cut -c-66 > `basename
$i .pdb`.pdbqt;done
```

Or

```
obabel receptor.pdb -xr -O receptor.pdbqt
```

Or by running AutoDock.py script (https://github.com/sarisabban):

```
python3 AutoDock.py -r receptor.pdb
```

b. Ligand's preparation

We downloaded the ligands from previously mentioned databases and combined them:

```
python3 AutoDock.py -d FILENAME.wget
```

The next step was splitting the ligands file for virtual screening into multiples files; each one contains 24 ligands to facilitates the docking:

```
python3 AutoDock.py -s FILENAME.pdbqt  24
```

c. Searching for the space center (x.y.z) and size (x.y.z) using autodock or pymol

In the PyMOL software command terminal, we typed Box (0,0,0,1,1,1), then we adjusted numbers, to get the search box. We deleted the Box and Position objects before adjusting the numbers. After that, we entered the next command line in the vina terminal:

```
pymol AutoDock.py -b FILENAME.pdb
```

d.   Docking

We used this command line for each target and adjusted it according to the target's coordinates:

```
for file in ./Ligands/*/*; do tmp=${file%.pdbqt}; name="${tmp##*/}";
./vina --receptor receptor.pdbqt --ligand "$file" --out $name_out.pdbqt --log
$name.log --exhaustiveness 8 --center_x 0 --center_y 0 --center_z 10 --
size_x 60 --size_y 60 --size_z 60; awk '/^[-+]+$/{getline;print
FILENAME,$0}' $name.log >> temp; done; sort temp -nk 3 > Results; rm
temp; mkdir logs; mv *.log *.out logs
```

For example: x,y,z center (0.0.10) and size (60*60*60)the exhaustiveness 8. This command generates the log file and result file with just the docking best poses; we could modify it by deleting this part: (awk '/^[-+]+$/{getline;print FILENAME,$0}' $name.log >> temp; done) part in case of error message.

At the end of the AutoDock script, there is PBS script to run Autodock vina using a high-performance computer (Optional).

In PBS generation command, we replaced Exhaustiveness by 8, false for output,1 for CPU and 3 for array and our email to get notification when the run finished):

```
python3 AutoDock.py -j Center_X Center_Y Center_Z Size_X Size_Y
Size_Z Seed Exhaustiveness Output CPUs your Email
```

8.2.8.   ADMET and drug-likeness evaluation

Absorption, distribution, metabolism, excretion, and toxicity (ADMET) property prediction could be thought to have started in 1863 with a research on the effect of aqueous solubility on toxicity, in 1884 with a QSPR for melting point, or in 1968 with a QSPR for aqueous solubility as a function of the octanol – water partition coefficient, P (K_{ow}) (Dearden, 2007, pp. 635–639).

To reduce failures in the drug discovery process, ADMET evaluation is considered necessary. ADME identifies the pharmacokinetic concerns that determine if the drug molecule reaches the target receptor in the human body and how far does it last in the

bloodstream. Simultaneous calculation of drug candidates' efficiency and biopharmaceutical features has been established, and extensive investigations of ADMET approaches are now frequently conducted at a preliminary phase of drug development (Dong et al, 2018, p. 29).

Using the free web server SwissADME: www.swissadme.ch/index.php (Daina, Michielin, and Zoete, 2017, p. 42717), important ADMET properties were calculated, SwissADME gives free access to a groop of rapid but rigorous calculations for physicochemical characteristics, pharmacokinetics, drug-likeness, and medicinal chemistry compatibility, including in-house approaches such as the BOILED-Egg, iLOGP, and Bioavailability Radar. A user-friendly interface ensures fast and straightforward input and interpretation. The input zone includes a molecular sketcher constructed on ChemAxon's Marvin JS (www.chemaxon.com), which allows the user to import (from a file or an external database), draw, and modify a 2D chemical structure before transferring it to a list of molecules (Daina, Michielin, and Zoete, 2017, p. 42717; Daina, Michielin, and Zoete, 2014, pp. 3284–3301). In addition, the polar surface area (PSA) has been evaluated and used as a molecular descriptor in the study of ligands transport properties like intestinal absorption and BBB penetration (Prasanna and Doerksen, 2009, pp. 21–41).

8.2.9. Lipinski's rule

The 'rule-of-five' RO5 (also referred to as 'Lipinski's rule of drug-likeness') is a highly effective approach for designing orally bioavailable small-molecule drugs (Zhang and Wilkinson, 2007, pp. 478–488) and based on the physicochemical properties of phase II drugs (Lipinski, 2016, pp. 34–41). The Lipinski rule of five helps in differentiating between drug-like and non-drug-like compounds. It suggests a great likelihood of accomplishment or failure caused by drug likeness for compounds that meet 2 or more of the following rules (Benet et al, 2016).

The Rule of 5 indicates that low absorption or permeation is more possible in the drug discovery context when there are more than 5 H-bond donors, 10 H-bond acceptors, the molecular weight is higher than 500 Da, and the calculated Log P (CLog P) is larger than 5 (Benet et al, 2016). When two or more of these conditions are violated, a molecule is predicted to be a non-orally bioavailable drug (Lipinski, 2016, pp. 34–41).

Furthermore, the "Rule of Three" is a fragment-specific extension of the Rule of Five (MW <300, logP <3, number of HD and HA <3, number of rotatable bonds< 3) (Lionta et al, 2014, pp. 1923–1938). The evaluation of drug likeness compounds in our research has been done using BIOVIA DS and the SwissADME web server.

8.2.10. Docking validation with AutoDock

The best poses selected from docking vina were subject to docking using another docking software (Autodock 4.2) validated in the last part of the study when we compared the experimental results with the calculated ones by docking the known inhibitors with their proteins.

A hundred complexes were docked by Autodock 4.2. The LGA search was used to create docked poses, and a semi-empirical FF-based scoring function was used to determine the free energy of binding. The graphical user interface (Autodock Tools (ADT) 1.5.6) was used to integrate non-polar hydrogens by assigning rotatable bonds to each constituent atom of the ligand and the enzyme before docking. To accelerate the interaction energy calculation during the conformational analysis, AutoGrid was utilized to produce grid maps for each atom type in the docked compounds that hold grids of interaction energy used as a reference table (sampling stage). For AutoGrid settings, the default values were employed. The maps were centered on the macromolecules and used a grid map with 60^3 points and a default grid spacing. The docking mechanism is semi-flexible, permitting the ligands to explore their structural space while maintaining the macromolecules rigid. The number of GA evaluations was set at 250000.

8.2.11. Docking analysis

In bioinformatics, computational docking is a critical approach. The evaluation and interpretation of docking results are also crucial. There is a variety of software provided for docking result analysis that can provide high-quality images. We used Pymol, a simple bioinformatics tool for visualizing macromolecules and interaction with ligands. It is simple to make high-quality images at various resolutions (90, 150, and 300 dpi). The better the dpi value, the higher the quality of the image. Also, we used Discovery Studio (DS) Visualizer, so we could easily visualize interactions between the receptor and the ligand. The label and font colors, as well as background and receptor colors, are easily customizable. We could also observe the receptor surface in several ways, such as aromatic, H-bond, charge, ionizability, and solvent accessibility (SAS). We could quickly generate a 2D interaction diagram and save it in PNG format. We could even save the entire session to restart later. We employed Autodock tools, in addition to docking and files's preparation, for the visualization of macromolecular structures and the production of images. It may also open the Vina docking output files, which we could simply analyze.

In addition, UCSF Chimera was a beneficial software for interactive molecular visualization and analysis, Chimera can scan molecular structures and supporting data in a variety of formats, visualizing the structures in a range of representations, and generating good quality images.

8.3. Molecular Dynamics Simulation

Molecular simulation is a tremendously important tool in current molecular modeling, allowing us to monitor and comprehend structure and dynamics in detail where individual atoms' motion can be traced (Lindahl E, 2008, pp. 3–23).

For MD studies of biomolecules, numerous software and force fields were created. MD analysis has revealed a variety of biological pathways that function at the atomic and molecular levels (protein folding and unfolding, protein-ligand interactions, protein-

protein interactions, DNA and RNA-protein interactions, proteins integrated into membranes, lipid-lipid interactions, drug transfer, and so on). (Kumari et al, 2017, pp.1163–1179).

To analyse the structural dynamics and steadiness of NOS-ligand complexes, either free nosS and their complexes with the best compounds discovered by VS were addressed to MD simulations using NAMD software (Phillips et al, 2005, pp. 1781–1802). All files were generated using CHARMM-GUI (A graphical tool that provides a Web-based approach to preparing files for use with CHARMM techniques. The platform assists in identifying any problem through visual inspection, which may then be readily solved with the help of the GUI) (Jo et al, 2014, pp. 235–265).

The targets 3D structures (PDB ID: 5VV0, 6AV7, 4CX7) were refined, including adjusting the side chain orientations, adding Hydrogens, and determining the best protonation states. The complexes and free NOSs were positioned in cubic boxes with explicit TIP3P water models with a thickness of 10.0 from protein surfaces. The systems were neutralized by providing counter ions, and a 0.15M NaCl salt solution was also employed to regulate the system's concentration. The Monte Carlo approach was utilized. We minimized the energy of the systems for 10000.

Following a 2 ns of equilibration run with a stable number of particles, volume, and temperature (NVT) ensemble, 100 ns-production-MD simulations were done for each system at a stable T (310.15 K) and pressure (NPT) ensemble. After the simulations of the free targets were completed, the protein-ligand complexes were thoroughly investigated with selected inhibitors using MD simulations.

8.3.1. Selected ligands for MD simulations

The following ligands (**Figure 8.1**) where optimized and prepared to be used in MD simulations according to the protocol.
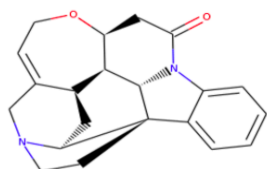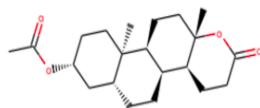
ZINC000000119434   ZINC000252517498   ZINC000253501597
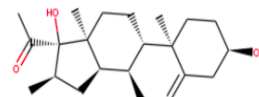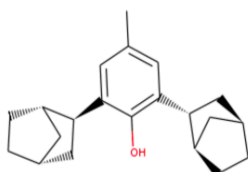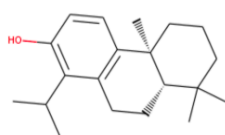
ZINC000001433941   ZINC000001872131   ZINC000003649911
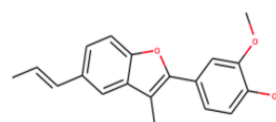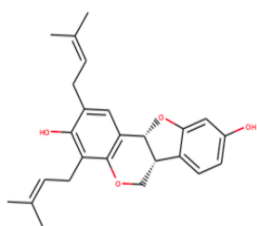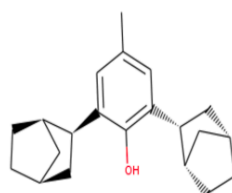
ZINC000013485422   ZINC000018183294   ZINC000013485423
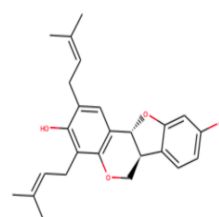
Figure 8.1 The 2D structure of the compounds used for MD simulation and retrieved from the virtual screening's best results.

8.3.2. Input files for NAMD

The following input files are important to run NAMD simulation (source: https://www.ks.uiuc.edu):

- **PDB file:** Provides the atomic coordinates of whole atoms in the molecular system. The angstrom unit is the default for pdb files.

- **PSF file:** Includes structural information about a molecular system.

- **Topology file:** (. top,.rtf) file provide the kind, mass, and partial charges of each atom for every residue, as well as bonding data needed to convert a list of residues to accomplish PSF files.

- **Parameter file:** (. prm,.str) file include all of the quantitative variables required to calculate forces and energy. Topology files for biological systems, including lipid membranes, proteins, carbohydrates, and nucleic acids in the CHARMM force field, are available online.

- **Configuration file:** NAMD defines configuration files with the Tcl Scripting language. A configuration input (also known as a.conf file,.inp file, or.namd file) is a display setting that provides a collection of parameters and settings for running the simulation. The parameters and values given in the configuration file govern NAMD's specific actions, such as whether functions are active or inactive, how long the simulation should run, etc. It is order-independent, and the entire file is evaluated before any data or computations are performed.

8.3.3. The output files generated by NAMD

(Source : https://www.ks.uiuc.edu)

- **Log file:** It contains the log for the entire simulation run. As well as this, it carries a massive amount of data like temperature, pressure, volume, and energy, among other things. In addition, it evaluates the simulation's benchmark time, which is utilized for performance optimization.

- **Trajectory (.dcd) File:** This file provides original atomic coordinates saved during simulation for all frames. When importing a .dcd file in VMD, we can see how

the system moves during the simulation. The frequency with which coordinates are saved for simulation runs is determined by the "dcd-freq" number specified in the NAMD config file.

- ***.xst File:** It keeps track of periodic cell parameters and prolonged system variables as they change during the simulation. The frequency with which this information is recorded can be specified in the NAMD configuration file using the "xstfreq" parameter.

- **Output *.coor, *.vel and *.xsc Files: *.coor and *.vel files:** Include the coordinates and velocities of whole atoms in the complex at the final step of a simulation, but *.xsc holds the system's periodic cell dimension and associated time step.

- ***. restart files:** Using the "restartfreq" command in the NAMD configuration file, NAMD can additionally generate the following restart files throughout the simulation run:

*.restart.coord (with the atomic coordinates)

*.restart.vel file (with the atom velocities)

*.restart.xsc file (with the system's periodic cell dimensions and time step).

8.3.4. Analysis of molecular dynamics simulations

VMD (Visual Molecular Dynamics) is a molecular graphics tool designed to present and analyze molecular assemblies, namely biopolymers like proteins and DNA/RNA. VMD includes a graphical user interface for software control and a text interface that utilizes the Tcl extensible syntax to support complex scripts. VMD has also explicitly been built to illustrate MD simulation trajectories retrieved from the outputs or the positive correlation to a running MD simulation (Humphrey, Dalke, and Schulten, 1996, pp. 33–38).

- **The Root Mean Square Deviation (RMSD):** The most popular quantitative measure of the connection between the two superimposed atomic coordinates is the root mean square deviation (RMSD).

The RMSD measurements are in Å and were determined using the following equation:

$$RMSD = \sqrt{\left(\frac{1}{n}\sum_{i=1}^{n} di^2\right)} \qquad (8.2)$$

Where: The estimation is done over n pairs of equivalent atoms, and di is the distance between the 2 atoms in the i-th pair (Kufareva and Abagyan, 2012).

Via VMD TkConsole (Extensions → Tk Console in the VMD Main window), we used the following command:

```
source rmsd.tcl
```

To generate rmsd.dat file that contained the measure of the RMSD of the protein backbone against time by running the following script:

```
set outfile [open rmsd.dat w];
set nf [molinfo top get numframes]
set frame0 [atomselect top "protein" frame 0]
set sel [atomselect top "protein"]
# rmsd calculation loop
for { set i 0 } {$i < $nf } { incr i } {
    $sel frame $i
    $sel move [measure fit $sel $frame0]
    puts $outfile "[measure rmsd $sel $frame0]"
}
close $outfile
```

- **RMSF (Root-Mean-Square Fluctuations):** The RMSF is a calculation of the fluctuation between particle i's position and an initial position:

$$RMSF = \sqrt{\left[\frac{1}{T}\sum_{tj=1}^{T}\left|ri(tj) - r_i^{ref}\ 2\right|\right]} \qquad (8.3)$$

Where:

T is the period of time over which the mean should be derived.

r_i^{ref} is the initial position of particle i

The variation between RMSD and RMSF is that the latter is estimated across period and offers a score for each particle, whilst the former does not. The RMSD, on the other hand, is estimated over the atoms and delivers time-specific information (Sneha and George Priya Doss, 2016, pp. 181–224).

Via VMD TkConsole (Extensions → Tk Console in the VMD Main window), we used the following command:

```
source rmsf.tcl
```

In order to generate rmsf.dat file that contained the value of the RMSF by running the following script:

```
set outfile [open rmsf.dat w]
set sel [atomselect top "name CA"]
set rmsf "[measure rmsf $sel first 0 last -1 step 1]"
for {set i 0} {$i < [$sel num]} {incr i} {
puts $outfile "[expr {$i+1}] [lindex $rmsf $i]"
}
close $outfile
```

- **The radius of gyration (Rg):** The radius of gyration (Rg) is described as the dispersion of its atoms around its axis. Rg is the length that reflects the distance between the point while it is rotating and the place where the energy transfer has the greatest effect. This idea particularly aids in detecting diverse polymer kinds, such as in the case of proteins. The computation of Rg and distance measurements are the two most important markers that are extensively utilized in estimating a macromolecule's structural activity. Determining the Rg also contributes to the prediction of drug and protein compactness and binding characteristics. (Sneha and George Priya Doss, 2016, pp. 181–224.). Rg is calculated according to:

$$\text{Rg} = \left(\frac{\sum_i ri^2 mi}{\sum_i mi}\right)^{\frac{1}{2}} \tag{8.4}$$

Where:

m_i : the MW of atom I

r_i : the location of i concerning the center of mass of the molecule.

Via VMD TkConsole (Extensions → Tk Console in the VMD Main window), we used the following command:

```
source rg.tcl
```

In order to generate rg.dat file that contained the value of the Rg by running the following script:

```
set mol [molinfo top]
set out [open rg.dat w]
set sel [atomselect top " (protein and resid 339) and backbone "]
# set sel [atomselect top " (same residue as within 4 of resname 18F)
 and    backbone "]
 set frames [molinfo $mol get numframes]
 for {set i 0} {$i < $frames} {incr i} {
$sel frame $i
$sel update
puts $out "$i [measure rgyr $sel]"
}
$sel delete
```

- **Hydrogen bond:** One of the essential biological mechanisms is hydrogen bonding. It is essential to the structure and function of many important molecules. It is usually needed for the stability of the receptor-ligand complexes. The H-bonding network is necessary in enzymatic activity because it allows NOS substrates or inhibitors to be positioned over the heme. Hydrogen bonds were generated in this study using the VMD plugin.

9. RESULTS AND DISCUSSION

9.1. Target Identification and Validation

- **Sequence alignment and structural superimposition:**

The sequence alignment and structural superimposition of the three human NOS isoforms: The amino acid sequences of hnNOS (PDB ID: 5VV5), heNOS (PDB ID:5VVB), and hiNOS (PDB ID: 3E7G) were aligned using BIOVIA DS software. Their corresponding three-dimensional (3D) structures were superimposed to calculate the sequence and structure similarity between the three NOS isoforms within the same species (**Figure 9.1**). The multiple sequence alignment of the the 3 hNOS isoforms listed above showed that the sequence identity was 52.6%, and the sequence similarity was 71.0%. Human nNOS has a structure that is quite like human iNOS and human eNOS, as predicted. **(Figure 9.2).**
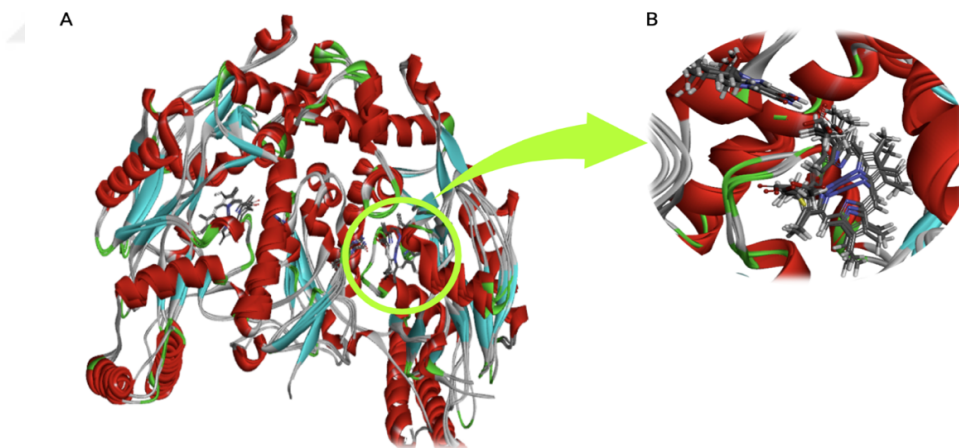
Figure 9.1 (A) Structural superimposition of hnNOS (PDB ID: 5VV5), heNOS (PDB ID:5VVB), and hiNOS (PDB ID: 3E7G). (B) Structural superimposition of the Cofactors (BH4 and heme) of hnNOS (PDB ID: 5VV5), heNOS (PDB ID:5VVB), and hiNOS (PDB ID: 3E7G)
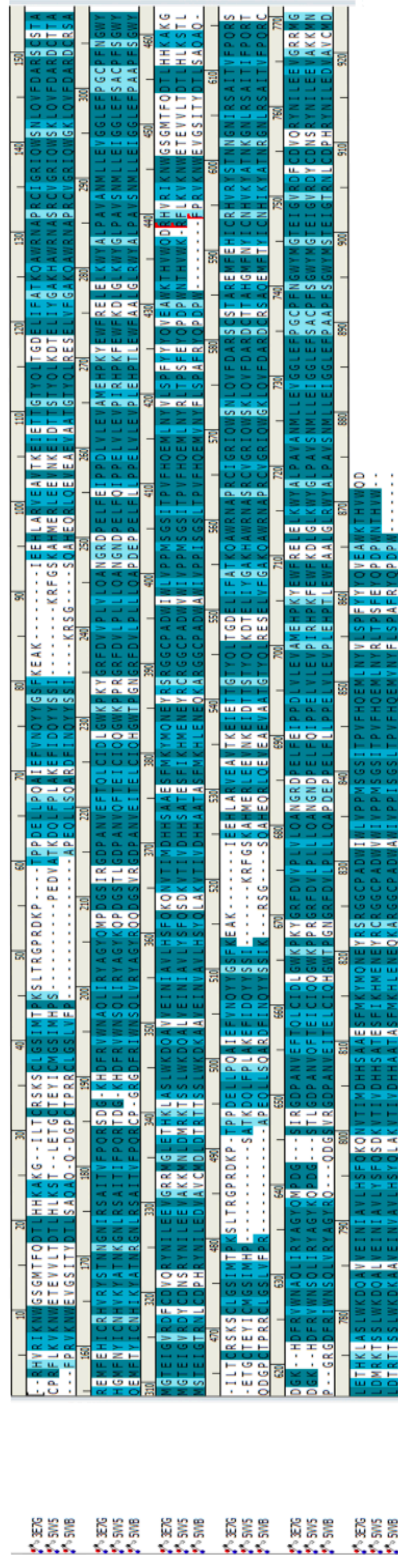
Figure 9.2 Multiple sequence alignment of hnNOS (PDB ID: 5VV5), heNOS (PDB ID:5VVB), and hiNOS (PDB ID: 3E7G) (Dark blue (Identity), light blue (Similarity), white (Difference)). The sequence identity is 52.6 % and sequence similarity is 71.0%.

The sequence and structure similarity of the neuronal NOS isoform of different species: The amino acid sequences of hnNOS (PDB ID: 5VV5) and Rat nNOS (PDB ID: 6NHE) were aligned using Biovia discovery studio software, and their corresponding three-dimensional (3D) structures were superimposed to calculate the sequence and structure similarity between neuronal NOS isoform of different species (**Figure 9.3**).

The architectures of human and rat nNOS are nearly identical, with sequence identity as far as 95.1 % and sequence similarity as high as 97.0 % (**Figure 9.4**). According to the literature, a large levels of freedom sequence of the Zn^{2+}-binding site is the only exception. This sequence is frequently disrupted in rnNOS (Ser 339 – Asp3 47). This sequence is fully organized in 1 subunit of each dimer of the hnNOS structure, whereas residues Ser 344 – Asp 352 are still deficient in the other subunit. In hiNOS, the same sequence region (Lys 123 – Asp131) is often very organized (Li et al, 2014, p. 5272).
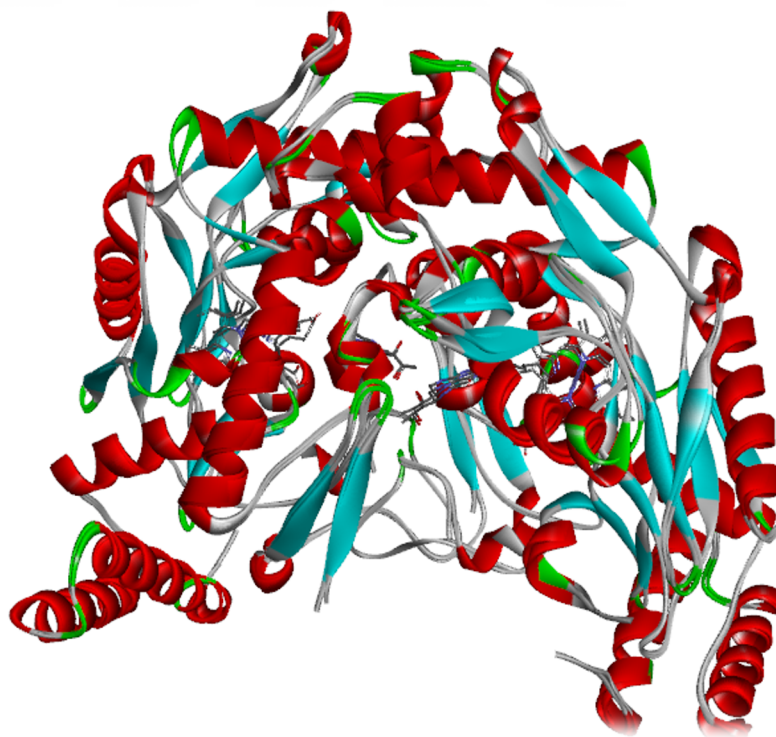
Figure 9.3 Structural superimposition of hnNOS (PDB ID: 5VV5) and Rat nNOS (PDB ID: 6NHE).

Figure 9.4 Multiple sequence alignment of hnNOS (PDB ID: 5VV5), and Rat nNOS (PDB ID: 6NHE). (Dark blue (Identity), light blue (Similarity), white (Difference)). The sequence identity is 95.1%, and sequence similarity is 97.0%.

- **Structure-based phylogenetic analysis:** The phylogenetic tree was created using various sequence alignments to explain the evolutionary connections between hnNOS (PDB ID: 5VV5), heNOS (PDB ID: 5VVB), hiNOS (PDB ID: 3E7G), and rat nNOS (PDB ID: 6NHE) (**Figure 9.5**). The phylogenetic tree indicated that hnNOS (PDB ID: 5VV5) and rat nNOS (PDB ID: 6NHE) are closely related and share an ancestral origin with the other isoforms, which confirmed the result of the sequence alignment.
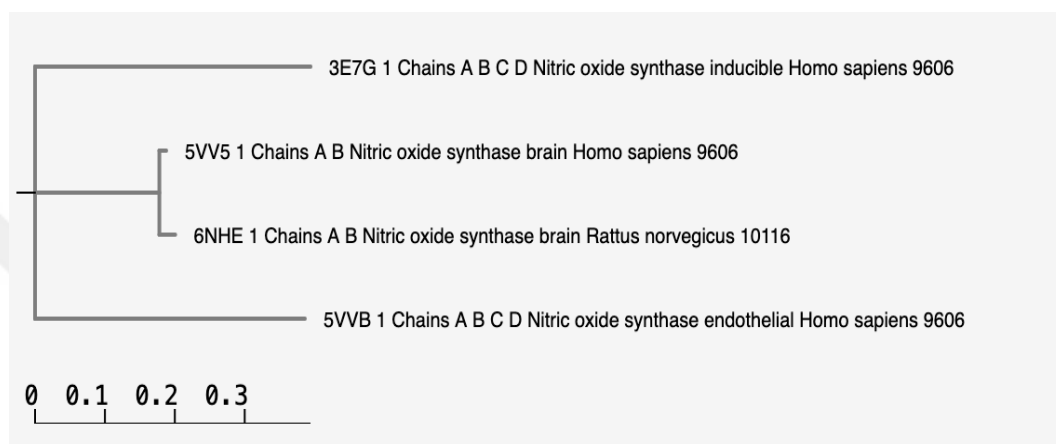
Figure 9.5 The phylogenetic tree of NOS (Human neuronal NOS (PDB ID: 5VV5), Human endothelial NOS (PDB ID: 5VVB), Human inducible NOS, (PDB ID: 3E7G) and Rat neuronal NOS (PDB ID: 6NHE)).

9.2. Re-Docking with Known Inhibitors

Docking algorithms are concerned with predicting ligand structure and orientation inside the receptor's designated active region. The docking technique significantly evolved considerably over the years to accommodate target and compound side-chain flexibility (Ghosh et al, 2006, pp. 194–202).

The co-crystallized ligands were removed from each protein structure. Employing Biovia Discovery Studio, missing loops were approximated, and hydrogen atoms were added according on the protonation state of the titratable residues at pH 7.4. These native ligands were later docked using AutoDock again into their original crystal structures. To validate the 3D structure of the targets and to select the average of Ki,

which will be used in the following steps as a reference, we compared the Ki experimental (nM) (or IC50) from the literature with the calculated resulting from AutoDock (**Table 9.1**).

Table 9.1 Binding energy (ΔG) and inhibition constant (Ki) calculated results of known inhibitors docking using Autodock compared with the experimental Ki.

PDB	ΔG kcal/mol	ki calculated (nM)	ki Exp (nM)	PDB	ΔG kcal/mol	ki calculated (nM)	ki Exp (nM)
6AV7	-10.88	10.52	83976	3E6L	-8,21	962,32	720
6AUS	-9,55	99,23	252	3E7I	-10,89	10,42	10
6AUV	-10,04	43,39	47	3E7M	-8,27	867,41	350
6AUW	-10,19	34,14	57	3E 68	-9,7	77,89	120
6AUX	-8,94	281,4	44	3EAI	-9,36	136,61	74
6CID	-10,24	31,12	110	3EBD	-8,65	454,32	40
5VUV	-8,99	256,57	768	4UGZ	-9,59	92,64	130
5VUX	-10,18	34,52	764	4UH0	-9,47	115,08	35 ± 2.0
5VUY	-10,23	31,5	274	4UH1	-10,54	18,92	17 ± 1.6
5VUZ	-10,95	9,34	108	4UH2	-9,37	134,8	67 ± 3.3
5VV0	-10,97	9,17	130	4UH3	-11,01	8,56	34 ± 1.2
5VV1	-11,04	8,15	73	4UH4	-10,84	11,24	24 ± 1.1
5VV2	-10,63	16,25	164	4D2Y	-9,41	127,24	40
5VV3	-11,38	4,58	32	4D2Z	-10,68	14,83	40
5VV4	-11,52	3,57	20	4D30	-9,69	79,18	54
5VV5	-11,89	1,92	30	4D31	-9,72	75,44	183
5UO1	-11,43	4,19	36	4D33	-5,3	131350	40000
5UO2	-10,77	12,72	125	4V3W	-9,58	94,68	138
5UO3	-12,06	1,45	31	4V3X	-10,59	17,2	19
5UO6	-12,19	1,15	65	4V3Z	-9,97	49,59	56
5UO7	-12,26	1,03	46	4CX7	-9,29	154.40	6629

- **Pearson correlation coefficient analysis:** We employed Pearson's correlation coefficient to evaluate the statistical link, or association, between ki experimental values and ki calculated values. Correlation can be between -1 and 1. The direction of the relationship is represented by the sign of the link coefficient, while the magnitude of the correlation (how near it is to -1 or +1) reflects the intensity of the relationship. We found that Pearson Correlation Coefficient r = 0.6475, which means a moderate positive correlation between the calculated and the experimental Ki results (**Figure 9.6**).
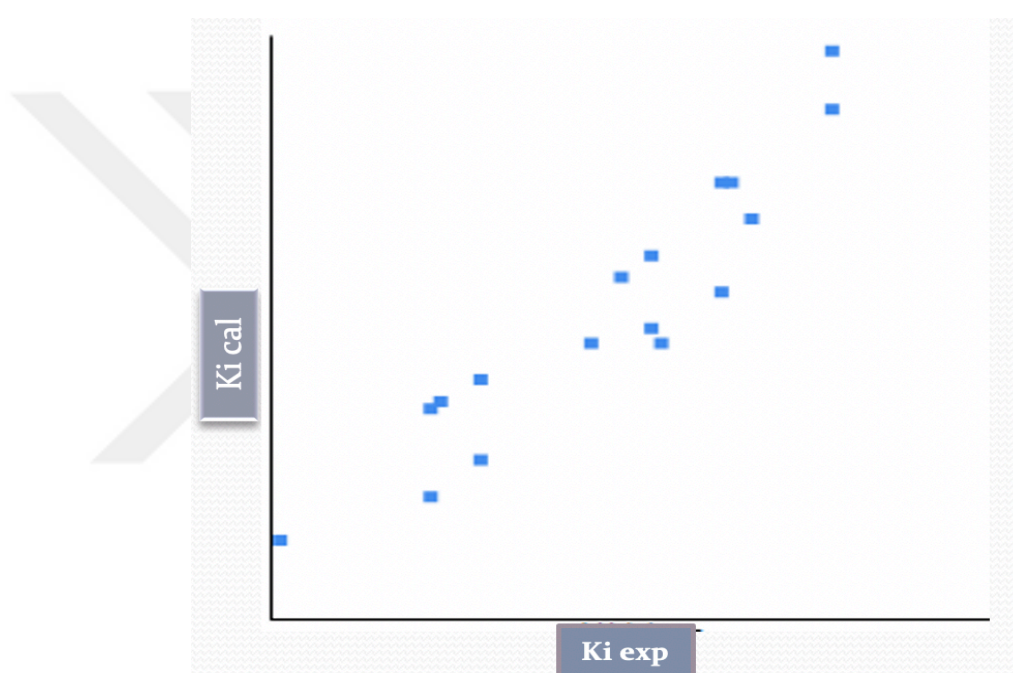
Figure 9.6 The scatterplot shows the correlation between the binding affinity (ki) of the experimental studies and the binding affinity of molecular docking.
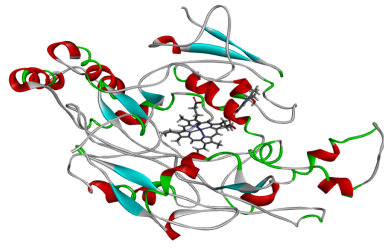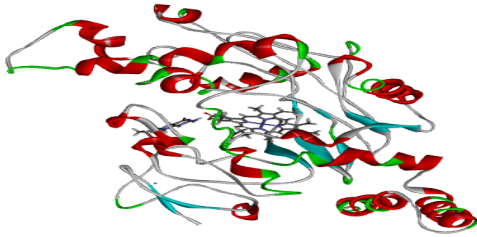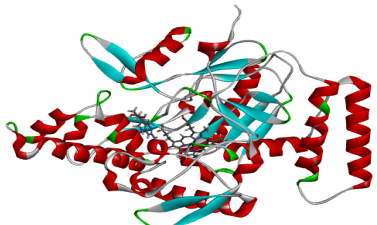
9.3. Structure-Based Virtual Screening

In drug discovery, VS is a good strategy for obtaining new drug molecules. Its goal is to select highly efficient compounds from a big chemical library for subsequent medical research. SBVS begins with a 3-D structure of a target receptor and a 3-D database of compounds, then employs virtual filtering, MD, and scoring to select credible lead candidates. Docking and scoring algorithms produce subgroups of a compound set with

increased affinity against a target by estimating their linking mode (through docking) and affinity (through scoring) and extracting those with the best scores (Ghosh et al, 2006, pp. 194–202).

- **Characterization of the macromolecular target:** We selected the following enzyme from the validation step to be used in the SBVS. The Chain A of each isoform was prepared and minimized (**Table 9.2**).

Table 9.2 The NOSs used for the VS.

PDB	Isoform	Organism	3D structure of chain A prepared
5VV0	nNOS	Homo sapiens	
6AV7	eNOS	Homo sapiens	
4CX7	iNOS	Homo sapiens	

- **Structures evaluation and validation of NOSs:** By evaluating the stereochemical quality of the target, errors in protein structures can be detected. The Ramachandran plot, which illustrates the phi (φ)and psi (ψ) backbone conformational angles for whole residue in a target, is a regularly used indication of protein quality (**Figure 9.7)**, and further analysis results are represented in **Table 9.3**, **Table 9.4, Figure 9.8, Figure 9.9, Figure 9.10,** and **Figure 9.11.**
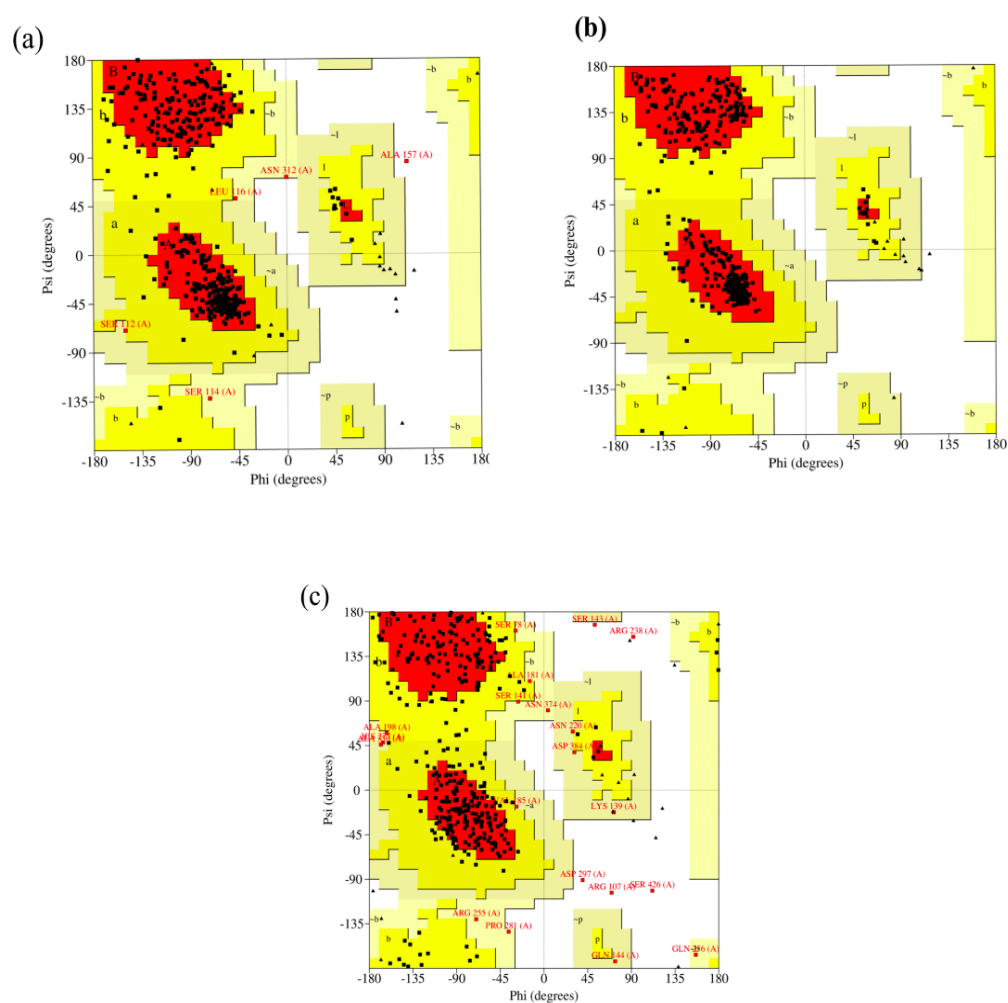
Figure 9.7 Ramachandran plot of (a) hiNOS (PDB ID:4CX7), (b) hnNOS (PDB ID: 5VV0), and (c) heNOS (PDB: 6AV7).

Table 9.3 Ramachandran plot results of the structure of hiNOS (PDB ID:4CX7), hnNOS (PDB ID: 5VV0), and heNOS (PDB: 6AV7).

PDB ID	4CX7	5VV0	6AV7
Highly Preferred observations	389 (92.840%)	398 (97.073%)	340 (84.788%)
Preferred observations	19 (4.535%)	7 (1.707%)	39 (9.726%)
Questionable observations	11 (2.625%)	5 (1.220%)	22 (5.486%)

Table 9.4 Hydrogen bond estimation (DSSP) score of hiNOS (PDB ID: 4CX7), hnNOS (PDB ID: 5VV0), and heNOS (PDB ID 6AV7).

PDB ID	4CX7	5VV0	6AV7
The residues % which have averaged 3D-1D score>= 0.2	89.55 Passed	83.7 Passed	85.15 Passed
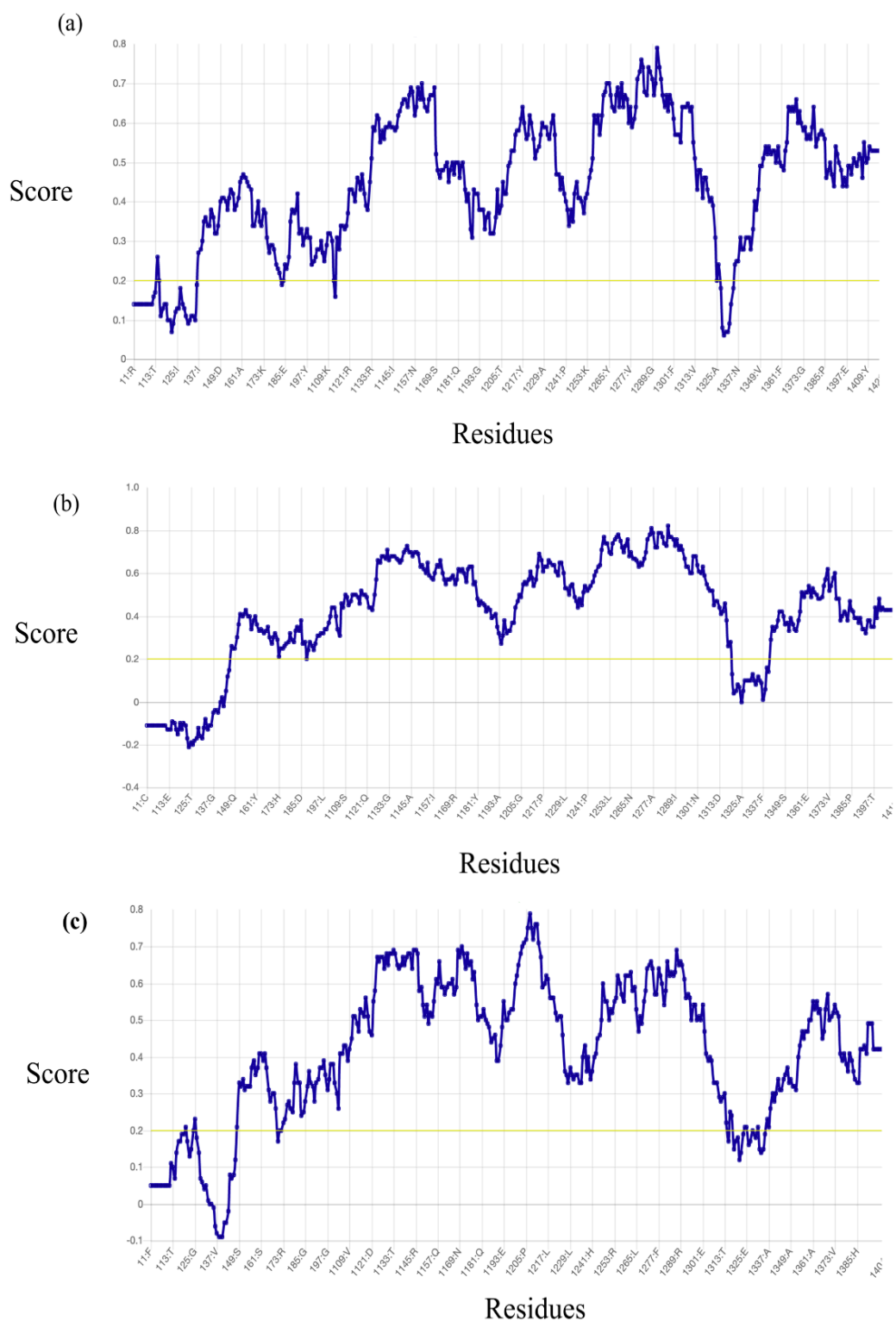
Figure 9.8 Hydrogen bond estimation (DSSP) of (a) hiNOS (PDB ID: 4CX7), (b) hnNOS (PDB ID: 5VV0), and (c) heNOS (PDB ID 6AV7).

Average Z–score

Z–score RMS

Distribution of atomic Z–scores
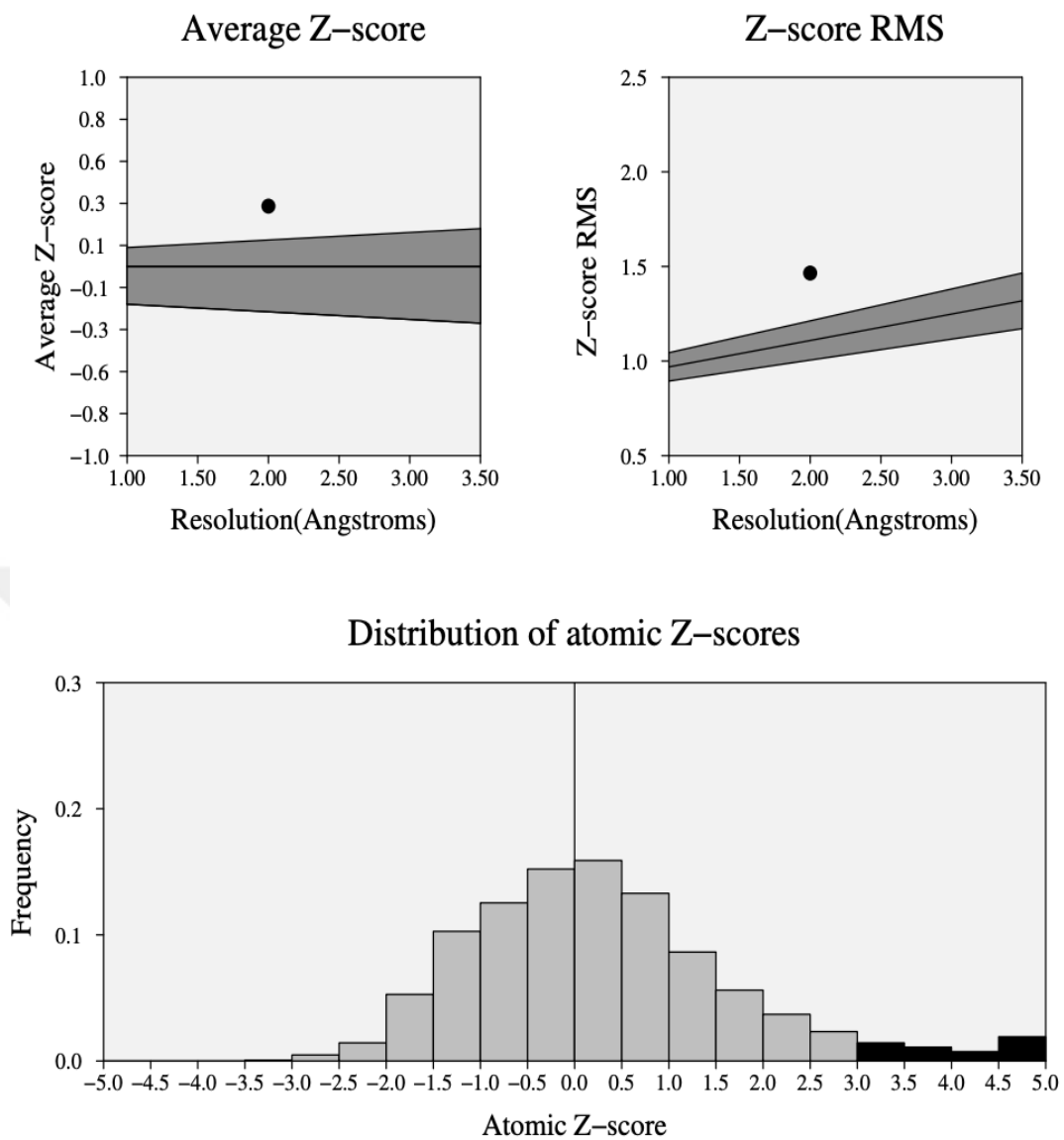
Z–score mean	0.319
Z–score stddev	1.430
Z–score RMS	1.465
# scored atoms	1658
# outliers	78
% outliers	4.700

Figure 9.9 Z-score of hiNOS (PDB ID:4CX7).

Average Z−score

Z−score RMS

Distribution of atomic Z−scores

Z−score mean	0.212
Z−score stddev	1.271
Z−score RMS	1.288
# scored atoms	1601
# outliers	53
% outliers	3.300
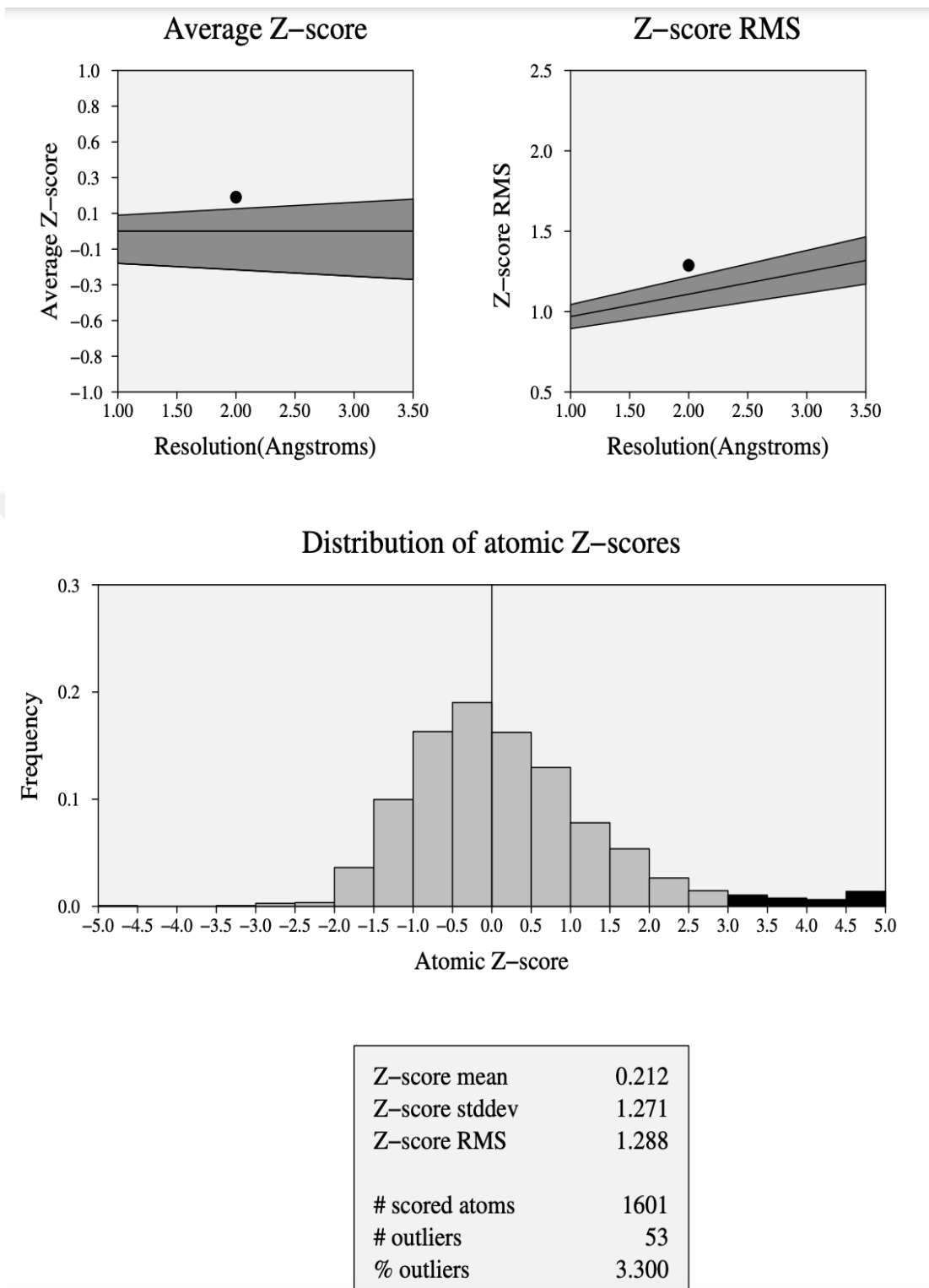
Figure 9.10 Z-score of hnNOS (PDB ID: 5VV0).

Average Z−score

Z−score RMS

Distribution of atomic Z−scores

Z−score mean	0.320
Z−score stddev	1.574
Z−score RMS	1.605
# scored atoms	1510
# outliers	95
% outliers	6.300
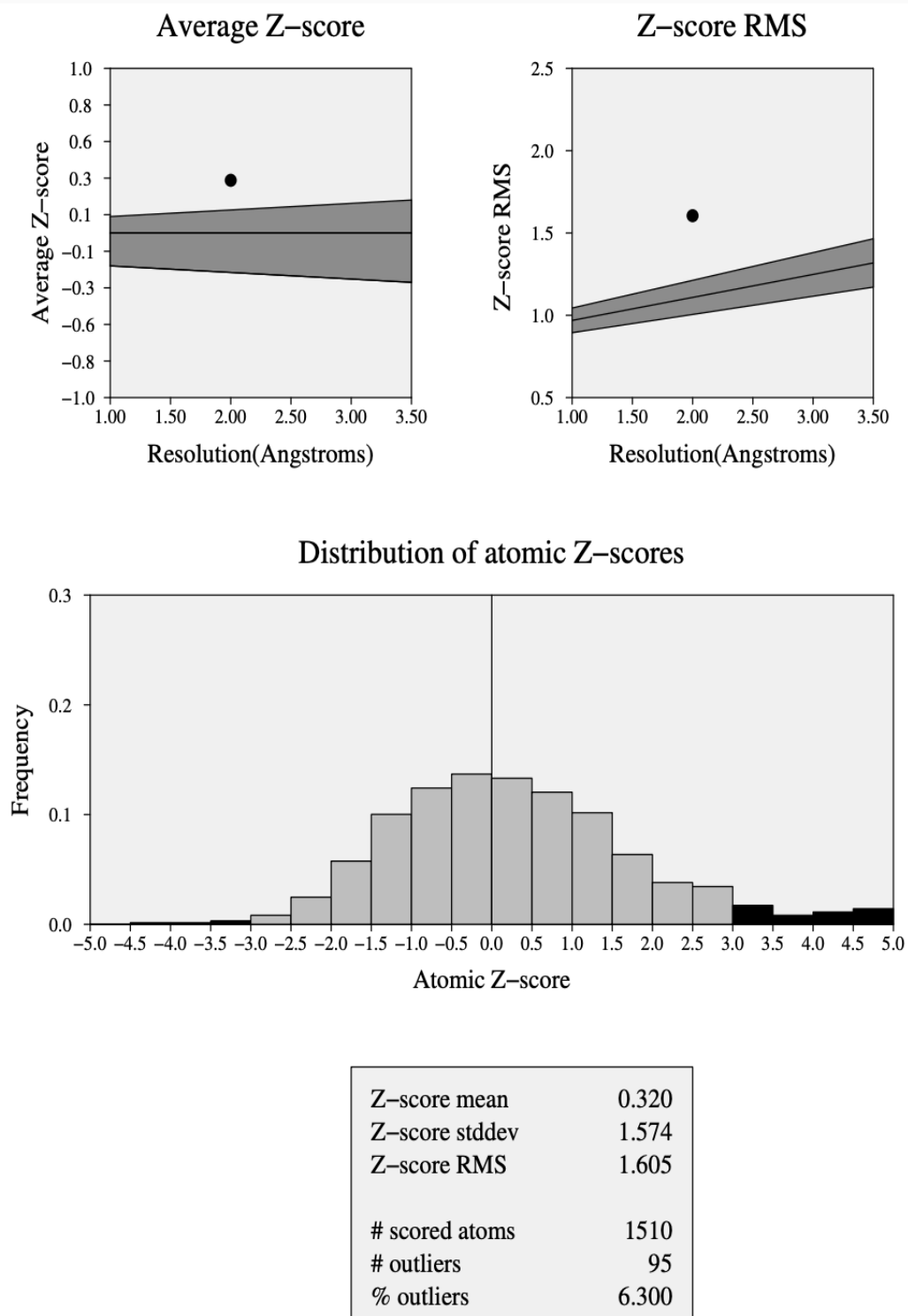
Figure 9.11 Z-score of heNOS (PDB ID 6AV7).

- **Binding site prediction:** The recognition and identification of functional regions on proteins are becoming increasingly important. Protein structures with indefinite functions and active sites are increasingly being discovered due to structural genomics investigations. Pocket detection pioneered binding site prediction because the binding site is generally observed in the biggest pocket (Laurie and Jackson, 2006, pp.395–406). According to the literature, In the active site pocket of all NOS isoforms (**Figure 9.12)**, there is a conserved Glu (Glu592 in nNOS and Glu363 in eNOS) that serves to attach the natural substrate, L-arginine. The substrate's C α terminus is fixed in a second pocket containing Asp597 in nNOS and Asn368 in eNOS (Delker et al, 2010, pp. 5437–5442) (**Table 9.5).**

Table 9.5 Binding site residues prediction of hiNOS (PDB ID: 4CX7), hnNOS (PDB ID: 5VV0), and heNOS (PDB ID 6AV7).

PDB ID	5VV0	4CX7	6AV7
	414W	194W	
	419R	197A	178W
	420C	198P	182P
	421V	199R	183R
	422G	200C	184C
	429L	201I	185V
	462S	202G	193L
	575M	205Q	226S
	589F	209L	339M
Binding residues	590S	242S	353F
	591G	355M	354S
	592W	369F	355G
	594M	370N	356W
	597E	371G	358M
	683W	372W	361E
	709F	377E	447W
	711Y	463W	473F
		489Y	475Y
		491Y	
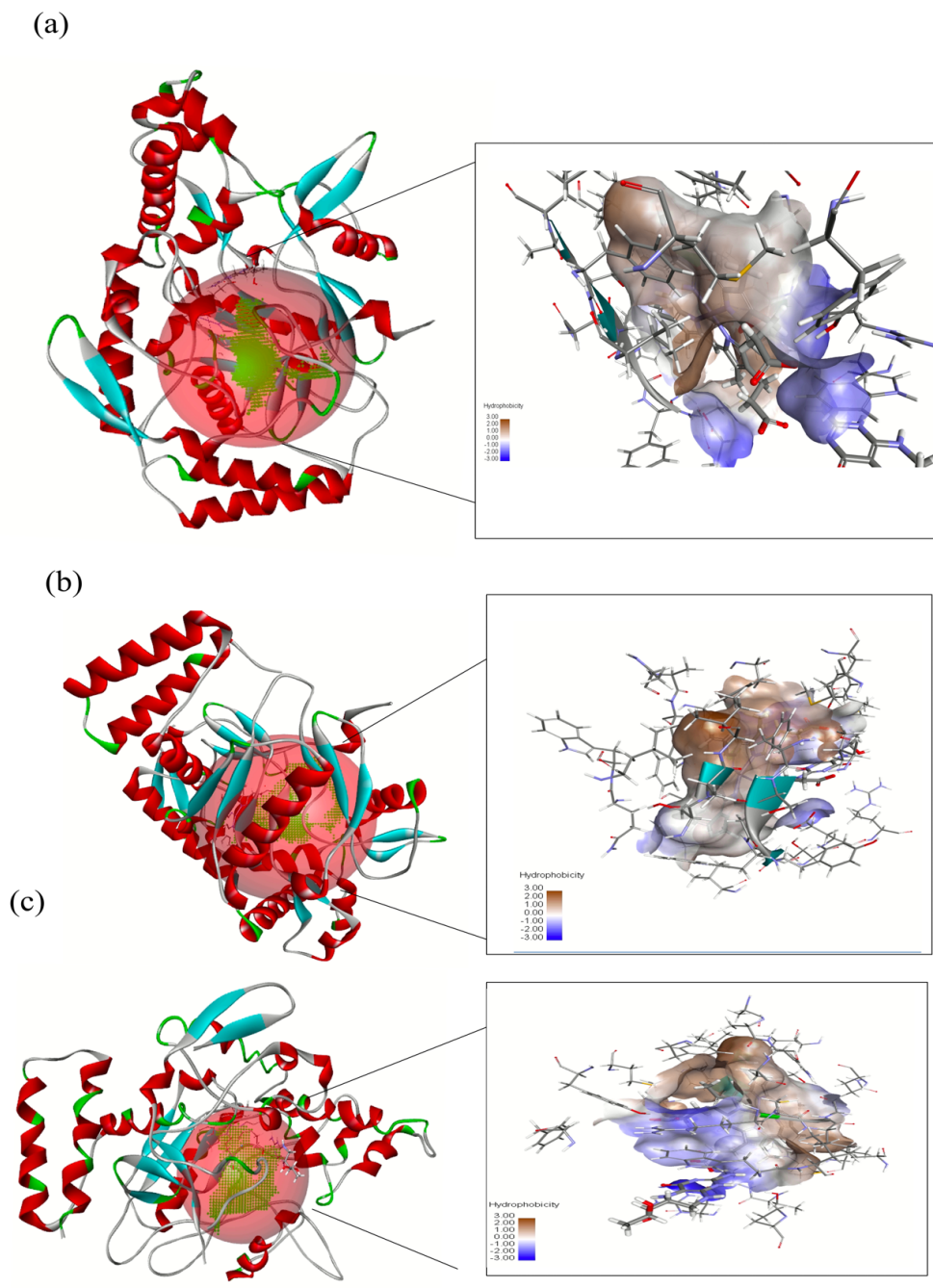
Figure 9.12   Predicted binding pocket of (a) hiNOS (PDB ID: 4CX7), (b) hnNOS (PDB ID: 5VV0), and (c) heNOS (PDB ID 6AV7).

9.4. Virtual Screening and Binding Energy Analysis

The virtual screening approach in drug design facilitates a rapid discovery of the bio-active hit compounds. In this study, we used AutoDock Vina to estimate the binding energies (ΔG) of different compounds from several databases (**Table 9.6**).

 The top compounds were subject to re-scoring by AutoDock 4.2 to approve the results obtained using Autodock Vina, to have the inhibition constants values (Ki) (**Table 9.7)**, and accordingly, to calculate the selectivity index (**Table 9.8**).

We noticed that the docking results of many compounds showed a high binding affinity for nNOS but did not satisfy selectivity criteria even with repetitive docking runs. Some compounds were inhibitors for eNOS and (or) iNOS and had a low binding affinity with nNOS. Conferring to studies that confirm our findings, the active sites of NOS isoforms are highly conserved. 16 of the 18 residues in the pocket within 6 Å of the substrate are indistinguishable; also, nNOS has a significant active site (1000 Å³~1100 Å³) which prevents the inhibitors to contact the enzyme ideally to increase the potency of inhibition (Ji et al, 2009, pp. 209–217).

Corresponding to the previous research, Asp597 and Glu592 are the two negatively charged side chains of nNOS that can electrostatically stabilize the inhibitor -amino group, and for better interaction, the inhibitor should curl, positioning the -amino group in the best possible place between Asp597 and Glu592 (Poulos and Li, 2017, pp. 68–77). To reveal the precise interactions of these potential inhibitors docked poses, the selected top compounds from VS were analyzed using BIOVIA DS 4.5.

Table 9.6 The binding energies (ΔG) of the top compounds predicted by Autodock vina.

Compound	hnNOS (5VV0) ΔG (kcal/mol)	heNOS (6AV7) ΔG (kcal/mol)	hiNOS (4CX7) ΔG (kcal/mol)	Compound	hnNOS (5VV0) ΔG (kcal/mol)	heNOS (6AV7) ΔG (kcal/mol)	hiNOS (4CX7) ΔG (kcal/mol)
ZINC000003649911	-9.3	-9.3	-9.0	ZINC000252517497	-8.8	-8.7	-9.3
ZINC000014928870	-10.5	-10.6	-9.4	ZINC000004612836	-8.6	-7.8	-7.9
ZINC000018102655	-9.3	-8.0	-8.2	ZINC000013302315	-9.7	-9.2	-9.5
ZINC000252477567	-8.4	-8.3	-8.5	ZINC000013311350	-8.5	-8.1	-8.4
ZINC000014824336	-9.6	-9.4	-9.5	ZINC000013485422	-11.1	-11.1	-10.5
ZINC000018144039	-9.2	-8.5	-8.5	ZINC000013485423	-10.5	-11.2	-10.6
ZINC000038140885	-10	-9.7	-9.8	ZINC000018183294	-7.8	-8.0	-7.8
ZINC000070691657	-8.8	-9.5	-9.1	ZINC000005132927	-9.0	-9.2	-8.6
ZINC000085576447	-9.6	-9.4	-9.9	ZINC000038563738	-9.1	-8.7	-9.0
ZINC000252477564	-8.7	-8.5	-8.3	ZINC000034045609	-8.6	-9.0	-7.6
ZINC000001433941	-9.2	-9.0	-9.4	ZINC000038358415	-8.6	-8.0	-8.0
ZINC000085602366	-8.1	-7.8	-8.3	ZINC000001872131	-8.8	-8.6	-8.6
ZINC000252517498	-9.1	-8.4	-9.1	ZINC000003881426	-9.0	-8.5	-8.4
ZINC000253388412	-8.2	-8.1	-8.1	ZINC000229903602	-8.2	-7.6	-7.5
ZINC000253497334	-8.6	-8.4	-8.6	ZINC000000119434	-12.0	-12.1	-11.7
ZINC000253501597	-8.2	-8.0	-8.4	ZINC000230017540	-11.0	-10.9	-9.7
ZINC000038563736	-9.5	-8.4	-8.2	ZINC000004023303	-10.9	-10.5	-10.1

Table 9.7 Calculated binding energies (ΔG) and inhibition constants (Ki) of the top compounds predicted by AutoDock 4.2.

Compound	hnNOS (5VV0) ΔG (kcal/mol)	hnNOS (5VV0) Ki (nM)	heNOS (6AV7) ΔG (kcal/mol)	heNOS (6AV7) Ki (nM)	hiNOS (4CX7) ΔG (kcal/mol)	hiNOS (4CX7) Ki (nM)
ZINC000003649911	-8.74	389.34	-8.38	722.14	-8.4	691.34
ZINC000014928870	-9.31	150.39	-9.77	69.14	-9.34	142.27
ZINC000018102655	-10.8	12.06	-9.98	48.57	-11.22	05.92
ZINC000252477567	-8.21	954.1	-6.96	7890	-9.8	65.33
ZINC000014824336	-8.63	475.45	-8.49	594.2	-9.41	126.38
ZINC000018144039	-11.15	01.76	-10.37	24.89	-11.39	04.46
ZINC000038140885	-10.07	41.47	-10.1	39.76	-9.79	66.54
ZINC000070691657	-8.78	366.49	-11.0	8.06	-11.37	04.61
ZINC000085576447	-7.18	5430	-7.58	2770	-8.44	645.51
ZINC000252477564	-10.41	23.57	-10.62	16.41	-9.99	47.22
ZINC000001433941	-10.77	12.67	-10.55	18.59	-10.58	17.45
ZINC000085602366	-8.21	967.14	-9.0	251.57	-8.9	300.42
ZINC000252517498	-9.31	150.9	-8.39	704.51	-7.6	2700
ZINC000253388412	-8.02	1310	-7.6	2670	-5.4	110990
ZINC000253497334	-7.69	2310	-7.61	2660	-7.5	3180
ZINC000253501597	-9.21	178.08	-8.12	1110	-8.37	729.49
ZINC000038563736	-8.06	1240	-10.55	18.58	-6.07	35510
ZINC000038563738	-8.49	593.86	-10.42	23.21	-5.43	104000
ZINC000252517497	-9.05	233.43	-1.12	151680000	-8.37	729.49
ZINC000004612836	-7.85	1780	-7.91	1580	-6.64	13560
ZINC000013302315	-7.13	5890	-7.87	1700	-8.14	1070
ZINC000013311350	-6.15	31080	-6.77	10990	-6.93	8280
ZINC000013485422	-9.47	114.06	-7.71	2220	-7.94	1510
ZINC000013485423	-9.92	53.41	-8.46	628.02	-8.16	1050
ZINC000018183294	-11.1	07.33	-10.12	38.34	-10.54	18.71
ZINC000005132927	-7.33	4260	-8.08	1190	-5.54	86950
ZINC000034045609	-6.95	8000	-7.29	4500	-4.01	1150000
ZINC000038358415	-8.2	972.37	-9.71	76.81	-9.6	91.39
ZINC000001872131	-8.64	467.31	-7.92	1560	-8.4	701.2
ZINC000003881426	-9.36	137.17	-8.2	972.59	-9.67	81.81
ZINC000229903602	-6.67	12930	-7.16	5680	-6.06	36110
ZINC000000119434	-9.08	222.51	-6.65	13390	-5.36	118370
ZINC000230017540	-8.92	290.74	-9.78	67.45	-8.27	874.01
ZINC000004023303	-8.97	264.73	-10.05	42.73	-7.6	2680

Table 9.8 Selectivity of hnNOS against heNOS and hiNOS.

Compound	Selectivity Index hnNOS/ heNOS	Selectivity Index hnNOS/ hi NOS	Compound	Selectivity Index hnNOS/ heNOS	Selectivity Index hnNOS/ hi NOS
ZINC000003649911	1.85	1.77	ZINC000252517497	649787.94	3.12
ZINC000014928870	0.45	0.94	ZINC000004612836	0.88	7.61
ZINC000018102655	4.02	0.49	ZINC000013302315	0.28	0.18
ZINC000252477567	8.26	0.06	ZINC000013311350	0.35	0.26
ZINC000014824336	1.24	0.26	ZINC000013485422	19.46	13.23
ZINC000018144039	3.68	0.65	ZINC000013485423	11.75	19.65
ZINC000038140885	0.95	1.60	ZINC000018183294	5.23	2.55
ZINC000070691657	0.02	0.01	ZINC000005132927	0.27	20.41
ZINC000085576447	0.51	0.11	ZINC000038563738	0.03	175.12
ZINC000252477564	0.69	2.00	ZINC000034045609	0.56	143.75
ZINC000001433941	1.46	1.37	ZINC000038358415	0.07	0.09
ZINC000085602366	0.26	0.31	ZINC000001872131	3.33	1.50
ZINC000252517498	4.66	17.89	ZINC000003881426	7.09	0.59
ZINC000253388412	2.03	84.72	ZINC000229903602	0.43	2.79
ZINC000253497334	1.15	1.37	ZINC000000119434	60.17	531.97
ZINC000253501597	6.23	4.09	ZINC000230017540	0.23	3.00
ZINC000038563736	0.01	28.63	ZINC000004023303	0.16	10.01

The best selective nNOS compounds were nominated for rendering their poses in the active sites of the enzyme. The 2D and 3D Ligand-protein (nNOS) binding modes representations after molecular docking of the designated compounds are illustrated in **Figures 9.13, 9.14,** and **9.15.**

For example, the compound ZINC000253501597 **(Figure 9.13 (a))** is entirely submerged in the active site of nNOS forming many interactions comprising pi-alkyl, a hydrogen bond interaction; in the same way, the compound ZINC000013485423 **(Figure 9.15 (a))** established several pi-alkyl interactions in addition to pi-sulfur and pi-cation interactions, which ingrained it in the active site of nNOS perfectly. The compound ZINC000013485422 **(Figure 9.14 (b))** has dual van der Waals interactions, multiple alkyl interactions, and one pi-cation interaction formed with nNOS, which keep the molecule firmly attached to the target.
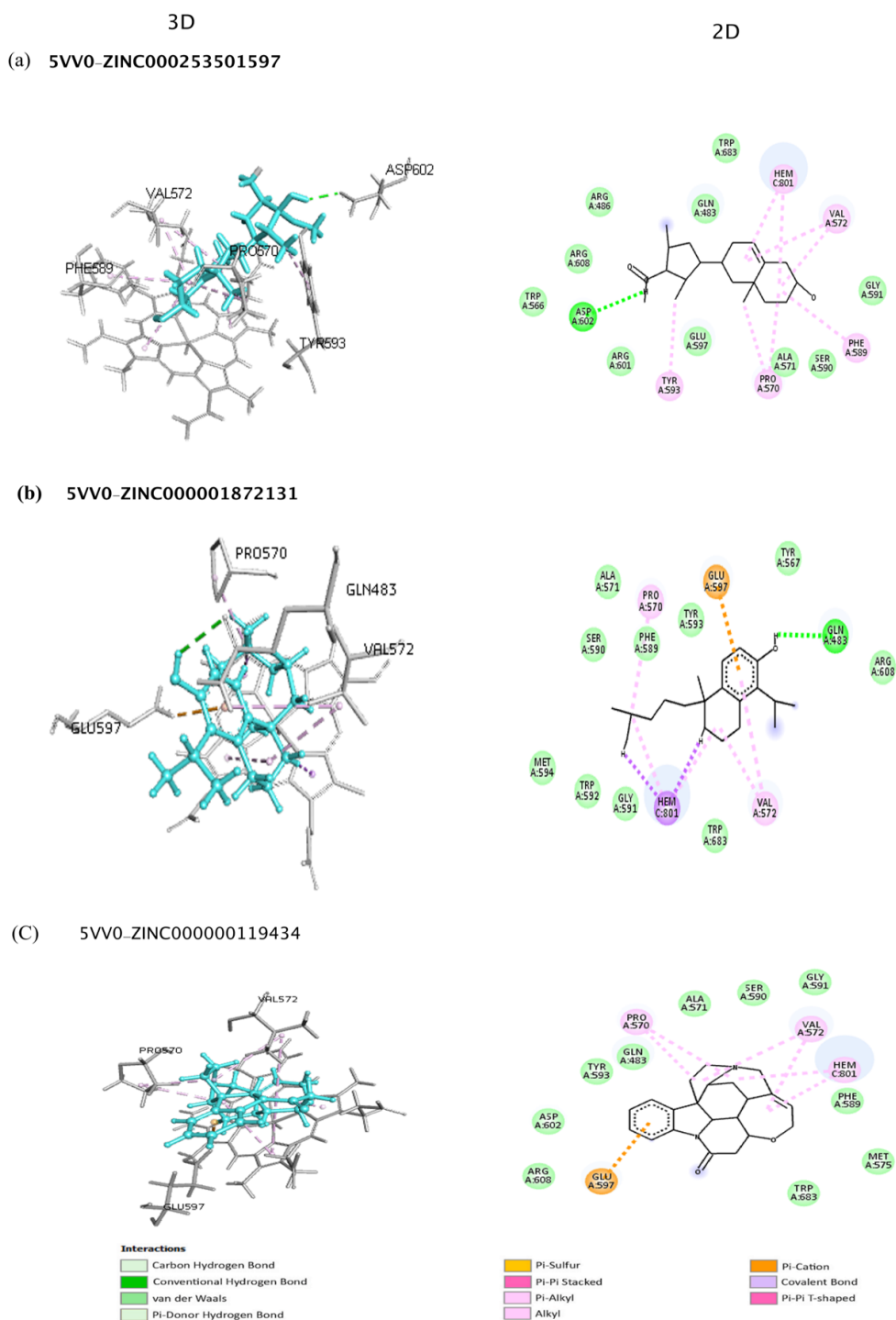
Figure 9.13 3D and 2D presentation of the chemical interactions after molecular docking of nNOS complexes ((a) 5VV0-ZINC000253501597, (b) 5VV0-ZINC000001872131, (c) 5VV0-ZINC000000119434) are represented in the left and right panels, respectively.

3D   2D

(a)   5VV0_ZINC000003649911

(b)   5VV0_ZINC000013485422

(c)   5VV0_ZINC000001433941

Figure 9.14 3D and 2D presentation of the chemical interactions after molecular docking of nNOS complexes ((a) 5VV0-ZINC000003649911, (b) 5VV0-ZINC000013485422, (c) 5VV0-ZINC000001433941) are represented in the left and right panels, respectively.

126

Figure 9.15 3D and 2D presentation of the chemical interactions after molecular docking of nNOS complexes ((a) 5VV0-ZINC000013485423, (b) 5VV0-ZINC000018183294, (c) 5VV0-ZINC000252517498) are represented in the left and right panels, respectively.

9.5. ADMET and Drug-Likeness Evaluation

The inappropriate ADMET proprieties cause the failure of a clinical trial of drug candidates which leads to time and money wasting. To avoid that, it is crucial to recognize the potential ADMET problems during the early stages of drug design. Many computational tools were developed to estimate the fate of drugs in the organism and calculate the toxicity risk to minimize failures. Because of the BBB, the successful delivery of nNOS inhibitors into the human brain is one of the most difficult missions.

18 of the 30 residues and cofactor side chains pointing toward the binding site of NOS are polar or charged, and clusters of acidic residues and cofactor side chains are detected, the heme propionate groups, as well as two low pKa polar side chains (residues Y562 and Y588), generate a very acidic local environment, as do residues E592 and D597, that is why the inhibitors must have positive charged electrostatic or HD groups, but unfortunately, their presence prevents the penetration via BBB (Ji et al, 2009, pp. 209–217).

Several findings aimed to solve this obstacle, for instance, by increasing the lipophilicity and rigidity of the inhibitors and adjusting the pKa of amino groups (Do et al, 2019, pp. 2690–2707). BIOVIA DS 4.5 and SwissADME were used in this study. **Table 9.9** illustrates the drug-likeness and ADMET profiles of the top-ranked compounds, which are considered drug-like compounds, passed Lipinski's rule of 5 and predicted to penetrate the BBB according to the calculations.

Table 9.9 Predicted ADMET properties of the best compounds.

Compound	MW g/mol	Rotatable bonds	HA	HD	TPSA	Consensus Log P	Compound	MW g/mol	Rotatable bonds	HA	HD	TPSA	Consensus Log P
ZINC000003649911	294.34	3	3	1	42.6	4.03	ZINC000252517497	348.48	2	4	0	52.6	3.83
ZINC000014928870	364.43	2	4	1	55.76	4.22	ZINC000004612836	346.5	1	3	2	57.53	3.44
ZINC000018102655	296.45	2	1	1	20.23	3.18	ZINC000013302315	314.42	2	3	1	54.37	3.9
ZINC000252477567	346.42	2	5	0	69.67	2.69	ZINC000013311350	374.43	9	6	2	77.38	3.24
ZINC000014824336	338.35	0	5	2	68.15	2.84	ZINC000013485422	392.49	4	4	2	58.92	5.1
ZINC000018144039	296.45	2	1	1	20.23	5.18	ZINC000013485423	392.49	4	4	2	58.92	5.1
ZINC000038140885	430.62	0	4	2	58.92	4.17	ZINC000018183294	296.45	2	1	1	20.23	5.19
ZINC000070691657	415.65	2	3	3	52.49	4.47	ZINC000005132927	340.41	5	4	0	36.92	4.23
ZINC000085576447	432.64	0	4	2	58.92	4.35	ZINC000034045609	306.48	1	2	2	40.46	3.9
ZINC000252477564	346.42	2	5	0	69.67	2.61	ZINC000038358415	374.56	4	3	2	57.53	4.64
ZINC000001433941	296.45	2	1	1	20.23	5.2	ZINC000001872131	286.45	1	1	1	20.23	5.26
ZINC000085602366	288.47	1	1	1	20.23	4.72	ZINC000003881426	270.37	0	2	1	37.3	3.32
ZINC000252517498	348.48	2	4	0	52.6	3.85	ZINC000229903602	334.49	3	3	0	35.53	4.41
ZINC000253388412	360.49	4	4	1	63.6	4.7	ZINC000000119434	334.41	0	3	0	32.78	2.11
ZINC000253497334	346.5	1	3	2	57.53	3.47	ZINC000230017540	364.43	2	4	1	55.76	4.28
ZINC000253501597	346.5	1	3	2	57.53	3.47	ZINC000004023303	386.52	2	4	0	52.60	2.26
ZINC000038563736	320.47	1	3	2	57.53	3.67	ZINC000038563738	320.47	1	3	2	57.53	3.66

9.6. Molecular Dynamics Simulation Analysis

MD simulations of 100 ns were used for the free enzymes and for the complexes to investigate the stability of the systems selected from virtual screening. To explore conformational changes in the enzymes's active site area, MD simulations of unbound nNOS, eNOS, and iNOS isoforms were done starting with the X-ray structures without the ligands (PDB ID: 5VV0, 4CX7, 6AV7)). We investigated the root mean square deviation (RMSD), root mean square fluctuation (RMSF), the radius of gyration (Rg), and hydrogen bond of the entire trajectories to evaluate the best candidates.

- **Root mean square deviation (RMSD):** RMSD is a resemblance measurement often employed in studying macromolecular structures and dynamics (Sargsyan, Grauffel, and Lim, 2017, pp.1518–1524). We analyzed RMSD to know how structures change over time compared to the initial point (**Figure 9.16**).

The free nNOS was stable at 57.2 ns with an RMSD of 2.6 Å, but it increased at 60 ns to reach 3.25 Å, gaining stability after 75.3 ns until the simulation was done with a slight oscillation.

The 5VV0-ZINC000253501597 complex became steady at 56.5 ns and reached the RMSD of 2.1 Å with a fluctuation at the end. For the 5VV0-ZINC000000119434 complex, the RMSD was unstable, suggesting the occurrence of a tremendous conformational modification during 86 ns, then it decreased from 3.2 Å to 2.09 Å. In addition, the 5VV0-ZINC000013485423 complex reached the steady-state at 37 ns and preserved its equilibrium mode until the end of the simulation with an RMSD of 2.3 Å. However, the 5VV0-ZINC000252517498 complex attained structural steadiness around 17 ns with the RMSD of 2.5 Å. Furthermore, the 5VV0-ZINC000018183294 complex showed a modest equilibrium between 40 and 50 ns and increased at 64 ns to reach 2.7 Å but dropped down then remained steady after that until the 100 ns.

Moreover, the 5VV0-ZINC000003649911 complex remained in the plateau state at the early stage of the simulation with an average backbone RMSD of 2 Å, then uncreased at

65 ns to reach 3 Å at 73 ns and decreased slowly to achieve the structural stability and the equilibrium state after that until the end of 100 ns. The 5VV0-ZINC000013485422 complex showed a plateau state between 30 ns and 100 ns.

The 5VV0-ZINC000001872131 complex gained steadiness since the beginning of the simulation with an RMSD around 2 Å with a minor fluctuation at the end, suggesting that the complex maintained its initial conformation throughout the simulation mechanism. Whereas the RMSD of the 5VV0-ZINC000001433941 complex progressively raised to 2.3 Å at 28 ns and persisted steady, but we mentioned a slight variability by the 100 ns.

The same compounds were subject to 100 ns duration MD simulations with iNOS and eNOS to investigate whether the structures were stable through the simulations. The RMSD of the free iNOS fluctuated between 2.5 and 3.6 Å when the RMSD of the free eNOS was around 3.5 and 4.6 Å. However, most of the iNOS and eNOS complexes were unstable with high RMSD profiles or a significant fluctuation during the simulations.
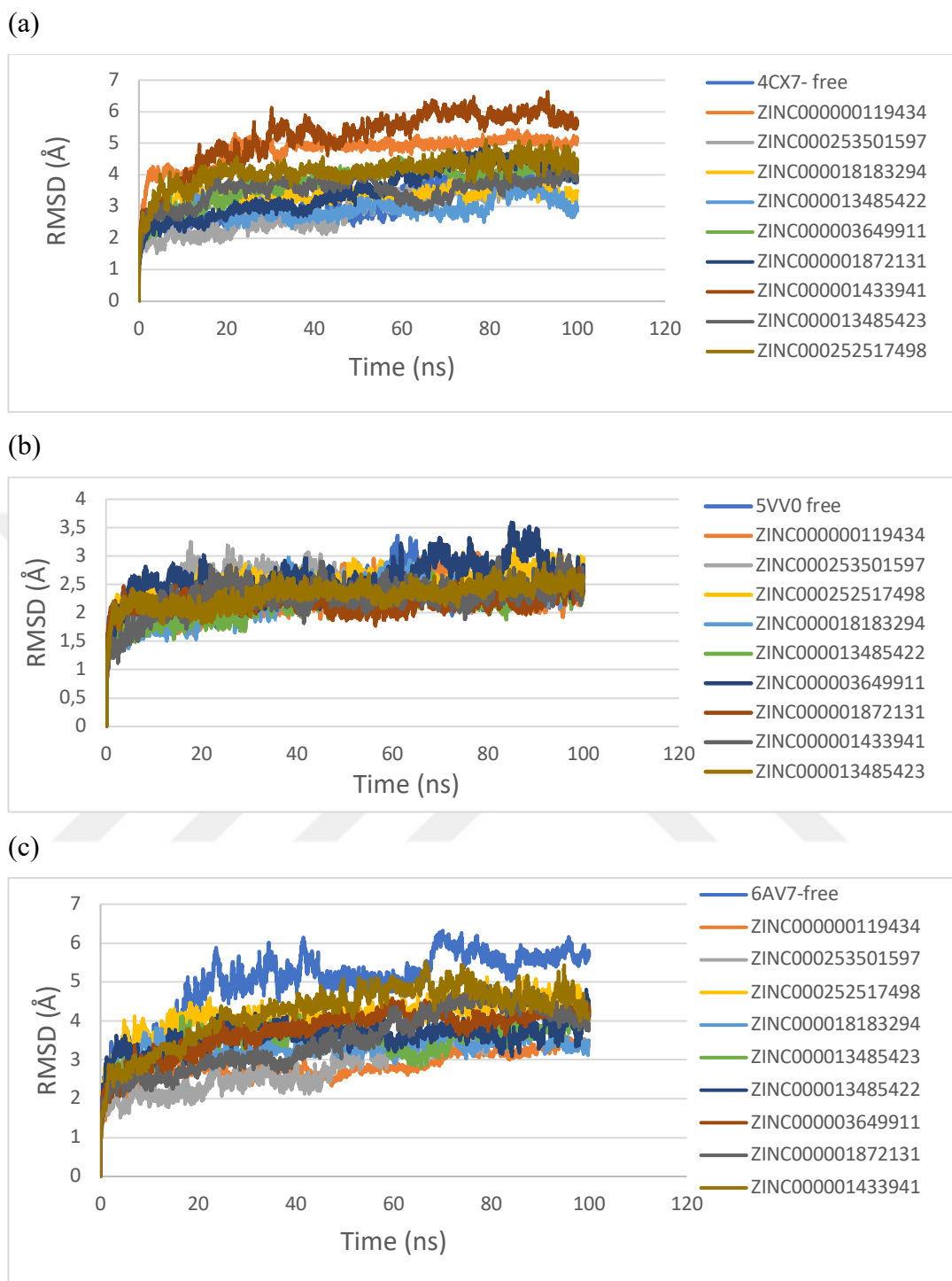
Figure 9.16 Root mean square derivation (RMSD) curves vs. simulation time (100 ns) for free NOSs and complexes. (a) hiNOS (PDB ID:4CX7), (b) hnNOS (PDB ID: 5VV0), and (c) heNOS (PDB: 6AV7).

- **Root mean square fluctuation (RMSF):** RMSF (Pitera, 2014, pp. 6526–6530) is a numerical measurement comparable to RMSD, but rather than revealing positional changes across complete structures over time, it measures individual residue flexibility or how much a specific residue fluctuates throughout a simulation (Martínez, 2015, p. e0119264).

RMSF is displayed vs. residue number and reveals which AA in the protein influence the most to molecular motion structurally. Greater flexibility during the simulations is shown by higher RMSF values and generally correspond to loops. The free nNOS was used as a control to demonstrate how the inhibitors affect the enzyme structure.

The presence of the most flexible areas of nNOS is shown by the high RMSF values. We observed that the average RMSF showed a noticed attenuation for some complexes like the 5VV0-ZINC000001872131 complex compared with the free enzyme, suggesting that the compound's binding reduces the flexibility. In some areas, the RMSF curves were similar but not totally matching except in the rigid areas, indicating that the fluctuated zones belong to the active site where the compounds behave in different manners (**Figure 9.17**).

(a)

(b)

(c)
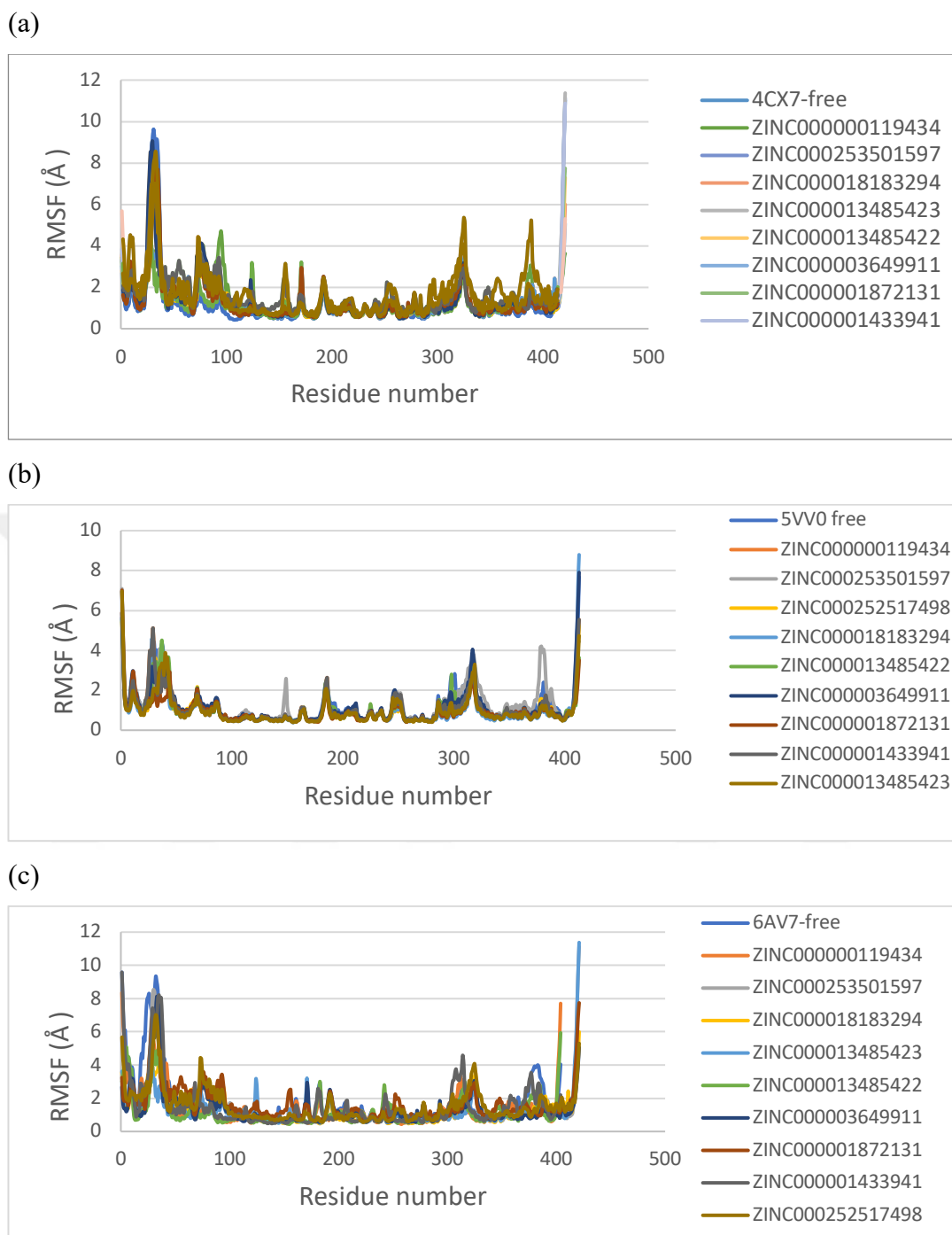
Figure 9.17 Root mean square fluctuation (RMSF) curves vs. Residue number for free NOSs and complexes. (a) hiNOS (PDB ID:4CX7), (b) hnNOS (PDB ID: 5VV0), and (c) heNOS (PDB: 6AV7).

- **The radius of gyration (Rg):** The mass-weighted root mean square distance of a group of atoms from their mutual center of mass is generally described as the Rg. This analysis provides the absolute dimensions of the target (Kumar et al, 2014, p. 502618). If the protein is folded stably, its Rg value will usually remain stable and diminished. When the compound binds to a protein, the radius of gyration changes due to a conformational modification.

The folding frequency of a protein is directly related to its compactness, which may be tracked using the advanced computational approach for determining the radius of gyration. Each structure's Radius of gyration diagram was recorded during the simulation duration to analyze structural deformation changes.

The average score of the free NOSs and the complexes were around 1.2 and 1.5 Å, and they persisted in the plateau state excluding the 5VV0-ZINC000013485423 complex, in which a sudden drop occurred at the last 10 ns, which suggests a structural transformation **(Figure 9.18).**
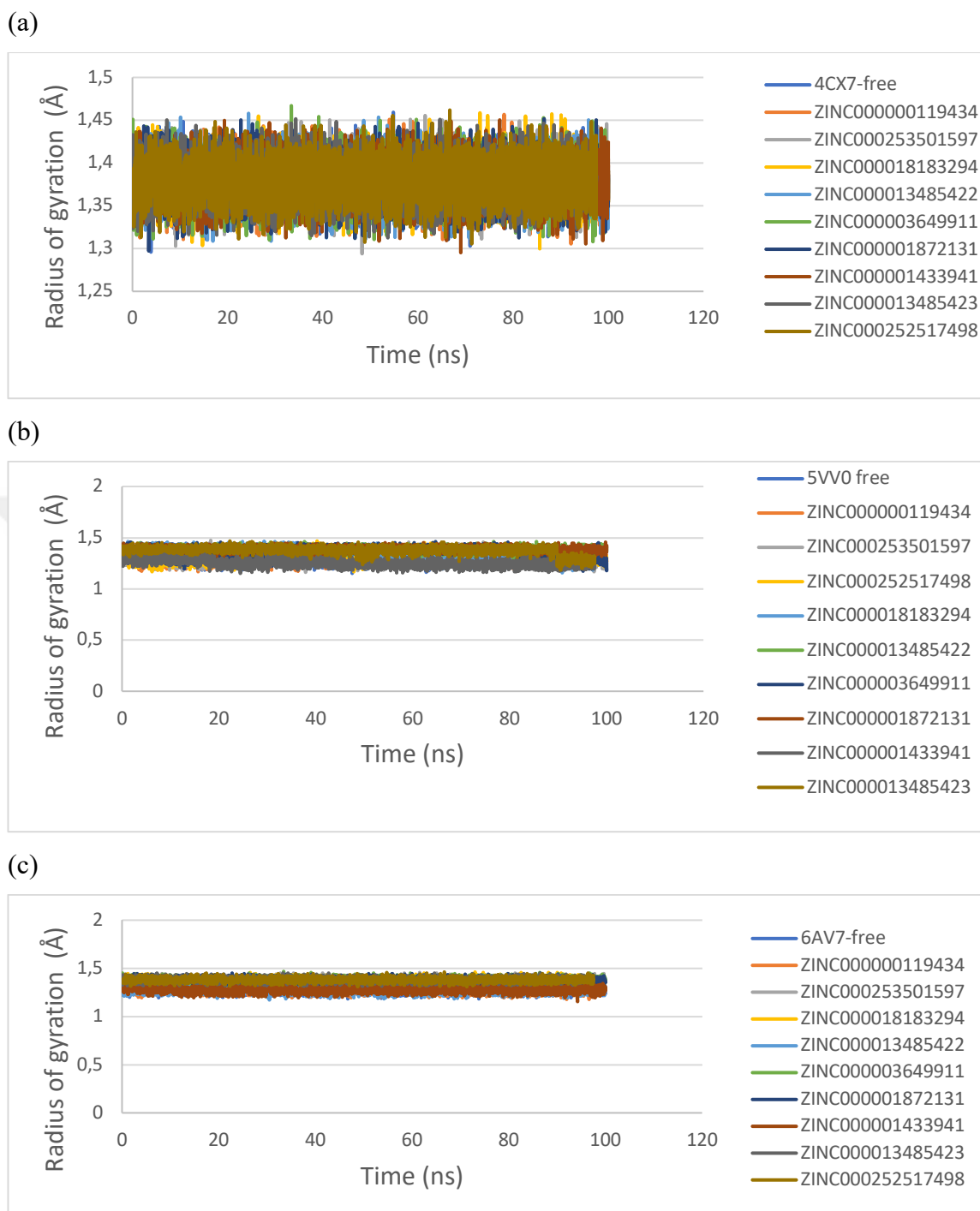
Figure 9.18 Radius of gyration (Rg) curves vs. simulation time for free NOSs and complexes. (a) hiNOS (PDB ID:4CX7), (b) hnNOS (PDB ID: 5VV0), and (c) heNOS (PDB: 6AV7).

- **Hydrogen bond:** One of the essential biological mechanisms is hydrogen bonding. It is indispensable to the structure and function of many important molecules and is usually needed for the protein-ligand complexe's stability.

The H-bonding network is required in enzymatic activity because it allows nNOS substrates or inhibitors to be positioned over the heme. We found that the complex 5VV0-ZINC000252517498 demonstrated a decrease in the H-bond interaction, which correlates with the RMSD results. Some complexes expressed more stable H-bond interactions, such as the 5VV0-ZINC000001433941 complex.

However, the 5VV0-ZINC000253501597 complex showed the minimum H-bond interactions at 100 ns **(Figure 9.19),** so we confirmed that the fewer hydrogen bonds there are, the more variations could be noticed, which ensure the RMSD values (**Figure 9.16).**

(a)

(b)

(c)
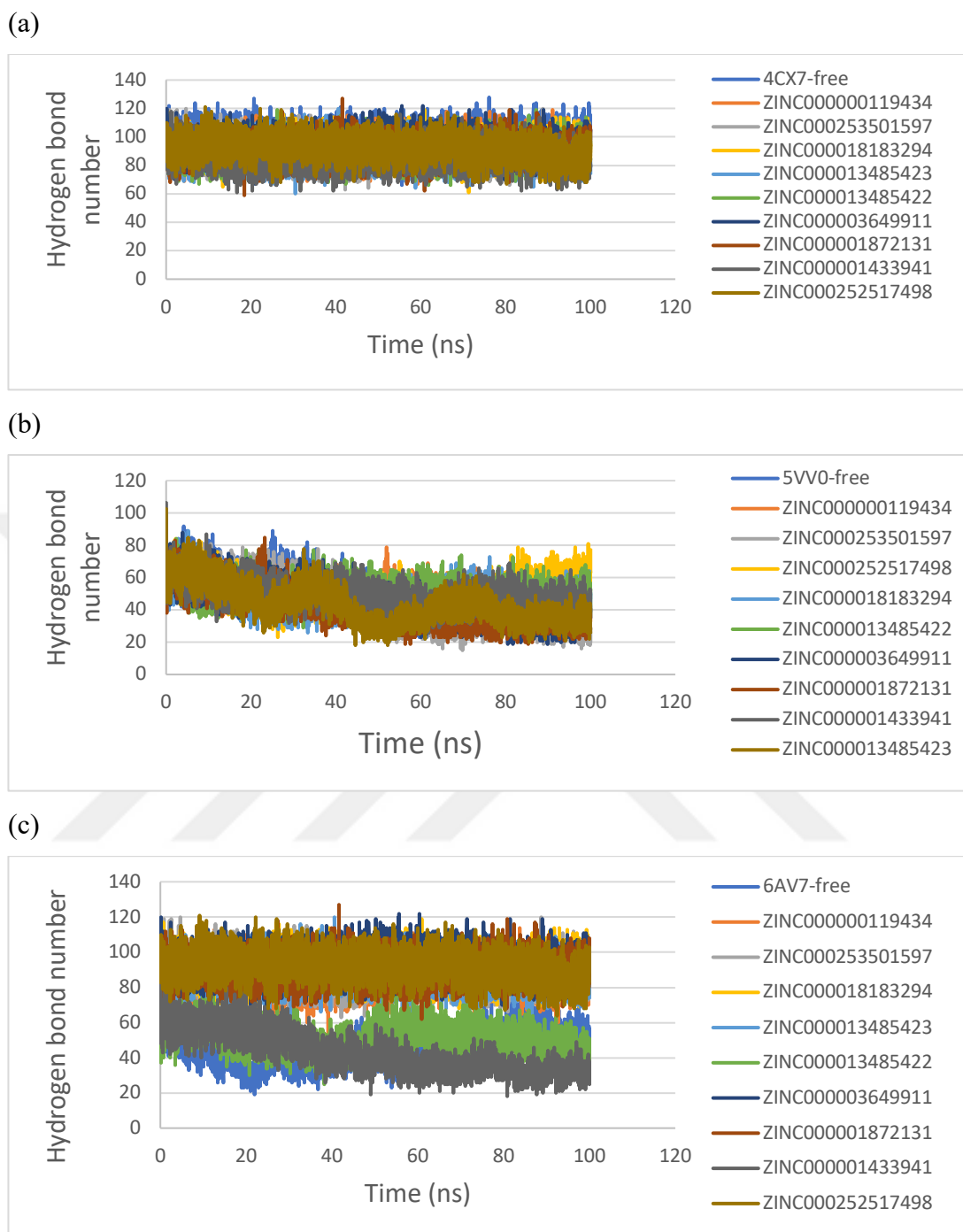
Figure 9.19 Hydrogen bond curves vs. simulation time for free NOSs and complexes. (a) hiNOS (PDB ID:4CX7), (b) hnNOS (PDB ID: 5VV0), and (c) heNOS (PDB: 6AV7).

- **Interaction study after MD simulations:** To investigate the interactions between the compounds and nNOS after performing 100 ns MD simulation, we loaded the trajectories on VMD software, and we retrieved the last frame from each simulation. The 3D and 2D presentations of the chemical interactions were generated using BIOVIA DS.

The final structures of nNOS complexes after MD simulations are shown in **Figures 9.20, 9.21,** and **9.22**. The complex 5VV0-ZINC000013485422 formed several interactions with nNOS. including pi-alkyl interactions with TRP 414, PHE 589, and PHE 709; alkyl interactions with ALA 417, ARG 601; pi-sigma interaction, and hydrogen bond with ARG 601, which maintains ZINC000013485422 attached to nNOS and stable in the active site.

3D
2D

(a) 5VV0-ZINC000253501597

(b) 5VV0-ZINC000001872131

(c) 5VV0-ZINC000000119434

Figure 9.20 3D and 2D presentation of the chemical interactions after MD simulations of nNOS complexes ((a) 5VV0-ZINC000253501597, (b) 5VV0-ZINC000001872131, (c) 5VV0-ZINC000000119434) are represented in the left and right panels, respectively.
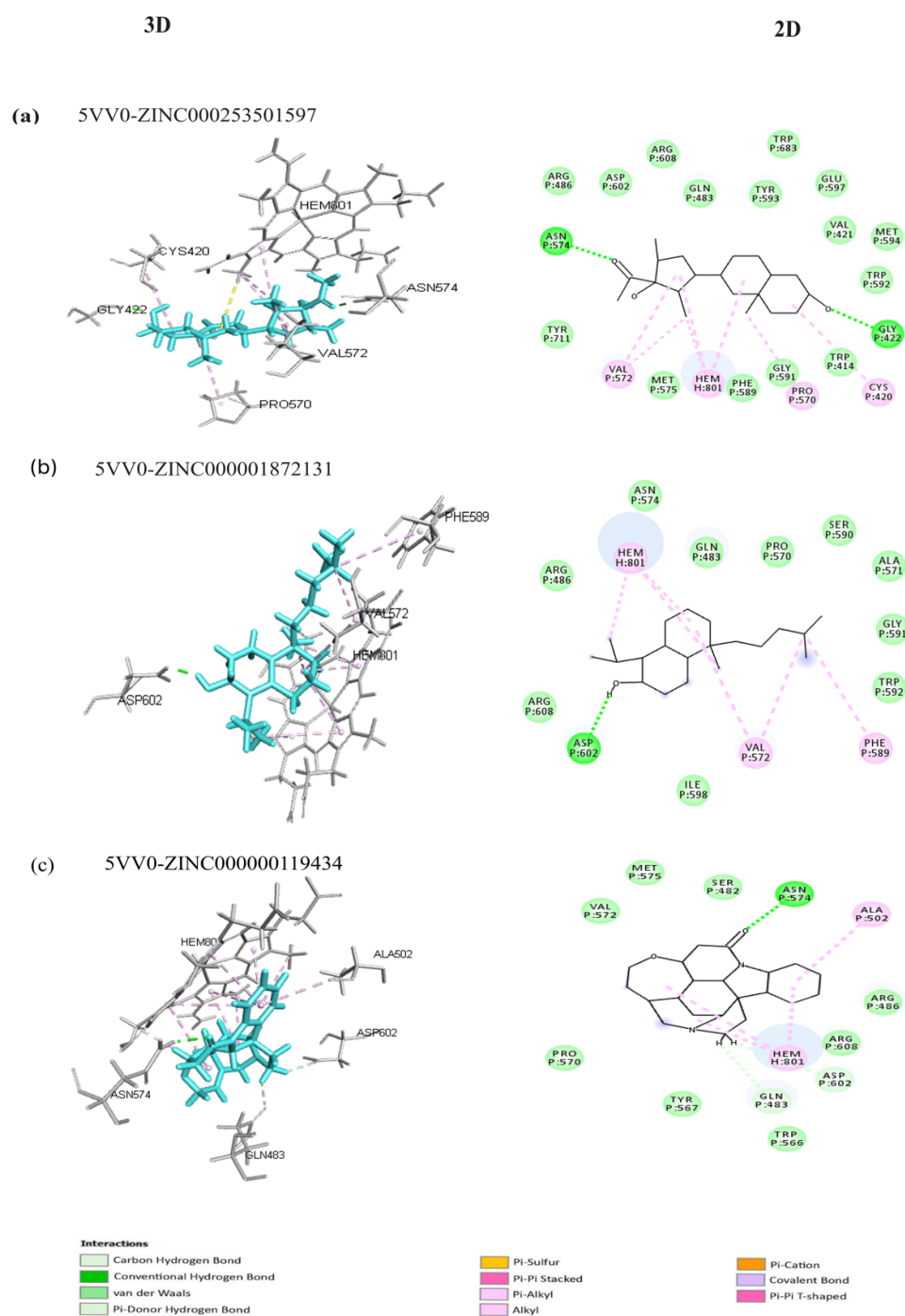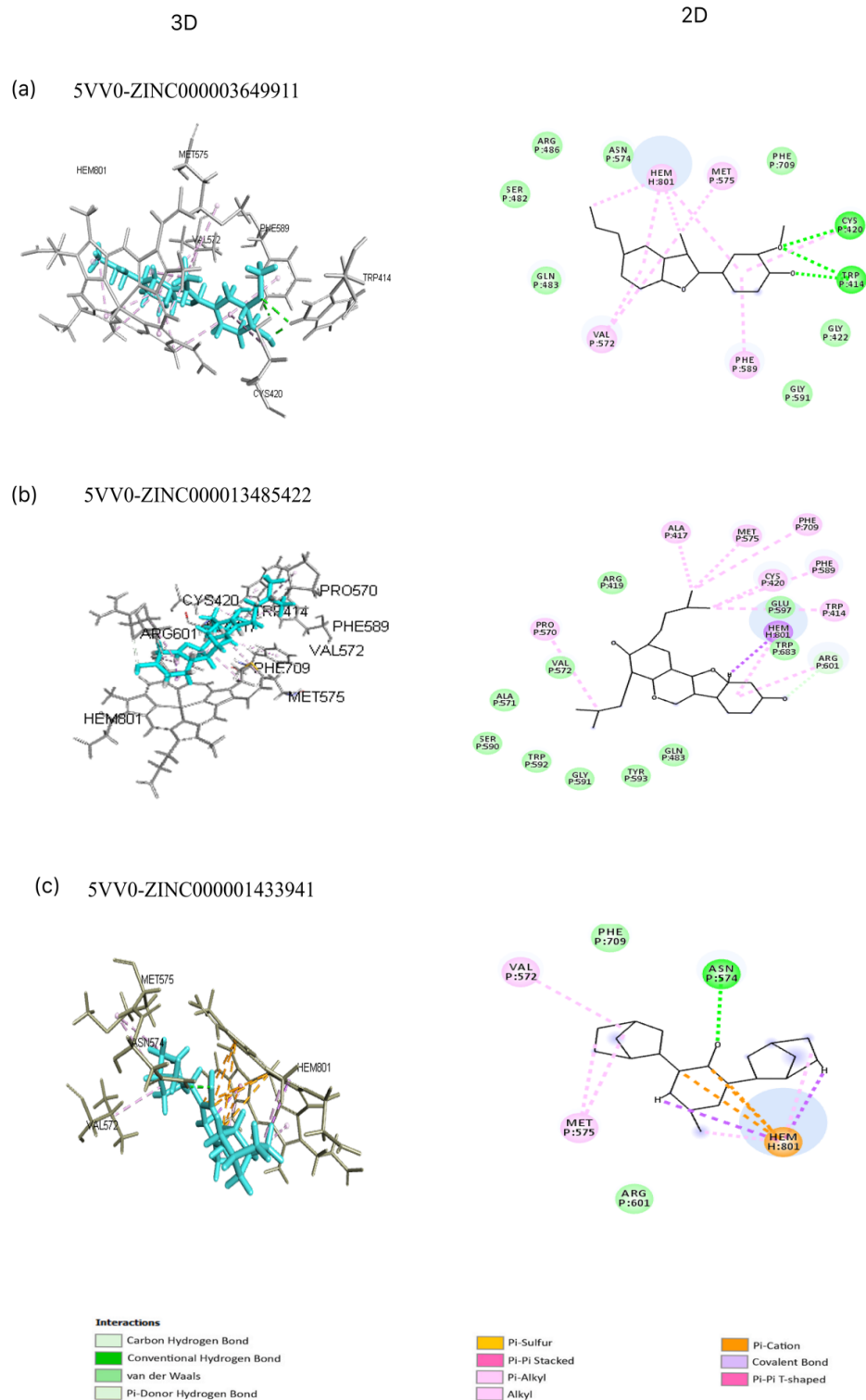
Figure 9.21 3D and 2D presentation of the chemical interactions after MD simulations of nNOS complexes ((a) 5VV0-ZINC000003649911, (b) 5VV0-ZINC000013485422, (c) 5VV0-ZINC000001433941) are represented in the left and right panels, respectively.
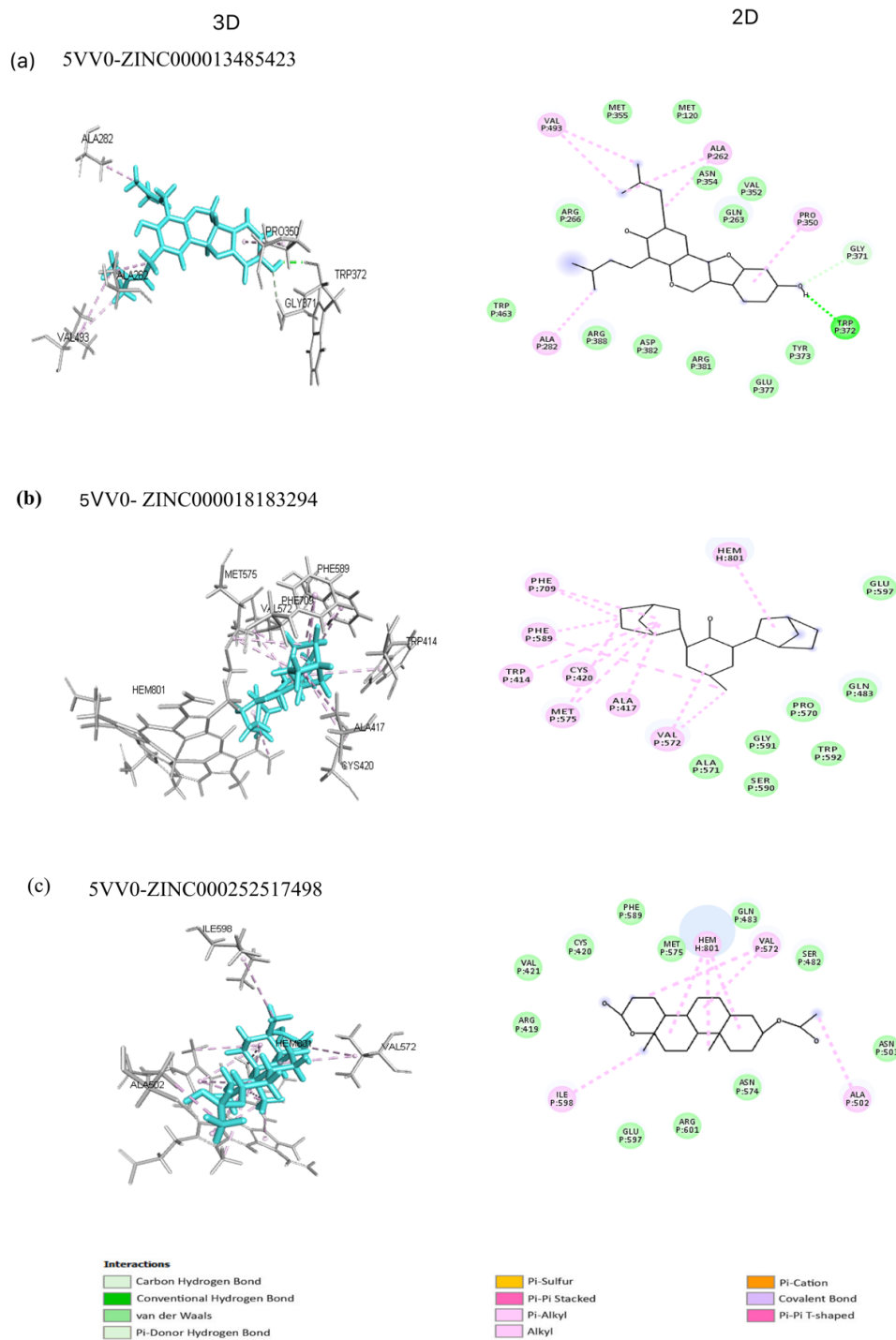
Figure 9.22 3D and 2D presentation of the chemical interactions after MD simulations of nNOS complexes ((a) 5VV0-ZINC000013485423, (b) 5VV0- ZINC000018183294, (c) 5VV0-ZINC000252517498) are represented in the left and right panels, respectively.

10. CONCLUSION

Nitric oxide as a free radical can regulate many physiological and pathological mechanisms. NO roles depend on the simulation of NOS in the enzymatic pathway, which converts the substrate L-Arg to L-citrulline, and NO. NOS activity necessitates the dimerization of enzyme monomers in addition to some cofactors present in each monomer, including reduced NADPH, FAD, FMN, iron protoporphyrin IX, BH4, and CaM. There are 3 isoforms of NOS (nNOS, iNOS, and eNOS) which catalyze the same reaction and share a high structure and sequence identity (50-60%) but have different regulation mechanisms.

In our research, we focused on the neuronal isoform (nNOS) inhibition; it is well known that the overexpression of nNOS is the leading cause of neurodegenerative disease, and due to the tremendous similarity of nNOS's binding site with the two other isoforms, targeting nNOS has always been a tremendous challenge in the drug discovery.

The vast number of people affected by neurodegenerative diseases would strain societies and their healthcare systems. There are over 600 NDs, according to the National Institute of Neurological Disorders and Stroke (NINDS), comprising AD, PD, HD, and ALS.

In certain cases, a particular diagnosis can only be made after analyzing brain tissue after death. Since autopsies are often not performed, there are apparent issues when using mortality data like death reports whether the neurologic disorder is not identified as a primary or secondary cause of death.

ND were found to contribute 12% of the total deaths globally conferring to the WHO Neurological disorders report, Chapter 2, 2015 (https://www.who.int/). AD is still the most common form of dementia affecting at least 27 million people and responsible for at least two-thirds of neurological disorders in the population aged 65 and above.

Unfortunately, there is almost no cure for NDs except for some symptomatic treatments. It is acknowledged that discovering a new drug is time-consuming and bringing a new drug to market is very expensive, and not all research leads to success; in fact, just one of 1000 drug candidates moves to phase 1 clinical trial, and only one of 5 drugs moves from phase 1 trials to the market. CADD became a helpful tool in drug discovery, compensating for the disadvantage of the classical methodologies despite its limitations. In this study, we used SBDD strategies to develop a new inhibitor against nNOS.

First, we started by the validation of NOS as a drug target. We compared the three isoform structures and sequence using BIOVIA DS and confirmed the similarity, which causes the difficulty to develop a new inhibitor against nNOS, which must be efficient and don't interfere with iNOS and eNOS activities (selective). Also, we evaluated the binding affinities of the known inhibitors, which have been compared with the experimental binding affinities values to select the elite NOS structures that can be used in the following stages of the research. We exploited structure-based virtual screening technic to narrow the vast list of compounds retrieved from several databases. We employed AutoDock Vina, a fast molecular docking tool, to select the top compounds which were selective for nNOS over the other isoforms in addition to their high affinity. These probable lead compounds were subject to another docking method to confirm AutoDock Vina's scores, so we got a new refined predictable lead compound list.

The top-ranked probable lead compounds were analyzed using the ADMET prediction tool to evaluate their drug-likeness profile. It is known that lipophilicity and solubility are the two most important molecular qualities in medication absorption. Lipinski rule was used to estimate the oral bioavailability of the compounds, which depends on their physicochemical properties. We know that nNOS is predominantly localized in the CNS. Therefore, the inhibitors should be BBB$^+$. The BBB consists of endothelial cells with tight connections that block external toxins from entering the brain that protect it and maintain its ideal physiological state. However, according to the analysis of the best compounds generated from docking results, we found that most of the compounds were BBB$^-$ which have been rejected.

Finally, the nine compounds that passed this filter were subject to 100 ns run MD simulation to evaluate the complexes' stability using NAMD software. The compound ZINC000013485422 demonstrated high binding mode stability with nNOS during the 100 ns MD run with a good ADMET profile, which may be a promising lead compound. ZINC000013485422 can be optimized *in silico* and in *vitro* to reach the appropriate selectivity as well as the desired potency to get approval for the clinical trials and cure or delay neurodegeneration in the coming years.

BIBLIOGRAPHY

Abraham, M. J. *et al.* (2015) 'GROMACS: High performance molecular simulations through multi-level parallelism from laptops to supercomputers', *SoftwareX*, 1–2, pp. 19–25. doi: 10.1016/J.SOFTX.2015.06.001.

Abreu, R. M. *et al.* (2010) 'MOLA*:* a bootable, self-configuring system for virtual screening using AutoDock4/Vina on computer clusters', *Journal of Cheminformatics*, 2(1), p. 10. doi: 10.1186/1758-2946-2-10.

Acharya, C. *et al.* (2011) 'Recent Advances in Ligand- Based Drug Design: Relevance and Utility of the Conformationally Sampled Pharmacophore Approach', *Current computer - aided drug design,* 7 (1), pp. 10 – 22. doi: 10.2174/157340911793743547.

Acun, B. *et al.* (2018) 'Scalable molecular dynamics with NAMD on the Summit system', *IBM Journal of Research and Development*, 62(6), pp. 4:1-4:9. doi: 10.1147/JRD.2018.2888986.

Ahsan, H. (2013) '3-Nitrotyrosine: A biomarker of nitrogen free radical species modified proteins in systemic autoimmunogenic conditions', *Human Immunology*, 74(10), pp. 1392–1399. doi: 10.1016/j.humimm.2013.06.009.

Alderton, W. K., Cooper, C. E. and Knowles, R. G. (2001) 'Nitric oxide synthases: structure, function and inhibition', *Biochemical Journal*, 357(3), pp. 593–615. doi: 10.1042/bj3570593.

Alkaitis, M. S. and Crabtree, M. J. (2012) 'Recoupling the Cardiac Nitric Oxide Synthases: Tetrahydrobiopterin Synthesis and Recycling', *Current Heart Failure Reports*, 9(3), pp. 200–210. doi: 10.1007/s11897-012-0097-5.

Anderson, A.C. (2011) ' Structure-based functional design of drugs: From target to lead compound ', *Methods in Molecular Biology*, pp.359–366. doi: 10.1007/978-1-60327-216-2_23.

Andersson, C. D., Chen, B. Y. and Linusson, A. (2010) 'Mapping of ligand-binding cavities in proteins', *Proteins: Structure, Function, and Bioinformatics*, 78(6), pp. 1408–1422. doi: 10.1002/prot.22655.

Annedi, S. C. (2015) 'Cell-Permeable Inhibitors of Neuronal Nitric Oxide Synthase Open New Prospects for the Treatment of Neurological Disorders', *Journal of Medicinal Chemistry*, 58(3), pp. 1064–1066. doi: 10.1021/acs.jmedchem.5b00057.

Aparoy, P., Kumar Reddy, K. and Reddanna, P. (2012) 'Structure and ligand based drug design strategies in the development of novel 5- LOX inhibitors', Current *Medicinal Chemistry*, 19(22), pp.3763–3778. doi: 10.2174/092986712801661112.

Araki, S. *et al.* (2020) 'Molecular Sciences Coordination between Calcium/Calmodulin-Dependent Protein Kinase II and Neuronal Nitric Oxide Synthase in Neurons', *International Journal of molecular sciences*, 21(21), p. 7997. doi: 10.3390/ijms21217997.

Arrouchi, H., Lakhlili, W. and Ibrahimi, A. (2019) 'Volume 15(2) Re-positioning of known drugs for Pim-1 kinase target using molecular docking analysis', *Bioinformation*, 15(2), pp. 116–120. doi: 10.6026/97320630015116.

Astashkin, A. V. *et al.* (2019) 'Positional Distributions of the Tethered Modules in Nitric Oxide Synthase: Monte Carlo Calculations and Pulsed EPR Measurements HHS Public Access', *J. Phys. Chem A*, 123 (32), pp. 7075 – 7086. doi: 10.1021/acs.jpca.9b05388.

Bach, A. *et al.* (2015) 'Biochemical investigations of the mechanism of action of small molecules ZL006 and IC87201 as potential inhibitors of the nNOS-PDZ/PSD-95-PDZ interactions', *Scientific Reports*. Nature Publishing Group, 5(1), p. 12157. doi: 10.1038/srep12157.

Baig, M. H. *et al.* (2016) 'Computer Aided Drug Design: Success and Limitations', *Current pharmaceutical design*, 22 5, pp. 572 – 581. doi: 10.2174/1381612822666151125000550.

Baig, M. H. *et al.* (2018) 'Computer Aided Drug Design and its Application to the Development of Potential Drugs for Neurodegenerative Disorders', *Current Neuropharmacology*, 16, pp. 740 – 748. doi: 10.2174/ 1570159X15666171016163510.

Bajorath, J. (2015) 'Open Peer Review Computer-aided drug discovery [version 1; referees: 3 approved]', *F1000Research*. doi: 10.12688/f1000research.6653.1.

Balaji, S. and Srinivasan, N. (2007) 'Comparison of sequence-based and structure-based phylogenetic trees of homologous proteins: Inferences on protein evolution', *Journal of Biosciences*, 32(1), pp. 83–96. doi: 10.1007/s12038-007-0008-1.

Balfour, J. A. and Wilde, M. I. (1997) 'Dorzolamide', *Drugs & Aging*, 10(5), pp. 384–403. doi: 10.2165/00002512-199710050-00006.

Balke, J. E., Zhang, L. and Percival, J. M. (2019) 'Neuronal nitric oxide synthase (nNOS) splice variant function: Insights into nitric oxide signaling from skeletal muscle', *Nitric Oxide*, 82, pp. 35–47. doi: 10.1016/j.niox.2018.11.004.

Bandookwala, M. and Sengupta, P. (2020) '3-Nitrotyrosine: a versatile oxidative stress biomarker for major neurodegenerative diseases', *International Journal of Neuroscience*, 130(10), pp. 1047–1062. doi: 10.1080/00207454.2020.1713776.

Barman, S. A. (2005) 'Effect of Nitric Oxide on Mitogen-Activated Protein Kinases in Neonatal Pulmonary Vascular Smooth Muscle', *Lung*, 183(5), pp. 325–335. doi: 10.1007/s00408-005-2545-4.

Bassil, M. and Anand-Srivastava, M. B. (2007) 'Cyclic GMP modulates the expression of Gi protein and adenylyl cyclase signaling in vascular smooth muscle cells', *Cell Biochemistry and Biophysics*, 47(1), pp. 99–108. doi: 10.1385/CBB:47:1:99.

Batool, M., Ahmad, B. and Choi, S. (2019) 'Molecular Sciences A Structure-Based Drug Discovery Paradigm', *International Journal of molecular sciences,* 20(11), p. 2783. doi: 10.3390/ijms20112783.

Baylis, C. (2006) 'Arginine, arginine analogs and nitric oxide production in chronic kidney disease', *Nature Clinical Practice Nephrology*, 2(4), pp. 209–220. doi: 10.1038/ncpneph0143.

Bazan, I. S. and Fares, H. (2015) 'Therapeutics and Clinical Risk Management Dovepress Pulmonary hypertension: diagnostic and therapeutic challenges', *Therapeutics and Clinical Risk Management*, pp. 11–1221. doi: 10.2147/TCRM.S74881.

Belov Kirdajova, D. *et al.* (2020) 'Ischemia-Triggered Glutamate Excitotoxicity From the Perspective of Glial Cells', *Frontiers in Cellular Neuroscience*, pp. 14 -51. doi: 10.3389/fncel.2020.00051.

Benet, L. Z. *et al.* (2016) 'BDDCS, the Rule of 5 and drugability', *Advanced Drug Delivery Reviews*, 101, pp. 89–98. doi: 10.1016/j.addr.2016.05.007.

Bibi, S. and Sakata, K. (2016) 'Current Status of Computer-Aided Drug Design for Type 2 Diabetes', *Current Computer-Aided Drug Design*, 12(2), pp. 167–177. doi: 10.2174/1573409912666160426120709

Bicket D. P. (2002) 'Using ACE inhibitors appropriately', *American family physician*, *66*(3), pp. 461– 468.

Bignon, E. *et al.* (2019) 'Use of Computational Biochemistry for Elucidating Molecular Mechanisms of Nitric Oxide Synthase', *Computational and Structural Biotechnology Journal*, 17, pp. 415 – 429. doi: 10.1016/j.csbj.2019.03.011.

Bivalacqua, T. J., Champion, H. C. and Hellstrom, W. J. G. (2002) 'Implications of nitric oxide synthase isoforms in the pathophysiology of Peyronie's disease', *International Journal of Impotence Research*, 14(5), pp. 345–352. doi: 10.1038/sj.ijir.3900872.

Boer, R . *et al*. (2000) 'The inhibitory potency and selectivity of arginine substrate site nitric-oxide synthase inhibitors is solely determined by their affinity toward the different isoenzymes', *Molecular pharmacology*, 58(5), pp.1026–1034.

Böhm, H.J. (1994) 'The development of a simple empirical scoring function to estimate the binding constant for a protein-ligand complex of known three-dimensional structure', *Journal of Computer-Aided Molecular Design*, 8(3), pp. 243–256. doi: 10.1007/BF00126743.

Bologa, C. G. and Oprea, T. I. (2012) 'Compound collection preparation for virtual screening', *Methods in molecular biology (Clifton, N.J.)*, *910*, pp. 125–143. doi: 10.1007/978-1-61779-965-5_7.

Bork, N. I. and Nikolaev, V. O. (2018) 'cGMP Signaling in the Cardiovascular System—The Role of Compartmentation and Its Live Cell Imaging', *International Journal of Molecular Sciences* , 19(3),p. 801. doi: 10.3390/ijms19030801.

Bossy-Wetzel, E., Petrilli, A. and Knott, A. B. (2008) 'MUTANT HUNTINGTIN AND MITOCHONDRIAL DYSFUNCTION', *Trends in neurosciences*, 31(12), pp. 609–616. doi: 10.1016/j.tins.2008.09.004.

Bourgognon, J.-M. *et al.* (2021) 'Inhibition of neuroinflammatory nitric oxide signaling suppresses glycation and prevents neuronal dysfunction in mouse prion disease', *Proceedings of the National Academy of Sciences*, 118(10), p. e2009579118. doi: 10.1073/pnas.2009579118.

Bowers, K. J. *et al.* (2006) 'Scalable Algorithms for Molecular Dynamics Simulations on Commodity Clusters', in *SC '06: Proceedings of the 2006 ACM/IEEE Conference on Supercomputing*, p. 43. doi: 10.1109/SC.2006.54.

Brooks, B. R. *et al.* (2009) 'CHARMM: The biomolecular simulation program', *Journal of Computational Chemistry*, 30(10), pp. 1545–1614. doi: 10.1002/jcc.21287.

Brown, F. K. *et al.* (2017) 'The evolution of drug design at Merck Research Laboratories', *Journal of Computer-Aided Molecular Design*, 31(3), pp. 255–266. doi: 10.1007/s10822-016-9993-1.

Bryan, N. S. and Grisham, M. B. (2007) 'Methods to detect nitric oxide and its metabolites in biological samples', *Free Radical Biology and Medicine*, 43(5), pp. 645–657. doi: 10.1016/j.freeradbiomed.2007.04.026. Epub 2007 Apr 29.

Burley, S. K. *et al.* (2017) 'Protein Data Bank (PDB): The single global macromolecular structure archive', in *Methods in Molecular Biology*, pp. 627–641. doi: 10.1007/978-1-4939-7000-1_26.

Butera, G. *et al.* (2019) 'Regulation of Autophagy by Nuclear GAPDH and Its Aggregates in Cancer and Neurodegenerative Disorders', *International Journal of Molecular Sciences*, 20(9), p. 2062. doi: 10.3390/ijms20092062.

Butterfield, D. A., Swomley, A. M. and Sultana, R. (2013) 'Amyloid β-Peptide (1-42)-induced oxidative stress in alzheimer disease: Importance in disease pathogenesis and progression', *Antioxidants and Redox Signaling*, pp. 823–835. doi: 10.1089/ars.2012.5027.

Calabrese, V. *et al.* (2007) 'Nitric oxide in the central nervous system: neuroprotection versus neurotoxicity', *Nature Reviews Neuroscience*, 8(10), pp. 766–775. doi: 10.1038/nrn2214.

Campos, F. *et al.* (2011) 'High blood glutamate oxaloacetate transaminase levels are associated with good functional outcome in acute ischemic stroke', *Journal of Cerebral Blood Flow & Metabolism*, 31, pp. 1387–1393. doi: 10.1038/jcbfm.2011.4.

Cao, J. *et al.* (2005) 'The PSD95–nNOS interface : a target for inhibition of excitotoxic p38 stress-activated protein kinase activation and cell death ', *Journal of Cell Biology*, 168(1), pp. 117–126. doi: 10.1083/jcb.200407024.

Cascione, C. *et al.* (2020) 'The New Frontiers in Neurodegenerative Diseases Treatment: Liposomal-Based Strategies', *Frontiers in Bioengineering and Biotechnology* , 8, p. 566767. doi: 10.3389/fbioe.2020.566767.

Case, D. A. *et al.* (2005) 'The Amber biomolecular simulation programs', *Journal of Computational Chemistry*, 26(16), pp. 1668–1688. doi: 10.1002/jcc.20290.

Chaguturu, R. (2013) 'Combinatorial Chemistry & High Throughput Screening. Editorial', *Combinatorial chemistry & high throughput screening*, 16(1), p.1. doi: 10.2174/1386207311316010001.

Chai, S. C., Lu, J.-P. and Ye, Q.-Z. (2009) 'Determination of binding affinity of metal cofactor to the active site of methionine aminopeptidase based on quantitation of functional enzyme', *Analytical Biochemistry*, 395(2), pp. 263–264. doi: doi: 10.1016/j.ab.2009.07.054.

Chartier, F. J. and Couture, M. (2004) 'Stability of the heme environment of the nitric oxide synthase from Staphylococcus aureus in the absence of pterin cofactor', *Biophysical Journal*, 87(3), pp. 1939–1950. doi: 10.1529/biophysj.104.042119.

Chegkazi, M. S. *et al.* (2018) 'Rational Drug Design Using Integrative Structural Biology*, Methods in molecular biology (Clifton, N.J.),* 1824, pp. 89–111. doi: 10.1007/978-1-4939-8630-9_6.

Chen, G., Seukep, A. J. and Guo, M. (2020) 'Recent Advances in Molecular Docking for the Research and Discovery of Potential Marine Drugs', *Marine drugs*, 18(11), p. 545. doi: 10.3390/md18110545.

Chen, Y. Z. and Zhi, D. G. (2001) 'Ligand–protein inverse docking and its potential use in the computer search of protein targets of a small molecule', *Proteins: Structure, Function, and Bioinformatics*, 43(2), pp. 217–226. doi: 10.1002/1097-0134(20010501)43:2<217::aid-prot1032>3.0.co;2-g.

Cheng, T. *et al.* (2012) 'Structure-Based Virtual Screening for Drug Discovery: a Problem-Centric Review', *The AAPS Journal*, 14(1), pp. 133–141. doi: 10.1208/s12248-012-9322-0.

Cherkasov, A. *et al.* (2014) 'QSAR Modeling: Where Have You Been? Where Are You Going To?', *Journal of Medicinal Chemistry*, 57(12), pp. 4977–5010. doi: 10.1021/jm4004285.

Choi, S. *et al.* (2019) 'A novel STAT3 inhibitor, STX-0119, attenuates liver fibrosis by inactivating hepatic stellate cells in mice', *Biochemical and Biophysical Research Communications*, 513(1), pp. 49–55. doi: 10.1016/j.bbrc.2019.03.156.

Chreifi, G. *et al.* (2014) 'Communication between the Zinc and Tetrahydrobiopterin Binding Sites in Nitric Oxide Synthase', *Biochemistry*, 53(25), pp. 4216–4223. doi: 10.1021/bi5003986.

Chung, K. K. *et al.* (2004) 'S-Nitrosylation of Parkin Regulates Ubiquitination and Compromises Parkin's Protective Function', *Science*, 304(5675), pp. 1328–1331. doi: 10.1126/science.1093891.

Cinelli, M. A. *et al.* (2017) 'Nitrile in the Hole: Discovery of a Small Auxiliary Pocket in Neuronal Nitric Oxide Synthase Leading to the Development of Potent and Selective 2-Aminoquinoline Inhibitors', *Journal* of *Medicinal Chemistry*, 60(9), pp. 3958–3978. doi: 10.1021/acs.jmedchem.7b00259 .

Costa, E. D. *et al.* (2016) 'Neuronal Nitric Oxide Synthase in Vascular Physiology and Diseases', *Front. Physiol*, 7, p. 206. doi: 10.3389/fphys.2016.00206.

Curtin, A. M. *et al*. (2015) 'Computational development of selective nNOS inhibitors: binding modes and pharmacokinetic considerations', *Current medicinal chemistry*, *22*(21), pp. 2558–2579. doi: 10.2174/0929867322666150429112600

Daff, S. (2010) 'NO synthase: Structures and mechanisms', *Nitric Oxide*, 23(1), pp.1–11. doi: 10.1016/j.niox.2010.03.001 .

Dai, Y. *et al.* (2013) 'Association of nNOS Gene Polymorphism with Ischemic Stroke in Han Chinese of North China', *The Scientific World Journal*, 2013, p. 891581. doi: 10.1155/2013/891581.

Daina, A., Michielin, O. and Zoete, V. (2014) 'iLOGP: A Simple, Robust, and Efficient Description of n-Octanol/Water Partition Coefficient for Drug Design Using the GB/SA Approach', *Journal of Chemical Information and Modeling*, 54(12), pp. 3284–3301. doi: 10.1021/ci500467k.

Daina, A., Michielin, O. and Zoete, V. (2017) 'SwissADME: a free web tool to evaluate pharmacokinetics, drug-likeness and medicinal chemistry friendliness of small molecules', *Scientific Reports*, 7(1), p. 42717. doi: 10.1038/srep42717.

Davis, A. M., Teague, S. J. and Kleywegt, G. J. (2003) 'Application and Limitations of X-ray Crystallographic Data in Structure-Based Ligand and Drug Design', *Angewandte Chemie International Edition*, 42 (24), pp. 2718–2736. doi: 10.1002/anie.200200539.

De Vivo M. *et al.* (2016) 'Role of Molecular Dynamics and Related Methods in Drug Discovery', *Journal of Medicinal Chemistry*, 59(9), pp. 4035-4061. doi: 10.1021/acs.jmedchem.5b01684.

Dearden, J. C. (2007) 'In silicoprediction of ADMET properties: how far have we come? ', *Expert Opinion on Drug Metabolism and Toxicology,* 3(5), pp. 635–639. doi: 10.1517/17425255.3.5.635.

Delker, S. L. *et al.* (2010) 'Role of Zinc in Isoform-Selective Inhibitor Binding to Neuronal Nitric Oxide Synthase', *Biochemistry*, 49(51), pp. 10803–10810. doi: 10.1021/bi1013479.

Delker, S. L. *et al.* (2010) 'Unexpected Binding Modes of Nitric Oxide Synthase Inhibitors Effective in the Prevention of a Cerebral Palsy Phenotype in an Animal Model', *Journal of the American Chemical Society*, 132(15), pp. 5437–5442. doi: 10.1021/ja910228a.

Dereeper, A. *et al.* (2010) 'BLAST-EXPLORER helps you building datasets for phylogenetic analysis', *BMC Evolutionary Biology*, 10(1), p. 8. doi: 10.1186/1471-2148-10-8.

Desai, P. V *et al.* (2004) 'Identification of Novel Parasitic Cysteine Protease Inhibitors Using Virtual Screening. 1. The ChemBridge Database', *Journal of Medicinal Chemistry*, 47(26), pp. 6609–6615. doi: 10.1021/jm0493717.

Do, H. T. *et al.* (2019) 'Optimization of Blood–Brain Barrier Permeability with Potent and Selective Human Neuronal Nitric Oxide Synthase Inhibitors Having a 2-Aminopyridine Scaffold', *Journal of Medicinal Chemistry*, 62(5), pp. 2690–2707. doi: 10.1021/acs.jmedchem.8b02032.

Dong, J. *et al.* (2018) 'ADMETlab: a platform for systematic ADMET evaluation based on a comprehensively collected ADMET database', *Journal of Cheminformatics*, 10(1), p. 29. doi: 10.1186/s13321-018-0283-x.

Dong, X., Wang, Y. and Qin, Z. (2009) 'Molecular mechanisms of excitotoxicity and their relevance to pathogenesis of neurodegenerative diseases', *Acta Pharmacologica Sinica*, 30(4), pp. 379–387. doi: 10.1038/aps.2009.24.

Dos Santos, R. N*.,* Ferreira, L. G. and Andricopulo, A. D. (2018) 'Practices in Molecular Docking and Structure-Based Virtual Screening', *Computational Drug Discovery and Design*, pp. 31–50. doi: 10.1007/978-1-4939-7756-7_3.

Drerup, C., Ermert, J. and Coenen, H. H. (2016) 'Synthesis of a Potent Aminopyridine-Based nNOS-Inhibitor by Two Recent No-Carrier-Added 18F-Labelling Methods', *Molecules*, 21(9), pp. 1160 . doi: 10.3390/molecules21091160.

Dunbar, A. Y. *et al.* (2004) 'Ubiquitination and Degradation of Neuronal Nitric-Oxide Synthase in Vitro: Dimer Stabilization Protects the Enzyme from Proteolysis', *Molecular Pharmacology*, 66(4), pp. 964 LP – 969. doi: 10.1124/mol.104.000125.

Dupanloup, I., Schneider, S. and Excoffier, L. (2002) 'A simulated annealing approach to define the genetic structure of populations', *Molecular Ecology*, 11(12), pp. 2571–2581. doi: 10.1046/j.1365-294X.2002.01650.x.

Durães, F., Pinto, M. and Sousa, E. (2018) 'Old Drugs as New Treatments for Neurodegenerative Diseases', *Pharmaceuticals*, 11(2), p. 44. doi: 10.3390/ph11020044.

Durrant, J. D. and McCammon, J. A. (2011) 'Molecular dynamics simulations and drug discovery', *BMC Biology*, 9(1), p. 71. doi: 10.1186/1741-7007-9-71.

Durrant, J. D., de Oliveira, C. A. F. and McCammon, J. A. (2011) 'POVME: An algorithm for measuring binding-pocket volumes', *Journal of Molecular Graphics and Modelling*, 29 (5), pp. 773 – 776. doi: 10.1016/j.jmgm.2010.10.007.

Džoljić, E., Grabatinić, I. and Kostić, V. (2015) 'Why is nitric oxide important for our brain?', *Functional neurolog, 30* (3), pp. 159 – 163. doi: 10.11138/fneur/2015.30.3.159.

Echagarruga, C. T. *et al.* (2020) 'nNOS-expressing interneurons control basal and behaviorally evoked arterial dilation in somatosensory cortex of mice', *eLife*, *9*, p. e60533. doi: 10.7554/eLife.60533.

Ekins, S., Mestres, J. and Testa, B. (2007) 'In silico pharmacology for drug discovery: methods for virtual ligand screening and profiling', *British Journal of Pharmacology*, 152(1), pp. 9–20. doi: 10.1038/sj.bjp.0707305.

El-Hachem, N. *et al.* (2017) 'AutoDock and AutoDockTools for Protein-Ligand Docking: Beta-Site Amyloid Precursor Protein Cleaving Enzyme 1(BACE1) as a Case Study', *Methods in molecular biology (Clifton, N.J.)*, 1598, pp. 391–403. doi: 10.1007/978-1-4939-6952-4_20.

Elber, R. (2016) 'Perspective.Computer simulations of long-time dynamics', *The Journal of Chemical Physics*, 144, p. 60901. doi: 10.1063/1.4940794.

Eldridge, M. D. *et al.* (1997) 'Empirical scoring functions: I. The development of a fast empirical scoring function to estimate the binding affinity of ligands in receptor complexes', *Journal of Computer-Aided Molecular Design*, 11(5), pp. 425–445. doi: 10.1023/A:1007996124545.

Entzeroth, M., Flotow, H. and Condron, P. (2009) 'Overview of High-Throughput Screening', *Current Protocols in Pharmacology*, 44(1), pp. 9.4.1-9.4.27. doi: 10.1002/0471141755.ph0904s44.

Erkkinen, M. G., Kim, M. O. and Geschwind, M. D. (2018) 'Clinical neurology and epidemiology of the major neurodegenerative diseases', *Cold Spring Harbor Perspectives in Biology*, 10(4), p. a033118. doi: 10.1101/cshperspect.a033118.

Esplugues, J. V (2002) 'NO as a signalling molecule in the nervous system', *British Journal of Pharmacology*, 135(5), pp. 1079–1095. doi: 10.1038/sj.bjp.0704569.

Fang, J. *et al.* (2007) 'S-nitrosylation of peroxiredoxin 2 promotes oxidative stress-induced neuronal cell death in Parkinson's disease', *Proceedings of the National Academy of Sciences*, 104(47), pp. 18742 LP – 18747. doi: 10.1073/pnas.0705904104.

Fang, M. *et al.* (2000) 'Dexras1: A G protein specifically coupled to neuronal nitric oxide synthase via CAPON', *Neuron*, 28(1), pp. 183–193. doi: 10.1016/S0896-6273(00)00095-7.

Fedorov, R. *et al.* (2004) 'Structures of nitric oxide synthase isoforms complexed with the inhibitor AR-R17477 suggest a rational basis for specificity and inhibitor design', *Proceedings of the National Academy of Sciences of the United States of America*, 101(16), pp. 5892 LP – 5897. doi: 10.1073/pnas.0306588101.

Feelisch, Martin *et al.* (1999) 'The soluble guanylyl cyclase inhibitor 1H-[1,2,4]oxadiazolo[4,3,-a] quinoxalin-1-one is a nonselective heme protein inhibitor of nitric oxide synthase and other cytochrome P-450 enzymes involved in nitric oxide donor bioactivation', *Molecular pharmacology,* 56 (2), pp. 243-53 . doi: 10.1124/MOL.56.2.243.

Feinstein, W. P. and Brylinski, M. (2015) 'Calculating an optimal box size for ligand docking and virtual screening against experimental and predicted binding pockets', *Journal of Cheminformatics*, 7(1), p. 18. doi: 10.1186/s13321-015-0067-5.

Félétou, M. (2011) *The Endothelium: Part 1: Multiple Functions of the Endothelial Cells — Focus on Endothelium-Derived Vasoactive Mediators*, *San Rafael (CA): Morgan & Claypool Life Sciences* (Chapter 4) , Endothelium - Dependent Regulation of Vascular Tone.

Feng, C. *et al.* (2014) 'Dissecting regulation mechanism of the FMN to heme interdomain electron transfer in nitric oxide synthases', *Journal of Inorganic Biochemistry*, 130, pp. 130–140. doi: 10.1016/j.jinorgbio.2013.09.005.

Fernando, V. *et al.* (2019) 'S-Nitrosylation: An Emerging Paradigm of Redox Signaling', *Antioxidants* , *8*, p. 404. doi: 10.3390/antiox8090404.

Ferreira, L. G. *et al.* (2015) 'Molecular Docking and Structure-Based Drug Design Strategies', *Molecules,* 20(7), pp. 13384–13421. doi: 10.3390/molecules200713384.

Fiscus, R. R. (2002) 'Involvement of Cyclic GMP and Protein Kinase G in the Regulation of Apoptosis and Survival in Neural Cells', *Neurosignals*, 11(4), pp. 175–190. doi: 10.1159/000065431.

Fisette, O. *et al.* (2012) 'Synergistic Applications of MD and NMR for the Study of Biological Systems', *Journal of Biomedicine and Biotechnology*. Edited by S. Pantano, 2012, p. 254208. doi: 10.1155/2012/254208.

Forli, S. *et al.* (2016) 'Computational protein–ligand docking and virtual drug screening with the AutoDock suite', *Nature Protocols*, 11(5), pp. 905–919. doi: 10.1038/nprot.2016.051.

Förstermann, U. and Li, H. (2011) 'Therapeutic effect of enhancing endothelial nitric oxide synthase (eNOS) expression and preventing eNOS uncoupling', *British Journal of Pharmacology*, 164(2), pp. 213–223. doi: 10.1111/j.1476-5381.2

Förstermann, U. and Sessa, W. C. (2012) 'Nitric oxide synthases: regulation and function', *European Heart Journal*, 33(7), pp. 829–837. doi: 10.1093/eurheartj/ehr304.

Foskett, J. K. *et al.* (2007) 'Inositol Trisphosphate Receptor Ca2+ Release Channels', *Physiological Reviews*, 87(2), pp. 593–658. doi: 10.1152/physrev.00035.2006.

Francis, S. H., Busch, J. L. and Corbin, J. D. (2010) 'cGMP-Dependent Protein Kinases and cGMP Phosphodiesterases in Nitric Oxide and cGMP Action', *Pharmacological Reviews*. Edited by D. Sibley, 62(3), pp. 525 LP – 563. doi: 10.1124/pr.110.002907.

Freudenberg, F., Alttoa, A. and Reif, A. (2015) 'Neuronal nitric oxide synthase (NOS1) and its adaptor, NOS1AP, as a genetic risk factors for psychiatric disorders', *Genes, Brain and Behavior*, 14(1), pp. 46–63. doi: 10.1111/gbb.12193.

Fricker, L. D. (2020) 'Proteasome Inhibitor Drugs', *Annual Review of Pharmacology and Toxicology*, 60(1), pp. 457–476. doi: 10.1146/annurev-pharmtox-010919-023603.

Friebe, A., Sandner, P. and Schmidtko, A. (2020) 'cGMP: a unique 2nd messenger molecule – recent developments in cGMP research and development', *Naunyn-Schmiedeberg's Archives of Pharmacology*, 393(2), pp. 287–302. doi: 10.1007/s00210-019-01779-z.

Fukunaga, K. *et al.* (2000) 'Inhibition of neuronal nitric oxide synthase activity by 3-[2-[4-(3-chloro-2-methylphenyl) -1- piperazinyl]ethyl] – 5 , 6 - dimethoxy- 1 - (4 - imidazolylmethyl) -1H-indazole dihydrochloride 3.5 hydrate (DY-9760e), a novel neuroprotective agent, in vitro and in cultured neuroblastoma cells in situ', *Biochemical Pharmacology*, 60(5), pp. 693–699. doi: 10.1016/S0006-2952(00)00370-1.

Fulton, D. J. R. (2016) 'Chapter Two - Transcriptional and Posttranslational Regulation of eNOS in the Endothelium', in Khalil, R. A. B. T.-A. in P. (ed.) *Endothelium*. Academic Press, pp. 29–64. doi: 10.1016/bs.apha.2016.04.001.

Furfine, E. S. *et al.* (1993) 'Selective inhibition of constitutive nitric oxide synthase by L-NG-nitroarginine', *Biochemistry*, 32(33), pp. 8512–8517. doi: 10.1021/bi00084a017.

Gachhui, R. *et al.* (1996) 'Characterization of the reductase domain of rat neuronal nitric oxide synthase generated in the methylotrophic yeast Pichia pastoris. Calmodulin response is complete within the reductase domain itself', *Journal of Biological Chemistry*, 271(34), pp. 20594–20602. doi: 10.1074/jbc.271.34.20594.

Gambaryan, S., Friebe, A. and Walter, U. (2012) 'Does the NO/sGC/cGMP/PKG pathway play a stimulatory role in platelets?', *Blood*, 119(22), pp. 5335–5336. doi: 10.1182/blood-2011-12-396374.

Gantner, B. N., LaFond, K. M. and Bonini, M. G. (2020) 'Nitric oxide in cellular adaptation and disease', *Redox Biology*, 34, p. 101550. doi: 10.1016/j.redox.2020.101550.

Garcin, E. D. *et al.* (2004) 'Structural Basis for Isozyme-specific Regulation of Electron Transfer in Nitric-oxide Synthase*[boxs]', *Journal of Biological Chemistry*, 279(36), pp. 37918–37927. doi: 10.1074/jbc.M406204200.

Garthwaite, J., Charles, S. L. and Chess-Williams, R. (1988) 'Endothelium-derived relaxing factor release on activation of NMDA receptors suggests role as intercellular messenger in the brain', *Nature*, 336(6197), pp. 385–388. doi: 10.1038/336385a0.

Garvey, E. P. *et al.* (1994) 'Potent and selective inhibition of human nitric oxide synthases. Inhibition by non-amino acid isothioureas', *Journal of Biological Chemistry*, 269(43), pp. 26669–26676. doi: 10.1016/s0021-9258(18)47071-8.

Gaulton, A. *et al.* (2012) 'ChEMBL: a large-scale bioactivity database for drug discovery', *Nucleic Acids Research*, 40(D1), pp. D1100–D1107. doi: 10.1093/nar/gkr777.

Geller, D. A. and Billiar, T. R. (1998) 'Molecular biology of nitric oxide synthases', *Cancer and Metastasis Reviews*, 17(1), pp. 7–23. doi: 10.1023/A:1005940202801.

Gerber, N. C. and de Montellano, P. R. O. (1995) 'Neuronal Nitric Oxide Synthase: EXPRESSION IN ESCHERICHIA COLI, IRREVERSIBLE INHIBITION BY PHENYLDIAZENE, AND ACTIVE SITE TOPOLOGY (∗)', *Journal of Biological Chemistry*, 270(30), pp. 17791–17796. doi: 10.1074/jbc.270.30.17791.

Ghasemi, N., Razavi, S. and Nikzad, E. (2017) 'Multiple sclerosis: pathogenesis, symptoms, diagnoses and cell-based therapy', *Cell J*, 19, pp. 1–10. doi: 10.22074/cellj.2016.4867.

Ghosh, A., Chawla-Sarkar, M. and Stuehr, D. J. (2011) 'Hsp90 interacts with inducible NO synthase client protein in its heme-free state and then drives heme insertion by an ATP-dependent process', *The FASEB Journal*, 25(6), pp. 2049–2060. doi: 10.1096/fj.10-180554.

Ghosh, D. K. and Salerno, J. C. (2003) 'Nitric oxide synthases: Domain structure and alignment in enzyme function and control', *Frontiers in Bioscience*, p. 193. doi: 10.2741/959.

Ghosh, S. *et al.* (2006) 'Structure-based virtual screening of chemical libraries for drug discovery', *Current Opinion in Chemical Biology*, 10(3), pp. 194–202. doi: 10.1016/j.cbpa.2006.04.002.

Giménez, B. G. *et al.* (2010) 'Evaluation of blockbuster drugs under the rule-of-five', *Pharmazie*, 65(2), pp. 148–152. doi: 10.1691/ph.2010.9733.

Gimeno, A. *et al.* (2019) 'The Light and Dark Sides of Virtual Screening: What Is There to Know?', *International Journal of Molecular Sciences*, 20(6), p. 1375 . doi: 10.3390/ijms20061375.

Gioia, D. *et al.* (2017) 'Dynamic Docking: A Paradigm Shift in Computational Drug Discovery', *Molecules* . doi: 10.3390/molecules22112029.

Gitler, A. D., Dhillon, P. and Shorter, J. (2017) 'Neurodegenerative disease: models, mechanisms, and a new hope', *Disease Models & Mechanisms*, 10(5), pp. 499–502. doi: 10.1242/dmm.030205.

Glaab, E. (2016) 'Building a virtual ligand screening pipeline using free software: a survey', *Briefings in Bioinformatics*, 17(2), pp. 352–366. doi: 10.1093/bib/bbv037.

Golde, T. E. (2009) 'The therapeutic importance of understanding mechanisms of neuronal cell death in neurodegenerative disease', *Molecular Neurodegeneration*, 4(1), p. 8. doi: 10.1186/1750-1326-4-8.

González-Castro, T. B. *et al.* (2019) 'Association between polymorphisms of NOS1, NOS2 and NOS3 genes and suicide behavior: a systematic review and meta-analysis', *Metabolic Brain Disease*, 34(4), pp. 967–977. doi: 10.1007/s11011-019-00406-3.

González, M. A. (2011) 'Force fields and molecular dynamics simulations', *JDN*, 12, pp. 169–200. doi: 10.1051/sfn/201112009.

Goodsell, D. S., Morris, G. M. and Olson, A. J. (1996) 'Automated docking of flexible ligands: Applications of autodock', *Journal of Molecular Recognition*, 9(1), pp. 1–5. doi: 10.1002/(SICI)1099-1352(199601)9:1<1::AID-JMR241>3.0.CO;2-6.

Grasemann, H. *et al.* (2000) 'A Neuronal NO Synthase (NOS1) Gene Polymorphism Is Associated with Asthma', *Biochemical and Biophysical Research Communications*, 272(2), pp. 391–394. doi: 10.1006/bbrc.2000.2794.

Green, D. V. S. B. T (2003) 'Virtual Screening of Virtual Libraries', *Elsevier*, pp. 61–97. doi: 10.1016/S0079-6468(02)41002-8.

Grek, C. and Townsend, D. M. (2014) 'Protein Disulfide Isomerase Superfamily in Disease and the Regulation of Apoptosis', *Cell Pathology*, 1(1), pp. 4–17. doi: 10.2478/ersc-2013-0001.

Gu, Y. and Zhu, D. (2021) 'nNOS-mediated protein-protein interactions: promising targets for treating neurological and neuropsychiatric disorders', *Journal of Biomedical Research*, 35(1), pp. 1–10. doi: 10.7555/JBR.34.20200108.

Guan, L. *et al.* (2018) 'ADMET-score - a comprehensive scoring function for evaluation of chemical drug-likeness', *MedChemComm*, 10(1), pp. 148–157. doi: 10.1039/c8md00472b.

Guedes, I. A., Pereira, F. S. S. and Dardenne, L. E. (2018) 'Empirical Scoring Functions for Structure-Based Virtual Screening: Applications, Critical Aspects, and Challenges ', *Frontiers in Pharmacology,* 9, p. 1089. doi: 10.3389/fphar.2018.01089.

Ha, K. S. *et al.* (2003) 'Nitric oxide prevents 6-hydroxydopamine-induced apoptosis in PC12 cells through cGMP-dependent PI3 kinase/Akt activation', *The FASEB Journal*, 17(9), pp. 1036–1047. doi: 10.1096/fj.02-0738com.

Hall, C. N. and Garthwaite, J. (2009) 'What is the real physiological NO concentration in vivo?', *Nitric Oxide*, 21(2), pp. 92–103. doi: 10.1016/j.niox.2009.07.002.

Hara, M. R. *et al.* (2005) 'S-nitrosylated GAPDH initiates apoptotic cell death by nuclear translocation following Siah1 binding', *Nature Cell Biology*, 7(7), pp. 665–674. doi: 10.1038/ncb1268.

Hardingham, N., Dachtler, J. and Fox, K. (2013) 'The role of nitric oxide in pre-synaptic plasticity and homeostasis ', *Frontiers in Cellular Neuroscience* , 7, p.190. doi: 10.3389/fncel.2013.00190.

Harigua-Souiai, E. *et al.* (2015) 'Identification of binding sites and favorable ligand binding moieties by virtual screening and self-organizing map analysis', *BMC Bioinformatics*, 16(1), p. 93. doi: 10.1186/s12859-015-0518-z.

Hartenfeller, M. and Schneider, G. (2011) 'De novo drug design', *Methods in molecular biology (Clifton, N.J.)*, 672, pp. 299–323. doi: 10.1007/978-1-60761-839-3_12.

Harvey, A. *et al.* (2016) 'Vascular Fibrosis in Aging and Hypertension: Molecular Mechanisms and Clinical Implications', *Canadian Journal of Cardiology*, 32(5), pp. 659–668. doi: 10.1016/j.cjca.2016.02.070.

Harvey, M. J., Giupponi, G. and Fabritiis, G. De (2009) 'ACEMD: Accelerating Biomolecular Dynamics in the Microsecond Time Scale', *Journal of Chemical Theory and Computation*, 5(6), pp. 1632–1639. doi: 10.1021/ct9000685.

Hassan, N. M. *et al.* (2017) 'Protein-Ligand Blind Docking Using QuickVina-W With Inter-Process Spatio-Temporal Integration', *Scientific Reports*, 7(1), p. 15451. doi: 10.1038/s41598-017-15571-7.

Heinrich, M., Gorath, M. and Richter-Landsberg, C. (1999) 'Neurotrophin-3 (NT-3) modulates early differentiation of oligodendrocytes in rat brain cortical cultures', *Glia*, *28*(3), pp. 244–255.

Hemmens, B. And Mayer, B. (1998) 'Enzymology of nitric oxide synthases', *Methods in molecular biology* , 100, pp. 1-32. doi: 10.1385/1-59259-749-1:1.

Hemmens, B. *et al.* (2000) 'Role of bound zinc in dimer stabilization but not enzyme activity of neuronal nitric-oxide synthase', *Journal of Biological Chemistry*, 275(46), pp. 35786–35791. doi: 10.1074/jbc.M005976200.

Ho, B. K. and Brasseur, R. (2005) 'The Ramachandran plots of glycine and pre-proline', *BMC Structural Biology*, 5(1), p. 14. doi: 10.1186/1472-6807-5-14.

Hollingsworth, S. A. and Dror, R. O. (2018) 'Molecular Dynamics Simulation for All', *Neuron*, 99(6), pp. 1129–1143. doi: 10.1016/j.neuron.2018.08.011.

Hollingsworth, S. A. and Karplus, P. A. (2010) 'A fresh look at the Ramachandran plot and the occurrence of standard structures in proteins', 1(3–4), pp. 271–283. doi: 10.1515/bmc.2010.022.

Honjo, Y. *et al.* (2017) 'Decreased levels of PDI and P5 in oligodendrocytes in Alzheimer's disease', *Neuropathology*, 37(6), pp. 495–501. doi: 10.1111/neup.12395.

Hoover, W. G. *et al*. (1983) 'Historical Development and Recent Applications of Molecular Dynamics Simulation', *Molecular-Based Study of Fluids*, pp.29–46. doi: 10.1021/ba-1983-0204.ch002.

Hornbeck, P. V *et al.* (2015) 'PhosphoSitePlus, 2014: mutations, PTMs and recalibrations', *Nucleic acids research*. 2014/12/16, 43, pp. D512–D520. doi: 10.1093/nar/gku1267.

Huang, H. *et al.* (2016) 'Genetic association of NOS1 exon18, NOS1 exon29, ABCB1 1236C/T, and ABCB1 3435C/T polymorphisms with the risk of Parkinson's disease: A meta-analysis', *Medicine*, 95(40), p. e4982. doi: 10.1097/MD.0000000000004982.

Huang, S. Y., Grinter, S. Z. and Zou, X. (2010) 'Scoring functions and their evaluation methods for protein-ligand docking: recent advances and future directions', *Physical chemistry chemical physics : PCCP,* 12(40), pp. 12899–12908. doi: 10.1039/c0cp00151a.

Huang, S.Y. and Zou, X. (2010a) 'Advances and Challenges in Protein-Ligand Docking', *International Journal of Molecular Sciences*, 11(8), pp. 3016–3034 . doi: 10.3390/ijms11083016.

Huang, S.Y. and Zou, X. (2010b) 'Inclusion of Solvation and Entropy in the Knowledge-Based Scoring Function for Protein−Ligand Interactions', *Journal of Chemical Information and Modeling*, 50(2), pp. 262–273. doi: 10.1021/ci9002987.

Hughes, J. P. *et al.* (2011) 'Principles of early drug discovery', *British Journal of Pharmacology*, 162(6), pp. 1239–1249. doi: 10.1111/j.1476-5381.2010.01127.x.

Humphrey, W., Dalke, A. and Schulten, K. (1996) 'VMD: Visual molecular dynamics', *Journal of Molecular Graphics*, 14(1), pp. 33–38. doi: 10.1016/0263-7855(96)00018-5.

Ignarro, L. J. (2000), *Nitric oxide: biology and pathobiology*, San Diego, Academic Press.

Ignarro, L. J. *et al.* (1986) 'Activation of purified soluble guanylate cyclase by endothelium-derived relaxing factor from intrapulmonary artery and vein: stimulation by acetylcholine, bradykinin and arachidonic acid.', *Journal of Pharmacology and Experimental Therapeutics*, 237(3), pp. 893 – 900.

Irwin, J. J. *et al.* (2012) 'ZINC: A Free Tool to Discover Chemistry for Biology', *Journal of Chemical Information and Modeling*, 52(7), pp. 1757–1768. doi: 10.1021/ci3001277.

Ivanova, K. and Hemmersbach, R. (2020) 'Guanylyl cyclase-cGMP signaling pathway in melanocytes: Differential effects of altered gravity in non-metastatic and metastatic cells', *International Journal of Molecular Sciences,* 21(3), p. 1139. doi: 10.3390/ijms21031139.

Jagadeb, M., Rath, S. N. and Sonawane, A. (2019) 'In silico discovery of potential drug molecules to improve the treatment of isoniazid-resistant Mycobacterium tuberculosis', *Journal of Biomolecular Structure and Dynamics*, 37(13), pp. 3388–3398. doi: 10.1080/07391102.2018.1515116.

Jaghoori, M. M., Bleijlevens, B. and Olabarriaga, S. D. (2016) '1001 Ways to run AutoDock Vina for virtual screening', *Journal of Computer-Aided Molecular Design*, 30(3), pp. 237–249. doi: 10.1007/s10822-016-9900-9.

Jakowec, M. W. and Petzinger, G. M. (2004) '1-methyl-4-phenyl-1,2,3,6-tetrahydropyridine-lesioned model of parkinson's disease, with emphasis on mice and nonhuman primates', *Comparative medicine*, 54(5), pp.497–513.

James, J. S. (1995) 'Saquinavir (Invirase): first protease inhibitor approved--reimbursement, information hotline numbers', *AIDS treatment news*, (237), pp. 1–2.

Janssens, S. P. *et al.* (1992) 'Cloning and expression of a cDNA encoding human endothelium-derived relaxing factor/nitric oxide synthase.', *Journal of Biological Chemistry*, 267(21), pp. 14519–14522. doi: 10.1016/S0021-9258(18)42066-2.

Jazwa, A. and Cuadrado, A. (2010) 'Targeting heme oxygenase-1 for neuroprotection and neuroinflammation in neurodegenerative diseases', *Current drug targets*, *11*(12), pp.1517–1531. doi: 10.2174/138945011009011517.

Jeffrey Man, H. S., Tsui, A. K. Y. and Marsden, P. A. (2014) 'Chapter Seven - Nitric Oxide and Hypoxia Signaling', in Litwack, G. B. T.-V. & H. (ed.) *Nitric Oxide*. Academic Press, pp. 161–192. doi: 10.1016/B978-0-12-800254-4.00007-6.

Ji, H. *et al.* (2009) 'Selective neuronal nitric oxide synthase inhibitors and the prevention of cerebral palsy', *Annals of Neurology*, 65(2), pp. 209–217. doi: 10.1002/ana.21555.

Jin, R. C.and Loscalzo, J. (2010) 'Vascular Nitric Oxide: Formation and Function', *Journal of blood medicine,* 2010 (1),pp. 147–162. doi: 10.2147/JBM.S7000.

Jo, S. *et al.* (2014) 'Chapter Eight - CHARMM-GUI PDB Manipulator for Advanced Modeling and Simulations of Proteins Containing Nonstandard Residues', in Karabencheva-Christova, T. B. T.-A. in P. C. and S. B. (ed.) *Biomolecular Modelling and Simulations*. Academic Press, pp. 235–265. doi: 10.1016/bs.apcsb.2014.06.002.

Johnson, T. O., Ermolieff, J. and Jirousek, M. R. (2002) 'Protein tyrosine phosphatase 1B inhibitors for diabetes', *Nature Reviews Drug Discovery*, 1(9), pp. 696–709. doi: 10.1038/nrd895.

Jurk, K. and Walter, U. (2019) 'New Insights into Platelet Signalling Pathways by Functional and Proteomic Approaches', *Hamostaseologie*, 39(2), pp. 140–151. doi: 10.1055/s-0038-1675356.

Kapetanovic, I. M. (2008) 'Computer-aided drug discovery and development (CADDD): In silico-chemico-biological approach', *Chemico-Biological Interactions*, 171(2), pp. 165–176. doi: 10.1016/j.cbi.2006.12.006.

Karplus, M. and Petsko, G. A. (1990) 'Molecular dynamics simulations in biology', *Nature*, 347(6294), pp. 631–639. doi: 10.1038/347631a0.

Katsila, T. *et al.* (2016) 'Computational approaches in target identification and drug discovery', *Computational and Structural Biotechnology Journal*, 14, pp. 177–184. doi: 10.1016/j.csbj.2016.04.004.

Kelm, M. (1999) 'Nitric oxide metabolism and breakdown', *Biochimica et Biophysica Acta (BBA) - Bioenergetics*, 1411(2-3), pp. 273–289. doi: 10.1016/s0005-2728(99)00020-1.

Kim, S. *et al.* (2016) 'PubChem Substance and Compound databases', *Nucleic Acids Research*, 44(D1), pp. D1202–D1213. doi: 10.1093/nar/gkv951.

Kim, S. H., Johnson, V. J. and Sharma, R. P. (2002) 'Mercury inhibits nitric oxide production but activates proinflammatory cytokine expression in murine macrophage: differential modulation of NF-κB and p38 MAPK signaling pathways', *Nitric Oxide*, 7(1), pp. 67–74. doi: 10.1016/S1089-8603(02)00008-3.

Kishimoto, J. *et al*. (1992) 'Localization of brain nitric oxide synthase (NOS) to human chromosome 12', Genomics, 14(3), pp. 802–804. doi: 10.1016/s0888-7543(05)80192-2.

Knott, A. B. and Bossy-Wetzel, E. (2009) 'Nitric Oxide in Health and Disease of the Nervous System', *Antioxidants & Redox Signaling*, 11(3), pp. 541–554. doi: 10.1089/ars.2008.2234.

Knowles, R. G. *et al.* (1989) 'Formation of nitric oxide from L-arginine in the central nervous system: a transduction mechanism for stimulation of the soluble guanylate cyclase', *Proceedings of the National Academy of Sciences*, 86(13), pp. 5159 LP – 5162. doi: 10.1073/pnas.86.13.5159.

Ko, H. R. *et al*. (2019) 'SIAH1 ubiquitin ligase mediates ubiquitination and degradation of Akt3 in neural development', *The Journal of biological chemistry, 294*(42), pp. 15435–15445. doi: 10.1074/jbc.RA119.009618.

Ko, J. *et al.* (2012) 'GalaxyWEB server for protein structure prediction and refinement', *Nucleic Acids Research*, 40(W1), pp. W294–W297. doi: 10.1093/nar/gks493.

Kore, P. P. *et al.* (2012) 'Computer-Aided Drug Design: An Innovative Tool for Modeling*, Open Journal of Medicinal Chemistry*, 02(04), pp. 139–148. doi: 10.4236/ojmc.2012.24017.

Kornberg, M. D. *et al.* (2010) 'GAPDH mediates nitrosylation of nuclear proteins', *Nature Cell Biology*, 12(11), pp. 1094–1100. doi: 10.1038/ncb2114.

Król, M. and Kepinska, M. (2021) 'Human Nitric Oxide Synthase—Its Functions, Polymorphisms, and Inhibitors in the Context of Inflammation, Diabetes and Cardiovascular Diseases', *International Journal of Molecular Sciences,* 22, p.56.   doi: 10.3390/ijms22010056.

Kufareva, I. and Abagyan, R. (2012) 'Methods of protein structure comparison', *Methods in molecular biology (Clifton, N.J.)*, 857, pp. 231–257. doi: 10.1007/978-1-61779-588-6_10.

Kumar, C. V. *et al.* (2014) 'Computational Analysis Reveals the Association of Threonine 118 Methionine Mutation in PMP22 Resulting in CMT-1A', *Advances in Bioinformatics*. Edited by P. Harrison, 2014, p. 502618. doi: 10.1155/2014/502618.

Kumari, I. *et al.* (2017) 'Molecular Dynamics Simulations, Challenges and Opportunities: A Biologist's Prospective', *Current protein and peptide science,* 18(11), pp.1163–1179. doi: 10.2174/1389203718666170622074741.

Lai, Y.-C. *et al.* (2014) 'Pulmonary Arterial Hypertension', *Circulation Research*, 115(1), pp. 115–130. doi: 10.1161/CIRCRESAHA.115.301146.

Lajoix, A.-D. *et al.* (2004) 'Changes in the Dimeric State of Neuronal Nitric Oxide Synthase Affect the Kinetics of Secretagogue-Induced Insulin Response', *Diabetes*, 53(6), pp. 1467–1474. doi: 10.2337/diabetes.53.6.1467.

Lancaster J. R. (2015) 'Nitric oxide: a brief overview of chemical and physical properties relevant to therapeutic applications', *Future science OA*, 1(1), p. FSO59. doi: 10.4155/fso.15.59.

Landmesser, U. *et al.* (2003) 'Oxidation of tetrahydrobiopterin leads to uncoupling of endothelial cell nitric oxide synthase in hypertension', *The Journal of Clinical Investigation*, 111(8), pp. 1201–1209. doi: 10.1172/JCI14172.

Laurie, A. T. and Jackson, R. M. (2006) 'Methods for the prediction of protein-ligand binding sites for structure-based drug design and virtual ligand screening', *Current protein and peptide science,* 7(5), pp.395–406. doi: 10.2174/138920306778559386.

Lavecchia, A. and Di Giovanni, C. (2013) 'Virtual screening strategies in drug discovery: a critical review', *Current medicinal chemistry*, 20(23), pp. 2839–2860. doi: 10.2174/09298673113209990001.

Lazarev, V. F. *et al.* (2018) 'GAPDH-targeted therapy – A new approach for secondary damage after traumatic brain injury on rats', *Biochemical and Biophysical Research Communications*, 501(4), pp. 1003–1008. doi: 10.1016/j.bbrc.2018.05.099.

Lea, A. P. and Faulds, D. (1996) 'Ritonavir', *Drugs*, 52(4), pp. 541–548. doi: 10.2165/00003495-199652040-00007.

Lee, S. B. *et al.* (2012) 'S-nitrosylation of B23/nucleophosmin by GAPDH protects cells from the SIAH1–GAPDH death cascade', *Journal of Cell Biology*, 199(1), pp. 65–76. doi: 10.1083/jcb.201205015.

Leelananda, S. P. and Lindert, S. (2016) 'Computational methods in drug discovery', *Beilstein Journal of Organic Chemistry*. Beilstein-Institut, 12(1), pp. 2694–2718. doi: 10.3762/bjoc.12.267.

Levine, A. B., Punihaole, D. and Levine, T. B. (2012) 'Characterization of the role of nitric oxide and its clinical applications', *Cardiology, 122*(1), pp. 55–68. doi: 10.1159/000338150.

Lewerenz, J. and Maher, P. (2015) 'Chronic Glutamate Toxicity in Neurodegenerative Diseases—What is the Evidence?', *Frontiers in Neuroscience*. 9, p. 469. doi: 10.3389/fnins.2015.00469.

Lexa, K. W. and Carlson, H. A. (2012) 'Protein flexibility in docking and surface mapping', *Quarterly reviews of biophysic*s, 45(3), pp. 301–343. doi.

Li A. P. (2004) 'A comprehensive approach for drug safety assessment', *Chemico-biological interactions*, 150(1), pp. 27–33. doi: 10.1016/j.cbi.2004.09.009.

Li, C. *et al.* (2007) 'Polymorphisms of the neuronal and inducible nitric oxide synthase genes and the risk of cutaneous melanoma', *Cancer*, 109(8), pp. 1570–1578. doi: 10.1002/cncr.22582.

Li, H. and Poulos, T. L. (2005) 'Structure–function studies on nitric oxide synthases', *Journal of Inorganic Biochemistry*, 99(1), pp. 293–305. doi: 10.1016/j.jinorgbio.2004.10.016.

Li, H. *et al.* (2014) 'Mobility of a Conserved Tyrosine Residue Controls Isoform-Dependent Enzyme-Inhibitor Interactions in Nitric Oxide Synthases', *Biochemistry*, 53, p. 5272. doi: 10.2210/PDB4CX7/PDB.

Li, H. *et al.* (2014) 'Structures of human constitutive nitric oxide synthases', *Acta crystallographica. Section D, Biological crystallography*, 70(Pt 10), pp.2667–2674. doi: 10.1107/S1399004714017064.

Li, H. *et al.* (2018) 'The Structural Basis for Isoform Selective Nitric Oxide Synthase Inhibition by Thiophene-2-Carboximidamides', *Biochemistry*. doi: 10.1021/acs.biochem.8b00895.

Li, Q.and Shah, S. (2017) 'Structure-Based Virtual Screening', *Methods in molecular biology (Clifton, N.J.),* 1558, pp. 111–124. doi: 10.1007/978-1-4939-6783-4_5.

Liao, C. *et al.* (2011) 'Software and resources for computational medicinal chemistry', *Future Medicinal Chemistry*, 3(8), pp. 1057–1085. doi: 10.4155/fmc.11.63.

Lin, F. Y. and MacKerell, A. D. (2019) 'Force Fields for Small Molecules', *Methods in molecular biology (Clifton, N.J.),* 2022, pp. 21–54. doi: 10.1007/978-1-4939-9608-7_2.

Lindahl, E. R. (2008) 'Molecular dynamics simulations', *Methods in molecular biology (Clifton, N.J.),* 443, pp. 3–23. doi: 10.1007/978-1-59745-177-2_1.

Lionta, E. *et al.* (2014) 'Structure-based virtual screening for drug discovery: principles, applications and recent advances'*, Current topics in medicinal chemistry*, 14(16), pp. 1923–1938. doi: 10.2174/1568026614666140929124445.

Lipinski, C. A. (2016) 'Rule of five in 2015 and beyond: Target and ligand structural limitations, ligand chemistry structure and drug discovery project decisions'*, Advanced drug delivery reviews*, 101, pp. 34–41. doi: 10.1016/j.addr.2016.04.029.

Liu, S. *et al.* (2012) 'Application of Consensus Scoring and Principal Component Analysis for Virtual Screening against β-Secretase (BACE-1)', *PLOS ONE*, 7(6), p. e38086. doi:10.1371/journal.pone.0038086.

Liu, T. *et al.* (2007) 'BindingDB: a web-accessible database of experimentally determined protein–ligand binding affinities', *Nucleic Acids Research*, 35(suppl_1), pp. D198–D201. doi: 10.1093/nar/gkl999.

Liu, X. *et al.* (2018) 'Molecular dynamics simulations and novel drug discovery', *Expert Opinion on Drug Discovery*, 13(1), pp. 23–37. doi: 10.1080/17460441.2018.1403419.

Long, F. *et al.* (2017) 'Validation and extraction of molecular-geometry information from small-molecule databases', *Acta crystallographica. Section D, Structural biology,* 73(Pt 2), pp. 103–111. doi: 10.1107/S2059798317000079.

Low, F. M., Hampton, M. B. and Winterbourn, C. C. (2008) 'Peroxiredoxin 2 and Peroxide Metabolism in the Erythrocyte', *Antioxidants & Redox Signaling*, 10(9), pp. 1621–1630. doi: 10.1089/ars.2008.2081.

Lu, J. *et al.* (2016) 'An effective sequence-alignment-free superpositioning of pairwise or multiple structures with missing data', *Algorithms for Molecular Biology*, 11(1), p. 18. doi: 10.1186/s13015-016-0079-3.

Luiking, Y. C., Engelen, M. P. K. J. and Deutz, N. E. P. (2010) 'Regulation of nitric oxide production in health and disease', *Current opinion in clinical nutrition and metabolic care*, 13(1), pp. 97–104. doi: 10.1097/MCO.0b013e328332f99d.

Lundberg, J. O., Weitzberg, E. and Gladwin, M. T. (2008) 'The nitrate–nitrite–nitric oxide pathway in physiology and therapeutics', *Nature Reviews Drug Discovery*, 7(2), pp. 156–167. doi: 10.1038/nrd2466.

Luo, W. *et al.* (2010) 'Heat shock protein 90 in neurodegenerative diseases', *Molecular Neurodegeneration*, 5(1), p. 24. doi: 10.1186/1750-1326-5-24.

Lyne, P. D. (2002) 'Structure-based virtual screening: an overview', *Drug Discovery Today*, 7(20), pp.1047–1055. doi: 10.1016/s1359-6446(02)02483-2.

Macalino, S. J. Y. *et al.* (2015) 'Role of computer-aided drug design in modern drug discovery', *Archives of Pharmacal Research*, 38(9), pp. 1686–1701. doi: 10.1007/s12272-015-0640-5.

Maccallini, C. and Amoroso, R. (2016) 'Targeting neuronal nitric oxide synthase as a valuable strategy for the therapy of neurological disorders', *Neural regeneration research*, 11(11), pp. 1731–1734. doi: 10.4103/1673-5374.194707.

Maia, E. H. B. *et al.* (2020) 'Structure-Based Virtual Screening: From Classical to Artificial Intelligence ', *Frontiers in Chemistry,* 8, p. 343. doi: 10.3389/fchem.2020.00343.

Major, L. L. and Smith, T. K. (2011) 'Screening the MayBridge Rule of 3 Fragment Library for Compounds That Interact with the Trypanosoma brucei myo-Inositol-3-Phosphate Synthase and/or Show Trypanocidal Activity', *Molecular biology international,* 2011, p. 389364. doi: 10.4061/2011/389364.

Makhoul, S .*et al*. (2018) 'Effects of the NO/soluble guanylate cyclase/cGMP system on the functions of human platelets', *Nitric oxide : biology and chemistry*, 76, pp.71–80. doi: 10.1016/j.niox.2018.03.008.

Manjunath, G. P., Ramanujam, P. L. and Galande, S. (2018) 'Structure function relations in PDZ-domain-containing proteins: Implications for protein networks in cellular signalling', *Journal of biosciences,* 43(1), pp.155–171.

Mansoor, A. and Mahabadi, N. (2020) *Volume of Distribution*, In StatPearls. StatPearls Publishing.

Marcus, A. J. *et al.* (*1997*) 'The endothelial cell ecto-ADPase responsible for inhibition of platelet function is CD39', *The Journal* of *clinical investigation*, 99(6), pp. 1351–1360. doi: 10.1172/JCI119294.

Marsden, P. A. *et al.* (1993) 'Structure and chromosomal localization of the human constitutive endothelial nitric oxide synthase gene', *The Journal of biological chemistry*, 268(23), pp.17478–17488.

Marsden, P. A.*et al*. (1992) 'Molecular cloning and characterization of human endothelial nitric oxide synthase', *FEBS letters*, 307(3), pp. 287–293. doi: 10.1016/0014-5793(92)80697-f.

Martin W. (2009) 'Robert F. Furchgott, Nobel laureate (1916-2009)- A personal reflection', *British Journal of pharmacology*, 158(3), pp. 633–637. doi: 10.1111/j.1476-5381.2009.00418.x.

Martínez L. (2015) 'Automatic identification of mobile and rigid substructures in molecular dynamics simulations and fractional structural fluctuation analysis', *PloS one*, 10(3), p. e0119264. doi: 10.1371/Journal.pone.0119264.

Martínez, B. *et al.* (2007) 'A NOS1 gene polymorphism associated with asthma and specific immunoglobulin E response to mite allergens in a Colombian population', *International archives of allergy and immuno*logy, 144(2), pp. 105–113. doi: 10.1159/000103221.

Mattila, J. T.and Thomas, A. C. (2014) 'Nitric oxide synthase: non-canonical expression patterns', *Frontiers in immunology*, 5, p. 478. doi: 10.3389/fimmu.2014.00478.

Maveyraud, L. and Mourey, L. (2020) 'Protein X-ray Crystallography and Drug Discovery', *Molecules (Basel, Switzerland)*, 25(5), p. 1030. doi: 10.3390/molecules25051030.

McCabe, T. J. *et al.* (2000) 'Enhanced electron flux and reduced calmodulin dissociation may explain "calcium-independent" eNOS activation by phosphorylation', *The Journal of biological chemistry*, 275(9), pp. 6123–6128. doi: 10.1074/jbc.275.9.6123.

McCarthy, S. M. *et al.* (2008) 'Nitric oxide regulation of MMP-9 activation and its relationship to modifications of the cysteine switch', *Biochemistry,* 47(21), pp. 5832–5840. doi: 10.1021/bi702496v.

McClellan, K. J. and Goa, K. L. (1998) 'Tirofiban. A review of its use in acute coronary syndromes', *Drugs,* 56(6), pp. 1067–1080. doi: 10.2165/00003495-199856060-00017.

Mejía-García, T. A. *et al. (*2013) 'Nitric oxide regulates AKT phosphorylation and nuclear translocation in cultured retinal cells', *Cellular signalling*, 25(12), pp. 2424–2439. doi: 10.1016/j.cellsig.2013.08.001.

Melikian, N. et al. (2009) 'Neuronal nitric oxide synthase and human vascular regulation', *Trends in cardiovascular medicine*, 19(8), pp. 256–262. doi: 10.1016/j.tcm.2010.02.007.

Meng, X. Y. *et al.* (2011) 'Molecular docking: a powerful approach for structure-based drug discovery', *Current computer-aided drug design*, 7(2), pp. 146–157. doi: 10.2174/157340911795677602.

Merino-Gracia, J. *et al.* (2016) 'Insights into the C-terminal Peptide Binding Specificity of the PDZ Domain of Neuronal Nitric-oxide Synthase: CHARACTERIZATION OF THE INTERACTION WITH THE TIGHT JUNCTION PROTEIN CLAUDIN-3', *The Journal of biological chemistry*, 291(22), pp. 11581–11595. doi: 10.1074/jbc.M116.724427.

Midgett, C. *et al.* (2011) 'Prostacyclin receptor regulation--from transcription to trafficking', *Current molecular medicine*, 11(7), pp. 517–528. doi: 10.2174/156652411800615144.

Mihm, M. J. *et al.* (2001) 'Free 3-nitrotyrosine causes striatal neurodegeneration in vivo', *The Journal of neuroscience : the official Journal of the Society for Neuroscience*, 21(11), p. RC149. doi: 10.1523/JNEUROSCI.21-11-j0003.2001.

Mirzaei, H. *et al.* (2015) 'Energy Minimization on Manifolds for Docking Flexible Molecules', *Journal of chemical theory and computation,* 11(3), pp. 1063–1076. doi: 10.1021/ct500155t.

Mittal, A. and Kakkar, R. (2020) 'Nitric Oxide Synthases and Their Inhibitors: A Review', *Letters in Drug Design and Discovery*, 17, p. 228. doi: 10.2174/1570180816666190222154457.

Mohs, R. C. and Greig, N. H. (2017) 'Drug discovery and development: Role of basic biological research', *Alzheimer's and dementia (New York, N. Y.),* 3(4), pp. 651–657. doi: 10.1016/j.trci.2017.10.005.

Moncada, S. and Higgs, E. A. (2006) 'The discovery of nitric oxide and its role in vascular biology', *British Journal of pharmacology,* 147 Suppl 1(Suppl 1), pp. S193–S201. doi: 10.1038/sj.bjp.0706458.

Moncada, S.and Bolaños, J. P. (2006) 'Nitric oxide, cell bioenergetics and neurodegeneration', *Journal of neurochemistry,* 97(6), pp. 1676–1689. doi: 10.1111/j.1471-4159.2006.03988.x.

Monni, R. *et al*. (2015) 'Tryptophan-to-heme electron transfer in ferrous myoglobins', *Proceedings of the National Academy of Sciences of the United States of America*, 112(18), pp. 5602–5606. doi: 10.1073/pnas.1423186112.

Morrell, N. W. *et al.* (2009) 'Cellular and molecular basis of pulmonary arterial hypertension', *Journal of the American College of Cardiology*, 54(1 Suppl), pp. S20–S31. doi: 10.1016/j.jacc.2009.04.018.

Morris, G. M., Huey, R. and Olson, A. J. (2008) 'Using AutoDock for ligand-receptor docking', *Current protocols in bioinformatics,* Chapter 8. doi: 10.1002/0471250953.bi0814s24.

Mukherjee, P. *et al.* (2014) 'Development of nitric oxide synthase inhibitors for neurodegeneration and neuropathic pain', *Chemical Society reviews*, 43(19), pp. 6814–6838. doi: 10.1039/c3cs60467e.

Mungrue, I. N. and Bredt, D. S. (2004) 'nNOS at a glance: implications for brain and brawn', *Journal of cell science*, 117(Pt 13), pp. 2627–2629. doi: 10.1242/jcs.01187.

Myers, S. and Baker, A. (2001) 'Drug discovery—an operating model for a new era', *Nature Biotechnology*, 19(8), pp. 727–730. doi: 10.1038/90765.

Nabeyrat, E. *et al*. (2003) 'Mitogen-activated protein kinases mediate peroxynitrite-induced cell death in human bronchial epithelial cells. American *Journal* of physiology', *Lung cellular and molecular physiology*, 284(6), pp. L1112-L1120. doi: 10.1152/ajplung.00178.2002.

Nagy, Z. and Smolenski, A. (2018) 'Cyclic nucleotide-dependent inhibitory signaling interweaves with activating pathways to determine platelet responses', *Research and practice in thrombosis and haemostasis*, 2(3), pp. 558–571. doi: 10.1002/rth2.12122.

Nakamura, T. and Lipton, S. A. (2008) 'Emerging roles of S-Nitrosylation in protein misfolding and neurodegenerative diseases', *Antioxidants and redox signaling,* 10(1), pp. 87–101. doi: 10.1089/ars.2007.1858.

Nakamura, T. and Lipton, S. A. (2011) 'S-Nitrosylation of critical protein thiols mediates protein misfolding and mitochondrial dysfunction in neurodegenerative diseases', *Antioxidants and redox signaling*, 14(8), pp. 1479–1492. doi: 10.1089/ars.2010.3570.

Nakamura, T. *et al.* (2013) 'Aberrant protein S-Nitrosylation in neurodegenerative diseases', *Neuron,* 78(4), pp. 596–614. doi: 10.1016/j.neuron.2013.05.005.

Napoli, C. *et al.* (2013) 'Effects of nitric oxide on cell proliferation: novel insights', *Journal of the American College of Cardiology*, 62(2), pp. 89–95. doi: 10.1016/j.jacc.2013.03.070.

National Center for Biotechnology Information. (2021a) *PubChem Compound Summary for CID 3394, Flurbiprofen.* Retrieved May 23, 2021, from https://pubchem.ncbi.nlm.nih.gov/compound/Flurbiprofen.

National Center for Biotechnology Information. (2021b) *PubChem Compound Summary for CID 1549120, Epalrestat.* Retrieved May 23, 2021, from https://pubchem.ncbi.nlm.nih.gov/compound/Epalrestat.

Nava, E. and Llorens, S. (2016) 'The paracrine control of vascular motion. A historical perspective', *Pharmacological research*, 113(Pt A), pp. 125–145. doi: 10.1016/j.phrs.2016.08.003.

Nicolas-Barreales, G., Sujar, A. and Sanchez, A. (2021) 'A web-based tool for simulating molecular dynamics in cloud environments', *Electronics (Switzerland),* 10(2), pp. 1–18. doi: 10.3390/electronics10020185.

Nitti, M. *et al.* (2018) 'Heme Oxygenase 1 in the Nervous System: Does It Favor Neuronal Cell Survival or Induce Neurodegeneration?', *International Journal of molecular sciences*, 19(8), p. 2260. doi: 10.3390/ijms19082260.

Noble, S. and Goa, K. L. (2000) 'Amprenavir: a review of its clinical potential in patients with HIV infection', *Drugs,* 60(6), pp. 1383–1410. doi: 10.2165/00003495-200060060-00012.

Obiol-Pardo, C. and Rubio-Martinez, J. (2007) 'Comparative evaluation of MMPBSA and XSCORE to compute binding free energy in XIAP-peptide complexes', *Journal of chemical information and modeling,* 47(1), pp. 134–142. doi: 10.1021/ci600412z.

Okada D. (1998) 'Tetrahydrobiopterin-dependent stabilization of neuronal nitric oxide synthase dimer reduces susceptibility to phosphorylation by protein kinase C in vitro', *FEBS letters*, 434(3), pp. 261–264. doi: 10.1016/s0014-5793(98)00993-4.

Okamoto, S. and Lipton, S. A. (2015) 'S-Nitrosylation in neurogenesis and neuronal development', *Biochimica et biophysica acta*, 1850(8), pp. 1588–1593. doi: 10.1016/j.bbagen.2014.12.013.

Oliveira, B. L. *et al.* (2013) 'Insights into the structural determinants for selective inhibition of nitric oxide synthase isoforms', *Journal of molecular modeling*, 19(4), pp. 1537–1551. doi: 10.1007/s00894-012-1677-8.

Olsbu, I. K.*et al.* (2018) 'Importance of Val567 on heme environment and substrate recognition of neuronal nitric oxide synthase', *FEBS open bio*, 8(9), pp. 1553–1566. doi: 10.1002/2211-5463.12503.

Onufriev, A. V. and Alexov, E. (2013) 'Protonation and pK changes in protein-ligand binding', *Quarterly reviews of biophysics*, 46(2), pp. 181–209. doi:

Orosz, F., Oláh, J. and Ovádi, J. (2006) 'Triosephosphate isomerase deficiency: facts and doubts', *IUBMB life*, 58(12), pp. 703–715. doi: 10.1080/15216540601115960.

Osuka, K. *et al.* (2002) 'Phosphorylation of Neuronal Nitric Oxide Synthase at Ser847 by CaM-KII in the Hippocampus of Rat Brain after Transient Forebrain Ischemia', *Journal of Cerebral Blood Flow & Metabolism*, 22(9), pp. 1098–1106. doi: 10.1097/00004647-200209000-00007.

Ou-Yang, S. S. *et al.* (2012) 'Computational drug discovery', *Acta pharmacologica Sinica*, 33(10.1017/S0033583513000024.9), pp. 1131–1140. doi: 10.1038/aps.2012.109.

Pacher, P., Beckman, J. S. and Liaudet, L. (2007) 'Nitric oxide and peroxynitrite in health and disease', *Physiological reviews*, 87(1), pp. 315–424. doi: 10.1152/physrev.00029.2006.

Pagadala, N. S., Syed, K. and Tuszynski, J. (2017) 'Software for molecular docking: a review', *Biophysical reviews*, 9(2), pp. 91–102. doi: 10.1007/s12551-016-0247-1.

Pajouhesh, H. and Lenz, G. R. (2005) 'Medicinal chemical properties of successful central nervous system drugs', NeuroRx : *the Journal of the American Society for Experimental NeuroTherapeutics*, 2(4), pp. 541–553. doi: 10.1602/neurorx.2.4.541.

Palumbo, A., Astarita, G. and d'Ischia, M. (2001) 'Inhibition of neuronal nitric oxide synthase by 6-nitrocatecholamines, putative reaction products of nitric oxide with catecholamines under oxidative stress conditions', *The Biochemical Journal*, 356(Pt 1), pp. 105–110. doi: 10.1042/0264-6021:3560105.

Panda, K. *et al.* (2002) 'Distinct dimer interaction and regulation in nitric-oxide synthase types I, II, and III', *The Journal of biological chemistry*, 277(34), pp. 31020–31030. doi: 10.1074/jbc.M203749200.

Panda, K. *et al.* (2003) 'Distinct influence of N-terminal elements on neuronal nitric-oxide synthase structure and catalysis', *The Journal of biological chemistry*, 278(39), pp. 37122–37131. doi: 10.1074/jbc.M304456200.

Papageorgiou, N.*et al.* (2015) 'Homoarginine in the shadow of asymmetric dimethylarginine: from nitric oxide to cardiovascular disease', *Amino acids*, 47(9), pp. 1741–1750. doi: 10.1007/s00726-015-2017-y.

Parasuraman S. (2012) 'Protein data bank', *Journal of pharmacology and pharmacotherapeutics*, 3(4), pp. 351–352. doi: 10.4103/0976-500X.103704.

Park, J.W. *et al.* (2020) 'Potential roles of nitrate and nitrite in nitric oxide metabolism in the eye', *Sci Rep* 10, p. 13166. doi: 10.1038/s41598-020-69272-9.

Parrish, A. B., Freel, C. D. and Kornbluth, S. (2013) 'Cellular mechanisms controlling caspase activation and function', *Cold Spring Harbor perspectives in biology*, 5(6), p. a008672. doi: 10.1101/cshperspect.a008672.

Patnaik D. (2020) 'Structure-based screening of chemical libraries to identify small molecules that are likely to bind with the SET and RING-associated (SRA) domain of Ubiquitin-like, PHD and Ring Finger-containing 1 (UHRF1)', *BMC research notes*, 13(1), p. 254. doi: 10.1186/s13104-020-05103-4.

Patra, C. *et al.* (2020) *Biochemistry, cAMP*. StatPearls Publishing.

Pellecchia, M. *et al.* (2008) 'Perspectives on NMR in drug discovery: a technique comes of age', *Nature reviews. Drug discovery*, 7(9), pp. 738–745. doi: 10.1038/nrd2606.

Pensa, A. V. *et al.* (2017) 'Hydrophilic, Potent, and Selective 7-Substituted 2-Aminoquinolines as Improved Human Neuronal Nitric Oxide Synthase Inhibitors', *Journal of Medicinal Chemistry*, 60(16), pp. 7146–7165. doi: 10.1021/acs.jmedchem.7b00835.

Pérez-Regidor, L. *et al.* (2016) 'Virtual Screening Approaches towards the Discovery of Toll-Like Receptor Modulators', *International Journal of molecular sciences*, 17(9), p. 1508. doi: 10.3390/ijms17091508.

Perrenoud, Q. *et al.* (2012) 'Characterization of Type I and Type II nNOS-Expressing Interneurons in the Barrel Cortex of Mouse', *Frontiers in neural circuits*, 6, p. 36. doi: 10.3389/fncir.2012.00036.

Perri, E. R. *et al.* (2016) 'The Unfolded Protein Response and the Role of Protein Disulfide Isomerase in Neurodegeneration', *Frontiers in cell and developmental biology*, 3, p. 80. doi: 10.3389/fcell.2015.00080.

Phillips, J. C. *et al.* (2005) 'Scalable molecular dynamics with NAMD', *Journal of computational chemistry*, 26(16), pp. 1781–1802. doi: 10.1002/jcc.20289.

Phillips, J. C. *et al.* (2020) 'Scalable molecular dynamics on CPU and GPU architectures with NAMD', *The Journal of chemical physics*, 153(4), p. 044130. doi: 10.1063/5.0014475.

Piazza, M., Guillemette, J. G. and Dieckmann, T. (2015) 'Dynamics of nitric oxide synthase-calmodulin interactions at physiological calcium concentrations', *Biochemistry*, 54(11), pp. 1989–2000. doi: 10.1021/bi501353s.

Picón-Pagès, P., Garcia-Buendia, J. and Muñoz, F. J. (2019) 'Functions and dysfunctions of nitric oxide in brain', *Biochimica et Biophysica Acta (BBA) - Molecular Basis of Disease*, 1865(8), pp. 1949–1967. doi: 10.1016/j.bbadis.2018.11.007.

Pihlstrøm, L., Wiethoff, S. and Houlden, H. (2017) 'Genetics of neurodegenerative diseases: an overview', *Handbook of clinical neurology*, 145, pp. 309–323. doi: 10.1016/B978-0-12-802395-2.00022-5.

Pinzi, L. and Rastelli, G. (2019) 'Molecular Docking: Shifting Paradigms in Drug Discovery', *International Journal of molecular sciences*, 20(18), p. 4331. doi: 10.3390/ijms20184331.

Pitera J. W. (2014) 'Expected distributions of root-mean-square positional deviations in proteins', *The Journal of physical chemistry*. B, 118(24), pp. 6526–6530. doi: 10.1021/jp412776d.

Pitt, W. R., Montalvão, R. W. and Blundell, T. L. (2014) 'Polyphony: superposition independent methods for ensemble-based drug discovery', *BMC bioinformatics*, 15(1), p. 324. doi: 10.1186/1471-2105-15-324.

Plosker, G. L. and Noble, S. (1999) 'Indinavir: a review of its use in the management of HIV infection', *Drugs*, 58(6), pp. 1165–1203. doi: 10.2165/00003495-199958060-00011.

Poulos, T. L. and Li, H. (2017) 'Nitric oxide synthase and structure-based inhibitor design', *Nitric oxide: biology and chemistry*, 63, pp. 68–77. doi: 10.1016/j.niox.2016.11.004.

Pradhan, A. A., Bertels, Z. and Akerman, S. (2018) 'Targeted Nitric Oxide Synthase Inhibitors for Migraine', *Neurotherapeutics : the Journal of the American Society for Experimental NeuroTherapeutics*, 15(2), pp. 391–401. doi: 10.1007/s13311-018-0614-7.

Prado, C. M., Martins, M. A. and Tibério, I. F. (2011) 'Nitric oxide in asthma physiopathology', *ISRN allergy*, 2011, p. 832560. doi: 10.5402/2011/832560.

Prasanna, S. and Doerksen, R. J. (2009) 'Topological polar surface area: a useful descriptor in 2D-QSAR', *Current medicinal chemistry*, 16(1), pp. 21–41. doi: 10.2174/092986709787002817.

Prentice, H., Modi, J. P. and Wu, J. Y. (2015) 'Mechanisms of Neuronal Protection against Excitotoxicity, Endoplasmic Reticulum Stress, and Mitochondrial Dysfunction in Stroke and Neurodegenerative Diseases', *Oxidative medicine and cellular longevity*, 2015, p. 964518. doi: 10.1155/2015/964518.

Priviero, F. B. and Webb, R. C. (2010) 'Heme-dependent and independent soluble guanylate cyclase activators and vasodilation', *Journal of cardiovascular pharmacology,* 56(3), pp. 229–233. doi: 10.1097/FJC.0b013e3181eb4e75.

Radusky, L. *et al.* (2017) 'LigQ: A Webserver to Select and Prepare Ligands for Virtual Screening', *Journal of Chemical Information and Modeling,* 57(8), pp. 1741–1746. doi: 10.1021/acs.jcim.7b00241.

Rajmohan, R. and Reddy, P. H. (2017) 'Amyloid-Beta and Phosphorylated Tau Accumulations Cause Abnormalities at Synapses of Alzheimer's disease Neurons', *Journal of Alzheimer's disease : JAD*, 57(4), pp. 975–999. doi: 10.3233/JAD-160612.

Raman, C. S. *et al.* (1998) 'Crystal structure of constitutive endothelial nitric oxide synthase: a paradigm for pterin function involving a novel metal center', *Cell,* 95(7), pp. 939–950. doi: 10.1016/s0092-8674(00)81718-3.

Raman, C. S. *et al.* (2001) 'Implications for isoform-selective inhibitor design derived from the binding mode of bulky isothioureas to the heme domain of endothelial nitric-oxide synthase', *The Journal of biological chemistry*, 276(28), pp. 26486–26491. doi: 10.1074/jbc.M102255200.

Rameau, G. A. *et al.* (2007) 'Biphasic coupling of neuronal nitric oxide synthase phosphorylation to the NMDA receptor regulates AMPA receptor trafficking and neuronal cell death', *The Journal of neuroscience : the official Journal of the Society for Neuroscience*, 27(13), pp. 3445–3455. doi: 10.1523/JNEUROSCI.4799-06.2007.

Rameau, G. A., Chiu, L. Y. and Ziff, E. B. (2003) 'NMDA receptor regulation of nNOS phosphorylation and induction of neuron death', *Neurobiology of aging,* 24(8), pp.1123–1133. doi: 10.1016/j.neurobiolaging.2003.07.002.

Rao, Y. M., Chaudhury, A. and Goyal, R. K. (2008) 'Active and inactive pools of nNOS in the nerve terminals in mouse gut: implications for nitrergic neurotransmission', *American Journal of physiology. Gastrointestinal and liver physiology*, 294(3), pp. G627–G634. doi: 10.1152/ajpgi.00519.2007.

Reierson, G. W. *et al.* (2011) 'cGMP Signaling, Phosphodiesterases and Major Depressive Disorder', *Current neuropharmacology*, 9(4), pp. 715–727. doi: 10.2174/157015911798376271.

Reif, A. *et al.* (2006) 'A neuronal nitric oxide synthase (NOS-I) haplotype associated with schizophrenia modifies prefrontal cortex function', *Molecular psychiatry*, 11(3), pp. 286–300. doi: 10.1038/sj.mp.4001779.

Reinhard, S. M., Razak, K. and Ethell, I. M. (2015) 'A delicate balance: role of MMP-9 in brain development and pathophysiology of neurodevelopmental disorders', *Frontiers in cellular neuroscience*, 9, p. 280. doi: 10.3389/fncel.2015.00280.

Rizvi, S. M., Shakil, S. and Haneef, M. (2013) 'A simple click by click protocol to perform docking: AutoDock 4.2 made easy for non-bioinformaticians', *EXCLI Journal*, 12, pp. 831–857.

Robichaux, W. G. 3rd. and Cheng, X. (2018) 'Intracellular cAMP Sensor EPAC: Physiology, Pathophysiology, and Therapeutics Development', *Physiological reviews*, 98(2), pp. 919–1053. doi: 10.1152/physrev.00025.2017.

Robinson-White, A. and Stratakis, C. A. (2002) 'Protein kinase A signaling: "Cross-talk" with other pathways in endocrine cells', *Annals of the New York Academy of Sciences*, 968, pp. 256–270. doi: 10.1111/j.1749-6632.2002.tb04340.x.

Roman, L. J. *et al.* (2000) 'The C termini of constitutive nitric-oxide synthases control electron flow through the flavin and heme domains and affect modulation by calmodulin', *The Journal of biological chemistry*, 275(38), pp. 29225–29232. doi: 10.1074/jbc.M004766200.

Rose-Jones, L. J. and Mclaughlin, V. V. (2015) 'Pulmonary hypertension: types and treatments', *Current cardiology reviews*, 11(1), pp. 73–79. doi: 10.2174/1573403x09666131117164122.

Rowen, R. C., Michel, D. J. and Thompson, J. C. (1987) 'Norfloxacin: clinical pharmacology and clinical use', *Pharmacotherapy*, 7(4), pp. 92–110. doi: 10.1002/j.1875-9114.1987.tb04030.x.

Russwurm, M. and Koesling, D. (2004) 'NO activation of guanylyl cyclase', *The EMBO Journal*, 23(22), pp. 4443–4450. doi: 10.1038/sj.emboj.7600422.

Ryan, J. J. and Archer, S. L. (2014) 'The right ventricle in pulmonary arterial hypertension: disorders of metabolism, angiogenesis and adrenergic signaling in right ventricular failure', *Circulation research*, 115(1), pp. 176–188. doi: 10.1161/CIRCRESAHA.113.301129.

Saleron, L. *et al.* (2002) 'Progress in the Development of Selective Nitric Oxide Synthase (NOS) Inhibitors', *Current Pharmaceutical Design*, 8(3), pp. 177–200. doi: 10.2174/1381612023396375.

Salo-Ahen, O. M. *et al.* (2020) 'Molecular Dynamics Simulations in Drug Discovery and Pharmaceutical Development', *Processes*, 9(1), pp. 71. doi: 10.3390/pr9010071.

Sánchez-Ruiloba, L. *et al.* (2014) 'Protein Kinase D Interacts with Neuronal Nitric Oxide Synthase and Phosphorylates the Activatory Residue Serine1412', *PLoS ONE*, 9(4), p. e95191. doi: 10.1371/journal.pone.0095191.

Saravi, S. S. S. (2017) *Nitric Oxide Synthase*- Simple Enzyme- Complex Roles. InTechOpen. London. doi: 10.5772/63170.

Sargsyan, K., Grauffel, C. and Lim, C. (2017) 'How Molecular Size Impacts RMSD Applications in Molecular Dynamics Simulations', *Journal of chemical theory and computation*, 13(4), pp.1518–1524. doi: 10.1021/acs.jctc.7b00028.

Sarkar, A. *et al*. (2015) 'Heat Shock Protein 90 Associates with the Per-Arnt-Sim Domain of Heme-free Soluble Guanylate Cyclase: IMplications for Enzyme Maturation',*The Journal of biological chemistry*, 290(35), pp. 21615–21628. doi: 10.1074/jbc.M115.645515.

Schiebel, J. *et al*. (2018) 'Intriguing role of water in protein-ligand binding studied by neutron crystallography on trypsin complexes', *Nature communications*, 9(1), p. 3559. doi: 10.1038/s41467-018-05769-2.

Schmidt, H. H. *et al*. (1992) 'Ca2+/calmodulin-regulated nitric oxide synthases',*Cell calcium*, 13(6-7), pp. 427–434. doi: 10.1016/0143-4160(92)90055-w.

Schober, P., Boer, C. and Schwarte, L. A. (2018) 'Correlation Coefficients: Appropriate Use and Interpretation', *Anesthesia and analgesia*, 126(5), pp. 1763–1768. doi: 10.1213/ANE.0000000000002864.

Schulte, J. and Littleton, J. T. (2011) 'The biological function of the Huntingtin protein and its relevance to Huntington's Disease pathology', *Current trends in neurology*, 5, pp. 65–78.

Sen, T., Saha, P. and Sen, N. (2018) 'Nitrosylation of GAPDH augments pathological tau acetylation upon exposure to amyloid-β', *Science signaling*, 11(522), p. eaao6765. doi: 10.1126/scisignal.aao6765.

Shah, R. C. *et al*. (2018) 'Redox regulation of soluble guanylyl cyclase', *Nitric oxide : biology and chemistry*, 76, pp. 97–104. doi: 10.1016/j.niox.2018.03.013.

Shahani, N. and Sawa, A. (2012) 'Protein S-nitrosylation: role for nitric oxide signaling in neuronal death', *Biochimica et biophysica acta*, 1820(6), pp. 736–742. doi: 10.1016/j.bbagen.2011.07.010.

Sharma, N. M. and Patel, K. P. (2017) 'Post-translational regulation of neuronal nitric oxide synthase: implications for sympathoexcitatory states', *Expert opinion on therapeutic targets*, 21(1), pp.11–22. doi: 10.1080/14728222.2017.1265505.

Sheldon, A. L. and Robinson, M. B. (2007) 'The role of glutamate transporters in neurodegenerative diseases and potential opportunities for intervention', *Neurochemistry international*, 51(6-7), pp. 333–355. doi: 10.1016/j.neuint.2007.03.012.

Shi, L. and Zhang, N. (2021) 'Applications of Solution NMR in Drug Discovery', *Molecules (Basel, Switzerland),* 26(3), p. 576. doi: 10.3390/molecules26030576.

Shimizu, S. *et al*. (2003) 'Hydrogen peroxide stimulates tetrahydrobiopterin synthesis through the induction of GTP-cyclohydrolase I and increases nitric oxide synthase activity in vascular endothelial cells',*Free radical biology and medicine*, 34(10), pp. 1343–1352. doi: 10.1016/s0891-5849(03)00172-2.

Si, Z. and Wang, X. (2020) 'The Neuroprotective and Neurodegeneration Effects of Heme Oxygenase-1 in Alzheimer's Disease', *Journal of Alzheimer's disease: JAD*, 78(4), pp. 1259–1272. doi: 10.3233/JAD-200720.

Silverman R. B. (2009) 'Design of selective neuronal nitric oxide synthase inhibitors for the prevention and treatment of neurodegenerative diseases', *Accounts of chemical research*, 42(3), pp. 439–451. doi: 10.1021/ar800201v.

Singh, S., Malik, B. K. and Sharma, D. K. (2006) 'Molecular drug targets and structure based drug design: A holistic approach', *Bioinformation,* 1(8), pp. 314–320. doi: 10.6026/97320630001314.

Sirotkin, A. V. *et al.* (2000) 'Effect of cGMP analogues and protein kinase G blocker on secretory activity, apoptosis and the cAMP/protein kinase A system in porcine ovarian granulosa cells in vitro', *The Journal of steroid biochemistry and molecular biology*, 74(1-2), pp. 1–9. doi: 10.1016/s0960-0760(00)00082-0.

Sliwoski, G. *et al.* (2013) 'Computational methods in drug discovery', *Pharmacological reviews*, 66(1), pp. 334–395. doi: 10.1124/pr.112.007336.

Smolenski A. (2012) 'Novel roles of cAMP/cGMP-dependent signaling in platelets', *Journal of thrombosis and haemostasis : JTH*, 10(2), pp. 167–176. doi: 10.1111/j.1538-7836.2011.04576.x.

Smyth, M. S. and Martin, J. H. (2000) 'x ray crystallography', *Molecular pathology : MP*, 53(1), pp. 8–14. doi: 10.1136/mp.53.1.8.

Sneha, P. and George Priya Doss, C. (2016) 'Molecular Dynamics', *Personalized Medicine*, pp. 181–224. doi: 10.1016/bs.apcsb.2015.09.004.

Soares-Silva, M. *et al.* (2016) 'The Mitogen-Activated Protein Kinase (MAPK) Pathway: Role in Immune Evasion by Trypanosomatids', *Frontiers in microbiology*, 7, p. 183. doi: 10.3389/fmicb.2016.00183.

Sobolewska-Stawiarz, A. *et al.* (2014) 'Energy landscapes and catalysis in nitric-oxide synthase', *The Journal of biological chemistry*, 289(17), pp. 11725–11738. doi: 10.1074/jbc.M114.548834.

Song, T. *et al.* (2004) 'Calcium/calmodulin-dependent protein kinase I inhibits neuronal nitric-oxide synthase activity through serine 741 phosphorylation', *FEBS letters*, 570(1-3), pp. 133–137. doi: 10.1016/j.febslet.2004.05.083.

Srivastava, A. *et al.* (2018) 'Role of Computational Methods in Going beyond X-ray Crystallography to Explore Protein Structure and Dynamics', *International Journal of molecular sciences,* 19(11) , p. 3401. doi: 10.3390/ijms19113401.

Stangherlin, A. and Zaccolo, M. (2012) 'Phosphodiesterases and subcellular compartmentalized cAMP signaling in the cardiovascular system', *American Journal of physiology. Heart and circulatory physiology*, 302(2), pp. H379–H390. doi: 10.1152/ajpheart.00766.2011.

Stank, A. *et al.* (2017) 'TRAPP webserver: predicting protein binding site flexibility and detecting transient binding pockets', *Nucleic acids research*, 45(W1), pp. W325–W330. doi: 10.1093/nar/gkx277.

Steele, J. W., Faulds, D. and Goa, K. L. (1993) 'Epalrestat. A review of its pharmacology, and therapeutic potential in late-onset complications of diabetes mellitus', *Drugs and aging*, 3(6), pp. 532–555. doi: 10.2165/00002512-199303060-00007.

Stephenson, J. *et al.* (2018) 'Inflammation in CNS neurodegenerative diseases', *Immunology*, 154(2), pp. 204–219. doi: 10.1111/imm.12922.

Sterling, T. and Irwin, J. J. (2015)' ZINC 15--Ligand Discovery for Everyone', *Journal of chemical information and modeling*, 55(11), pp. 2324–2337. doi: 10.1021/acs.jcim.5b00559.

Subramaniam, S. R. and Chesselet, M. F. (2013) 'Mitochondrial dysfunction and oxidative stress in Parkinson's disease', *Progress in neurobiology*, 106-107, pp. 17–32. doi: 10.1016/j.pneurobio.2013.04.004.

Sugiki, T., Kobayashi, N. and Fujiwara, T. (2017) 'Modern Technologies of Solution Nuclear Magnetic Resonance Spectroscopy for Three-dimensional Structure Determination of Proteins Open Avenues for Life Scientists', *In Computational and Structural Biotechnology Journal* ,15, pp. 328–339.

Sugrue M. F. (1996) 'The preclinical pharmacology of dorzolamide hydrochloride, a topical carbonic anhydrase inhibitor', *Journal of ocular pharmacology and therapeutics,* 12(3), pp. 363–376. doi: 10.1089/jop.1996.12.363.

Sumbalova, L. *et al.* (2018) 'HotSpot Wizard 3.0: web server for automated design of mutations and smart libraries based on sequence input information', *Nucleic acids research*, 46(W1), pp. W356–W362. doi: 10.1093/nar/gky417.

Sundaresan, L., Giri, S. and Chatterjee, S. (2016) 'Inhibitors of Nitric Oxide Synthase: What's up and What's Next? ', *Current Enzyme Inhibition*, 12(1), pp. 81–107. doi: 10.2174/1573408012666151126185922.

Talevi A. (2018) 'Computer-Aided Drug Design: An Overview', *Methods in molecular biology (Clifton, N.J.),* 1762, pp. 1–19. doi: 10.1007/978-1-4939-7756-7_1.

Tang, Y. *et al.* (2006) 'New technologies in computer-aided drug design: Toward target identification and new chemical entity discovery', *Drug discovery today. Technologies*, 3(3), pp. 307–313. doi: 10.1016/j.ddtec.2006.09.004.

Taylor S. D. (2003) 'Inhibitors of protein tyrosine phosphatase 1B (PTP1B)', *Current topics in medicinal chemistry*, 3(7), pp. 759–782. doi: 10.2174/1568026033452311.

Taylor, B. S., Alarcon, L. H. and Billiar, T. R. (1998) 'Inducible nitric oxide synthase in the liver: regulation and function', *Biochemistry. Biokhimiia*, 63(7), pp. 766–781.

Tejero, J. and Stuehr, D. (2013) 'Tetrahydrobiopterin in nitric oxide synthase', *IUBMB life,* 65(4), pp. 358–365. doi: 10.1002/iub.1136.

Tejero, J. *et al.* (2019) 'Mechanism and regulation of ferrous heme-nitric oxide (NO) oxidation in NO synthases', *The Journal of biological chemistry*, 294(19), pp. 7904–7916. doi: 10.1074/jbc.RA119.007810.

Tejero, J. *et al.* (2010) 'Surface charges and regulation of FMN to heme electron transfer in nitric-oxide synthase', *The Journal of biological chemistry*, 285(35), pp. 27232–27240. doi: 10.1074/jbc.M110.138842.

Tengan, C. H., Rodrigues, G. S. and Godinho, R. O. (2012) 'Nitric oxide in skeletal muscle: role on mitochondrial biogenesis and function', *International Journal of molecular sciences*, 13(12), pp. 17160–17184. doi: 10.3390/ijms131217160.

Teramoto, R. and Fukunishi, H. (2007) 'Supervised consensus scoring for docking and virtual screening', *Journal of chemical information and modeling*, 47(2), pp. 526–534. doi: 10.1021/ci6004993.

Teramoto, R. and Fukunishi, H. (2008) 'Structure-based virtual screening with supervised consensus scoring: evaluation of pose prediction and enrichment factors', *Journal of chemical information and modeling*, 48(4), pp. 747–754. doi: 10.1021/ci700464x.

Thomas, D. D. *et al.* (2008) 'The chemical biology of nitric oxide: implications in cellular signaling', *Free radical biology and medicine*, 45(1), pp. 18–31. doi: 10.1016/j.freeradbiomed.2008.03.020.

Todorov, I. T. *et al.* (2006) 'DL_POLY_3: new dimensions in molecular dynamics simulations via massive parallelism', *Journal of Materials Chemistry*, 16(20), p. 1911. doi: 10.1039/b517931a.

Tohgi, H. *et al.* (1999) 'Alterations of 3-nitrotyrosine concentration in the cerebrospinal fluid during aging and in patients with Alzheimer's disease', *Neuroscience letters*, 269(1), pp. 52–54. doi: 10.1016/s0304-3940(99)00406-1.

Tripathi, A.and Bankaitis, V. A. (2017) 'Molecular Docking: From Lock and Key to Combination Lock', *Journal of molecular medicine and clinical applications*, 2(1), p. 10.16966/2575-0305.106. doi: 10.16966/2575-0305.106.

Trott, O. and Olson, A. J. (2010) 'AutoDock Vina: improving the speed and accuracy of docking with a new scoring function, efficient optimization, and multithreading', *Journal of computational chemistry,* 31(2), pp. 455–461. doi: 10.1002/jcc.21334.

Tuteja, N. *et al.* (2004) 'Nitric Oxide as a Unique Bioactive Signaling Messenger in Physiology and Pathophysiology', *Journal of biomedicine and biotechnology*, 2004(4), pp. 227–237. doi: 10.1155/S1110724304402034.

Uehara, T. *et al.* (2006) 'S-nitrosylated protein-disulphide isomerase links protein misfolding to neurodegeneration', *Nature,* 441(7092), pp. 513–517. doi: 10.1038/nature04782.

Underly, R. G. and Shih, A. Y. (2021) 'Rapid, Nitric Oxide Synthesis-Dependent Activation of MMP-9 at Pericyte Somata During Capillary Ischemia in vivo', *Frontiers in physiology*, 11, p. 619230. doi: 10.3389/fphys.2020.619230.

Vakser I. A. (2014) 'Protein-protein docking: from interaction to interactome', *Biophysical Journal*, 107(8), pp. 1785–1793. doi: 10.1016/j.bpj.2014.08.033.

Venema, R. C. *et al.* (1997) 'Subunit interactions of endothelial nitric-oxide synthase', Comparisons to the neuronal and inducible nitric-oxide synthase isoforms. *The Journal of biological chemistry*, 272(2), pp. 1276–1282. doi: 10.1074/jbc.272.2.1276.

Vijayakrishnan R. (2009) 'Structure-based drug design and modern medicine', *Journal of postgraduate medicine*, 55(4), pp. 301–304. doi: 10.4103/0022-3859.58943.

Villalobo A. (2006) 'Nitric oxide and cell proliferation', *The FEBS Journal*, 273(11), pp. 2329–2344. doi: 10.1111/j.1742-4658.2006.05250.x.

Villanueva, C. and Giulivi, C. (2010) 'Subcellular and cellular locations of nitric oxide synthase isoforms as determinants of health and disease', *Free radical biology and medicine*, 49(3), pp. 307–316. doi: 10.1016/j.freeradbiomed.2010.04.004.

Viola, K. L. and Klein, W. L. (2015) 'Amyloid β oligomers in Alzheimer's disease pathogenesis, treatment, and diagnosis', *Acta neuropathologica*, 129(2), pp. 183–206. doi: 10.1007/s00401-015-1386-3.

Víteček, J. *et al.* (2012) 'Arginine-based inhibitors of nitric oxide synthase: therapeutic potential and challenges', *Mediators of inflammation*, 2012, p. 318087. doi: 10.1155/2012/318087.

Vyas, V. K. *et al.* (2012) 'Homology modeling a fast tool for drug discovery: current perspectives', *Indian Journal of pharmaceutical sciences*, 74(1), pp. 1–17. doi: 10.4103/0250-474X.102537.

Wang, M. *et al.* (1997) 'Three-dimensional structure of NADPH-cytochrome P450 reductase: prototype for FMN- and FAD-containing enzymes', *Proceedings of the National Academy of Sciences of the United States of America*, 94(16), pp. 8411–8416. doi: 10.1073/pnas.94.16.8411.

Wang, X. *et al.* (2018) 'Structure-Based Drug Design Strategies and Challenges', *Current Topics in Medicinal Chemistry*, 18. doi: 10.2174/1568026618666180813152921 .

Wang, Y. and Marsden, P. A. (1995) 'Nitric oxide synthases: gene structure and regulation', *Advances in pharmacology* (San Diego, Calif.), 34, pp. 71–90. doi: 10.1016/s1054-3589(08)61081-9.

Wang, Y., Newton, D. C. and Marsden, P. A. (1999) 'Neuronal NOS: gene structure, mRNA diversity, and functional relevance', *Critical reviews in neurobiology,* 13(1), pp. 21–43. doi: 10.1615/critrevneurobiol.v13.i1.20.

Webb R. C. (2003) 'Smooth muscle contraction and relaxation', *Advances in physiology education*, 27(1-4), pp. 201–206. doi: 10.1152/advan.00025.2003.

Williams M. (2003) 'Target validation', *Current opinion in pharmacology*, 3(5), pp. 571–577. doi: 10.1016/j.coph.2003.06.001.

Williams, A. J. *et al.* (2010) 'ChemSpider - building a foundation for the semantic web by hosting a crowd sourced databasing platform for chemistry', *Journal of Cheminformatics*, 2(Suppl 1), p. O16. doi: 10.1186/1758-2946-2-S1-O16.

Wishart, D. S. *et al.* (2008) 'DrugBank: a knowledgebase for drugs, drug actions and drug targets', *Nucleic acids research*, 36, pp. D901–D906.

Wishart, D. S. *et al.* (2018) 'DrugBank 5.0: a major update to the DrugBank database for 2018', *Nucleic acids research*, 46(D1), pp. D1074–D1082. doi: 10.1093/nar/gkx1037.

Wlodawer, A. *et al.* (2008) 'Protein crystallography for non-crystallographers, or how to get the best (but not more) from published macromolecular structures', *The FEBS Journal*, 275(1), pp. 1–21. doi: 10.1111/j.1742-4658.2007.06178.x.

Wu, K. L. *et al.* (2014) 'Role of nitric oxide synthase uncoupling at rostral ventrolateral medulla in redox-sensitive hypertension associated with metabolic syndrome', *Hypertension.* Lippincott Williams and Wilkins, 64(4), pp. 815–824. doi: 10.1161/HYPERTENSIONAHA.114.03777.

Xie, A. *et al.* (2014) 'Shared mechanisms of neurodegeneration in Alzheimer's disease and Parkinson's disease', *BioMed research international*, 2014, p. 648740. doi: 10.1155/2014/648740.

Xie, Z. R. *et al.* (2013) 'LISE: a server using ligand-interacting and site-enriched protein triangles for prediction of ligand-binding sites', *Nucleic acids research,* 41, pp. W292–W296. doi: 10.1093/nar/gkt300.

Yabluchanskiy, A. *et al.* (2013) 'Matrix Metalloproteinase-9: Many Shades of Function in Cardiovascular Disease', *Physiology. American Physiological Society Bethesda, MD*, 28(6), pp. 391–403. doi: 10.1152/physiol.00029.2013.

Yang, J., Roy, A. and Zhang, Y. (2013) 'Protein-ligand binding site recognition using complementary binding-specific substructure comparison and sequence profile alignment', *Bioinformatics (Oxford, England),* 29(20), pp. 2588–2595.

Yang, L. *et al.* (2016) 'Development of novel proteasome inhibitors based on phthalazinone scaffold', *Bioorganic and medicinal chemistry letters,* 26(12), pp. 2801–2805. doi: 10.1016/j.bmcl.2016.04.067.

Yang, X. *et al.* (2017) 'Oxidative Stress-Mediated Atherosclerosis: Mechanisms and Therapies', *Frontiers in physiology*, 8, p. 600. doi: 10.3389/fphys.2017.00600.

Yang, Y. *et al.* (2015) 'Nitric oxide synthase inhibitors: a review of patents from 2011 to the present', *Expert opinion on therapeutic patents*, 25(1), pp. 49–68.

Yong, T. *et al.* (2005) 'Regulation between nitric oxide and MAPK signal transduction in mammals', *Progress in Natural Science*, 15(1), pp. 1–9. doi: 10.1080/10020070512331341700.

Zacharia, I. G. and Deen, W. M. (2005) 'Diffusivity and solubility of nitric oxide in water and saline', *Annals of biomedical engineering*, 33(2), pp. 214–222.

Zhang, M. Q. and Wilkinson, B. (2007) 'Drug discovery beyond the 'rule-of-five'', *Current opinion in biotechnology*, 18(6), pp. 478–488.

Zhang, M., Zhu, W. and Li, Y. (2013) 'Discovery of novel inhibitors of signal transducer and activator of transcription 3 (STAT3) signaling pathway by virtual screening', *European Journal of medicinal chemistry*, 62, pp. 301–310.

Zhang, Y. *et al.* (2018) 'nNOS-CAPON interaction mediates amyloid-β-induced neurotoxicity, especially in the early stages', *Aging cell*, 17(3), p. e12754. doi: 10.1111/acel.12754.

Zhang, Y. H. *et al.* (2014) 'Molecular mechanisms of neuronal nitric oxide synthase in cardiac function and pathophysiology', *The Journal of physiology*, 592(15), pp. 3189–3200. doi: 10.1113/jphysiol.2013.270306.

Zhang, Z. *et al.* (2015) 'Evidence for the contribution of NOS1 gene polymorphism (rs3782206) to prefrontal function in schizophrenia patients and healthy controls', *Neuropsychopharmacology: official publication of the American College of Neuropsychopharmacology,* 40 (6), pp. 1383 – 1394. doi: 10.1038/npp.2014.323.

Zheng, H. *et al.* (2014) 'The future of crystallography in drug discovery. Expert opinion on drug discovery, 9 (2), pp. 125 – 137. doi: 10.1517/17460441.2014.872623.

Zhou, L. and Zhu, D. Y. (2009) 'Neuronal nitric oxide synthase: structure, subcellular localization, regulation, and clinical implications', *Nitric oxide: biology and chemistry*, 20(4), pp. 223–230. doi: 10.1016/j.niox.2009.03.001.

Zhou, L. *et al.* (2010) 'Treatment of cerebral ischemia by disrupting ischemia-induced interaction of nNOS with PSD-95', *Nature medicine*, 16(12), pp. 1439–1443. doi: 10.1038/nm.2245.

Zhu, M. and Gong, D. (2020) 'A Mouse Model of 1-Methyl-4-Phenyl-1,2,3,6-Tetrahydropyridine (MPTP)-Induced Parkinson Disease Shows that 2-Aminoquinoline Targets JNK Phosphorylation', *Medical Science Monitor. International Scientific Information, Inc.*, 26. doi: 10.12659/MSM.920989.

APPENDIX A

Script 1 '**AutoDock.py**': The script used for Autodock vina (Source and authorization from: https://github.com/sarisabban).

```python
#!/usr/bin/python

import os
import sys
import math
#import numpy
#import pymol
import argparse
import itertools
#from pymol.cgo import *

def Box(pX, pY, pZ, x, y, z):
        '''
        Sets up the search box within the protein, which is
        used in the docking protocol
        '''
        pymol.cmd.pseudoatom('Position', pos=[pX, pY, pZ])
        ([X, Y, Z],[a, b, c]) = pymol.cmd.get_extent('Position')
        pymol.cmd.show('spheres', 'Position')
        minX = X+float(x)
        minY = Y+float(y)
        minZ = Z+float(z)
        maxX = X-float(x)
        maxY = Y-float(y)
        maxZ = Z-float(z)
        boundingBox = [BEGIN, LINES,
                VERTEX, minX, minY, minZ,
                VERTEX, minX, minY, maxZ,
                END]
        boxName = 'Box'
        pymol.cmd.load_cgo(boundingBox, boxName)
        return(boxName)

def download(filename):
        '''
        Download, unzip, combine, renumber ligands
        '''
        with open(filename, 'r')as infile:
                for line in infile:
                        try:
                                namegz = line.split()[-1]
                                name = line.split()[-1].split('gz')[0][:-1]
                                get = line.split()[1]
                                wget = 'wget {} -O {}'.format(get, namegz)
                                gunzip = 'gunzip {}'.format(namegz)
                                cat = 'cat {} >> temp'.format(name)
                                os.system(wget)
                                os.system(gunzip)
                                with open(name) as f:
                                        first = f.readline()
                                if first.split()[0] == 'MODEL':
                                        os.system(cat)
                                else:
                                        os.system('echo "MODEL        1" >> temp')
                                        os.system(cat)
                                        os.system('echo "ENDMDL" >> temp')
                        except:
                                with open('error', 'a') as e:
```

```
                                                        e.write(line)
                count = 0
                with open('temp', 'r') as infile:
                        with open('temp2', 'a') as outfile:
                                for line in infile:
                                        if line.startswith('MODEL'):
                                                count += 1
                                                outfile.write('MODEL {:15}\n'.format(count))
                                        else:
                                                outfile.write(line)
                os.system('ls *.pdbqt | grep -v receptor.pdbqt | xargs rm')
                os.remove('temp')
                os.rename('temp2', 'ZINC15.pdbqt')

def receptor(filename):
        '''
        Prepares the receptor by first removing all the water molecules from
        the protein's structure, then adds only the polar hydrogens, then
        it exports the resulting structure and converts it to a .pdbqt file.
        '''
        cmd.load(filename)
        cmd.remove('resn HOH')
        cmd.h_add(selection='acceptors or donors')
        cmd.save('protein.pdb')
        os.system('babel protein.pdb temp.pdbqt -xh')
        os.system('grep ATOM temp.pdbqt > receptor.pdbqt')
        os.remove('temp.pdbqt')
        os.remove('protein.pdb')

def split(filename, direct, prefix, limit):
        '''
        Separates a .pdbqt file with multiple molecules into separate files with
        singles molecules segmented over sub directories.
        '''
        with open(filename) as infile:
                count = 0
                in_dir_count = 0
                dircount = 0
                for dircount in itertools.count():
                        for line in infile:
                                if line.strip() == 'MODEL{:16}'.format(count+1):
                                        directory = os.path.join(direct, '{}'.format(dircount+1))
                                        os.makedirs(directory, exist_ok=True)
                                        name = '{}_{:09}.pdbqt'.format(prefix, count+1)
                                        out = os.path.join(directory, name)
                                        with open(out, 'w') as outfile:
                                                for line in infile:
                                                        if line.strip() == 'ENDMDL':
                                                                break
                                                        if line.split()[0] == 'REMARK' and\
                                                                                          line.split()[1] ==
'Name':
                                                                NewName = os.path.join(directory,\
        '{}.pdbqt'.format(line.split()[3]))
                                                        outfile.write(line)
                                        os.rename(out, NewName)
                                        count += 1
                                        in_dir_count += 1
                                        if in_dir_count >= limit:
                                                in_dir_count = 0
                                                print('[+] Finished directory {}'.format(directory))
                                                break
                                else: break
        print('----------\n[+] Done')

def PBS(pX, pY, pZ, x, y, z, seed, exhaust, out, CPU, array, email):
        '''
        Write a PBS file for HPC virtual screening
        '''
        if out == 'True' or out == 'true':
                output = '''out_$n'''
        elif out == 'False' or out == 'false':
```

```python
                output = '/dev/null'
        with open('dock.pbs', 'w') as dock:
                dock.write('#!/bin/bash\n\n')
                dock.write('#PBS -N Docking\n')
                dock.write('#PBS -m e\n')
                dock.write('#PBS -M {}\n'.format(email))
                dock.write('#PBS -q thin_1m\n')
                dock.write('#PBS -l select=1:ncpus=24:ompthreads=24\n')
                dock.write('#PBS -j oe\n')
                dock.write('#PBS -J 1-{}\n\n'.format(array))
                dock.write('cd $PBS_O_WORKDIR\n\n')
                dock.write('mkdir -p ../Ligands_Completed/${PBS_ARRAY_INDEX}\n')
                dock.write('process() { local n=${1##*/}\n')
                dock.write('\t./vina \\\n')
                dock.write('\t\t--receptor receptor.pdbqt \\\n')
                dock.write('\t\t--ligand "$1" \\\n')
                dock.write('\t\t--out {} \\\n'.format(output))
                dock.write('\t\t--log "log_$n" \\\n')
                dock.write('\t\t--exhaustiveness {} \\\n'.format(exhaust))
                dock.write('\t\t--cpu {} \\\n'.format(CPU))
                dock.write('\t\t--seed {} \\\n'.format(seed))
                dock.write('\t\t--center_x {} \\\n'.format(pX))
                dock.write('\t\t--center_y {} \\\n'.format(pY))
                dock.write('\t\t--center_z {} \\\n'.format(pZ))
                dock.write('\t\t--size_x {} \\\n'.format(x))
                dock.write('\t\t--size_y {} \\\n'.format(y))
                dock.write('\t\t--size_z {} \\\n'.format(z))
                dock.write('"\t\t| awk -v name="$n" \'$1 == "1" {print name "\\t" $0;exit}\' >>
Docks_${PBS_ARRAY_INDEX} \\\n"')
                dock.write('\t\t&& rm log_$n \\\n')
                dock.write('\t\t&& mv "$1" ../Ligands_Completed/${PBS_ARRAY_INDEX}\n')
                dock.write('}\n')
                dock.write('export -f process\n')
                dock.write('"find ../Ligands/${PBS_ARRAY_INDEX}/ -type f -print0 | xargs -0 -P 24 -I{} bash
-c \'process "$1"\' _ {}"')

def Kd_to_dG(Kd):
        Kd = float(Kd)
        dG = 0.0019872036*298*numpy.log(Kd)
        print('{} Kcal/mol'.format(round(dG, 2)))

def dG_to_Kd(dG):
        dG = float(dG)
        Kd = math.e**(dG/(0.0019872036*298))
        print('{:0.2e} dG'.format(Kd))

parser = argparse.ArgumentParser(description='Prep ligands for AutoDock Vina')
parser.add_argument('-r',
                                        '--receptor',
                                        nargs='+',
                                        help='Prep and convert protein receptor from PDB to PDBQT')
parser.add_argument('-b',
                                        '--box',
                                        nargs='+',
                                        help='Draw search box')
parser.add_argument('-d',
                                        '--download',
                                        nargs='+',
                                        help='Download, unzip, renumber, combine ligands')
parser.add_argument('-s',
                                        '--split',
                                        nargs='+',
                                        help='Split a file with multiple models into single files\
                                                        segmented into directories')
parser.add_argument('-j',
                                        '--job',
                                        nargs='+',
                                        help='Write the PBS file for HPC virtual screaning')
parser.add_argument('-c',
                                        '--combine',
                                        nargs='+',
                                        help='Sort and combine the docking results into a file')
parser.add_argument('-Kd',
```

```python
                                        '--Kd_to_dG',
                                        nargs='+',
                                        help='Convert Kd to delta G')
parser.add_argument('-dG',
                                        '--dG_to_Kd',
                                        nargs='+',
                                        help='Convert delta G to Kd')
args = parser.parse_args()

def main():
        if args.receptor:
                receptor(sys.argv[2])
        elif args.box:
                pymol.cmd.load(str(sys.argv[2]))
                pymol.cmd.extend('Box', Box)
        elif args.download:
                download(sys.argv[2])
        elif args.split:
                split(sys.argv[2], 'Ligands', 'model', int(sys.argv[3]))
        elif args.job:
                PBS(sys.argv[2], # pX
                        sys.argv[3],        # pY
                        sys.argv[4],        # pZ
                        sys.argv[5],        # x
                        sys.argv[6],        # y
                        sys.argv[7],        # z
                        sys.argv[8],        # Seed
                        sys.argv[9],        # Exhaustiveness
                        sys.argv[10],       # Output
                        sys.argv[11],       # CPUs
                        sys.argv[12],       # Array
                        sys.argv[13])       # Email
        elif args.combine:
                os.system('cat {}/Docks_* | sort -nk 3 > Result'.format(sys.argv[2]))
        elif args.Kd_to_dG:
                Kd_to_dG(sys.argv[2])
        elif args.dG_to_Kd:
                dG_to_Kd(sys.argv[2])

if __name__ == '__main__': main()
```

CURRICULUM VITAE

Personal Information

Name Surname: Sarah Boumezber

Education

Undergraduate Education : University of Science and Technology Houari Boumediene (USTHB), Algeria. Bachelor in biochemistry (2004).

Graduate Education : University of Science and Technology Houari Boumediene (USTHB), Algeria. Master's in biotechnology and molecular pathologies (2008).

Foreign Language Skills : Mother tongues: Arabic, French

Other languages : English (advanced speaker), Turkish (basic), German (basic).

Work Experience

2012-2017: Medical tourism agent. Istanbul

2011-2012: Lecturer at the department of biotechnology. Islamic university of Gaza.

2010-2011: Lab assistant. Nasser hospital. Gaza.

2010-1011: Lab assistant. Kuwaiti hospital. Gaza.

2009-2010: lab assistant at Mustapha pasha university hospital center. Department of neurology. Algeria.

2008-2009: lab assistant at local medical laboratory. Poly clinique Dely Ibrahim. Algeria.

Publications and Presentations Derived from the Thesis

Boumezber. S. and Yelekci. K. (2022) 'Screening of novel and selective inhibitors for neuronal nitric oxide synthase (nNOS) via structure-based drug design techniques', *Journal of Biomolecular Structure and Dynamics.* doi: 10.1080/07391102.2022.2054471.